TEMPOROMANDIBULAR JOINT INJURIES DURING WHIPLASH

Ciaran Simms

Department of Mechanical and Manufacturing Engineering

Trinity College
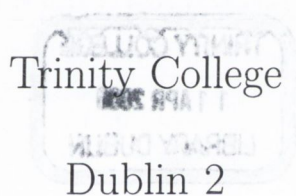
Dublin 2

Ireland

September 1999

A thesis submitted to the University of Dublin for the degree

of PhD.
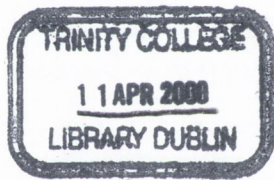
Abstract

Whiplash injuries occur due to differential accelerations in the human body. Neck injuries are predominant, but a considerable body of clinical evidence suggesting a close relationship between whiplash and temporo-mandibular joint (TMJ) disorders has also accumulated. These soft–tissue injuries are generally treated conservatively and may take several years to resolve. The symptoms are well established but their cause is unclear as the validity of retrospective clinical studies is compromised by their subjective nature. Two main injury hypotheses have been proposed, but these lack experimental evidence. This thesis presents the development and sled–testing of a physical model of the head, neck and mandible designed to simulate *in vivo* behaviour in a low velocity rear–end collision. Extensive instrumentation and a new angular displacement transducer for the head have given detailed kinematic information regarding mouth–opening and accelerations at the TMJ. Soft–tissue tensile tests using *in vitro* specimens have given an indication of the structural properties of the TMJ. The results indicate clearly that the mandible and TMJ are not harmed during a low-velocity rear–end collision. Excessive levels of mouth–opening do not occur during whiplash resulting from Δv's of up to 9.2km/h. Active bracing of the jaw muscles prevents mouth–opening. A 2–D kinematic model of the head/jaw complex has been developed. The input to this model is given by the measured rotational kinematics of the model head. Simulations have shown a good correlation with experimental data and a parametric analysis showed remarkable stability of the model. The latter indicates that normal geometric variations are unlikely to influence loading at the TMJ significantly. The model was used to estimate the magnitude of loading at the TMJ during retroflexion. Comparison with a simple free body diagram of the mandible shows that reactive forces across the TMJ in functional chewing are much higher. These results are in direct conflict with the predominant Inertial Injury Theory. In contrast, the results of this thesis are in agreement with the post–accident neuro–muscular changes proposed by the Late TMJ Injury Theory.

Declaration

I declare that I am the author of this thesis and that all the work described herein is my own, unless otherwise referenced. This work has not been submitted, in whole or in part, to any other university or college for any degree or qualification. I authorise the library of Trinity College, Dublin to lend this thesis.

Acknowledgements

Nomenclature

COG_{head} — Centre of gravity of the head (m)

$\triangle v$ — Change in vehicle velocity (ms^{-1})

E' — Elastic modulus (Pa)

E" — Storage modulus (Pa)

E* — Complex modulus (Pa)

g — Acceleration due to gravity (ms^{-2})

P_{sled_X} — X–direction displacement of the sled (m)

P_{head_X} — X–direction displacement of COG_{head} (m)

P_{head_Z} — Z–direction displacement of COG_{head} (m)

P_{TMJ_X} — X–direction displacement of the TMJ (m)

P_{TMJ_Z} — Z–direction displacement of the TMJ (m)

θ_{head} — Angular displacement of the head (rad)

θ_{jaw} — Angular displacement of the jaw (rad)

$\dot{\theta}_{jaw}$	Angular velocity of the jaw (rads^{-1})
$\dot{\theta}_{opening}$	Rate of mouth–opening (rads^{-1})
$\theta_{opening}$	Magnitude of mouth–opening (rad)
sp	Cadaveric TMJ specimen
$\tan\delta$	Phase angle (rad)

Derivatives of a function with respect to time are denoted by the 'dot' operator.

Abbreviations

CNS	Central nervous system
COG	Centre of gravity
CSA	Cross–sectional area
DMTA	Dynamic materials testing analyser
DOF	Degrees of freedom
EMG	Electromyography
FBD	Free body diagram

HSV   High speed video

ICR   Instantaneous centre of rotation

IIT   Inertial injury theory

LTIT   Late TMJ injury theory

MDF   Medium density fibre

MHD   Magneto–hydrodynamic (sensor)

MPD   Myofascial pain dysfunction

MRI   Magnetic resonance imaging

MVA   Motor vehicle accident

PTFE   Polytetrafluoroethylene

RID   Rear impact dummy

SCM   Sternocleidomastoid

SED   Sierra engineering dummy

SNR   Signal to noise ratio

TA   Tibialis anterior

TMJ   Temporomandibular joint

TMD   Temporomandibular dysfunction

TML   Temporomandibular ligament

VC   Viscous criterion

Contents

List of Figures

List of Tables

Chapter 1

Introduction

Whiplash injuries to the human Temporomandibular Joint (TMJ) are a subset of the larger family of whiplash injuries. The public perception is that whiplash refers only to neck injuries following a rear–end motor vehicle accident. In fact, it includes any injuries to the head and neck region due to differential acceleration of the head relative to the body. The accuracy of the term has long been disputed, but the compact and descriptive appeal of 'whiplash' has ensured its continued use.

Whiplash commonly occurs in rear impact automobile collisions but can equally result from other forms of accident. The classic event occurs in an urban environment, where the front vehicle is stationary at an intersection and the driver is unaware of the impending collision. A second vehicle travelling towards the intersection fails to stop and collides with the rear of the front vehicle. The driver of the striking vehicle is unharmed as he/she is aware of the impending impact and the $\triangle v$ is often low due to emergency braking and low urban speed limits. However, the crash pulse applied to the struck vehicle causes both the vehicle and its occupants to accelerate and then decelerate in a sequence that frequently causes soft–tissue injuries in the upper body region. Injuries to the cervical spine are predominant, but a considerable body of clinical data has also accumulated which suggests a close relationship between whiplash and TMJ injuries.

1

1.1 Historical Perspective

Injuries caused by inertial loading of the human body are an inevitable consequence of the transport revolution. Today's whiplash injury has origins in railroad accidents and a condition known as 'Railway Spine' which became an accepted phenomenon in the latter half of the nineteenth century [1]. The US Navy may have been the first to identify the essential cause of the injury when in the 1920's it was found that pilots of catapult-launched fighter aircraft sometimes lost consciousness during take-off. This caused a loss of aircraft and manpower and was quickly remedied by the installation of head–rests to support the head and thus prevent damage to the cervical spine [2]. Amazingly, it was not until 1969 that head–rests became mandatory in the USA for front seats of vehicles in the civilian sector.

The incidence of reported neck injuries grew as the world car population expanded. There was, as yet, no consciousness of the possibility of TMJ damage. In the USA, where the transport revolution was greatly boosted by the availability of cheap fuel, public awareness of the injury manifested itself earlier than in Europe or elsewhere. Victims of rear–end collisions reporting to hospitals precipitated the medical community's interest in this phenomenon and the early reports are largely clinical findings coupled with conjecture on the nature of the injury. In 1919, the *Boston Journal of Medical Surgery* published a report listing automobile accidents as one of the causes of mild neck injuries. In 1928, a report of eight cases of neck injuries all resulting from traffic accidents was presented to the Western Orthopaedic Association in San Francisco. (Years later Crowe, the author, stated that he had alluded to the term 'whiplash' in this report, but the proceedings were not published. Later again, he is said to have denied having ever used the phrase. The dispute continues mainly in the medical fraternity.) By the 1950's the term 'whiplash' had become widely accepted and *'Common whiplash injuries of the neck'* published by Gay & Abbott in 1953 [3] has since become regarded as one of the seminal medical works in the field. In this report, the jaw is only mentioned as a site of referred pain.

It took some time before awareness in the medical world was translated into action by car manufacturers. At that time, there were no standardised tests with deformable barriers (or otherwise) to test safety features in a new vehicle. 'Crash-worthiness' has become such a catch-phrase in the safety–conscious 1990's that it is difficult to imagine now how little attention was paid to injury prevention by car designers in the 1950's. Some idea of 1950's contemporary thinking on safety can be gleaned from this report by Severy et al. [4]: *'Reliable appraisal of the complete collision performance of new car models could be made only when based on evaluations which include experimentally staged collisions. It is suggested that this criteria be included in judging the merits of new cars.'*

The modern history of whiplash investigations began with these suggestions. That report recognised the importance of incorporating the findings of experimental crash–tests into the design of future cars. Severy et al. [4] carried out the first controlled rear–impact crash tests using human subjects and anthropometric dummies. This impressive body of work draws conclusions which are still relevant today. It marks the beginning of attempts to measure what actually happens to the occupants of a vehicle in a classic rear–end collision, providing indispensable kinematic data relating to vehicle and occupant behaviour. This was a significant departure from having to rely on subjective clinical reports.

By the 1950's low–speed rear impact collisions were recognised as being one of the most common types of car crash injury, while at the same time being largely misunderstood and therefore treated with suspicion. The primary difficulty is the paradox that resulting body injuries are rarely accompanied by commensurate vehicular damage. This is compounded by the fact that there may be no tangible signs of injury immediately after the accident, so that an injured occupant may initially be unaware of his/her condition. Symptoms frequently requiring considerable recovery time and medical attention may only develop between twelve and twenty-four hours post–accident. This has led to the publication of articles since the mid '60s with titles such as 'The enigma of whiplash injury' [5] and 'Whiplash syndrome – fact or fiction?' [6]. In the majority of rear–end collisions legal responsibility for the accident lies with the driver of the striking vehicle, while the

3

occupants of the struck vehicle are more likely to be injured. This frequently results in legal proceedings which considerably colours the nature of research in this area. Thirty years later, the same lingering suspicion continues to tarnish the credibility of all research in this field. It is a dubious tribute to the media that the *volksmund* has remained largely unaware that most reputable authors have found that litigation is not statistically significant in determining the outcome of whiplash injuries [7, 8, 9, 10, 11]. TMJ injuries during whiplash are subject to the same distrust and although there are many clinical reports and hypotheses suggesting a causal relationship between whiplash and TMJ dysfunction, there has been a dearth of experimental work to accompany the existing clinical evidence. This is due to difficulties in obtaining useful volunteer data, and the complexity required in an experimental model.

1.2   The Rear–end Collision

It is instructive to have a clear concept of vehicle and driver kinematics following impact. This has been the goal of several research teams since the 1950's [12, 13, 14, 15, 16, 17, 18] and broad consensus has been reached regarding the motion of the occupant(s) of the struck vehicle. There are some differences between reports as vehicle design has changed dramatically during the last four decades: the 1947 Plymouth used by Severy et al. [4] had very different crush characteristics (no energy absorbing bumpers) and cabin layout than the 1986 Dodge 600 Convertible used by McConnell et al. [19, 20]. More importantly, head–rests were not a standard feature in US vehicles prior to 1969. Improvements in instrumentation have meant that two recent studies by McConnell et al. [19, 20] provide the most accurate descriptions to date. A brief summary of these reports provides a good understanding of occupant kinematics during a low–velocity rear–end collision. The following description refers to a test run of 4.87mph with a male volunteer and a zero incidence–angle impact. McConnell et al. [19, 20] have divided the event into five phases for convenient description and the temporal origin is defined at impact. These observations are probably the best attempt at describing body kinematics

4

following a low velocity rear impact, but even here it should be remembered that the collisions were staged. Despite considerable efforts to shield volunteers from awareness of the impending impact, this can never be fully successful and may affect occupant behaviour.

1. **Initial phase (0–100ms).** There is no detectable body motion for at least 50–60ms after bumper contact. In this time, the base of the seat travels forward ca. 7cm and the seat–back deflects an average of 3–5°. The result of this motion is that the lower seat–back is compressed into the occupant's back and the seat–back is deflected rearwards relative to the vehicle. The upper torso and head remain stationary. Between 60–80ms the vehicle and seat–base have moved forward by 10cm from rest and seat–back deflection is 6–7°. The lower portion of the body now begins to drag the torso forward and the lower portion of the trunk contacts the increasingly rearward sloping seat–back. Rearward deflection of the seat–back lowers the vertical seat height and the shoulders ramp up 5–8cm over the seat–back incline. The mid back is pushed forward by the advancing seat–back and this straightens the thoracic curve, further increasing the ramping effect. During this period the head has not moved at all, even though the base of the neck has begun to move. The result is that tension in the neck causes an anterior pull on the base of the skull and by 100ms the top of the neck has begun to move forward.

2. **Principal Forward Acceleration (100–200ms).** Early in the second phase (110–120ms), the seat–back reaches its maximum rearward deflection of 10–14° and the acceleration of the top of the neck also reaches its maximum of 5–15g (note the very large variation). The vehicle has now moved forward ca. 16cm, T1 (the first thoracic vertebra) has moved forward 8–10cm (about half as much as the vehicle), and the neck is still largely vertical. It can be deduced from film evidence of clear bulging of the sternocleidomastoid muscle that considerable tension has developed in the neck. Between 110–170ms, 10–15° of almost pure rotation of the head occurs, after which continued

5

forward motion of the top of the neck forces a translational component of head motion. By 200ms the head has reached maximum retroflexion of 18–51° (again a large variation). It is in this phase, when head accelerations (both linear and rotational) are at a maximum, that damage to the TMJ is most likely to occur.

3. **Head overspeed/torso recovery (200–300ms).** Early in this phase the seat regains its pre–impact displacement relative to the car. The torso has a velocity close to that of the vehicle while the head is now travelling forward at a higher rate and is being decelerated by the neck. Between 280–320ms the head reaches its pre-impact upright position.

4. **Head deceleration/torso rest (300–400ms).** The head continues to be decelerated in the flexion motion while the body assumes its resting position with respect to the vehicle. Voluntary stabilisation of the occupant's position was in evidence here.

5. **Restitution phase (400–600ms).** The occupant now comes to final rest relative to the vehicle in a position that is slightly higher in the seat than the pre-impact situation. The authors conjecture that this is due to the sloped seat–base and the manner in which the body lands after leaving the seat–base in phase 1.

1.3 Objectives and Outline of the Thesis

The literature contains numerous physical models of the head/neck complex (of which the Hybrid III is the best known) but there are no published models including a movable jaw. In addition, there is a lack of information regarding the soft–tissue properties of the TMJ. This thesis reports on two main approaches: the development and sled–testing of a mechanistic model of the head, neck and mandible, and soft–tissue testing of cadaveric TMJ specimens. The former has provided detailed information on the kinematic behaviour of the mandible and the TMJ during a rear–impact collision, while the latter gives a measure of robustness of the TMJ. The aim of this thesis is to collate the results from these two experimental approaches to determine the likelihood of TMJ trauma during whiplash. In addition, a two–dimensional Lagrangian model of the head/jaw complex has been developed and used to investigate the parametric stability of the physical model. This is used to address the effect of geometric variations on the likelihood of injury.

Chapter 1 contains a brief introduction to the classic whiplash event and its connection to TMJ injuries. An outline of the relevant anatomy is provided in appendix B. The literature survey in chapter 2 reviews the epidemiological evidence and the various injury hypotheses. Current research into crash–test investigations and experimental muscle modelling is also assessed. In chapter 3 the design, construction and validation of the experimental sled–testing facility are detailed. Results of sled–testing are reported in chapters 4 and 5. Force/extension testing of *in vitro* TMJ specimens is described in chapter 6. Simulations using the Lagrangian model developed to investigate the stability of the experimental whiplash model are covered in chapter 7. In chapter 8, a summary of results is given and this is used to assess the injury hypotheses detailed in the literature survey. The strengths and limitations of this work are discussed. In chapter 9, conclusions are drawn and recommendations for future work are made.

Chapter 2

Review of the Literature

There are three research areas directly relating to the work in this thesis:

- Epidemiological evidence of TMJ injuries as a result of whiplash.

- Experimental crash–tests including whiplash investigations.

- Characterisation and physical modelling of human muscle behaviour.

A glossary of medical terms is included in appendix A. Appendix B provides an outline of the anatomy of the neck and a more detailed description of the structure and function of the mandible and TMJ. A brief description of muscle physiology is also given.

2.1 Epidemiology

An early reference to non–direct injury of the TMJ comes from Pringle, who stated in 1918 that the temporomandibular disc may become anteriorly displaced by excessive mouth movements, as can occur in the physiologic motions of a yawn or sneeze [21]. In 1948, Wakeley suggested that anterior displacement of the disc could occur without a direct blow to the mandible due to sudden or irregular contraction of the lateral pterygoid muscle [22]. Wakeley speculated that the posterior attachment of the disc was especially susceptible to damage if the mouth were open and the attachment already stretched. In some patients there was

anecdotal evidence that this may become chronic, with 'persistent snapping' of the joint and associated pain.

An article by Roydhouse commenting on the similarity between some of the symptoms of TMJ dysfunction and those of whiplash appeared in *The Lancet* in 1973 [23]. Roydhouse admitted that these symptoms (which included head pains, stuffy noses, plugged ears, blurred vision, sore throats and stiff jaws) were too vague to enable a clear prognosis. Deceleration effects on the mandible and hence on the TMJ are cited as the cause of these symptoms, but no further explanation is given. The suggestion was that although pain in the TMJ and muscles of mastication is sometimes seen as referred pain, these locations may in fact be origins, but again no further comment is made. The importance of this article is that it appears to be the first to correlate whiplash and TMJ dysfunction explicitly. It is also the first of many articles by clinicians with personal experience of patients claiming TMJ disorders resulting from whiplash.

The medical literature can be subdivided into two categories. There are several papers reporting the findings of surveys carried out at dental clinics. In these the authors present a list of symptoms reported in a retrospective survey of a sample group of patients. An assessment is made of the likelihood of a causal link between TMJ dysfunction and whiplash. Theories explaining what injuries are responsible for the reported symptoms are proposed. In most cases, an explanation of how crash kinematics cause these injuries is also given. The second category has many papers by clinicians in which the causal link is presupposed and the aetiology of a plethora of injuries is then discussed. Individual case studies are often chosen to illustrate the author's point of view. Papers published by Frankel in the 1960's are probably the first of this kind [24, 25]. Both categories are valuable because they represent the only information available on real car crash injuries. Although some symptoms are too generalised, others relate to injury of specific tissues and are present in several reports.

However, extreme caution is necessary when considering the external validity of such investigations. Retrospective studies always contain an element of self-evaluation for the patient, and there are numerous examples of the unreliability

of this procedure, even when the intention of the patient is honourable. The most striking of these are the repeated reports by victims of rear-end motor vehicle accidents (MVA), stating that flexion of the head occurred before retroflexion [3]. If litigation is involved, it becomes untenable to regard a patient's subjective report as scientific fact. In a recent article, McKay & Christensen [26] have ridiculed the entire process of retrospective clinical studies as pseudo-scientific, accusing it of being detrimental to the general scientific process. This aggressive attack overlooks some undoubtedly positive contributions of these papers, but reflects frustration at their lack of objectivity. Subjective clinical methods are unavoidable and commonplace in the medical community. Pain cannot be measured on an absolute scale and is necessarily defined as a subjective entity. Thus, there is no clear distinction between objective fact and opinion, and Christensen & McKay [26] are correct in drawing attention to this problem. The following chronological review of published medical reports should be seen in the context of these limitations.

Medical Reports

In 1977, Brooke, Stenn & Mothersill [27] published their findings of two hundred and seventy-four patients (with symptoms in one or both TMJ's) referred to the Department of Oral Medicine at the University of Western Ontario. The following categories were identified:

- Seventy percent were diagnosed as Myofascial Pain Dysfunction (MPD) syndrome patients.

- Seventeen percent suffered from other TMJ associated disorders.

- Eleven percent had conditions unrelated to the TMJ. This means that more than ten percent of patients reporting pain, trismus (spasm of the muscles) or other TMJ dysfunction actually had no injury in that region.

The major symptoms of those with MPD were pain (96%), clicking (82%) and difficulty in mouth–opening or closing, and deviation (76%). None of the patients had abnormal radiographs and in five percent of cases pain was the only symptom.

Seventy–five percent of patients described themselves as 'stressed', but it is not clear whether this was a cause or an effect of the TMJ symptoms. Ten percent of MPD patients reported that they had received either direct or indirect trauma of the TMJ in a road traffic accident, and that this had precipitated their symptoms. These patients were found to respond far less favourably to conservative treatment. Treatment was found to be successful in eighty–one percent of the MPD group as a whole, whereas in the trauma–induced injury group there was only a forty percent success rate. It is frustrating that no attempt was made to distinguish between those suffering from direct and indirect trauma, as this is critical in assessing the statistical correlation between whiplash and TMJ dysfunction. In a further paper concentrating on the differences in the success of treatment between non-traumatic and traumatic MPD groups no differences in the symptoms were observed [28]. The sample of trauma–induced cases was increased to thirty–seven patients and there was still a poor response to conservative treatment. The authors suggest that stress resulting from litigation may be responsible for the continuation of symptoms. With prolonged constriction of the muscle, spasm becomes more likely. When this occurs in the temporalis, it is perceived as 'headache', when it occurs in masseter or the pterygoids it is perceived as 'jaw pain'. However, only 14% of the trauma group were involved in litigation. It is reasonable to conclude that injuries to the TMJ due to extrinsic trauma are more difficult to treat, but the lack of a distinction between direct and indirect trauma precludes any definite conclusions regarding a causal link between TMJ injury and whiplash.

Harkins and Marteney [29] collected data from seven hundred and twenty–seven symptomatic patients who sought treatment for temporomandibular dysfunction (TMD). Data was gathered by interview, clinical examination and a self-administered questionnaire. Nineteen percent reported that whiplash had resulted in head or neck trauma and seventeen percent reported whiplash as the precipitating factor in TMJ dysfunction. However, nearly all of these (exact percentage unclear) were involved in litigation, and there is again no indication whether trauma to the TMJ was direct or indirect.

11

Truelove et al. [30] studied two hundred and twenty–four patients who presented with symptoms of facial pain:

- thirty percent reported a history of trauma, but this was not limited to MVA implicated patients.

- ten percent reported that trauma had precipitated their symptoms.

- five percent reported that their trauma was a result of an MVA.

Direct and indirect impacts in the MVA subgroup were not differentiated and there is no record of whether litigation was involved. This report is inconclusive, but probably suggests no causal link between TMJ dysfunction and whiplash.

Weinberg & Lapointe [31] studied twenty–eight patients who reported TMJ symptoms. All had medically diagnosed cervical whiplash symptoms following an MVA. Eighteen accidents were rear-end MVA's, six were front–end and four were lateral impacts. The following initial symptoms were reported:

- nineteen (67%) suffered pain as their major initial symptom.

- nine (32%) patients had restricted mouth–opening.

- four (14%) patients had TMJ clicking and numbness.

The onset of symptoms varied from the day of the accident (57%) to over one week after the accident (11%). A large variety of symptoms were reported:

- pain localised in the TMJ.

- temporo–parietal, occipital and frontal headaches.

- painful and tender muscles of mastication, cervical musculature and muscles of the upper back.

- clicking in the TMJ.

- painful limitation of mouth–opening associated with mandibular deviation.

- ear-aches, vertigo, tinnitus and retro-orbital pain.

Inferior joint–space arthrographic examinations were carried out in twenty–five patients (three patients refused arthrograms) with the following diagnosis:

- anterior disc displacement with reduction in twelve patients.

- anterior disc displacement without reduction in eight patients.

- anterior disc displacement without reduction and perforation in one patient.

- degenerative joint disease in one patient.

- three patients had normal arthrograms and were diagnosed as suffering from MPD.

Ten patients elected to have surgery and the arthrographic findings were confirmed in every case. One patient showed perforation of the lateral third of the posterior attachment tissue. These are some of the more compelling clinical findings, not least because of the surgical affirmation lacking in other reports. However, a sample of twenty–eight patients is small and again there is no mention of whether trauma was direct or indirect.

Pullinger & Monteiro [32] studied one hundred and fifty–two TMD patients and compared their histories and symptoms with a control group of three hundred and thirty–one students attending the *UCLA Temporomandibular and Facial Pain Clinic*. Amazingly, sixty–five percent of the control group exhibited some symptoms. If this is representative of a typical control group, then the utility of these surveys is questionable: if sixty–five percent of a control group are symptomatic it becomes difficult to draw any conclusions from the test group. However, the authors do not address this and state that the patient group had a significantly higher likelihood of a trauma history. Again, there is no mention of whether TMJ trauma was direct or indirect. Within the control group, a report of moderate or severe trauma was significantly associated with specific symptoms of internal derangement, dental or occlusal discomfort and headache or cervical pain. The sequellae of TMJ trauma may be traumatic arthritis [33], disc displacement [34], disc dislocation [35] and intra–articular haemorrhage [35].

13

Heise, Laskin & Gervin [36] studied one hundred and fifteen whiplash victims. Patients were interviewed, examined and a follow-up interview was carried out one month later. These were divided into two categories, those with radiological evidence of cervical skeletal injury (forty patients), and those without (seventy-five patients). None in the first category reported TMJ symptoms at the first interview, and after one month only two reported TMJ pain. In the group without radiological evidence, one patient reported TMJ symptoms at the initial interview, but no additional cases of pain were reported after one month. The authors concluded that there is no nexus between cervical musculoskeletal injury and TMJ pain. In a second paper by the same authors [37], the sample was increased to one hundred and fifty-five patients, and the conclusions drawn are similar. Contrary to the findings of Brooke et al. [27], this study found that the incidence of masticatory myalgia and joint spasm was low in patients with whiplash injuries, and that conservative treatment was generally successful when it did occur. The study shows that although some patients with neck injuries do develop TMJ pain/dysfunction, the likelihood of this is very low (4%).

Burgess [38] examined one hundred patients with symptoms of TMJ pain who had suffered overt trauma (31 patients), whiplash with overt trauma (35 patients) or whiplash with no direct impact (34 patients). However, the report is unclear because in a table showing symptoms of those with whiplash, only fifty-one percent report pain in the TMJ. According to the study design, all patients in this category were chosen because they had both TMD symptoms and were whiplash victims. The study concludes that pain symptoms from each of the three categories vary significantly.

Pressman et al. [39] examined thirty-three symptomatic whiplash patients (66 TMJ's) who reported no direct trauma to the jaw, head, mouth or face due to the accident and no prior history of TMJ dysfunction. These underwent Magnetic Resonance Imaging (MRI) and the images were retrospectively analysed. Twenty-nine patients (88%) had some abnormality in the TMJ. Displacement of the disc was seen in thirty-seven (56%) joints:

- twenty-one (32%) had anterior disc displacement with reduction.

14

- nine (14%) had anterior disc displacement without reduction.

- six (6%) had lateral or medial displacement.

- one (2%) had posterior displacement.

Joint effusion and/or oedema was seen in sixty–five percent of TMJ's. MRI clearly shows the cases of disc displacements, but the localised joint effusions and signs of oedema are not so obvious. McKay & Christensen [26] contend that TMJ effusion detected by MRI is often an expression of normal synovial fluid as well as displaced saliva within the upper joint cavity. The article concedes that the quality of the medical histories may have been compromised by compensation claims pursued by some of the patients, but the percentage involved in litigation is not stated. The statement that no direct injury of the head, jaw or face occurred relies on the accurate memory of the patient in recalling the details of a sudden and brief event.

A review paper in 1993 by Brady et al. [40] includes a report of a new clinical study. One hundred and ninety-four patients referred for craniofacial pain evaluation were examined. Twenty-seven patients (14%) with internal derangement of the TMJ reported whiplash as the precipitating factor. However, the paper does not state how internal derangement was diagnosed, whether impact was direct or indirect, and there is no mention of litigation and how this may affect the patient's self-reports.

Magnusson [41] reports on thirty-eight patients with late whiplash syndrome. The original sample had one hundred patients. However, sixty–two were disqualified due to earlier whiplash injury, history of direct trauma, involvement in a roll-over accident or a history of musculoskeletal disorder prior to the accident. In the screened sample of thirty–eight, Magnusson found that eleven (29%) had pain and tenderness in the TMJ, unilaterally in five and bilaterally in six. Four also had signs of TMD and were diagnosed with oromandibular dysfunction. The symptoms of this are

- joint crepitation.

- bruxism.

15

- pain on jaw function.

- locking of jaw–opening (in one patient).

- articular pain.

- tender points in the capsule.

Magnusson remarks that TMD symptoms in whiplash are generally secondary to muscle tension in the masticatory muscles.

A sense of perspective of overall accident statistics can be gained from an Australian study by Probert et al. [42] in Melbourne. In 1987, over twenty thousand compensation claims were accepted following MVA's. Whiplash accounted for ca. two thousand (10%) of these and was found to be the most frequent injury associated with subsequent TMJ dysfunction. However, only twenty–eight patients (1%) were identified with TMD. The authors note that in some cases TMJ problems are not reported and that the figures quoted are thus likely to be a conservative estimate. Nonetheless, the relative importance of TMJ dysfunction following an MVA is very low in this report.

In a recent study, Garcia & Arrington [43] carried out MRI in eighty–seven consecutive MVA whiplash patients who presented with TMJ symptoms. According to self–reports, none of the patients had suffered a direct trauma to the head, neck or mandible and none had TMJ symptoms prior to their accident. The MRI tests were carried out within one year of the accident in eighty–five percent of cases and were evaluated for disk displacement, reduction, effusion and inflammation/oedema. The authors report internal derangement in eighty–seven percent of cases based on T1 weighted images. Abnormal joint fluid was seen in T2 weighted samples. It should be noted that all of these whiplash patients had presented with TMJ symptoms, so the high percentage of joint derangements and abnormal joint fluid cases is not surprising. By its own admission, this study lacks a suitable MRI–evaluated control group. Further, McKay & Christensen [26] have stated that the T2 weighted MRI images interpreted by the authors as showing abnormal joint fluid are in fact simply showing saliva from the parotid gland. In addition,

16

Internal derangement	No. of TMJ's (total = 164)	%
Disk displacement with reduction	118	72
Disk displacement without reduction	25	14
Normal (no derangement)	21	13

Table 2.1: Internal derangement of the TMJ seen on T1 weighted MRI [43].

the definition of 'normal' disc position (taken here to be when the middle section of posterior band of the disc lies over the mid–portion of the condyle) may have increased the number of joints being classified as abnormal. Nonetheless, anterior disc displacement is clearly visible in the MRI images and comparisons with studies of normal TMJ subjects show that the instances of abnormalities in the joint are much higher in the symptomatic group.

Comment On Medical Reports

The difficulty with this body of evidence is that no two reports are sufficiently similar in structure to allow cross-comparison. In addition, some critical questions do not seem to have been asked. With the exception of Magnusson [41], none of the surveyors attempted to differentiate between injuries caused by direct and indirect trauma, and this fundamentally reduces the utility of most of these reports

Joint fluid	no. of TMJ's	%
Effusion	113	69
Inflammation/oedema	84	51
Normal	32	20

Table 2.2: Abnormal fluid seen in T2 weighted MRI [43].

17

Category	Example
Autoimmune Disorders	Temporal arthritis
Bone disorders	Avascular necrosis
Central nervous system disorders	Cerebrospinal fluid rhinorrhea
Dental problems	Dental infections
Diseases of the ears, nose and throat	Middle–ear infection, sinusitis, vocal dystonia
Inflammation	Labyrinthitis
Neurologic disorders	Trigeminal neuralgia
Psychological Disorders	Depression
Rheumatic Disease	Rheumatoid Arthritis
Salivary gland disorders	Sialolith
Tumours	Acoustic neuroma

Table 2.3: Disorders with similar symptoms to TMJ dysfunction.

when trying to establish the connection between whiplash and temporomandibular disorders. The percentage of a sample involved in litigation is important in assessing the reliability of self-reports, yet this is not documented in several studies. The small sample size of most surveys is a problem, but this is not adequately addressed. There are a disproportionate number of females in almost all samples, but it has also been noted that females are more prone to seeking healthcare in general. (The ratio of head mass to neck muscle strength is higher in women than in men [44].)

More recently, McKay & Christensen have contended that the painful symptoms reputed to be the result of whiplash injuries are in fact a manifestation of progressive synovitis, osteoarthritis and internal derangement that evolves throughout adult life in 25–35% of the population [26]. It is certainly true that there are many disorders that share some or all of the same signs and symptoms as those claimed by victims of mandibular whiplash (see table 2.3), and this casts further doubt on the reliability of the epidemiological reports.

A small majority of surveys conclude that there is a causal link, but the clinical evidence as a unit is inconclusive – neither the proponents nor the opponents of 'jawlash' have conclusive proof of their respective theories. There are too many factors involved: how were the patients chosen? Were they predisposed to injury? Was litigation involved? What kind of patient is likely to attend a given clinic? Was the patient relaxed? Was the patient facing forward? (An individual with his/her head turned at the moment of impact has a greatly reduced range of neck motion [16].) A common finding was that stress was frequently related to the onset of complaints – in one study, sixty–eight percent of TMJ patients also suffered from nervous stomach disorders [45]. These clinical surveys show that there are a considerable number of patients with dysfunction of the TMJ. There is no evidence that conclusively links whiplash to TMJ dysfunction, but it has not been possible to demonstrate adequately that there is no causal link.

2.1.1   Types of Injury

Identification of the TMJ as a site of pathology may be difficult due to the presence of cervical injuries which produce symptoms in the same area [46]. However, Myofascial Pain Dysfunction (MPD) and internal joint trauma (TMD) are the two main injury classifications that have been identified. MPD is linked to muscle spasm and the symptoms are muscle discomfort with particular tenderness in the origins and insertions. Internal joint trauma refers to physical disorders occurring within the joint itself. Joint derangements are demonstrated by mechanical blockage of mandibular motion with no bounce or elasticity demonstrable in excursion end–points. Patients either have, or have had, periods of locking, in which they are unable to open their mouth fully. These are manifestations of loss of coordination of the condyle and the disc. Brooke & Lapointe [47] describe four stages of internal derangement of the joint.

1. The disc is displaced antero–medially in the joint space when the patient is in the mouth–closed position. As the mouth opens, the disc clicks back (reduces) to a normal relationship with the condyle: between the condyle and

articular eminence. As the mouth closes, the disc returns to its abnormal position with a further click. Pain may occur in the mouth–open position due to impingement of the innervated posterior attachment tissues when they are stretched across the articulation due to displacement of the disc.

2. Classic stage one derangements progress to locking. The disc fails to reduce an opening – i.e. it does not click back into place during mouth–opening. This results in pain and limitation of mouth–opening, and often deviation to the affected side. If this continues, the disc then either scars and improves (both symptomatically and functionally), or perforates.

3. A perforated posterior attachment with a non–reducing disc is stage III. This results in direct bone–to–bone contact through the perforation. Remodelling of the convex surfaces of the condyle may occur.

4. If remodelling is too destructive, degenerative changes in the bones of the joint are seen. This results in pain and grinding in the TMJ.

Both MPD and TMD are reflected in three main clinical complaints (identified by Frankel in the 1960's and early 1970's [24, 25]) that are considered tell-tale symptoms of TMJ dysfunction:

- pain in the TMJ.

- clicking.

- limited range of motion.

Internal joint derangement may be caused by MPD, and the two injuries often occur in conjunction with each other. Some argue that an alteration in the disc–condyle relationship is the initiating factor and that concomitant muscle spasm is secondary. Others argue that muscle spasm is primary and that this causes disc displacement. Most patients present with the symptomatology of both conditions in varying proportions [47]. Symptoms are often not identified until several weeks or months after the accident [48, 49, 31, 50].

20

2.1.2 Possible Injury Mechanisms

There are two main categories of proposed injury mechanisms: those contending that injury occurs due to inertial behaviour of the mandible during the whiplash event, and those postulating that neurological changes in the post–accident period cause muscle spasm and, with time, internal derangement of the TMJ.

The Inertial Injury Theory

The following is the basis of the Inertial Injury Theory (IIT). Stretching of the posterior discal attachments occurs during retroflexion of the head. The inertia of the mandible causes it to move posteriorly more slowly than the head and this results in downward and forward displacement of the disc–condyle complex relative to the cranial base. Excessive mouth–opening occurs because the lower jaw does not keep up with head motion [51, 31, 52, 23]. Hypertranslation of the mandible occurs easily because of the lack of a well defined anterior capsule which has been referred to as the anatomical 'Achilles heel' of the TMJ [53, 31]. This can lead to stretching and tearing of the posterior attachments, synovial tissues and lateral condylar poles [29, 31, 23]. The hyoid bone has no bony articulation, but attaches to the mandible via the suprahyoid muscles, and to the clavicle, sternum and rib cage via the infrahyoid muscles. In the extension phase, there is insufficient time for the supra–hyoid and infra–hyoid muscles to lengthen, thereby anchoring the mandible and holding it still. This increases mouth–opening and contributes to anterior displacement of the condyles [51, 31]. With forward displacement of the disc–condyle complex, the stretched posterior attachment is suspended in a vulnerable position across the glenoid fossa. Reflex reaction to involuntary mouth–opening will create an over–contraction of the masticatory muscles, resulting in the characteristic tenderness of the temporalis, masseter, suprahyoid, and pterygoid muscles [51]. During the flexion phase of head motion, the previously injured posterior attachment tissues are crushed between the mandibular condyle and glenoid fossa of the temporal bone. This reapplication of stress can cause further stretching, crushing, tearing or perforation of the posterior attachment tissue [31].

The Late TMJ Injury Theory

Voluntary control of anatomical position and movement is governed by the skeletal musculature which is controlled by neural impulses. The central nervous system (CNS) carries both afferent and efferent impulses – the former carries messages to the brain from a receptor, the latter from the brain to an effector (gland or muscle). Afferent input is supplied to the CNS via specialised nerve–endings called mechanoreceptors. These are cells that respond to mechanical distortion and are very sensitive to minor postural changes. Proprioceptors are sensory nerve endings in the muscle spindles that monitor internal changes in the body. Mechanoreceptors located in the upper cervical spine are sensitive to very slight postural changes of the head, neck and mandible. By sensing and reflexively correcting deviations from the normal postural position, these mechanoreceptors maintain a physiologically stable relationship between the head, neck and mandible. They can also initiate protective reflex arcs in an attempt to protect the body against injury. However, if the postural position is altered by injury, misinterpretation by the proprioceptors could produce ongoing neurologic signalling resulting in pathofunction of the related structures. It is possible that pathofunction in the cervical musculature is an important aetiological factor in the development of pain syndromes in the face or TMJ, and this is the core of the Late TMJ Injury Theory (LTIT).

Lader describes this in detail and suggests that post–accident occlusal discrepancies manifest as symptoms of pain in the face and head, and also as masticatory and/or articular dysfunction [54]. Lader describes the chronology of how this domino–effect can occur: Cervical myospasm causes an alteration in the normal craniovertebral posture. This stimulates the neuroreceptors in the cranial musculature to attempt to compensate this change by reflex action. The functional demand on the suprahyoid muscles is heightened, increasing their tonus. Hypertonicity in the suprahyoid muscle group generates postero–inferior load on the mandible, altering its position relative to the maxilla. This changes the occlusion, and the neuroreceptors in the periodontal ligament and in the TMJ respond with affer-

ent CNS signals which trigger efferent signalling to the masticatory muscles [55]. The result is muscle–bracing, which reduces stress resistance and increases the likelihood of muscle spasm. Spasm of the masticatory muscles is known to be an important aetiological factor in the development of joint pain and dysfunction [56].

Mannheimer describes a similar aetiology as the primary cause of TMJ disorders weeks, and even months, after the accident. This can occur even when the initial event is insufficient to cause direct trauma to the TMJ. [51]. In addition, posterior displacement of the mandible is a prime cause of otalgia (pain in the ear), tinnitus, dizziness, and a feeling of fullness in the ear [57]. Innervation of the tensor tympani and tensor palatini muscles (muscles of the ear) is via the mandibular nerve, which also innervates the masseter, temporalis, pterygoids, mylohoid and anterior digastric muscles via its motor branch. Constant reflex contraction of the tensor tympani and tensor palatini muscles can maintain this symptomatology. Research using electromyographic analysis supports the production of abnormal masticatory muscle activity due to a change in cranial and mandibular posture [58, 59, 60].

Discussion

These two categories of injury mechanism are very different but not mutually exclusive. The IIT is older and is still quoted as the primary cause of TMJ dysfunction. Superficially it appears to explain the clinically reported symptoms adequately. It has two major flaws: if the injuries are caused directly during the accident, why is the onset of symptoms often considerably delayed? Secondly, do the described rearward motions of the head and mandible actually occur in retroflexion? Supporters of the IIT claim that the late reporting of symptoms occurs because the patient is initially preoccupied with more serious injuries [47]. In contrast, the LTIT is supported by the late onset of symptoms, but cannot be experimentally investigated. However, if TMJ injuries as a result of whiplash do exist, but loading at the TMJ during whiplash is benign, then this constitutes strong evidence in favour of the LTIT.

2.2 Experimental Crash–tests

Crash–test investigations of the whiplash injury began with the series of real crash tests performed by Severy et al. in the 1950's [4] [61] [62]. At that time, the whiplash phenomenon was already well established, but little information was available in textbooks or medical literature. In 1953, Gay & Abbott had reported on a range of neck injuries of fifty whiplash patients they had examined [3]. The commonest complication reported was cervical radiculitis (inflammation of the root of a cervical nerve) and radiated pain into the lower jaw was among the lesser symptoms of this. The report made no mention of the TMJ, neither as a site of referred pain nor as an injury location. The authors also reported that the neck was first forced into flexion and then into extension. This theory was formed from descriptions of the accident by whiplash victims and illustrates the unreliability of such sources. However, there were no investigations into car and body kinematics at the time, so theories on the kinematics of the event lacked corroborative evidence.

Severy et al. used human subjects in both front and rear vehicles for low–speed collisions (up to 10mph), while anthropometric dummies were used for higher velocity impacts (up to 20mph). The dummy was also used in the lower speed impacts to provide a correlation estimate between human and dummy. Accelerometers and high speed film were used to monitor the event. It should be noted that the 1941 Plymouths used did not feature head–restraints, seat belts or shoulder harnesses. A number of important observations were made:

- The acceleration pulse of the struck vehicle is almost complete before significant acceleration of the occupant begins, and the authors attributed this to inertia, seat-back compressibility and flexure. This is the kernel of whiplash: the components of the vehicle and the body are accelerated at differing rates.

- The motion described by crash victims as 'whiplash' was found to be rearward rotation of the head (retroflexion), followed by forward rotation of the head (flexion), after which the head returned to its normal upright position.

24

- Body posture and state of preparedness influence the injury potential of a given collision. An unprepared occupant will not be able to brace prior to impact.

- Loading of the neck is via both translational and rotational accelerations, and flexure in the seat–back may be partially capable of cancelling the effects of one against the other.

- Vehicles should be rated on their collision performance as well as their acceleration and braking performance. In addition, the interior environment of the vehicle, especially the steering wheel and dashboard, can be responsible for direct facial injuries and this should be taken into account at the design stage.

These observations may appear self–evident today, but in the 1950's none of this had been formally observed and crash victims' reports are notoriously unreliable. The attempt at correlating dummy and human crash responses showed markedly differing acceleration patterns, and improving the biofidelity of anthropometric dummies is still a dominant focus, since volunteers can only be used for relatively benign impacts. The Sierra Engineering Dummy (SED) used by Severy et al. [4] had a shorter pulse and a far higher peak acceleration than human volunteers in the same crash environment, indicating that the dummy was too stiff.

In 1967 a research team at Wayne State University in Detroit led by H. Mertz and L.M. Patrick investigated the effect of head–rests in rear impact collisions [63]. This was two years before they became a legal requirement in the US, but they had already been fitted by several car manufacturers. Mertz & Patrick [63] simulated rear–end collisions using cadavers, dummies and a volunteer (L. M. Patrick himself) on a horizontal sled and track system. The sled was accelerated to a given velocity and could then be decelerated as desired using a hydraulic snubber. (Colonel Stapp of the US Air Force was one of the first to use volunteers to experiment on human tolerances to acceleration, often using himself as volunteer. On one occasion he had to cancel an aircraft–launching experiment because his

eyes began to bulge in their sockets). Mertz & Patrick [63] made a number of observations:

- For the unsupported head simulations, cadavers gave responses representative of persons unaware of an impending collision. The SED dummies responded differently from each other, and also from the cadavers and the volunteer. However, with the head initially close to the head–rest, the response of all subjects was similar.

- Controlled seat–back collapse reduces the severity of injury. It was suggested that an optimum rotational characteristic might be found for seat–backs. Severy et al. [4] had made the same observation.

- Neck torque measured at the occipital condyles rather than axial or shear force was proposed as a measure of likelihood of injury.

The theory of neck torque as a good indicator of injury was further investigated and the authors developed a head-angle/torque 'loading corridor', within which the response of a human neck could be expected to lie [64]. The highest peak deceleration pulse experienced by the volunteer was 14g. This caused sharp pain extending from the neck into the back that lasted for two days. The angle between the head and neck was found to be a poor indicator of trauma for neck extension because a small change in angle produces a large change in resisting torque. The best indicator was the equivalent moment which consists of the moments of neck and chin contact forces taken with respect to the occipital condyles. The authors note that there is no unique neck response curve, and that a response corridor is therefore more appropriate. Their suggested tolerance level to bending moment is 190Nm in flexion and 57Nm in retroflexion. These are considered lower bound estimates, as similar bending moments cause no discernable ligamentous damage in cadavers.

There have been other experimental crash–tests, and those prior to 1986 are reviewed by Huelke & Nusholtz [65]. More recent reports have included measurement of muscle activity using electromyography [66, 67, 68] and attempts to define body

motions more precisely [19, 20]. West et al. [69] carried out low speed rear–end collision tests with an unspecified number of volunteers and were the first to refer to possible TMJ injuries. These authors were aware of the IIT as a mechanism of TMJ injuries in low–velocity impacts, but stated that their videotapes showed no evidence of mouth–opening. Although the volunteers were wearing helmets firmly attached to the head and no mention is made of the state of awareness of the impending crash, they conclude that the reason there is no mouth–opening is that there are no forces acting to open the mouth. There is no explanation given for this speculation and no further comment is made regarding TMJ injuries.

2.2.1 TMJ Investigations

A focussed effort at investigating TMJ injuries in real crash simulations arose from the work of the Biodynamic Research Corporation in Texas. Two sets of low velocity rear–end car crash simulations resulted in the publication of the detailed description of occupant kinematics during whiplash given in section 1.2. A second research team led by Howard has concentrated on the behaviour of the jaw, drawing on experimental evidence to support new claims.

Testing with cadavers precludes measuring jaw kinematics because of rigor mortis. The ratio of head mass to neck muscle strength is such that rigor mortis is not capable of significantly altering the response of the neck: Mertz & Patrick [63] found that cadaver neck response was a good approximation to the *in vivo* response [63]. However, this is not the case for the jaw. The muscles of mastication are powerful as they are required to generate high chewing forces. By contrast, the mass of the mandible is only 0.16kg [70]. This means active clenching of the jaw elevator muscles will almost certainly prevent inertial injury of the jaw. Crash–test investigations of possible jaw injuries must be carried out with suitable dummies or volunteers, but not with cadavers.

However, even when volunteers are used, the same problem of muscle clenching arises. The critical aspect of TMJ injuries during whiplash is that the victim is unaware of the impending crash and the musculature is therefore in a relaxed con-

27

dition. It is doubtful whether this can be faithfully reproduced in any experimental set–up. Volunteers will always have some awareness of the impending impact and this causes a degree of pre–impact bracing. One report claims that pre–impact EMG indicated a relaxed musculature, but this study involved an accelerometer bite–block arrangement [20] that disturbs the normal occlusal relationship. This almost certainly generates heightened muscle activity.

Howard et al. [71] predicted that there is no absolute rearward motion of the mandible during retroflexion of the head and that this was a fundamental flaw in the IIT. The IIT claims that the head travels rearwards relative to ground during retroflexion, when in fact the head is travelling rearward relative to the upper torso, which is travelling forward. A considerable degree of cancellation occurs, and the resultant displacement of the head centre of gravity is small but forward. This is experimentally substantiated in this thesis. The result of this modified view of head motion is that the direction of load on the TMJ is altered and does not cause anterior dislocation of the condyles during retroflexion. Instead, Howard et al.[71] predicted that loading is primarily compressive during whiplash. Since large compressive loads are sustained without injury during functional chewing [72] this indicates that there is no potential for injury due to this kind of motion. Howard et al.[71] have not investigated the likely influence of mouth–opening or the possible effects of loading rate during whiplash but their conclusions are closely connected to some of the experimental findings in this thesis.

2.3 Experimental Muscle Modelling

A sensible approach to simplifying muscle response is crucial to all experimental investigations involving human kinematic behaviour. In fact, muscle response is the main obstacle preventing true biofidelity in crash dummy design, and the poor performance of many current surrogates in low–speed impacts is probably because existing dummies do not model muscle behaviour satisfactorily [66].

Muscle models

Two classic muscle models form the basis of all subsequent analyses. Most simulations of muscle behaviour use the Hill model [73], largely because of its inherent simplicity. The origins of this lie with William Thompson (Lord Kelvin), who introduced the Standard Linear Model, a three–element model approximating features of polycrystalline metals (this had been adapted from the work of James Clerk Maxwell and Waldemar Voigt). The basic principle of the Kelvin model is to place spring and dashpot components in series and parallel, see figure 2.1. Each component represents a different physical characteristic of the material. Vivian Hill modified this by adding a contractile element (dashpot) in series with an elastic spring, and found that this was a good approximation to active skeletal muscle behaviour. Hill developed his classic Force–Velocity Equation, a linear differential equation relating muscle force, shortening velocity and stiffness. The limitation of this model is that it is incapable of modelling the change from passive to active: changes in the value of elasticity and viscosity are not sufficient to produce tension in a muscle which has zero tension prior to stimulation.

The Huxley model is two–state and more complex. It is based on the sliding filament theory of muscle contraction proposed by A. F. Huxley in 1957 [74], see appendix B. It is still considered the most accurate model but due to its complexity many researchers have continued with the Hill model.

However, neither of these mathematical muscle models can be implemented in an experimental process. An experimental model relies on simplifying muscle response to a degree where surrogates can be constructed. In addition, total mechanical response of the bone–tendon–muscle–tendon–bone complex is more important than modelling individual muscle components. Ideally, surrogate muscles exhibiting the same force–length and force–velocity characteristics as live skeletal muscle are required.
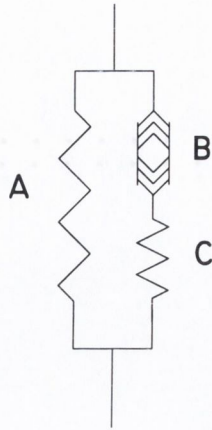
Figure 2.1: Hill's fundamental muscle model: parallel element (A), contractile element (B) and series component (C).

Experimental Approach

An approach utilising data from published experimental work is significantly easier to implement. To this end, empirical force/length relationships for skeletal muscle were investigated. Muscle response consists of passive and active components. The passive response is the stress–strain curve obtained when muscle is stretched in the absence of active stimulation. This has been experimentally determined both *in vivo* and *in vitro* [75, 76]. Constitutive equations governing passive muscle response have been derived but satisfactory equations governing active skeletal muscle behaviour have not been found. The contractile characteristics of muscle depend on muscle architecture and cell properties, see appendix B. Although all vertebrate skeletal muscle fibres are similar in their structural arrangement of the actin and myosin proteins, other complex variations at cellular level cause differences in fibre contractile characteristics. These include fibre force, maximum shortening velocity and resistance to fatigue. In addition, the architectural arrangement of muscle fibres determines how much load is transferred to the bones [75]. The relationships between muscle force and length and between muscle force and shortening velocity are the two classic characteristic curves that define active muscle response. Both of these have been experimentally determined and
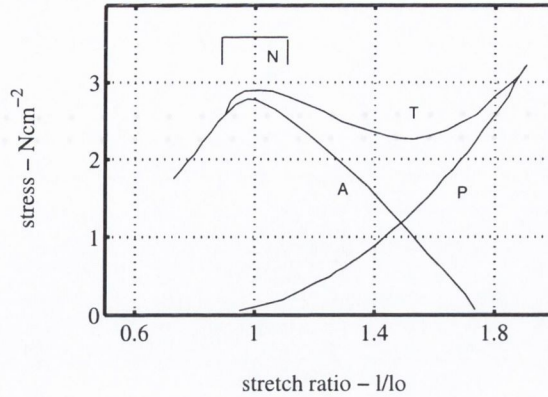
Figure 2.2: Stress/stretch–ratio relationships in skeletal muscle: active (A), passive (P) and total (T) muscle responses. The normal working range (N) is also shown.
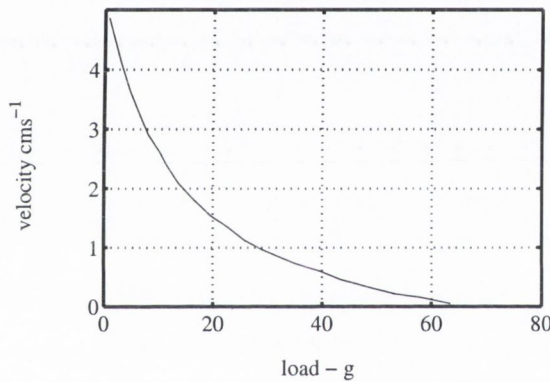
Figure 2.3: Muscle force versus shortening velocity.

characteristic curves are shown in figures 2.2 and 2.3. The classic experiment in which live muscle is isolated and artificially stimulated is described by Gordon et al. [77]. A micrometer is attached to one end of the muscle, a force transducer to the other and an electrical stimulus is applied to the muscle belly (direct excitation rather than through the nerve) causing a fused tetanus, see appendix B. The force/length curve shows that there is an optimum working length for a muscle, which is usually the resting length. Alternatively, the optimum length might be the position where most force is required. In the masseter, this has been shown to be at ca. 20mm incisal opening, thereby developing optimal chewing forces [78].

31

The force/velocity curve shows that the tension produced by a muscle decreases rapidly as the rate of shortening is increased. However, these fundamental relationships are considerably complicated by the influence of history, so that there is no unique force/length or force/velocity relationship for muscle [79, 80, 81].
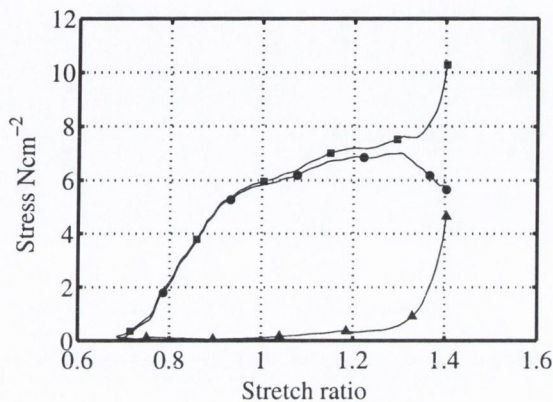
Figure 2.4: Experimental muscle response [75]: active ($\bullet$), passive ($\blacktriangle$) and total ($\blacksquare$).

Hawkins & Bey [75] developed an experimental procedure for studying partially intact rat tibialis anterior (TA) muscle–tendon complexes in a physiological environment. The rats were anaesthetised, the tissue around the TA was removed and an electrode was attached to the nerve. A 3mA signal of 50μs duration repeated every 4ms was sufficient to create a fused tetanus of the muscle. The bone was directly clamped, eliminating the need for soft–tissue clamps which can distort the tissue being investigated. The partially intact muscle–tendon complex maintains a physiological environment while kinematics, activation–level and force were controlled directly. Active and passive force/length curves were generated. All force data were normalised with respect to muscle cross–sectional area and length data were normalised with respect to muscle resting length to give stretch ratio. The active stress data were calculated by subtracting the passive data from the total stress data obtained in the active force–length tests, see figure 2.4.

Yamada carried out extensive tests on the passive strengths of *in vitro* biological tissues [76]. Figure 2.5 shows a comparison between the force/extension curve

32

of the human sternocleidomastoid and the rat TA data of Hawkins & Bey [75]. Although there are differences between the curves in the higher stretch–ratio region, there is good agreement in the lower stretch–ratio. These curves have been used as the basis for the experimental muscle models in this thesis. Their implementation is detailed in section 3.4.
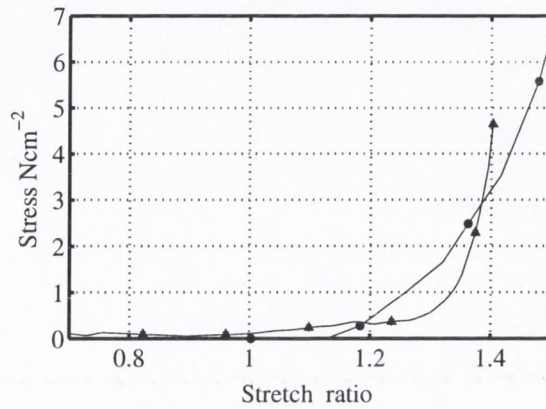
Figure 2.5: Passive muscle response: Hawkins & Bey (▲) and Yamada (•).

Chapter 3

Sled–test Setup and Validation

The complexity of the human body must necessarily be reduced in a physical model: only factors affecting dynamic behaviour were included. Direct impacts of the head and jaw were not investigated, allowing simplified modelling of these structures. A sled and track system with a pneumatic impact ram was used to simulate the crash pulse of the vehicle. Instrumentation was implemented to measure linear and angular kinematic parameters on the sled and dummy. Instrumentation measurements were calibrated and human volunteer tests were used to validate the dummy neck response.

3.1   The Model Head

The head was constructed from lamina of medium density fibre-board (MDF), see figure 3.1. Important characteristics of a mechanistic head for whiplash sled–tests are mass, centre of gravity and correct location and geometry of relevant contacting structures. The *in vivo* mass of a 50th percentile male skull is quoted by Hybrid III designers as 4.5kg [82], but this has been disputed by Clemens & Burow [83], who reported a mass of between 3.8 and 4.1kg. An independent test using displacement of water showed the mass to be closer to 4.5kg, and this value was adopted. The centre of gravity of the skull was found to average 1cm anterior and 2cm superior to the external auditory meatus [84], but it is unclear what proportion of the
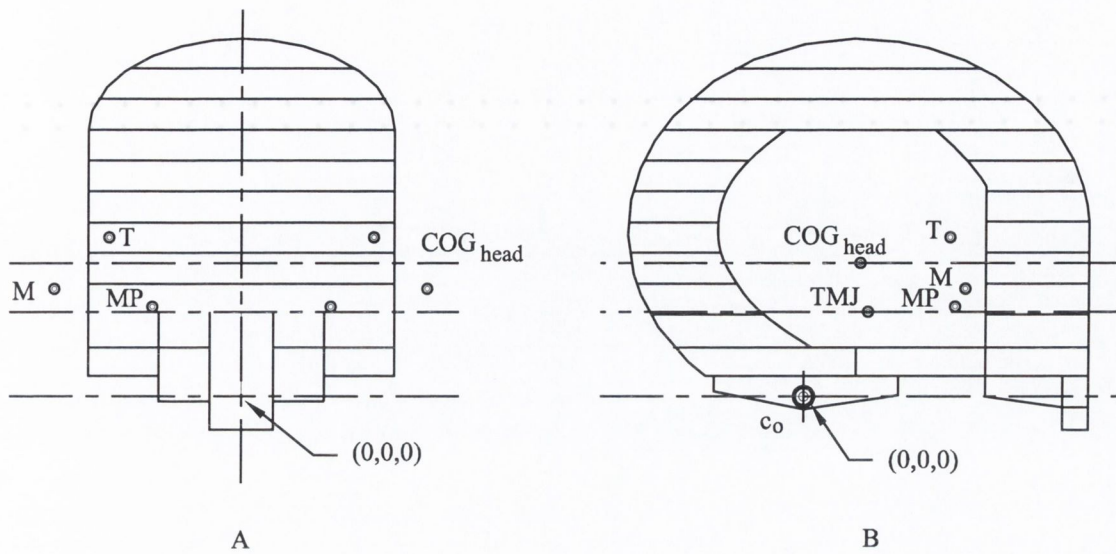
Figure 3.1: The model head, showing the TMJ, centre of gravity, c_o and temporalis (T), masseter (M) and medial pterygoid (MP) muscle insertions in frontal (A) and lateral (B) views.

neck was included in that calculation. The mass centre of a sealed cadaveric skull filled with water was found to be higher than 2cm above the ear, but this did not incorporate any material in the neck. For validation purposes, the value quoted in the literature was used. Correction of mass and centre of gravity on the model head was done iteratively. The unamended MDF head was too light, and holes were bored and filled with close fitting lead cylinders to correct the mass of the head. When the correct mass was approximately achieved, steel pins were inserted into either side of the head at the desired centre of gravity location and masses were added and adjusted until stable equilibrium was reached when the model head was supported on these pins. The full 4.5kg mass of an *in vivo* head was achieved by replacing one of the MDF lamina with mild steel at the approximate height of the centre of gravity of the head.

The shape of the skull was formed by two merging ellipsoids and does not represent the true shape of a human skull. However, the base of the skull at c_o was
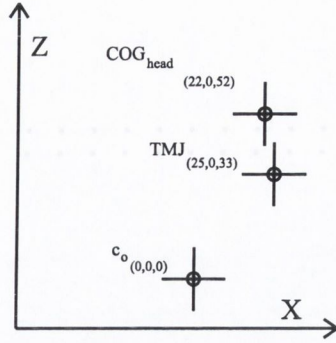
Figure 3.2: Important landmarks on the model head (units in mm).

used as a reference point for locating important landmarks. The location of centre of gravity (COG_{head}), the TMJ's, the maxilla and muscle insertions were measured on a 50th percentile dry male skull and reproduced on the model head. The spatial relationship between c_o, the TMJ and COG_{head} is given in figure 3.2. The muscle origins and insertions are given in table 3.1 and the insertion points on the head are shown schematically in figure 3.1. The origin is taken at the midpoint of the c_o axis. These have been adapted from Baragar & Osborn [85] and compared with the insertion locations on a 50% male cadaveric skull. Baragar & Osborn subdivided the individual jaw elevator muscles into anterior/posterior sections. The increased accuracy this provides in their theoretical model does not sufficiently compensate the complexity added to an experimental model, and muscles have thus been assigned a single location for insertion and origin respectively.

	Origin (jaw)			Insertion (skull)		
muscle	X_j (mm)	Y_j (mm)	Z_j (mm)	X_h (mm)	Y_h (mm)	Z_h (mm)
masseter	38	45	-13	63	69	39
temporalis	55	48	19	57	52	61
medial pterygoid	34	37	-13	57	28	36

Table 3.1: Cartesian coordinates of the elevator muscle origins and insertions.

3.2 The Model Neck

The model neck must reproduce the load–transfer characteristics between the shoulder and the head that occur *in vivo* in a low velocity rear–end collision. In the 1980's the Hybrid III neck became the industrial standard, but this was only suitable for higher velocity impacts. The need for an improved dummy neck arose from clear evidence that the Hybrid III neck was too stiff to model low–velocity collisions [86, 87]. A robust model neck designed for low velocity rear-end collision simulations was developed by Svensson et al. at Chalmers Technical University in Goteborg [88]. The Rear Impact Dummy (RID III) neck with subsequent improvements has since been accepted as the best surrogate neck. The RID III neck consists of seven cervical and two thoracic vertebrae connected by pin–joints and is designed solely for rear-end tests. Each vertebra is the same height. The total range of motion of the RID III neck is 83° in extension and 43° in flexion. The cervical vertebrae and the occipital joint all have the same range of motion: 10° in extension and 5.6° in flexion. The first thoracic vertebra has an angular range of 3° in both extension and flexion relative to the second thoracic vertebrae. The latter is attached rigidly to the shoulders. The interspaces between the vertebrae are filled with blocks of foam and the thickness of the foam determines the stiffness of the neck.

A RID III neck was constructed and adapted for use in this experimental process, see figure 3.3. The advantage of the RID III is that neck stiffness can be easily altered, and the foam 'stiffness' components can be replaced. This results in a very robust structure suitable for repeated crash–testing. There are also disadvantages. The pin–joint design only allows angular movement of the neck in the sagittal plane. This is a major limitation, as oblique–angle impacts are not possible. Further, cervical vertebrae can slide relative to each other as well as rotate, but there is no facility for this motion on the RID III neck. These limitations are further considered in chapter 8. However, the RID III neck accurately models the angular kinematics of the neck in a sagittal plane impact and provides a strong basis for investigating the kinematics of the TMJ during whiplash.
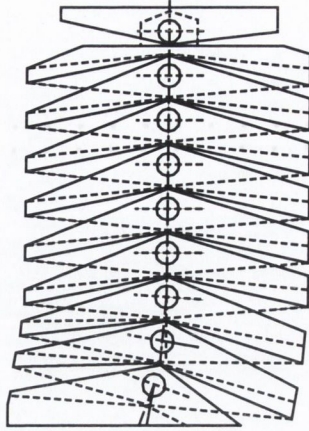
Figure 3.3: The RID III neck.

3.3 The Model Jaw

The jaw motion under investigation does not include direct impacts of the mandible and this facilitates some important simplifications. The limits of jaw motion are effected through the TMJ's, occlusal contacts and the biomechanical constraints of the muscles and ligaments. In a true whiplash, occlusal strike is the only contact between the mandible and surrounding structures. Therefore, it is sufficient to model correctly the

- inertial characteristics of the mandible.

- geometry and material properties of the TMJ and occlusal contact surfaces.

- soft–tissue components (muscles and ligaments).

There are no commercially available crash–test dummy mandibles: a mandible and TMJ were therefore constructed from measurements of a 50th percentile male dry skull and mandible. An anatomical text [89] was also used for reference.

Inertial Properties of the Jaw

A coordinate system is necessary in order to establish locations on the jaw. Most researchers have adopted the convention in figure 3.4, where the origin lies midway
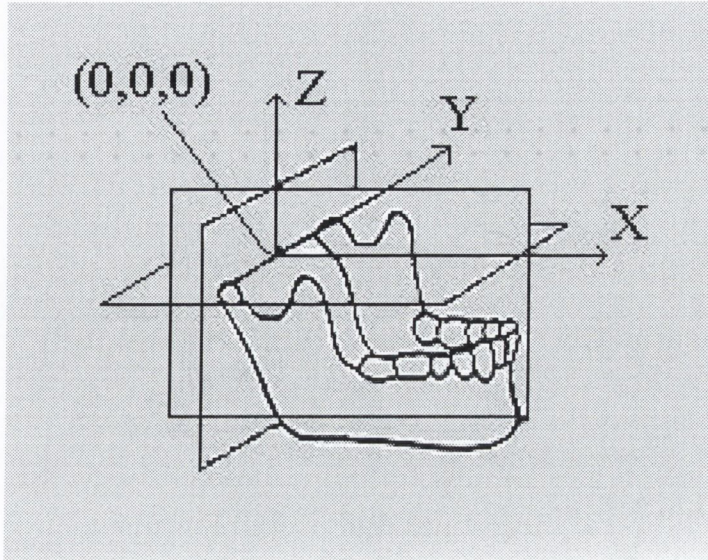
Figure 3.4: Local coordinate frame for the mandible.

along the intercondylar axis. The XZ plane is equivalent to the sagittal plane, while the XY and YZ planes correspond to the horizontal (Frankfort plane) and frontal planes respectively. Schneider et al. [70] describe a simple hanging method to determine the mass centre of a dry mandible. The mandible is hung from two locations and the intersection of the two lines of gravity is the location of the mass centre, see figure 3.5. Maintaining a reference of the first line of gravity when the mandible is hung from the second point involved marking entry and exit points on the interior surfaces of the mandible. Wire struts joining these points then provided a line collinear with the first gravity line. This procedure was performed repeatedly on a single dry mandible (matching the 50th percentile skull used to construct the model head), and the average coordinates of the mass centre relative to the centre of the intercondylar axis were X = 44mm, Y = 0mm and Z = -14mm. Referred to the global origin (the centre of the c_o axis), the coordinates of the mass centre of the model mandible are X = 69mm, Y = 0mm and Z = 19mm.

Schneider et al. [70] quote 0.16kg for the mass of the mandible, not including the tongue, and this value has been adopted. Inclusion of the tongue would be complicated by the fact that its behaviour is unknown and it can therefore not be modelled as a lumped mass in a fixed location. It has not been included.
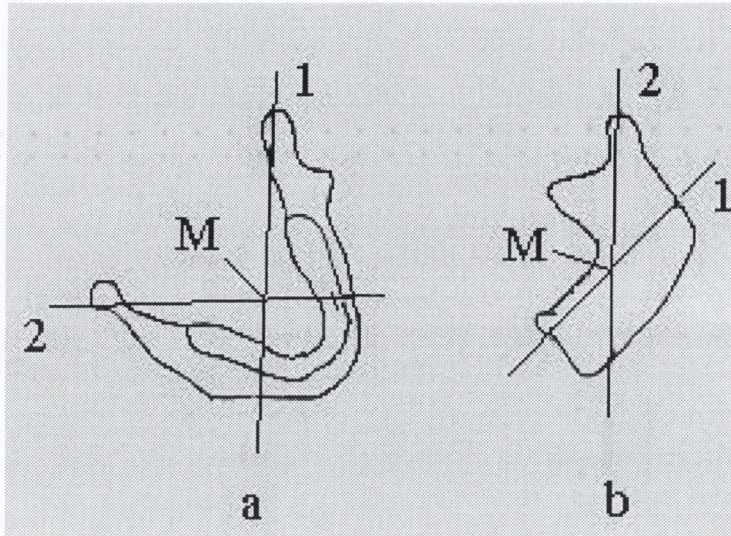
Figure 3.5: Determination of mass centre (M) of the jaw: (a) position 1; (b) position 2. Lines of gravity in each case (1 & 2) are shown.

Construction of the mandible

The body of the mandible was formed from 3mm mild steel plate bent into the desired shape using a suitable template, see appendix D and figure 3.6. Steel was chosen in preference to aluminium for two reasons. In a previous model using aluminium, the condylar neck was too compliant. In addition, the aluminium mandible was too light and required the addition of corrective masses. In the steel model, excess mass could be easily reduced by drilling holes in the steel plate. This prevented the problem of corrective masses interfering with surrounding structures. Geometric data from a single 50th percentile male dry mandible were implemented on the model jaw. The end–view of the articular portion of the condyles was ellipsoid with a semi–major radius of ca. 5.5mm and a semi–minor radius of ca. 3.75mm. The plan–view length of the condyles was 20mm. The condyles were machined from teflon (PTFE) and bolted onto a flange plate glued to the superior surface of the condylar neck. This provided a strong attachment. Final sculpting of the condyles to emulate correctly the bony articulating surfaces was carried out manually using surgical blades.
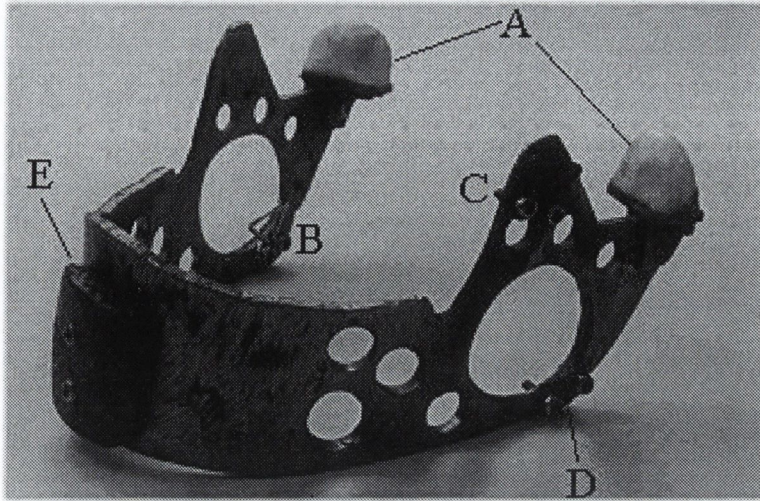
Figure 3.6: Photograph of model mandible: condyles (A), medial pterygoid attachment (B), temporalis attachment (C), masseter attachment (D) and corrective mass (E).

3.4 Soft–tissue Components

The mandible is connected to the skull and neck by muscles, ligaments, fascia and other soft–tissue components. The most important of these are the jaw elevator muscles and the temporomandibular ligament, see appendix B. The stiffness of fascia and the other remaining tissues covering the TMJ is small compared to that of the collagenous muscles and ligaments. Thus only the three main elevator muscles and the temporomandibular ligament are included in this model. The digastric muscle has not been included and the effect of this omission is addressed in chapter 8.

Muscle Modelling

The muscles are the most important and also the most complicated soft–tissue component because instantaneous muscle stiffness is a combination of both active and passive stretching of the muscle. The experimental tests on rat TA muscle [75] introduced in chapter 2 form the basis of the model muscle characteristics used in this thesis. The stress/stretch–ratio graph in figure 2.4 is repeated here for clarity,

41
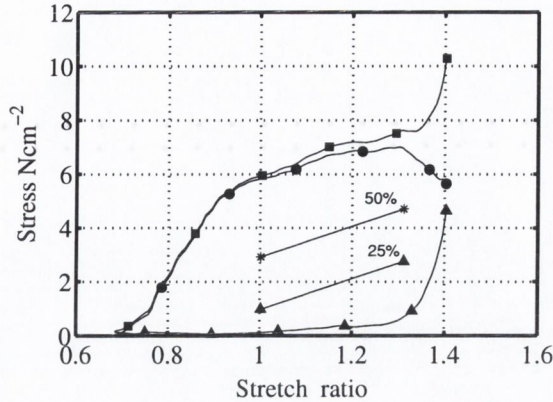
Figure 3.7: Experimental muscle response [75]: active (•), passive (▲) total (■) and linearly scaled 25% and 50% active response.

see figure 3.7. The level of muscle activity of a seated vehicle occupant prior to impact may vary considerably. If relaxed, the muscle tone should approach the passive curve shown in figure 3.7. In the unlikely event of total pre–impact bracing, muscle tone approaches the total curve shown. All other muscle states must lie between these two limits. A scaling procedure is suitable for testing the effect of varying muscle activity. It can be seen that the total muscle response is broadly linear for stretch–ratios between 1–1.35, and this exceeds the normal physiological envelope. For simplicity, muscle response is thus scaled linearly between the passive and fully active limits, see figure 3.7. Muscle bundles corresponding to the passive, 25%, 50% and 100% active muscle states were prepared for sled–testing.

Force in a muscle can be determined easily from the product of physiological cross–sectional area (CSA) and the current stress. The lengths of the muscles were measured from the origin and insertion points located in the skull and mandible used to construct the model head and jaw. The CSA's of the elevator muscles have been measured [90] and these data are presented in table 3.2. This was sufficient information to generate desired force–extension curves for each muscle.

It is uncertain whether the stretch characteristics of a rat TA muscle adequately model the behaviour of human jaw–elevator muscles. Yamada's [76] extensive work on the properties of *in vitro* biological tissue includes a stress/stretch–ratio graph

42

muscle	length (m)	area (m^2)
masseter	0.06	3.4e^{-4}
medial pterygoid	0.054	1.9e^{-4}
temporalis	0.05	4.2e^{-4}

Table 3.2: Muscle lengths and cross–sectional areas.

for the human sternocleidomastoid muscle (SCM), see figure 2.5. A comparison of Yamada's [76] data with those of Hawkins & Bey [75] shows that both have the same strongly non-linear features, but there are some differences in the higher stretch–ratio range: these differences can probably be accounted for by post–mortem changes in Yamada's samples and also by difference in species. Application of the Hawkins & Bey [75] experimental procedure to the human SCM is clearly not feasible and so a compromise is necessary: Yamada's [76] human SCM curve has been used to generate the purely passive response, while the active response of rat TA measured by Hawkins & Bey [75] is used to produce the scaled muscle activity curves, see appendix E.

Muscle Construction

Synthetic muscles were constructed using rubber elastic and cord. Both of these are largely linear in the elastic range but were combined in several strips arranged to become taut at different lengths and the non–linear passive muscle curve was thus successfully approximated. A standard tensile testing machine (Instron 1011) was used to construct and test these muscles, see appendix E. Miniature metal hooks were used to secure the muscle bundles to the head and jaw at their correct origin and insertion points: the bundles were spliced onto the hooks and these were then secured to the model head and jaw using 2mm bolts.

Ligaments

The temporomandibular ligament (TML) is the primary ligamentous reinforcement of the TMJ (see appendix B), and is the only ligament included in this

43

model. The TML is a stiff collagenous structure and has been modelled using stiff inextensible cord. This is connected to the lateral wall of the pre–glenoid plane and lateral surface of the condylar neck on the model head and jaw using 2mm bolts, see figure B.10. The model TML was taut but under no tension in the mouth–closed position.

3.5   The Sled and Track

A sled and track rig suitable for simulating rear–end collisions was designed and constructed. The following were the main requirements:

- portability for access to data logging hardware and compressed air supply.

- a propulsion system capable of applying a repeatable acceleration pulse corresponding to various impact velocities.

- ability to withstand repeated sled–testing.

- sufficient space to house instrumentation.

- adaptability for subsequent changes and additions.

- low–friction travel of the sled and sufficient track length.

Figure 3.8 shows a photograph of the model head, neck and jaw mounted on the sled and track. A plan, end–view and elevation schematic of the complete rig are shown in figure 3.9. A number of iterative improvements were made to the original design. The initial propulsion system was via the kinetic energy of a 6kg steel ball rolling on an incline before impacting the sled. However, this simple system had several disadvantages and was replaced by a pneumatic impact ram (Martonair S565E/40 - Norgren LTD, Slaney Close, Dublin Ind Estate, Dublin 11, Ireland). Support struts for the guide tracks were added to prevent vertical oscillations of the sled. The shape of the acceleration pulse can be varied using the impact cylinder settings and also via a damped plunger mounted on the rear

of the sled at the contact point with the pneumatic ram. However, full control of sled acceleration remained a problem.

3.6 Instrumentation

The choice of instrumentation used is crucial to the quality of results. High Speed Video (HSV) provides the best visual aid, but considerable post–processing is required. More traditional transducers give no visual aid but allow direct conversion to numerical data. It is desirable (but not practical) to measure all of the following by independent means:

1. linear displacement, velocity and acceleration of the sled.

2. linear displacement, velocity and acceleration of COG_{head}.

3. rotational displacement, velocity and acceleration of the head.

4. linear displacement, velocity and acceleration of the jaw.

5. rotational displacement, velocity and acceleration of the jaw.

6. forces reacted across the TMJ.

Noise Analysis And Kinematic Treatment Of Noise

Velocity and acceleration are first and second derivatives of displacement respectively, and it is possible to use numerical techniques to estimate integrals and differentials of kinematic data. However, experimental data consists of discrete data points with a noise component, and curve-fitting techniques or numerical calculus must be used. The effects of noise in numerical calculus are readily seen:

Let $x_m(t)$ represent the measurement of $x(t)$, which varies sinusoidally at a frequency ω_o. In practice, there will be noise from the measurement chain that interferes with the measurement. Let $n(t)$ be the noise in the system. This has a frequency ω_n. Then

$$x_m(t) = x(t) + n(t) = A_o \sin \omega_o t + N_n \sin \omega_n t, \tag{3.1}$$
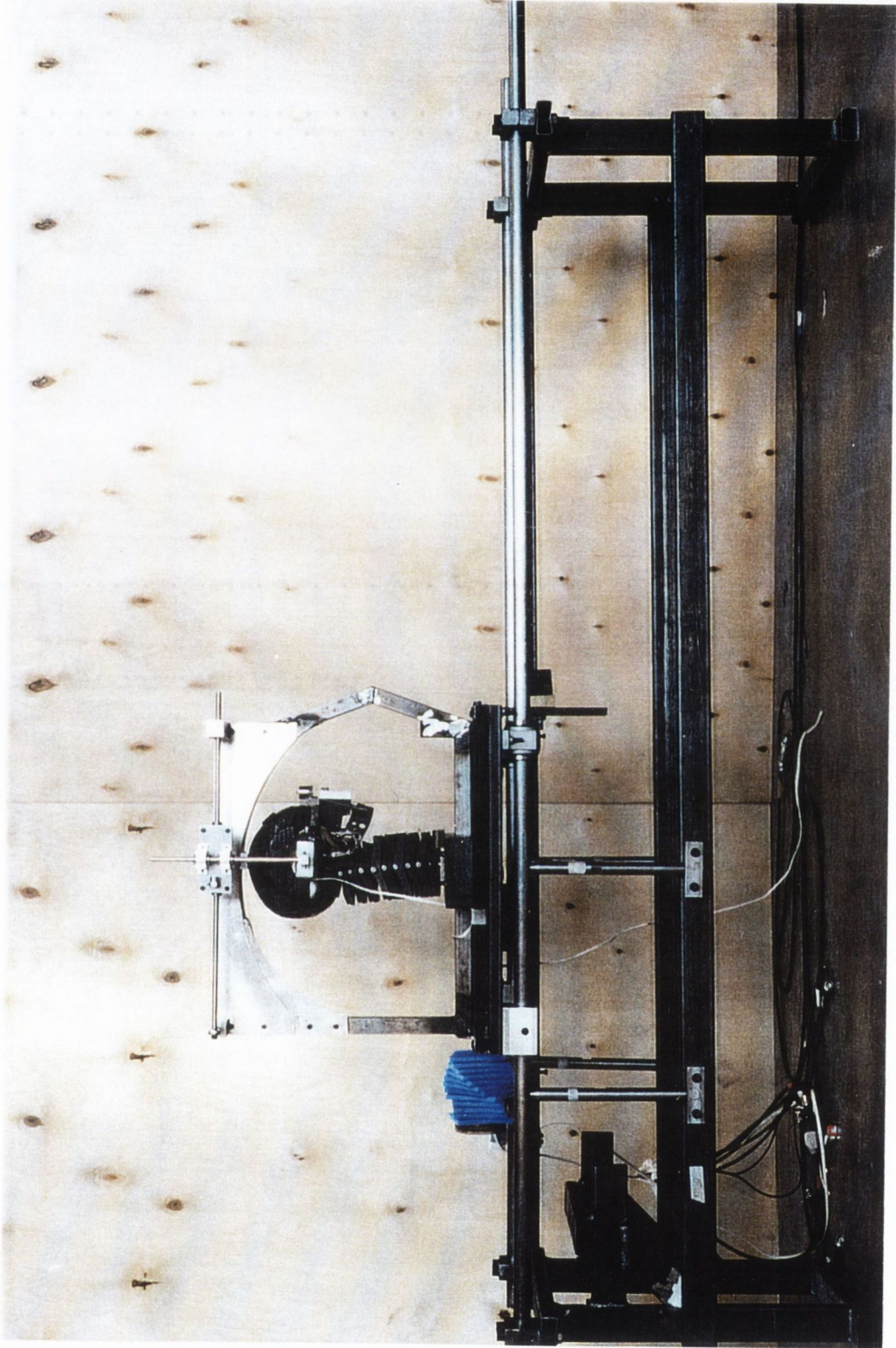
Figure 3.8: Photograph of experimental rig.
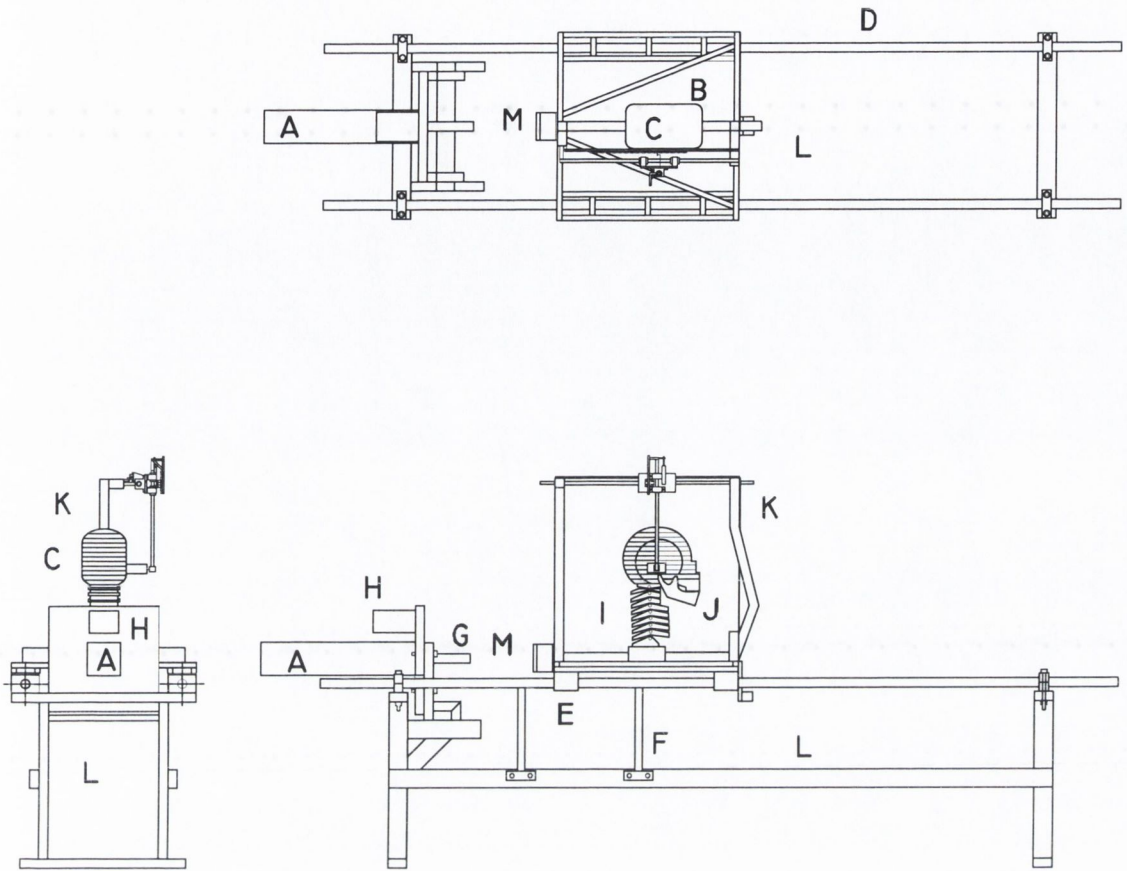
A	pneumatic cylinder	B	sled
C	dummy head	D	guide track
E	linear bearing	F	support strut
G	impact piston	H	pneumatic controller board
I	dummy neck	J	dummy jaw
K	support frame	L	instrumentation housing
M	plunger and damper	N	rotational potentiometer
O	bearing system		

Figure 3.9: Schematic of experimental rig.

where A_o and N_n are the respective magnitudes of the signal and noise components. The signal to noise ratio (SNR) is given by

$$SNR_{x(t)} = \frac{A_o}{N_n}. \qquad (3.2)$$

The first derivative of equation 3.1 is

$$\dot{x}_m(t) = \dot{x}(t) + \dot{n}(t) = A_o\omega_o cos\omega_o t + N_n\omega_n \cos\omega_n t, \qquad (3.3)$$

and the SNR of the derivative signal is

$$SNR_{\dot{x}} = \frac{A_o\omega_o}{N_n\omega_n} = \frac{\omega_o}{\omega_n}SNR_x \qquad (3.4)$$

From this it is clear that the effect of differentiation is to reduce the SNR when the noise is predominantly high frequency. The effect of a second differentation is to further reduce the SNR by a factor of $\frac{\omega_o}{\omega_n}$. This phenomenom has caused serious problems in related disciplines, including gait analysis [91], where the usual remedy is to apply a low pass filter to the measured signal prior to numerical differentiation. Modern digital filters can be applied in both directions at the post-acquisition stage to minimise the phase shift normally associated with filtering. It is important that the bandwidth of the filter is tuned to pass as much of the desired frequency as possible [91].

The influence of numerical integration can be similarly investigated. As before, let $x_m(t)$ represent the measurement of $x(t)$, which varies sinusoidally at a frequency ω_o. Then,

$$\int x_m(t)dt = \int x(t)dt + \int n(t)dt = -\frac{A_o}{\omega_o}\cos\omega_o t - \frac{N_n}{\omega_n}\cos\omega_n t, \qquad (3.5)$$

and the SNR is now given by

$$SNR_{\int x} = \frac{\omega_n}{\omega_o}SNR_x, \qquad (3.6)$$

which is the inverse of the previous result. Thus, the integration process accentuates low frequency noise, particularly errors in the calibration constants of transducers. As before, the effect of successive integrations is to reduce the SNR

by a factor of $\frac{\omega_n}{\omega_o}$ each time. This also causes problems, and when used in a blind manner, numerical integration may lead to serious inaccuracies [92].

It is therefore problematic to use the second derivative of displacement data to give an acceleration estimate. Vibration of the steel structures in the experimental rig combined with 50Hz mains inteference introduce high frequency noise. The choice of a suitable cut-off frequency for a low pass filter is difficult. The lower the cut-off frequency, the smoother the output, but the signal magnitude is also affected. A good example of this given in figure 3.22: comparison of phase from the accelerometer data compared to the differentiated film data is satisfatory, but the peak magnitudes are quite different.

Similarly, displacement calculations from acceleration data can yield unreliable data. This problem is exacerbated by the fact that piezo-electric accelerometers have a poor steady state response [93]. Thus when a constant velocity is reached, there is a large potential for errors. As a result, acceleration transducers have not become widespread in the measurements of motion analysis [94, 95]. It is therefore preferable to perform direct measurement of all kinematic parameters required. In practice, this is often not feasible and numerical techniques are a necessity.

Morris [93] developed a method of calculating the 3-dimensional motions of a body in space using accelerometer measurements. This method applies Euler's theorem which states that the general displacement of a body can be found from the knowledge of one fixed point on the body combined with a rotation about a suitable fixed axis through that point. The latter is established by the use of three orthogonal parallel pairs of accelerometers. An algorithm involving repeated numerical integration with a first–order trapezoidal scheme was then applied to calculate the angular velocity and angular displacement vectors respectively. Morris applied this method in gait analysis and reported positive results [93].

The difficulty in applying the above method to the present experimental procedure is that the low mass of the mandible severely curtails the choice of transducer that can be attached to the model jaw without significantly affecting its kinematic behaviour. Morris' elegant method was therefore not applicable to calculation of motion of the mandible in this thesis. Further, recent research has found that a

minimum of nine accelerometers per body segment are required [96].

Sled Displacement

The dummy neck is directly connected to the sled which therefore represents the shoulders in a real impact. Commercially available linear potentiometers capable of measuring the desired sled displacement span (ca. 0.5m) proved prohibitively expensive and an alternative mechanism was required. An attempt was made to construct a linear potentiometer using tensioned stainless steel wire running parallel to the track with a spring–mounted contact point attached to the sled. However, the SNR ratio for this device was very poor. Instead, sled displacement was measured using a slotted opto–switch (Radionics RS 304–560, Herberton Road, Rialto, Dublin 12, Ireland) incorporated into a beam–breaker circuit. The opto–switch was attached to the sled and a strip of crenellated plastic running parallel to the track was positioned to slot between the emitter and collector. As the sled moves the beam is alternately passed and interrupted by the crenellated strip, see figure 3.10. The tooth and gap widths were measured using a Vernier's Calipers and a Matlab function was used to sum voltage changes and convert this to displacement.

Sled Acceleration

Sled acceleration was measured using a piezo-electric accelerometer (DJB A20, Birchall LTD, Finchley Ave, Mildenhall IP28 7B6, England) mounted on the front vertical face of the wood shoulders of the dummy, pointing in the direction of travel of the sled. Some high–frequency vibration of the sled was shielded from the accelerometer by avoiding direct contact between the transducer and the steel frame of the sled.

Sled Velocity

Sled velocity was not independently measured, but was estimated numerically by integration of the acceleration data and by differentiation of the displacement data.
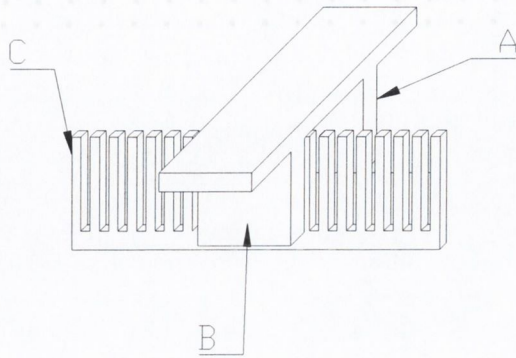
Figure 3.10: Optical displacement measurement: emitter (A), collector (B) and crenellated strip (C).

Head Angular Displacement

A rigid body in planar motion has three degrees of freedom: its position in space is fixed by specifying two orthogonal linear displacements of a point on the body and the inclination of the body about that point. In the case of head motion during a sagittal whiplash sequence, there is no fixed centre of rotation. Therefore, it is not possible to connect the body of a contact–style transducer (e.g. a rotational potentiometer) to the head with the shaft in a fixed location normal to the sagittal plane. This has traditionally limited direct measurement of head angular displacement, and other techniques including HSV analysis have been developed instead. Angular motion of the head in the sagittal plane can then be calculated using fiducial reference markers. However, HSV is expensive and requires considerable data processing (object identification and compensation for angle changes as the subject moves relative to the camera). The problems associated with successive numerical integration of angular acceleration data have been discussed.

Instead, a new design has been developed. If it is possible to allow the shaft of

a potentiometer to follow both vertical and horizontal linear motions of the head, then rotation in the potentiometer measures the inclination of the head in the sagittal plane. A precision mechanism formed by a system of rods (F & G) and linear bearings (H & I) was used to achieve this, see figure 3.11. The components of this mechanism are as follows:

- A – Housing for the body of the rotational potentiometer, which is bolted into the head at the centre of gravity with its long axis normal to the sagittal plane.

- B – The shaft of the potentiometer. This is connected through a radial bearing for support.

- C – Horizontal guide rod. This is fixed at both ends to the sled frame. The plate (G) connecting D and F is free to travel horizontally along this guide rod.

- D – Vertical connecting rod (8mm diameter). This is connected to the the potentiometer shaft via a hinge joint. The top end of this rod is free.

- E – Horizontal linear bearings. These are light–weight bearings mounted with an overall L/D ratio greater than three.

- F – Vertical linear bearings. These are of the same type as (E), similarly mounted and are attached on the opposite side of the same plate as the horizontal linear bearings. The two sets of bearings are orthogonal.

- G – Connecting plate for horizontal and linear vertical bearings. This also serves as a platform for subsequent instrumentation.

Head Linear Displacements

The bearing and rod assembly used to measure head angular displacement provides a convenient means to measure the horizontal and vertical linear displacements of COG_{head}. The movement of the bearing plate (G) relative to the horizontal
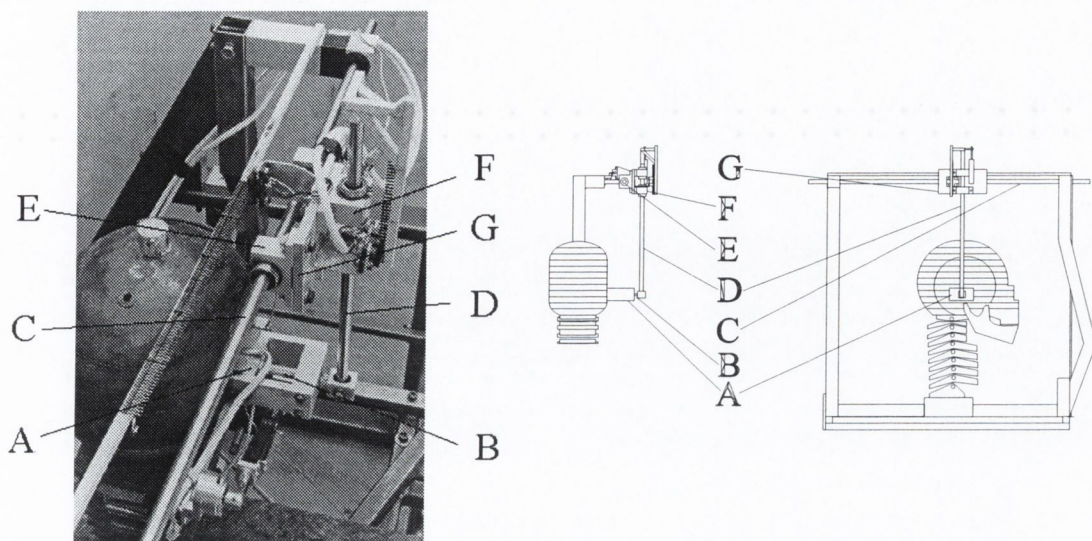
Figure 3.11: Bearing and rod mechanism for angular displacement measurement.

guide rod (C) is the horizontal component of COG_{head} translation, see figure 3.11. Similarly, the motion of the bearing plate (G) relative to the vertical connecting rod (D) is the vertical component of COG_{head} translation. The horizontal component was measured using a slotted opto–switch system, as on the sled. The opto–switch was mounted on the bearing plate (G) with the crenellated strip running parallel to the horizontal connecting rod and passing between the emitter and collector, as before. The vertical component was initially measured in the same way: the opto–switch was attached to the bearing plate (G) and the crenellated strip was mounted parallel to the vertical connecting rod. An added complication using opto–switches to measure this motion is that a single switch cannot register a change in direction. This does not occur on the sled, but does for both horizontal and vertical head motion. This problem can be overcome by either knowing the time at which the direction change occurs, or by using a second opto–switch mounted out of phase with the first. However, it was found that the resulting resolution ($\pm$1mm) was too low. Maximum vertical displacement at COG_{head} was less than 0.02m and a 0.025m stroke linear potentiometer (S-13-FLP-25A, Techni Measure, Alexandra
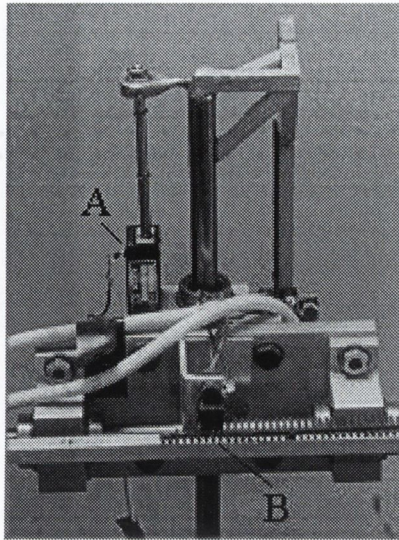
Figure 3.12: Measurement of vertical (A) and horizontal (B) head displacements.

Buildings, 59 Alcester Road, Studley, Warwickshire, England) was used instead. This was connected vertically between the bearing plate (G) and the vertical guide rod (D), see figure 3.12.

Displacement of the condyles

Hypertranslation of the condyles has long been postulated as an injury mechanism and measurement of condylar motion is therefore desirable. However, even if it can be assumed that non-sagittal plane displacements do not occur, motion of the condyles has a 3 degrees of freedom. As stated, the low inertia of the mandible is a critical problem for any method of contact transducer. The difficulty arises from the fact that the mass of an attached transducer can significantly influence the kinematic behaviour of the model mandible. Measurement of this motion therefore poses difficulties. A brief review of common contact style transducers for measuring joint motions shows their unsuitability for this application.

- Single DOF goniometers are easy to use, but these are sensitive to out–of–plane movement. Complex arrangements of goniometers have been used to measure the true kinematic angles between joints but this requires a difficult yet accurate setup [97].

54

- Accelerometry has been used to measure the spatial position of limb segments in gait analysis, but is not generally used for this purpose. The disadvantages outweigh the advantages and optical methods are generally preferred [98].

- Magnetic tracking methods can be used to measure displacements between two bodies. One half of the device is the emitter. This forms a magnetic field and the position of the sensor device is then measured relative to the axis system in the emitter. The accuracy of these devices decreases with distance between emitter and collector. Generalised planar motion of the mandible is thus difficult to track with this method.

- Optical methods of position measurement have become more widely available. Current methods involve identification of the motion of markers fixed to a body. There are two kinds of optical sensors: array sensors, which measure the location of two points; and linear sensors, which only measure the location of one point. Both types convert light intensity from a focussed image into digital form. Both are constructed from a set of minute, discrete photodetectors. The resolution of the sensor is primarily determined by the number of individual photodetectors present.

These devices were all either unsuitable or too expensive and an alternative measurement system was attempted: motion of the mandible in the sagittal plane has 3 DOF. Thus if the X and Z–direction displacements of one point on the mandible and the rotation of the mandible about that point are known, then sagittal motion of the mandible can be fully characterised.

An experimental procedure was devised to measure the displacement of one condyle using a polar coordinate measuring system. Figure 3.13 shows the principle applied: The body (A) of a linear potentiometer (S-13-FLP-25A, Techni Measure) was connected via a rotational potentiometer to a fixed point (B) on the skull. The piston was fixed to the condyle (C) via a radial bearing. Sagittal plane displacements between the fixed point on the head and the condyle can then be found in polar terms (r, θ) from the linear and angular displacements in the respective potentiometers.
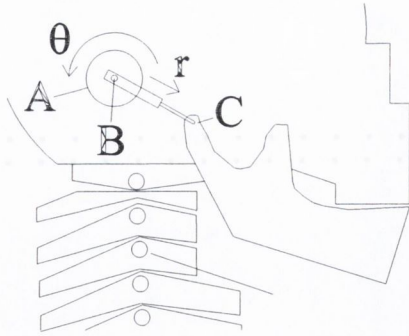
Figure 3.13: Attempted measurement of condylar displacement in the sagittal plane:

However, the practical application of this method was unsuccessful. The SNR from the rotational potentiometer was very poor, making sensible interpretation of the data difficult. Further, although the assembly was light and the connection to the mandible was at the TMJ (and therefore likely to be in the region of the centre of rotation), it was not easy to determine the inertial influence of this device. If the method yielded sensible data, an estimate of the inertial influence could have been found by comparing $\dot{\theta}_{jaw}$ with and without the device attached, but this was not the case. Therefore this measurement was not fulfilled.

The disadvantages of this omission are not trivial: loading at the TMJ could therefore not be directly calculated from the experimental measurements and could only be estimated from the results of the simulations discussed in chapter 7.2. However, this did not affect the ability to measure the rate of mouth-opening.

Angular Velocity of the Head and Jaw

Angular rate of the head and jaw was measured using magneto–hydrodynamic sensors (MHD's) - (ARS -4E M479&m458, ATA Sensors, 4300 Annaheim Ave NE, Suite B-6, Albuquerque, New Mexico, 87113 USA). These devices have a magnetic fluid enclosed in a case with a permanent magnet. The operating principle is that angular motion about the sensitive axis creates a velocity differential between the fluid and the case, generating an electric potential proportional to angular

rate. These relatively new devices are available in a miniature series with several important advantages. They are non–contact transducers and their extremely low mass (0.006kg) permits their use on the model jaw without seriously affecting the jaw's inertial behaviour. They are highly insensitive to linear velocity, which means they are ideal for measuring the rate of angular displacement of a body with a moving centre of rotation (i.e. when rotation is accompanied by translation). This is the case for both the head and the jaw. One MHD (m458) was mounted on the side of the head at COG_{head} with the sensitive axis normal to the sagittal plane. A second MHD (m479) was mounted on the jaw so that its sensitive axis was collinear with the intercondylar axis. This measures angular rate of the jaw in the sagittal plane, assuming symmetry of jaw motion.

Head Acceleration

Sagittal plane accelerations of selected points on the model head were measured using DJB A20 piezo-electric accelerometers (Birchall LTD). Angular acceleration of the head was calculated using the numerical derivative of angular velocity of the head. When angular velocity and angular displacement of the head are known, measurement of acceleration at one point on the head allows calculation of sagittal plane accelerations of any other point on the head, see chapter 5.

3.6.1   Data Acquisition

The data aquisition hardware used was an 8–channel, 14 bit A/D data–logging system produced by Leuven Measurement Systems. This was interfaced with a Hewlett Packard Unix–based Work–Station. The sample rate for all tests was 16384Hz. All data was logged unfiltered and exported into the Matlab software package, where a digital low–pass Butterworth filter was applied. The sample length in each case was 500ms, with a trigger delay of -100ms. This was sufficient to include the pre–impact period, and the retroflexion and flexion phases of head motion.

3.7 Validation

Calibration and validation of the experimental rig was a lengthy procedure. Problems were eliminated and an acquisition procedure in Matlab was developed. Individual transducers were validated and the behaviour of the head and neck complex was compared to volunteer sled–tests.

3.7.1 Instrumentation Calibration

Vibration

Impact causes broadband excitation and so it was necessary to minimise resonance in the sled and track. All time traces were low–pass filtered using a digital filter system in Matlab, but it is preferable to remove noise at the source. A rear–impact collision occurs over ca. 600ms and during this time retroflexion and flexion of the head occur. Although the event is caused by impact, the high mass of the head results in predominantly low–frequency motion of the head. A typical time history of head angular displacement is shown in figure 3.14. Head rotation approximates a half–sine wave in 300ms, corresponding to a frequency of 1.6Hz. This indicates that the motion of interest is primarily the low–frequency behaviour of the dummy and sled as it moves forward after impact. High–frequency vibrations in the sled
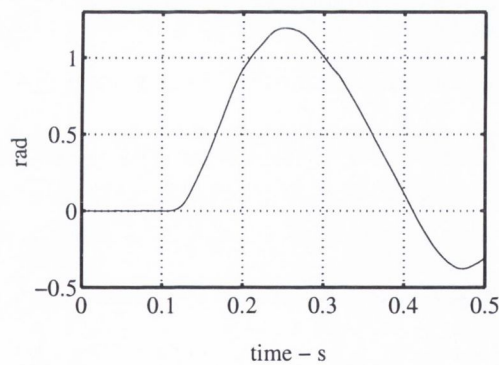

Figure 3.14: Head angular displacement.

and track needed to be minimised. In the initial design, impact was effected by

a steel ball striking the sled after rolling down an inclined plane, see figure 3.15. The vertical support struts along the track shown in figure 3.9 had not yet been fitted and, even with padding on the guide plane, this resulted in considerable vertical vibration in the sled. The addition of vertical support struts along the track required replacement of the two closed linear bearings at the rear of the sled with open linear bearings, but vertical vibrations were suppressed.
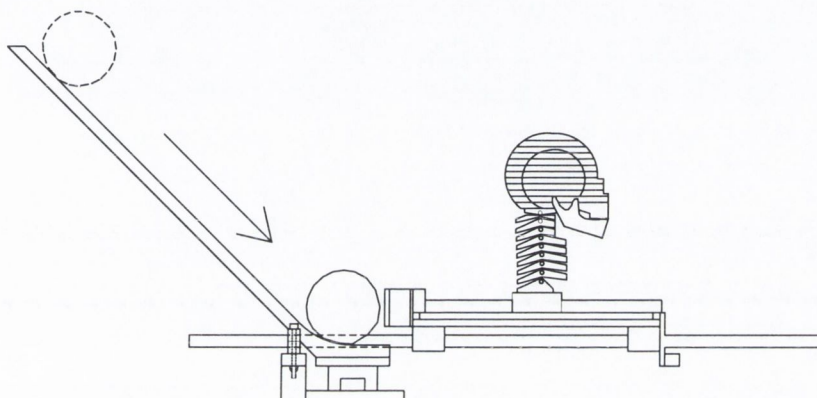

Figure 3.15: Steel ball impact system.

Neck Problems

The stiffness of the Hybrid III neck is a function of the foam layers placed in the inter–vertebral spaces. However, a machining error caused the fit between some vertebrae to be looser than desired. During the retroflexion sequence this caused the angular displacement curve of the head to be less smooth as some slip was possible between the vertebrae, see figure 3.16. Inflection points at $t = 0.25$s and $t = 0.31$s are clearly visible. This problem was minimised by placing extra padding between the vertebrae where slip occurred and the resulting head displacement curve was smooth, see figure 3.14.

Effect of Potentiometer Apparatus

Changes in the inertial characteristics of the head due to addition of the angular displacement mechanism were investigated. This device supports no moment and

59

is bolted into the skull at the line of the centre of gravity, so the net result is an increase in head inertia but no change in its distribution. The effect was monitored by comparing angular velocity traces of the head for nominally equal impacts with, and without, the bearing mechanism attached. The result is shown in figure 3.17 and the difference is unimportant. This is because the mass of the skull is 4.5kg and the proportional mass increase due to the potentiometer housing is small.

The Opto Switches

A Matlab script was used to convert the optical sensor output to displacement. The signal alternates between high and low as the sensor passes over the strip, see figure 3.18a. The transducer rise time is very short ($<200~\mu$s), but there is overshoot and ripple. The data was converted to binary output and at each time–step where a voltage change occurred, the displacement counter was incremented. The result is a step–like displacement curve which is clearly an artefact of the measurement device, see figure 3.18a. An improved curve was achieved using averaging, see figure 3.18b.

Numerical Data manipulation

Sled velocity was not measured directly and needed to be estimated by numerical means. This involved integration and differentiation of the measured accelera-
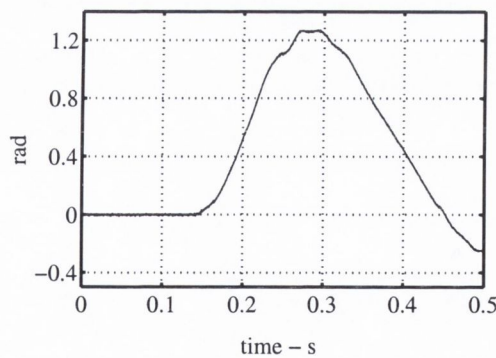

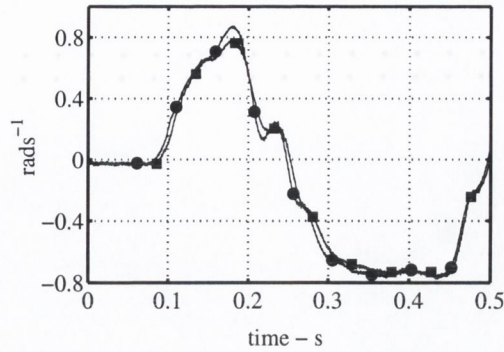Figure 3.16: Problems with the RID III neck.

60

Figure 3.17: $\dot{\theta}_{head}$ with (●) and without (■) rod and bearing mechanism.
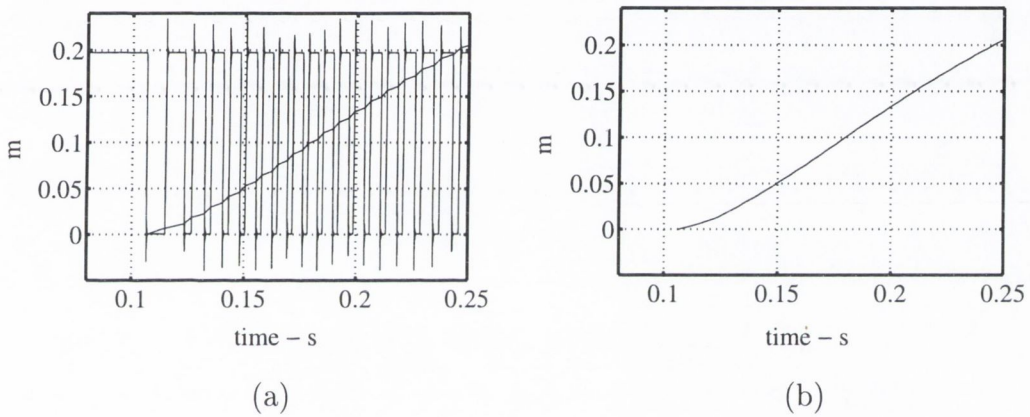

(a)   (b)

Figure 3.18: P_{sled_X}: (a) optical signal with discrete curve; (b) smooth curve.

tion and displacement data respectively. Figure 3.19 illustrates the characteristics associated with each method: numerical differentiation produces a very uneven curve, while numerical integration produces a smooth curve. Both methods are subject to considerable error. The low level of high–frequency noise remaining in the displacement data after smoothing is strongly amplified by numerical differentiation. This causes the 'jagged' effect in the resulting velocity curve. The integrated acceleration curve is smooth but the cumulative error of low–frequency drift causes the non–sensical negative velocity seen after $t = 0.3$s. A least squares fit to the differentiated displacement curve is probably a good estimation of true
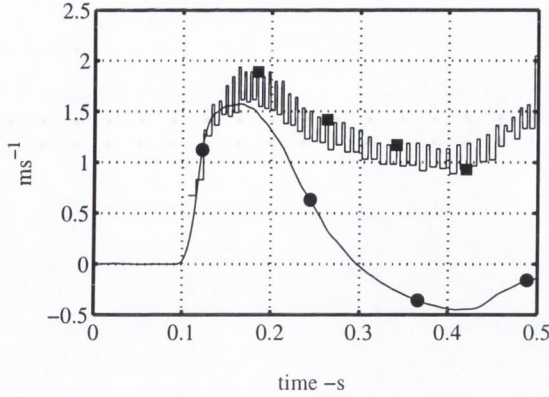
Figure 3.19: $\dot{P}_{sled_X}$: derivative of P_{sled_X} (■) and integral of $\ddot{P}_{sled_X}$ (●) data.

sled velocity but a precise measurement is not possible by these means.

Calibration of MHD's

Calibration of the MHD's was time consuming because erroneous calibration constants were supplied by the manufacturers. The values supplied were 115.93 mV/rads^{-1} for m458 and 120.98mV/rads^{-1} for m479, both measured at 10 Hz. An independent simple–pendulum test with a period of 0.6s (ca. 1.6Hz) gave the following calibration constants: 120.98mV/rads^{-1} for m479 (same as before) but 77.89mV/rads^{-1} for m458. However, the specification that both sensors were insensitive to linear velocity was correct: when connected directly to the sled (i.e. a body with high linear velocity but zero rotational velocity), the sensor output was noise with a magnitude less than 4% of the signal magnitude produced when the sensor was placed on the rotating head. The frequency response characteristics for both m458 and m479 are given in appendix C.

Accuracy of Mouth-opening Measurement

The rate of mouth-opening was calculated from the algebraic difference of the measured angular velocities of the model head and mandible. This method has the major advantage that a non-contact system is used to measure the relative angular velocity between the head and jaw. This is far preferable to a contact style
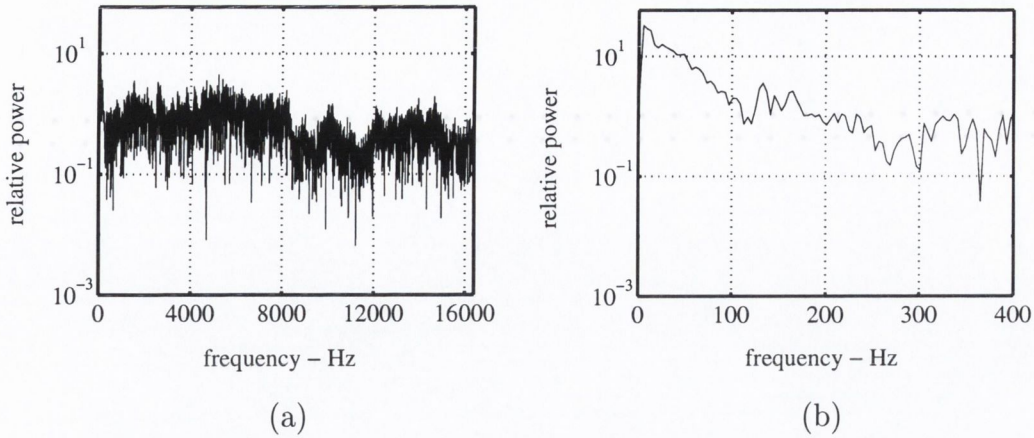
62

Figure 3.20: Discrete Fourier Transform of sled acceleration: (a) full frequency range; (b) low–frequency range.

transducer which would interfere with the movement to be measured. However, this system relies on the motion of the mandible being limited to the sagittal plane and any out-of-plane movement will introduce errors. Moreover, a further drawback of this method becomes clear when there is little relative motion between the model head and jaw. The difference between two measurements is more sensitive to error when the absolute magnitudes of the signals are similar. Thus it will be seen that the ability to determine accurately the relative motion between the head and jaw reduces as the applied muscle stiffness increases and hence relative motion decreases. Figure 4.12a shows that the angular velocities of the head and jaw are very similar when 50% muscle bundles are applied. The computed rate of mouth-opening is thus subject to substantial error, see figure 4.13a.

The advantage of direct measurement of relative motion between the head and jaw is the insensitivity to error introduced by subtraction of two similar measurements. However, this is significantly offset by the disadvantages of the inertial and frictional effects of a contact style transducer. An ideal measurement would be a non-contact transducer which directly measures relative motion between the head and jaw, but that was not achieved in this work. However, inspection shows that although the exact angular rate at a time t cannot be measured, the extent of mouth-opening in the tests described by figures 4.12 and 4.13 is clearly negligible.

63

Filtering

All data traces were loaded into Matlab. A first order 100Hz low–pass filter was used to smooth the kinematic data: a discrete Fourier Transform (function FFT.m in Matlab) of sled acceleration showed signal power above 100Hz to be low, see figure 3.20. The FILTFILT zero–phase forward and reverse digital filter in the Matlab Signal Processing Toolbox was used for all filtering operations. This causes zero phase distortion but results in a correspondingly higher magnitude distortion.

Triggering

The trigger for the data acquisition system was provided by the first voltage change from the opto–switch on the sled.

3.7.2   Model Validation

There have been no experimental investigations of jaw behaviour during whiplash, and it is therefore not possible to compare the current model jaw with published data. The model head is a rigid body whose inertial characteristics conform to those of its *in vivo* counterpart, and this requires no experimental validation. The RID III neck has been validated by Svennson & Lovsund [88]. However, since the neck for the current model was constructed rather than commercially purchased, independent validation of the dummy neck was necessary. A model gains credence if it can be validated against existing experimental data, and correlation of sled–test data from the current model with published crash data is important. However, the number of crash–tests using volunteers is limited and there is a good deal of variation in the manner of their reporting. Crash–tests using volunteers usually report some (or all) of the following parameters:

- peak vehicle acceleration.

- vehicle $\triangle v$.

- time–histories of angular displacement, velocity and acceleration of the head.

64

- time–histories of linear head accelerations.

A direct comparison between sled acceleration on the current rig with vehicle acceleration from volunteer tests is not meaningful: the sled is a rigid structure (no deformable bumper, etc.) to which the shoulders are directly attached. In a real crash, energy absorption occurs as the acceleration pulse passes through the vehicle to the occupant. In this investigation, the neck is directly connected to the sled and therefore sled acceleration should represent shoulder accelerations from volunteer crash tests. Unfortunately, shoulder accelerations are rarely measured by other researchers, so there is no direct basis for comparison. However, a suitable alternative is available. The primary body under investigation is the mandible. This is light (ca. 0.16kg) and is connected to the head which has a high inertia (ca. 4.5kg). This mass–ratio means that the jaw is strongly influenced by the head, and head behaviour largely governs inertial loading at the TMJ. Therefore, accurate modelling of head kinematics is crucial to the overall validity of the model. It follows that close correspondence between the kinematic behaviour of the dummy head and human head data from volunteer investigations constitutes validation for the head/neck complex. Further, comparison with published crash data allows calibration of the impact severity of the sled–tests performed.

Few published volunteer tests are suitable for direct comparison to the current model. One of the earliest whiplash investigations using volunteers was reported by Severy et al. [4], see section 2. It has already been stated that this seminal study made many important recommendations. However, the design of the vehicles used (no headrests or deformable bumpers) and the quality of the instrumentation have compromised the relevance of the measured data from these reports. More recently, West et al. [69] have also reported on low velocity impact tests using volunteers. However, this report does not include vehicle Δv's or any angular kinematic data: only linear accelerations of the volunteer's head are reported. The location on the head of these acceleration measurements is unclear and there is thus no basis for comparison to the current sled tests.

In contrast, the recent volunteer tests reported by McConnell et al. [20] are well documented, see section 1.2. A total of fourteen test collisions using two tar-

Test	$\triangle v$ (km/h)	Symptoms (Driver)	Symptoms (Passenger)
5	7.7	'Awareness' of posterior neck base, onset a few minutes, lasting twelve hours.	Mild neck 'awareness', onset a few minutes, lasting a few hours.
7	9.2	Mild neck awareness, onset a few minutes, lasting a few hours.	Dull headache from head–restraint strike, gone in a few seconds, one–two hours later, mild frontal headache, lasting a few hours.
12	8.7	Frontal headache, onset a few minutes, lasting five minutes. Additional neck discomfort (mild), lasted ca. three days.	Soreness in anterior strap muscles, pre–existing, lasted one–two more days.

Table 3.3: Details of McConnell et al. [20] volunteer tests.

get vehicles were performed. Data from each test consisted of a medical history, observations obtained before and after each test exposure, HSV data and acceleration measurements from sensors mounted on both the vehicle and its occupants. This provides a good reference basis for the current work. Table 3.3 details $\triangle v$ and occupant symptoms of three of these tests. Figures 3.21 and 3.22 show the corresponding time–histories of head angular displacement, velocity and acceleration. There are some differences between the film and transducer measurements. This is because HSV is less sensitive to high–frequency signal components than the electrical transducers.

A comparison was made between these data and the angular kinematics of the model head during different sled tests. Test 7 best compares with the maximum
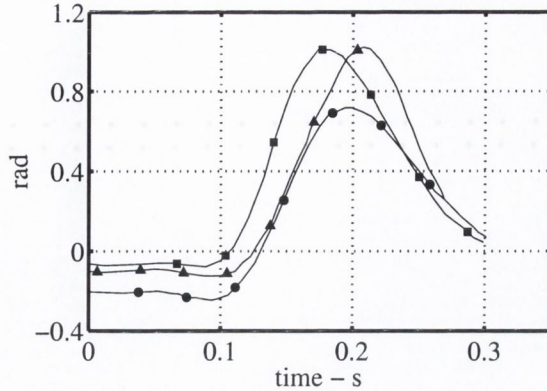
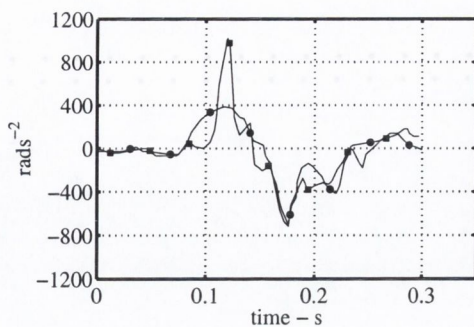Figure 3.21: Volunteer data [20], head angular displacement: test 5 (•), test 7 (▲) and test 12 (■).

impact severity that can be achieved with the impact cylinder. This corresponds to a Δv of 9.2 km/h. Figure 3.23 shows comparisons between the angular displacement, velocity and acceleration obtained by McConnell et al. [20] in test 7 and the same parameters measured during sled–tests with the current model. The pre–impact posture of the volunteers seen in figure 3.21 has been chosen as the 'upright' position for clearer comparison with the dummy data. The period of dummy head displacement is larger than that of the volunteers, because the volunteer tests included a head–rest which prevented full retroflexion of the head. In addition, the earlier return of the volunteer to the neutral position is due to tensing of the neck muscles. However, the difference in neck response during this time is not critical since damage is more likely to occur earlier in the retroflexion phase, when head acceleration is higher. There is good correspondence between the two curves during the complete retroflexion phase of head motion. The angular velocity and particularly the angular acceleration curves in figure 3.23 also show good correspondence between the dummy response and volunteer data.

Conclusions

It can be concluded that the dummy head response is close to that of a vehicle occupant in a rear impact collision. This means that loading applied to the model
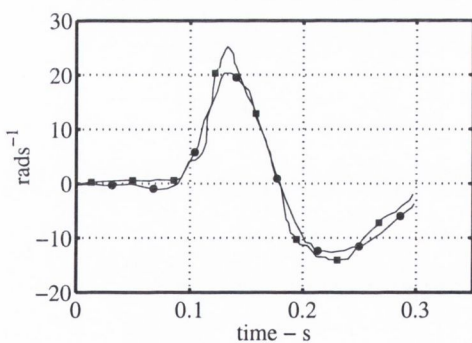
67
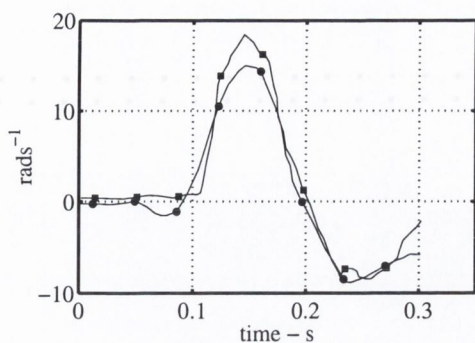
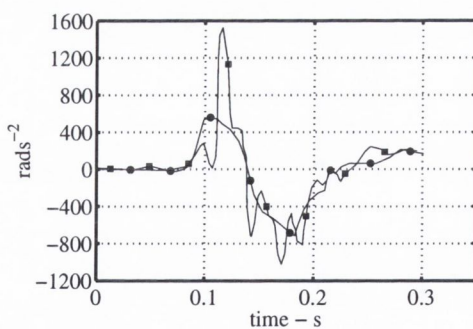angular velocity – test 5

angular acceleration – test 5
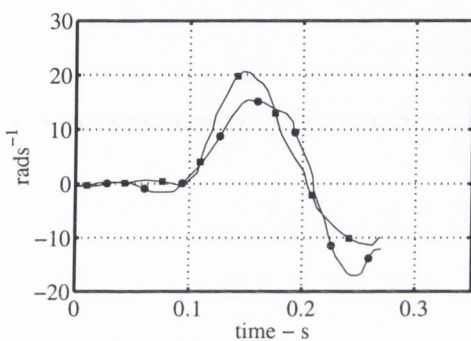
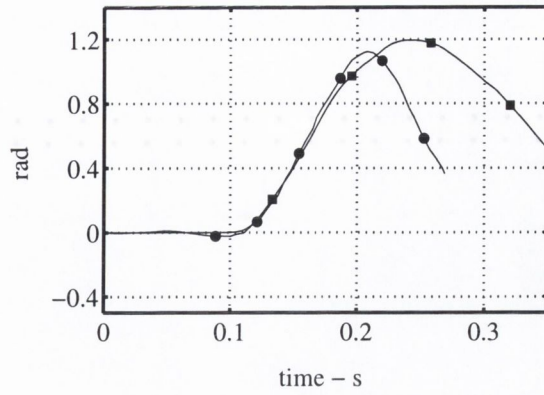angular velocity – test 7
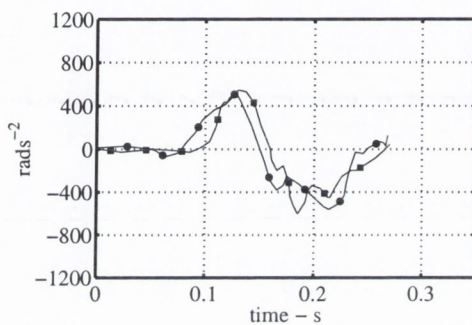
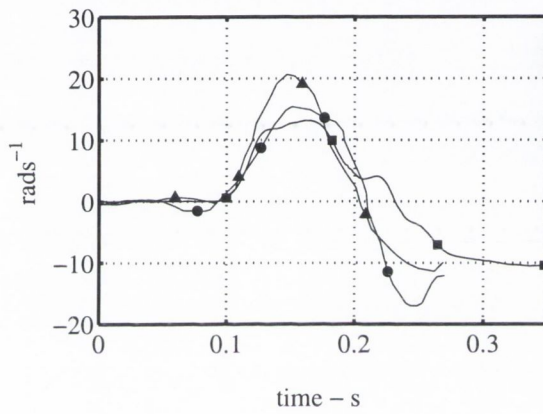angular acceleration – test 7

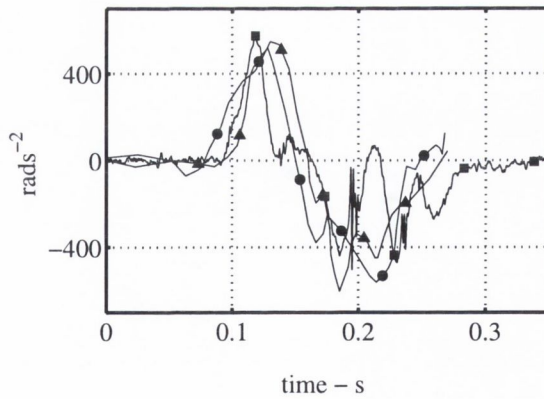angular velocity – test 12

angular acceleration – test 12

Figure 3.22: Volunteer data [20], head kinematics: transducer data (■) and digitized film data (●).

angular displacement

angular velocity

angular acceleration

Figure 3.23: Head kinematics: dummy – this work (■); volunteers [20]: trans-
ducer (▲) and film (•).

69

jaw through the motion of the model head accurately represents loading of the mandible and TMJ during a low velocity rear impact collision.

Chapter 4

Sled–test Results – I

The first experimental series investigated mouth–opening during whiplash. The three primary jaw elevator muscles (masseter, temporalis and medial pterygoid) will be collectively referred to as the jaw muscles. Sled–tests were performed with three different jaw muscle stiffnesses corresponding to the following muscle states:

1. 0% active (passive response).

2. 25% active.

3. 50% active.

It had also been intended to test 100% stiffness (or fully active) jaw muscles but this proved unnecessary. The following experimental measurements were taken in all three test–series, see figure 4.1:

1. sled displacement (P_{sled_X}).

2. sled acceleration ($\ddot{P}_{sled_X}$).

3. head acceleration at the nose ($\ddot{P}_{head_Z}$) – initial orientation vertical.

4. head angular displacement (θ_{head}).

5. head angular velocity ($\dot{\theta}_{head}$).
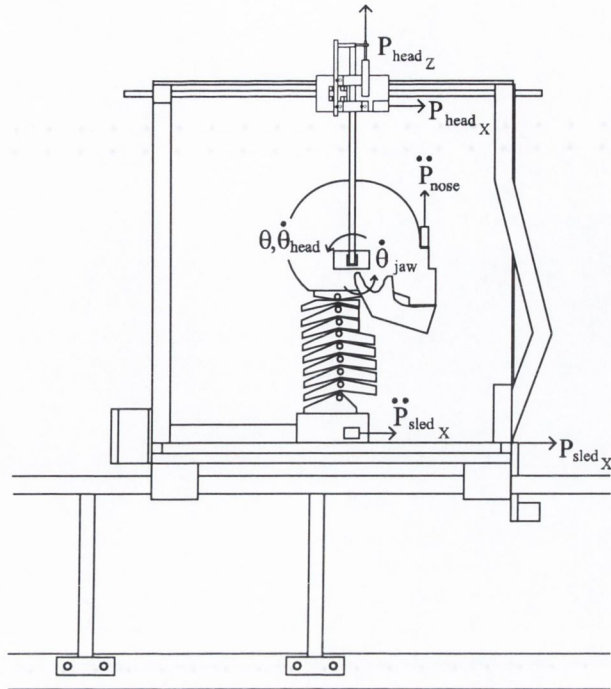
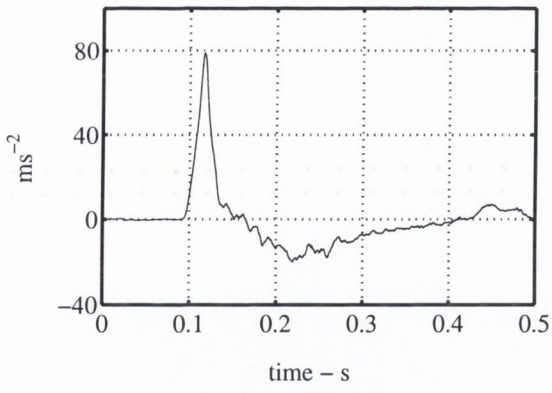6. jaw angular velocity ($\dot{\theta}_{jaw}$).

Figure 4.1: Transducer locations.

The positive X–axis lies along the track. The Z–axis is vertical, (upwards is positive), and the Y–axis lies perpendicular to the X and Z–axes to complete the right–handed coordinate system.

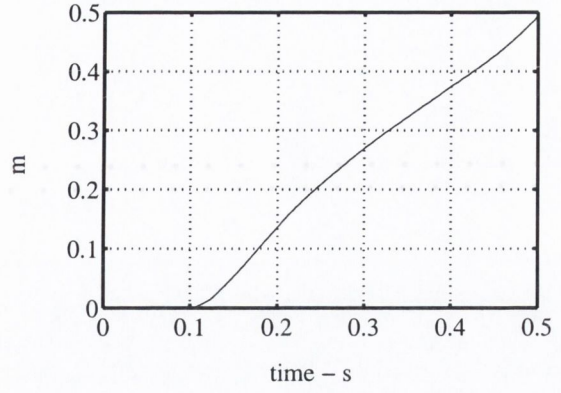## 4.1 Passive Jaw Muscle Tests

The first set of sled–tests was performed with 0% active jaw muscles: these simulate mandibular motion governed only by inertial forces and the passive component of muscle response, i.e. in the absence of any active stimulus. These tests are designed to model a rear–end impact in which the occupant is relaxed, facing forward and unaware of the impending collision.
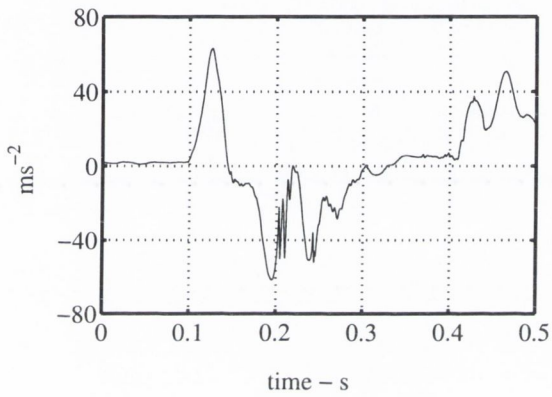
Discussion

Data from each sled–test were converted to SI units using Matlab scripts. Results of a standard test are presented in figure 4.2. It was difficult to produce two iden-
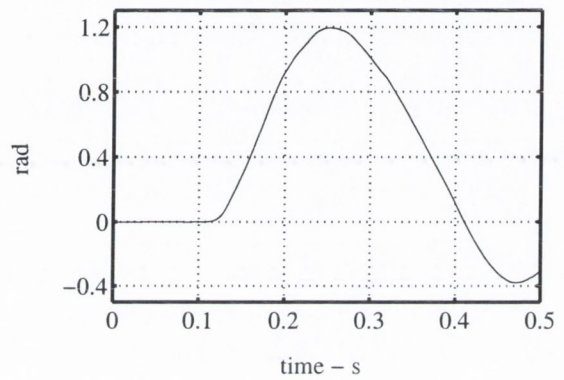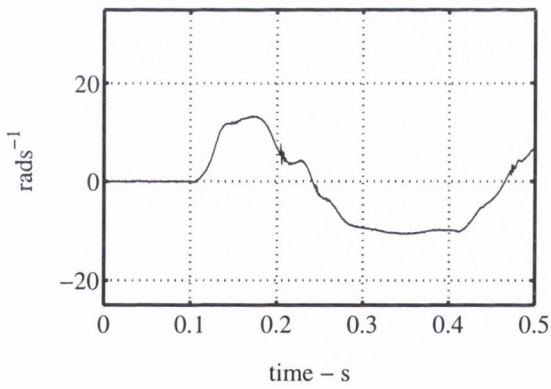
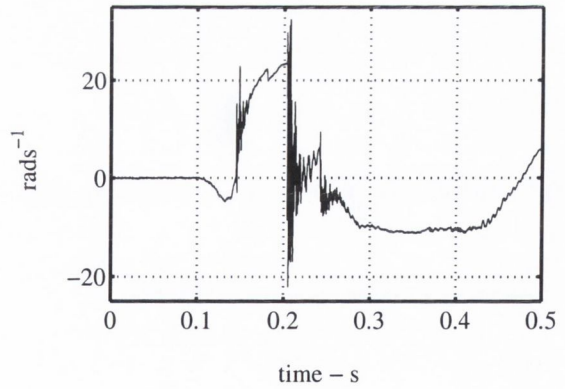(a) Sled acceleration.

(b) Sled displacement.

(e) Head linear acceleration.

(f) Head angular displacement.

(c) Head angular velocity.

(d) Jaw angular velocity.

Figure 4.2: Passive jaw muscle sled–test data – I.

tical sets of experimental data in consecutive sled–testing with the dummy and pneumatic impact cylinder. This is because the impact ram provides a slightly variable pulse and the dummy neck has nine degrees of freedom. However, it can be seen from figures F.1 and F.2 in appendix F that there is good repeatability between nominally equal impact tests. In addition, since sled and head/jaw kinematics are all measured, it is also possible to view each test individually. Head kinematics from these tests correspond well to the 9.2km/h $\triangle v$ volunteer tests from McConnell et al. [20], see section 3.7.2. The occupant symptoms following those tests were dull headache and soreness in the neck but no symptoms remained after two days: the impact severity was marginally harmful. On the test–rig, maximum sled acceleration was ca. 8g and the maximum head angular acceleration was 580rads^{-2}.
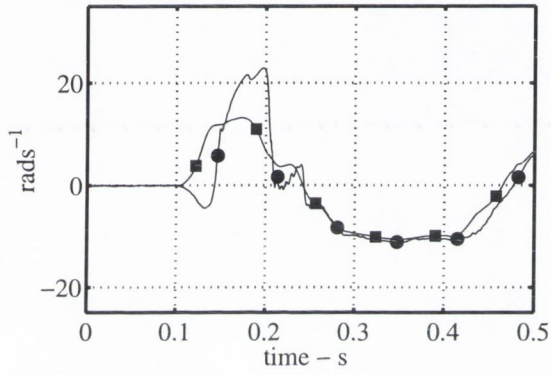
Head and Jaw Angular Velocities

The two MHD sensors measure angular velocity of the head and jaw respectively. Filtered and unfiltered time histories of these are shown in figure 4.3a&b. The unfiltered trace allows easy identification of occlusal impact when the mouth has closed at $t = 0.21$s, while the filtered curve gives a clearer overall view of $\dot{\theta}_{head}$ and $\dot{\theta}_{jaw}$. The accuracy of the $\dot{\theta}_{head}$ measurement can be judged from figure 4.3c, which compares the MHD measurement of head angular velocity with the differentiated potentiometer measurement of head angular displacement. There is good agreement throughout retroflexion. A similar check for $\dot{\theta}_{jaw}$ is not possible, but since both MHD's are the same, it is assumed that the jaw sensor is also accurate. When the mandible was held tightly shut, the two MHD measurements were identical, illustrating their insensitivity to linear velocity.
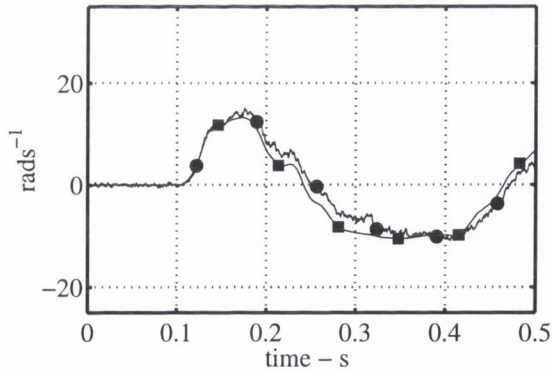
Contra–rotation of the Jaw

The $\dot{\theta}_{head}$ curve is quite smooth with the exception of the inflection point at $t = 0.22$s, see figure 4.3a&b. The cause of this is the slight machining fault in the neck described in section 3.7.1. The $\dot{\theta}_{jaw}$ curve is more complex: the direction of

74
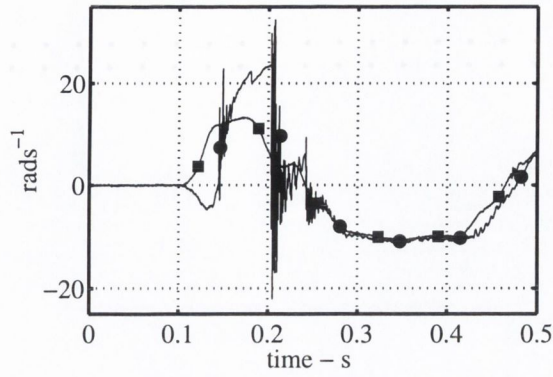
(a) unfiltered

(b) filtered

(c)

Figure 4.3: a & b: Angular velocity, head (■) & jaw (•); (c): $\dot{\theta}_{head}$, MHD (■) and derivative of θ_{head} (•).
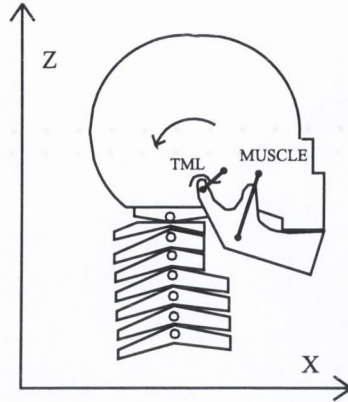
Figure 4.4: Schematic of soft–tissue connections between the model head and jaw.

rotation between $t = 0.10\text{s}$ and $t = 0.15\text{s}$ appears counter–intuitive, but can be explained. The mandible is constrained to follow retroflexion of the head through the ligaments at the TMJ and the elevator muscles. The TMJ is located forward of the articulating surfaces of the neck, see figure 4.4. This means that retroflexion of the head initially causes the TMJ to move in the $+Z$ direction. The condyles are tightly bound into the TMJ by the stiff temporomandibular ligament (TML), whereas the passive jaw muscles are less stiff. As the head rotates away from the mandible during retroflexion, the TML pulls the condyles in the $+Z$ direction before the jaw muscle bundles become taut. The condyles are thus lifted earlier than the body of the mandible and this causes the contra–rotation of the mandible seen in figure 4.3. Figure 4.1 shows the directions of positive angular velocity adopted in this thesis. From this it can be seen that the negative angular velocity of the mandible between $t = 0.1\text{s}$ and $t = 0.14\text{s}$ in figure 4.3 is the contra–rotation of the mandible early in the retroflexion phase.

Maximum Angular Velocity

The other important aspect of the $\dot{\theta}_{jaw}$ curve is that it reaches a significantly higher maximum than the $\dot{\theta}_{head}$ curve and at a slightly later stage: $max(\dot{\theta}_{head}) = 13\text{rads}^{-1}$ at $t = 0.17\text{s}$, while $max(\dot{\theta}_{jaw}) = 23\text{rads}^{-1}$ at $t = 0.12\text{s}$. This is because the mandible has a much lower mass than the head (0.16kg compared to 4.5kg) and

76

when the muscle bundles become taut after $t = 0.14$s and $\dot{\theta}_{jaw}$ changes direction, tensile loading through the muscle connections causes the mandible to rapidly follow head motion. This results in the mandible attaining a higher maximum angular velocity than the head.
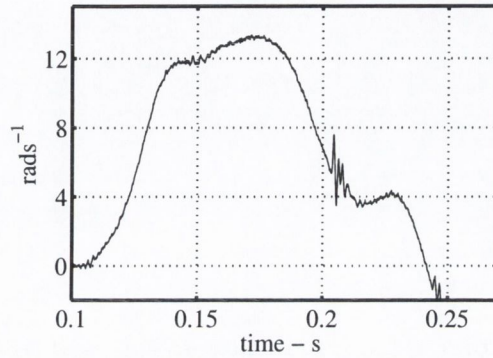

Figure 4.5: Head oscillation due to mouth–closing.

Mouth–opening

The rate of mouth–opening is the algebraic difference between the angular velocities of the head and jaw, see figure 4.6. This curve is largely symmetric between $t = 0.10$s and $t = 0.21$s. The maximum velocities of mouth–opening and closing are both ca. 15rads^{-1}. By $t = 0.21$s the mouth has closed again and figure 4.3a clearly shows the impact between the model jaw and head (occlusal contact). This is followed by nearly 50ms of decaying vibration between $t = 0.21$s and $t = 0.25$s, after which the relative velocity between the model head and jaw becomes negligible. The sensitivity to error during this stage has been discussed in section 3.7.1. Inspection of the $\dot{\theta}_{head}$ curve shows a small oscillation caused by the impact of mouth–closing at $t = 0.21$s, see figure 4.5.

An estimate of the extent of mouth–opening can be made by integrating figure 4.6a, see figure 4.6b. The maximum magnitude of mouth opening is 0.35rad, (ca. 20 degrees). This is considerably aided by the contra–rotation of the mandible in the early stages. The negative mouth–opening after $t = 0.2$s is an artefact of
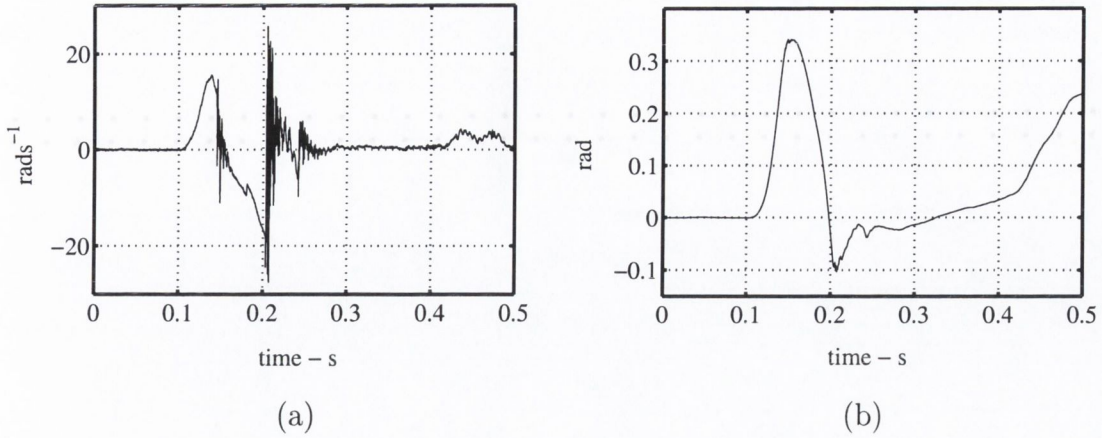
Figure 4.6: Mouth–opening: (a) rate & (b) magnitude.

numerical integration: the high–frequency spikes resulting from the impact of mouth–closing preclude sensible integration over this period. The numerical integration error after $t = 0.2s$ is clearly very large, and that section of the curve is meaningless. When mouth closing is complete and the head and jaw have similar angular rates, the error in the calculation of the rate of mouth-opening is considerable, see section 3.7.1. Numerical integration errors are cumulative, and the error after mouth-closing is therefore large.

The smaller disturbance in the $\dot{\theta}_{jaw}$ curve at $t = 0.15s$ is of uncertain origin, see figure 4.3. It also appears in some of the other passive jaw muscle tests, see appendix F. The most likely explanation is a minor impact between the body of the mandible and the muscle bundles: the passive muscles are loose and bulky in the rest position and could easily cross the trajectory of the mandible.

Mouth–opening and Retroflexion

Figure 4.7 shows the relationship between mouth–opening rate and magnitude and retroflexion angle of the head. It is clear that mouth–opening and closing occur early: all relative jaw motion has occurred by 0.89rad rotation of the head. The significance of this is addressed in chapter 8.
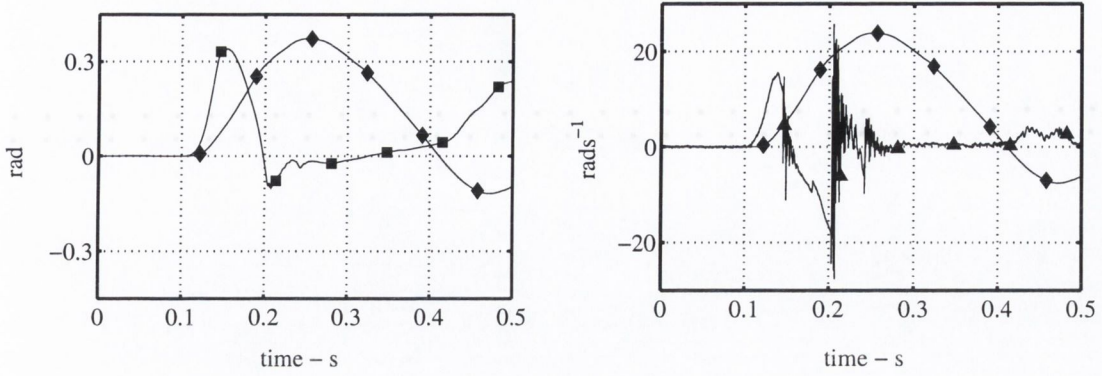
78

Figure 4.7: (a) Rate (■) and (b) magnitude (▲) of mouth–opening as a function of retroflexion of the head (•) – head angle not to scale.

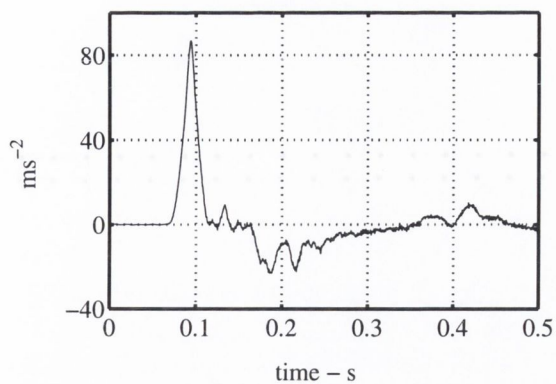## 4.2 25% Active Jaw Muscle Tests

In these sled–tests the passive jaw muscles were replaced by 25% active jaw muscles. All other parameters were unaltered and the same kinematic measurements were taken as in the passive jaw muscle tests. Two sets of impact data are included from this series, see figure 4.8 and figure F.3 in appendix F.
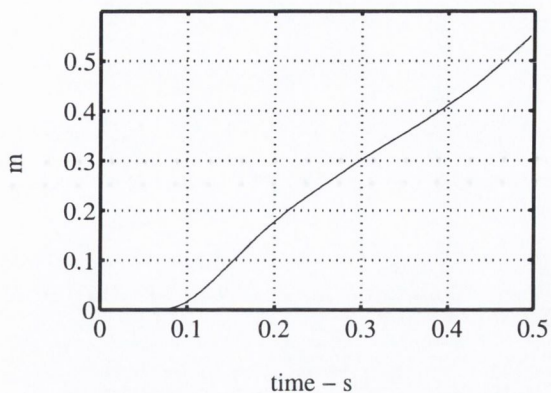
Head and Jaw Angular Velocities

Figure 4.9 again shows the unfiltered and filtered $\dot{\theta}_{head}$ and $\dot{\theta}_{jaw}$ curves. Compared to figure 4.3, the two curves are clearly far more similar, showing a strongly reduced level of relative motion between the head and jaw.

### Contra–rotation of the Mandible

In contrast to the passive jaw muscle tests, there is no initial contra–rotation of the mandible at the onset of retroflexion. This is because the 25% jaw muscles are stiffer and a static muscle force is produced even before impact has occurred. Muscle stress at zero–stretch for 25% activity is ca. 1.5Ncm^{-2}, see figure 3.7. Assuming the mandibular rest position to correspond to zero–stretch of the muscles, and taking the total cross–sectional area of elevator muscle to be 19 cm^2 (see figure 3.2), the closing force on the mandible in the rest–position will be ca. 28N
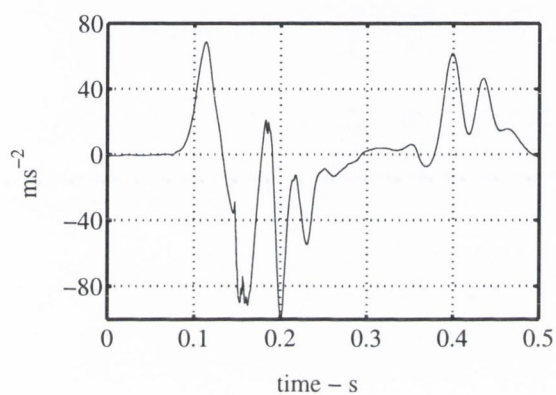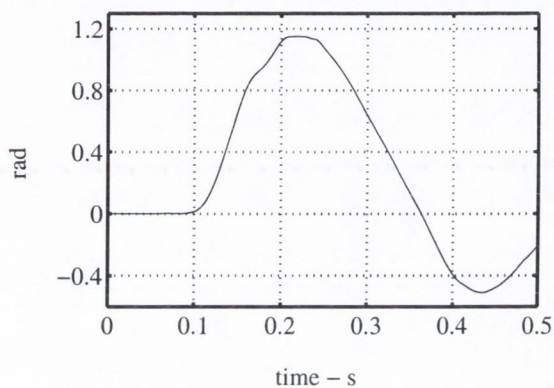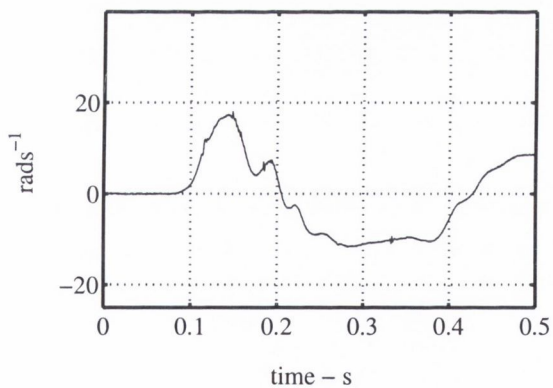
79

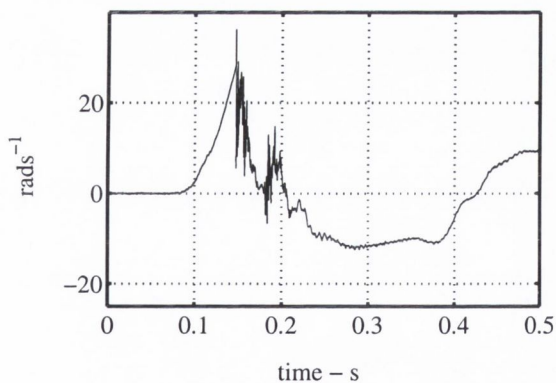(a) Sled acceleration.

(b) Sled displacement.

(e) Head linear acceleration.

(f) Head angular displacement.

(c) Head angular velocity.

(d) Jaw angular velocity.

Figure 4.8: 25% active jaw muscle sled–test data – I.

80

(a) unfiltered   (b) filtered
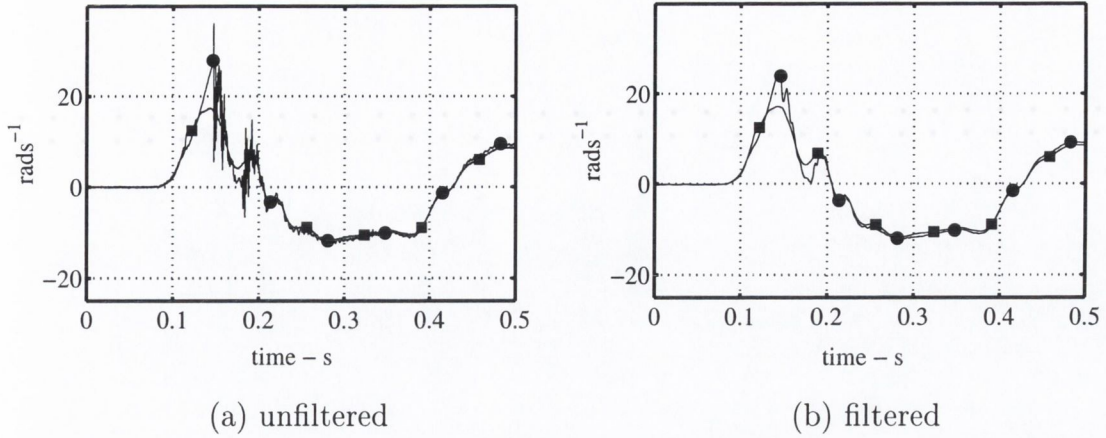
Figure 4.9: Angular velocity: head (■) & jaw (•).

spread over the six elevator muscles (three on each side). When retroflexion of the head begins, tensile load in the muscles is greater than in the soft–tissue connections at the TMJ. This loading configuration causes the mandible to follow the rotational motion of the skull, but no contra–rotation occurs.

Mouth–opening

The rate of mouth–opening is determined by the algebraic difference between the $\dot{\theta}_{head}$ and $\dot{\theta}_{jaw}$ curves, and is shown in figure 4.10a. The max level of $\dot{\theta}_{opening}$ has

(a)   (b)

Figure 4.10: Mouth–opening: (a) rate & (b) magnitude.

81

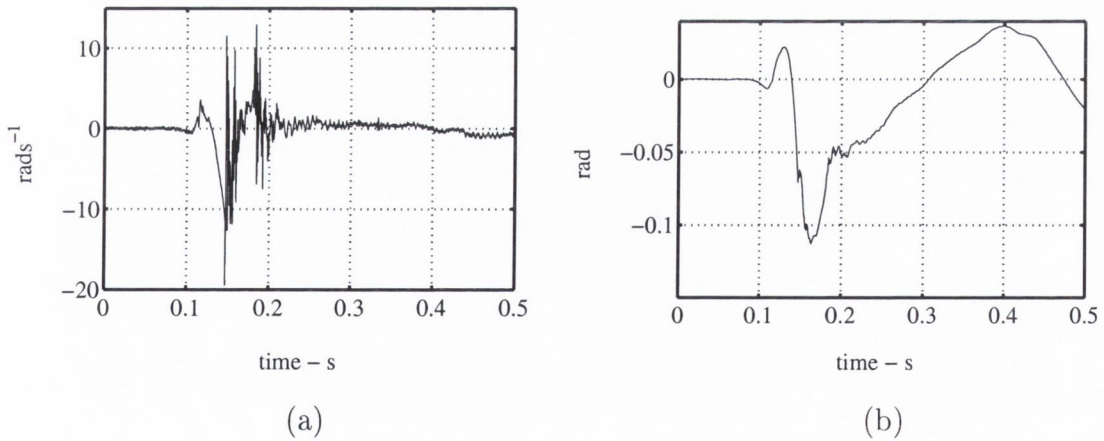now dropped to ca. 3rads^{-1}, compared to 15rads^{-1} for the passive jaw muscle tests. In addition, the mouth has closed again by $t = 0.145\text{s}$, which means that the mouth–opening and closing sequence occurs in the first 50ms after retroflexion begins. In the passive muscle tests the same sequence occurred over a period of 100ms. The shorter time frame for the 25% muscle tests is due to the increased stiffness of the muscle bundles acting on the mandible in this test series. The impact occurring at full occlusal contact can be seen clearly at $t = 0.145\text{s}$. After mouth–closing there is some vibration as further (smaller) impacts between the head and jaw occur at the occlusal surfaces, but the mouth remains closed for the remainder of the test. Figure 4.10a shows that there is little difference between the $\dot{\theta}_{head}$ and $\dot{\theta}_{jaw}$ curves after $t = 0.2\text{s}$.

The extent of mouth–opening ($\theta_{opening}$) can be estimated by numerically integrating the $\dot{\theta}_{opening}$ curve, see figure 4.10b. Maximum mouth–opening is 0.02rad which occurs at $t = 0.13\text{s}$. This is much less than the mouth-opening of 0.35rad occurring in the passive jaw muscle tests. After the mouth has closed (at $t = 0.145\text{s}$), the integrated $\dot{\theta}_{opening}$ curve has little meaning and this portion of the graph must therefore be disregarded. As before, this is due to the accumulated integration error as vibration between the model head and jaw occurs after the mouth closes. Further, it can be seen that there is a small time lag between the mouth–closing impact at $t = 0.145s$ in figure 4.10a and the time for zero mouth–opening in figure 4.10b. The latter occurs at $t = 0.14s$ and the graphs therefore indicate that the mouth has fully closed $7ms$ before the corresponding impact occurs. If this were true, then negative mouth–opening would occur. However, this is unlikely since the soft–tissue connections in the TMJ are stiff. Cumulative integration error has caused this small time gap: the two curves ($\theta_{opening}$ and $\dot{\theta}_{opening}$) are computed from the same transducer measurement.
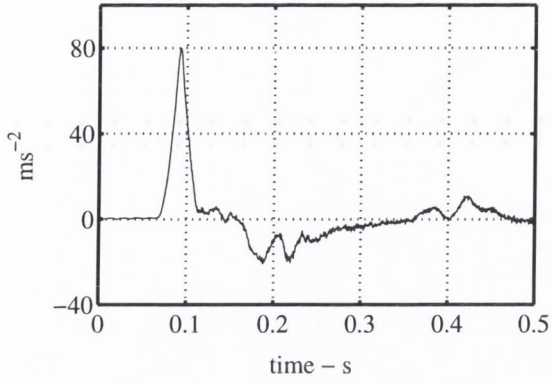
4.3   50% Active Jaw Muscle Tests

In these sled–tests the 25% muscle bundles were replaced with 50% active jaw muscle models. All other parameters were unaltered and the same kinematic

measurements were taken. A single set of impact data is included from this series, see figure 4.11.

Discussion

These tests confirm the tendency for dramatically reduced mouth–opening as muscle activity is increased. The rate of mouth–opening is negligible, see figure 4.13a. The magnitude of $\dot{\theta}_{opening}$ is insignificant and results in no measurable mouth–opening occurring, see figure 4.13b. This is because strong jaw muscle forces act to close the mouth. With reference to figure 3.7, muscle stress at zero–stretch is ca. $3.25 \mathrm{Ncm}^{-2}$. Assuming (as before) that the mandibular rest position corresponds to zero–stretch of the muscles and taking the total cross–sectional area of elevator muscle to be $19cm^2$ (see figure 3.2), then a mouth–closing force 61N is spread over the six jaw muscles (three on each side). This prevents relative motion between the head and mandible throughout the whiplash sequence.

(a) Sled acceleration.
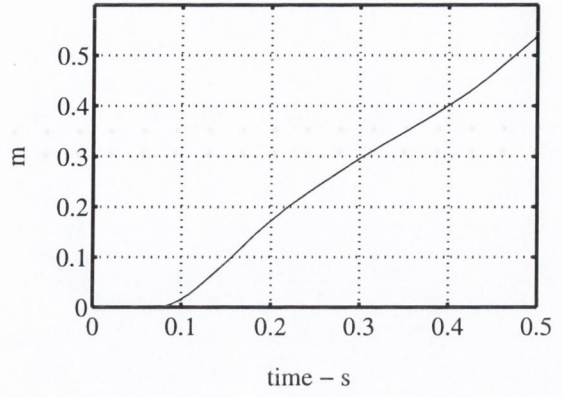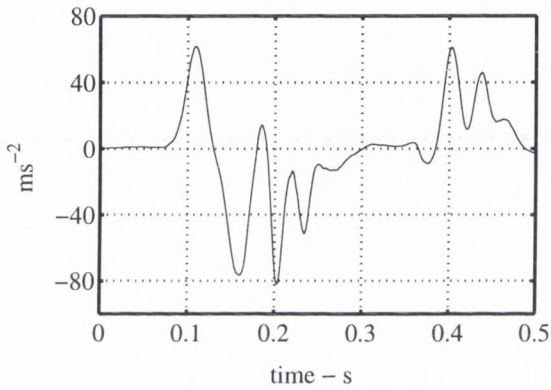
(b) Sled displacement.

(e) Head linear acceleration.

(f) Head angular displacement.

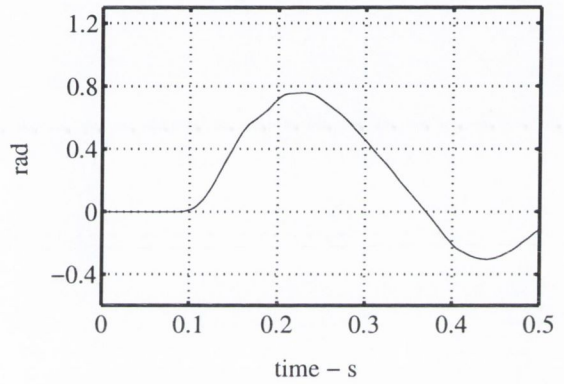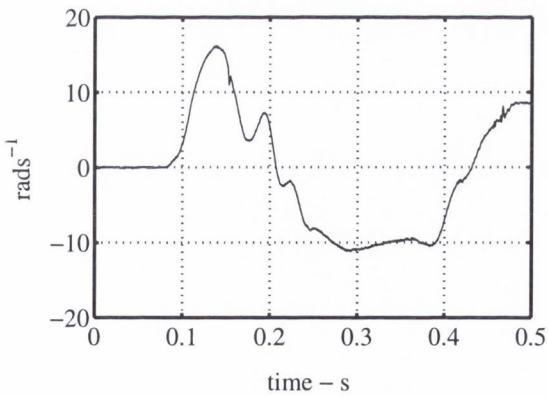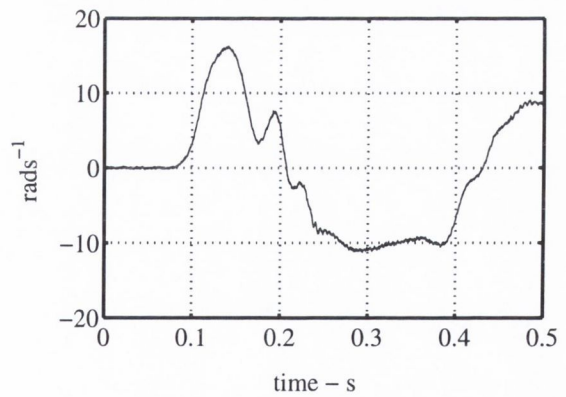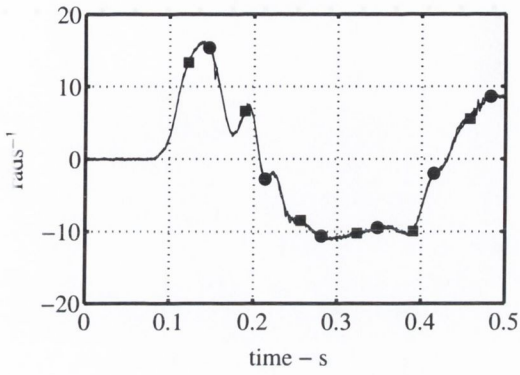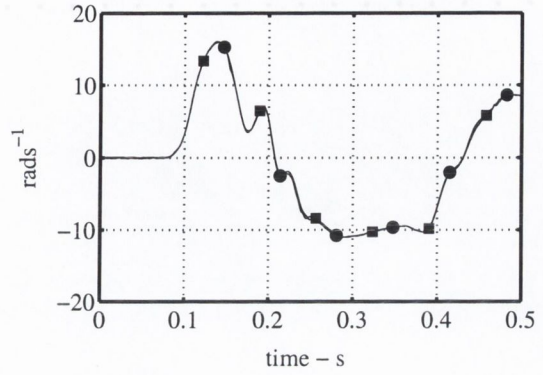(c) Head angular velocity.

(d) Jaw angular velocity.

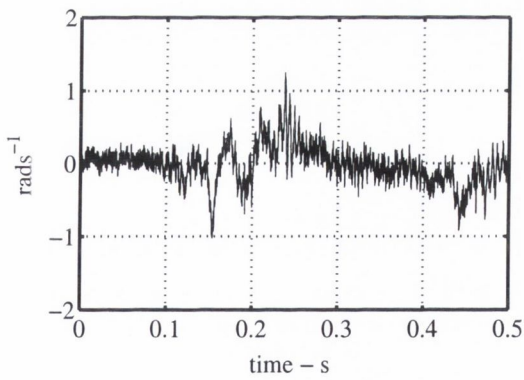Figure 4.11: 50% active jaw muscle sled–test data – I.

(a) unfiltered

(b) filtered

Figure 4.12: Angular velocity: head (■) & jaw (•).

(a)
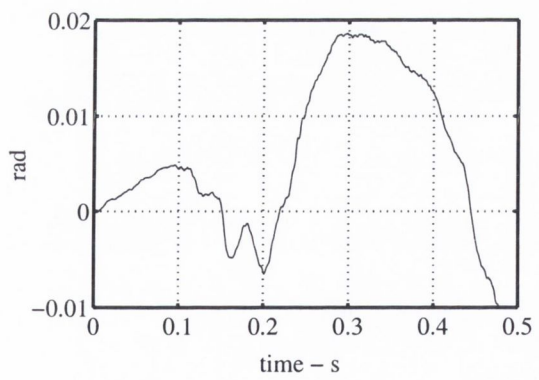
(b)

Figure 4.13: Mouth–opening: (a) rate & (b) magnitude.

Chapter 5

Sled–test Results – II

The first experimental series investigated the degree of mouth–opening during retroflexion of the head. It was also desirable to establish the kinematics of the TMJ, and a further experimental test series was necessary to achieve this. The TMJ is at a fixed location on the skull and experiences forces corresponding to the kinematic behaviour of the head and jaw. Two approaches were adopted: direct measurement of sagittal plane accelerations of the skull portion of the TMJ (He_h, He_v), and measurement of displacements of the head centre of gravity (COG_{head}) and TMJ and the location of the instantaneous centre of rotation of the head (ICR_{head}) during retroflexion. For simplicity, head displacements (P_{head_X}, P_{head_Z}) always refer to COG_{head}.

Calculation of kinematic loading at the TMJ requires measurement of the relative acceleration between the head and jaw portions of the TMJ. It was not feasible to attach a bi-axial accelerometer array to the jaw at the TMJ, and direct measurement of the loads reacted across the articular surface could therefore not be realised. The disadvantage of this has been recognised, see section 3.6. However, it is possible to carry out a more limited analysis by examining the accelerations at the skull portion of the TMJ.

Prior to impact the head and jaw are at rest. Forces applied to the head through the neck following impact then cause relative acceleration between the head and jaw. Measurement of acceleration at the skull portion of the TMJ (He_h, He_v) gives

an indication of loading at the TMJ during the brief post-impact period before the mandible has begun to follow head movement. It should be clear that these measurements alone cannot be used to quantify TMJ loading once relative motion between the head and jaw has begun. An estimate of the load reacted across the TMJ will be made using the results of a numerical simulation in chapter 7. In this chapter, the (skull portion) TMJ acceleration measurements are used to show qualitatively that proximity to the COG_{head} protects the TMJ from large linear accelerations.

The measurement of ICR_{head}, and head and sled displacements provide an understanding of the kinematic behaviour of the TMJ during retroflexion. Mouth–opening is not considered in the following discussion. The origin of the system is the pre–impact position of COG_{head}. As before, the X–axis lies along the track. The Z–axis is vertical, and the Y–axis completes the right–handed coordinate system.

5.1   TMJ Acceleration

Two orthogonal linear accelerometers (He_h and He_v) fixed at the TMJ in the sagittal plane were used to measure accelerations directly, see figure 5.1a. The pre–impact orientations of He_h and He_v are in the X and Z–directions respectively. Coupled with head angular displacement data (θ_{head}), these measurements allow direct calculation of $\ddot{P}_{TMJ_X}$ and $\ddot{P}_{TMJ_Z}$:

$$\ddot{P}_{TMJ_X} = He_h \cos\theta_{head} - He_v \sin\theta_{head} \tag{5.1}$$

$$\ddot{P}_{TMJ_Z} = He_h \sin\theta_{head} + He_v \cos\theta_{head}. \tag{5.2}$$

Typical time–histories of $\ddot{P}_{TMJ_X}$ and $\ddot{P}_{TMJ_Z}$ are given in figure 5.2a&b. The resultant magnitude of acceleration in the sagittal plane is shown in 5.2c, and the corresponding $\dot{\theta}_{head}$ curve is also given, see figure 5.2d. Given the two orthogonal, sagittal plane accelerations (He_v, He_h) at a point on the head and the angular kinematics of the head (θ_{head} and its derivatives) in the sagittal plane, then the
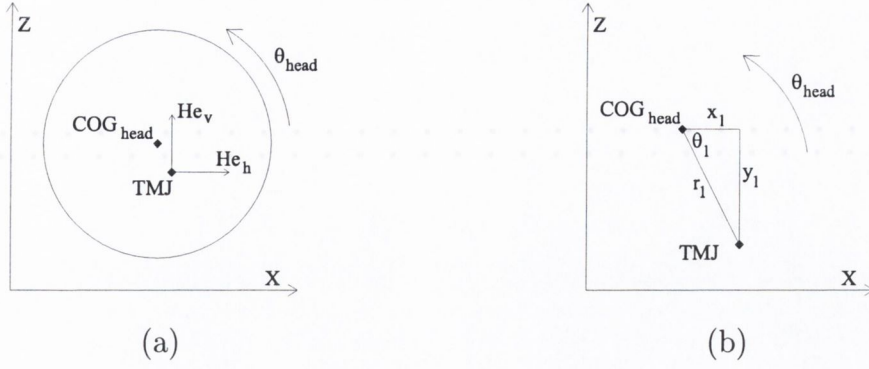
Figure 5.1: Accelerometer locations at the TMJ.

acceleration components of any other point in the sagittal plane are

$$
\ddot{P}_{C_X} = He_v \sin\theta_{head} + He_h \cos\theta_{head} + r_1\dot{\theta}_{head}^2 \cos\left(\theta_1 - \theta_{head}\right)
$$
$$
- r_1\ddot{\theta}_{head} \sin\left(\theta_1 - \theta_{head}\right) \tag{5.3}
$$

$$
\text{and} \quad \ddot{P}_{C_Z} = He_v \cos\theta_{head} - He_h \sin\theta_{head} + r_1\dot{\theta}_{head}^2 \sin\left(\theta_1 - \theta_{head}\right)
$$
$$
+ r_1\ddot{\theta}_{head} \cos\left(\theta_1 - \theta_{head}\right). \tag{5.4}
$$

where r_1 and θ_1 are the polar coordinates describing the fixed relationship between the points on the body, see figure 5.1b. The reliability of the TMJ acceleration measurements shown in figure 5.2 was tested by applying equations 5.3 and 5.4 to successive sled–tests. In the first, orthogonal accelerometers were placed at a location A on the head and $\ddot{P}_{A_X}$, $\ddot{P}_{A_Z}$ were measured directly while $\ddot{P}_{TMJ_X}$, $\ddot{P}_{TMJ_Z}$ were calculated using equations 5.3 and 5.4. In the second, orthogonal accelerometers were placed at a location B on the head: $\ddot{P}_{B_X}$ and $\ddot{P}_{B_Z}$ were measured directly and $\ddot{P}_{TMJ_X}$, $\ddot{P}_{TMJ_Z}$ were again calculated. A good correlation between these readings was achieved, see figure 5.3a & b. Figure 5.3c shows the corresponding $\dot{\theta}_{head}$ traces for both sled–tests. The maximum resultant level of TMJ acceleration does not exceed 30ms^{-2}, see figure 5.2c. The X–component is positive throughout retroflexion. However, it can be seen that the magnitude of these compressive accelerations is small ($\leq$ 1g) and fluctuating during the early stages of head motion.
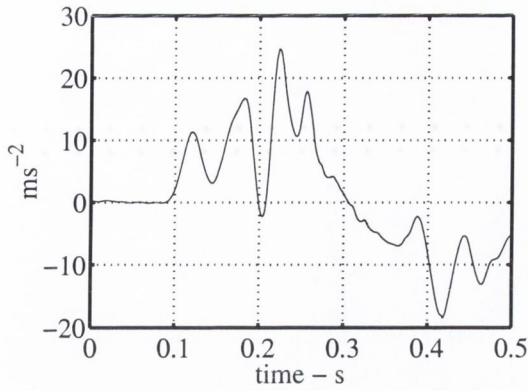
(a) X–direction
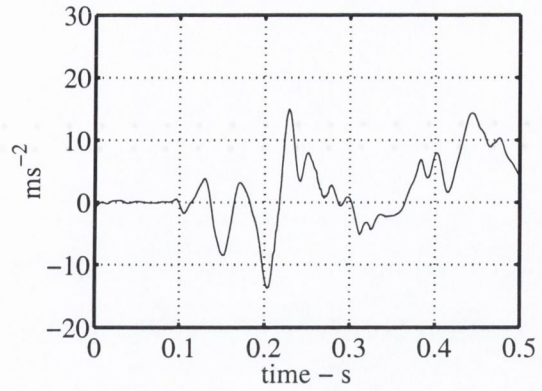
(b) Z–direction
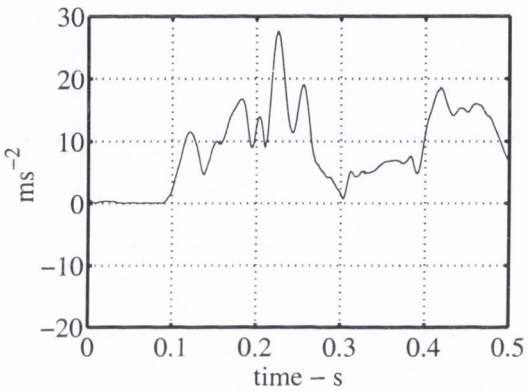
(c) Resultant
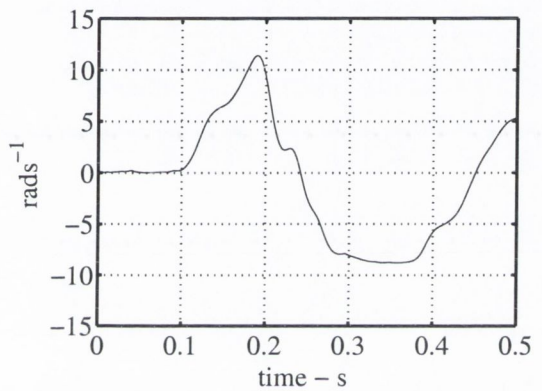
(d)

Figure 5.2: (a)–(c): TMJ accelerations; (d) time–history of $\dot{\theta}_{head}$.

5.2 TMJ Displacement

At any instant, there is one point of a lamina moving in planar motion (not in pure translation) which has zero velocity. This is the instantaneous centre of rotation (ICR) and any point on a rotating body experiences forces proportional to the distance to the ICR. The human skull does not have a unique pivot point: its ICR is therefore not fixed and so it is of interest to establish the locus of ICR_{head} during the whiplash sequence. There are several simple methods available: Synge & Griffith describe a system using known velocity vectors of any two points on the body [99]. The ICR can also be found if displacements of any two points on the
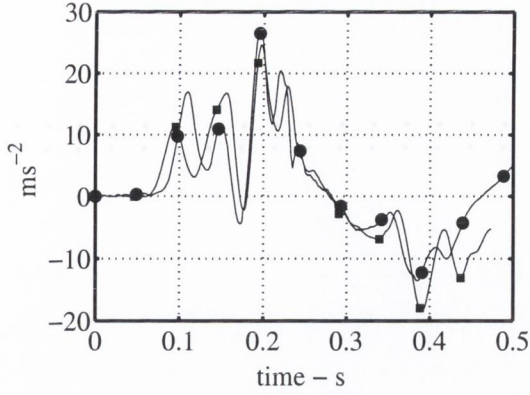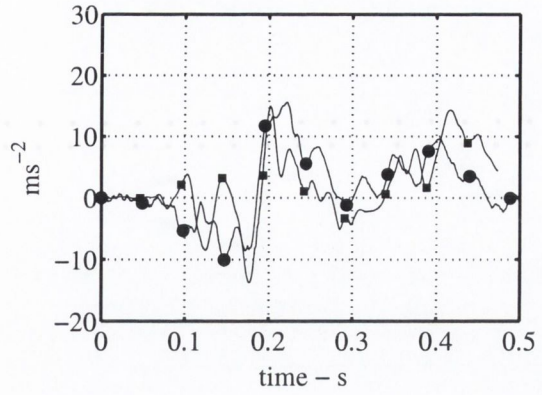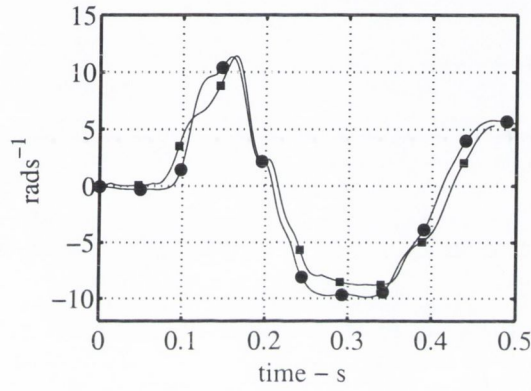
Figure 5.3: (a)&(b) TMJ accelerations (skull portion) measured from two locations on the head; (c) corresponding $\dot{\theta}_{head}$ traces.

body are known. Displacement measurements of the head and sled were provided directly by the instrumentation whereas velocities could only be determined by numerical manipulation and the displacement method was therefore used in this analysis. The following displacement measurements are relevant:

1. absolute X–displacement of the sled (P_{sled_X}).

2. relative X–displacement between COG_{head} and the sled ($P_{head_X/sled_X}$).

3. relative Z–displacement between COG_{head} and the sled ($P_{head_Z/sled_Z}$).

4. angular displacement of the head (θ_{head}).

Slotted opto–switches were used to measure P_{sled_X} and $P_{head_X/sled_X}$, and linear and rotational potentiometers were used for $P_{head_Z/sled_Z}$ and θ_{head} respectively, see section 3.6. The absolute X–displacement of COG_{head} is the algebraic sum of P_{sled_X} and $P_{head_X/sled_X}$. Since the sled is constrained to move in the X–direction, $P_{head_Z/sled_Z}$ is equal to absolute Z–displacement of the head (P_{head_Z}). Time histories of the sagittal plane displacements of COG_{head} (P_{head_X}, P_{head_Z}) can thus be established. Angular displacement of the head (θ_{head}) can then be used to calculate the displacement of the TMJ. In the upright, pre–impact position, the TMJ lies 0.01m anterior and 0.02m inferior to COG_{head}, see figure 5.1b. Thus its relative coordinates are $x_1 = 0.01$m and $z_1 = 0.02$m. In polar coordinates $r_1 = |x_1^2 + z_1^2|^{0.5}$ and $\theta_1 = tan^{-1}(z_1/x_1)$. As the head rotates,

$$P_{TMJ_X} = P_{head_X} + r_1 cos(\theta_1 - \theta_{head}) \tag{5.5}$$

$$P_{TMJ_Z} = P_{head_Z} - r_1 sin(\theta_1 - \theta_{head}). \tag{5.6}$$

The displacement of any other point can be found similarly: the (X,Z) coordinates of two points on the head are then known and the locus of ICR_{head} can be calculated.

Results

Typical time–histories of X–direction displacements are shown in figure 5.4a–d:

- figure 5.4a – absolute displacement of the sled (P_{sled_X}).

- figure 5.4b – displacement of the COG_{head} relative to the sled ($P_{head_X/sled_X}$).

- figure 5.4c – absolute COG_{head} displacement (P_{head_X}).

- figure 5.4d – P_{head_X} is the algebraic sum of figure 5.4a and figure 5.4b.

The relationship between retroflexion angle of the head (θ_{head}) and (P_{head_X}) is given in figure 5.4e&f.
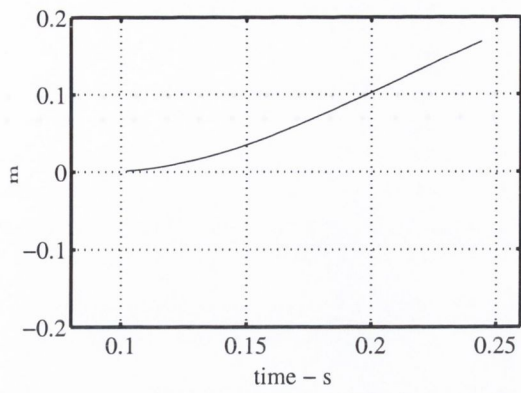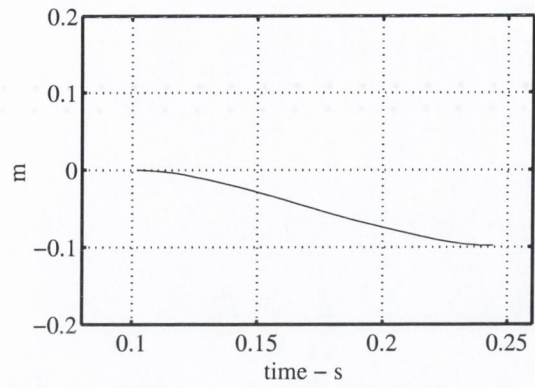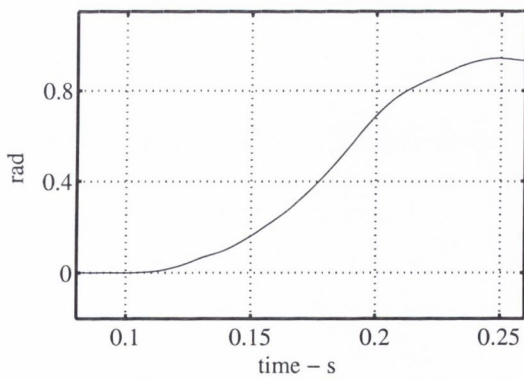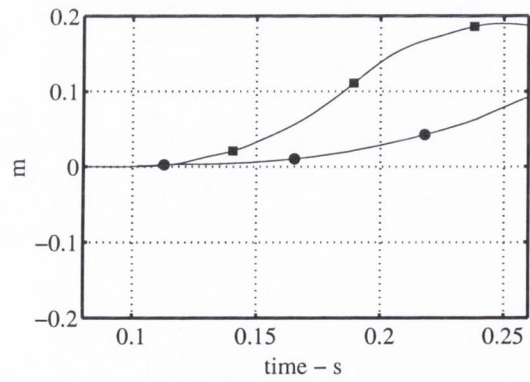
Figure 5.4: (a)–(d): X–direction displacements: (a) P_{sled}, (b) $P_{head/sled}$, (c) P_{head}, (d) P_{sled} (•), $P_{head/sled}$ (▲) and P_{head} (■); (e) θ_{head} and (f) P_{head} (•) and θ_{head} (■) – not to scale.

92

Discussion

After impact, X–direction motion of the sled occurs. The velocity increases for 50ms after which a steady speed is maintained. The high inertia of the head causes its displacement to lag behind sled motion. The result is that COG_{head} travels rearward relative to the sled. The sled and head are at rest prior to impact and inertial loading at the TMJ is thus a function of its kinematic behaviour relative to a fixed reference frame rather than a frame fixed in the sled. (This is not the case for the neck, which also experiences direct loading corresponding to the spatial relationship between the head and shoulders). Thus the critical factor for the TMJ is its displacement relative to a fixed reference frame. Total X–direction head displacement (P_{head_X}) is equal to the algebraic sum of sled displacement and COG_{head} displacement relative to the sled. A considerable degree of cancellation occurs: as the sled travels forward, relative motion of the head is rearward. From figure 5.4 it is clear that P_{head_X} is small during the entire retroflexion sequence of the head.

Equations 5.5 and 5.6 were used to calculate TMJ displacements from head displacements, see figure 5.5a&b. TMJ displacements differ from head displacements only due to head rotation. It can be seen that the maximum X–direction displacement of the TMJ occurs gradually throughout the retroflexion sequence and this accounts for the low level of acceleration measured using accelerometers located at the TMJ, see figure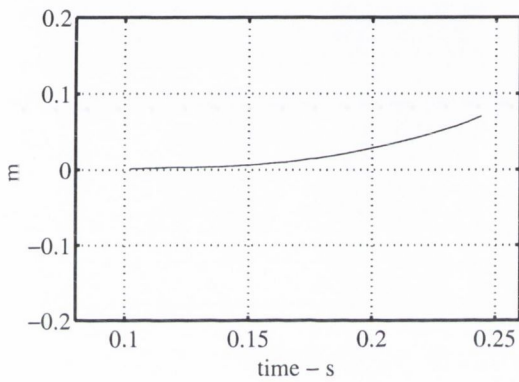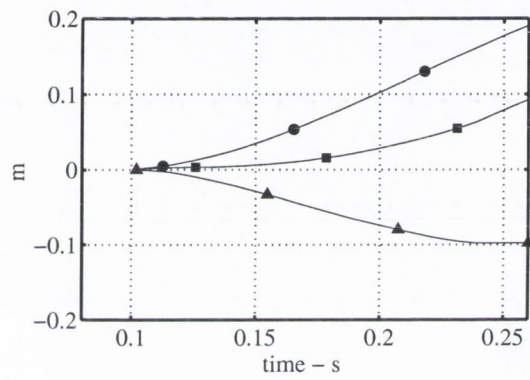 5.2. After impact, head rotation causes +Z displacement of the TMJ until retroflexion is almost complete, see figure 5.5b. The TMJ lies anterior to the COG_{head} and Z–displacement of the TMJ is less than that of COG_{head}. These results are not surprising: high inertia causes the head response to minimise its kinetic energy. This is achieved by reducing the linear velocity $(\dot{P}_{head_X}, \dot{P}_{head_Z})$ and angular velocity $(\dot{\theta}_{head})$ of COG_{head}. The TMJ lies close to the COG_{head} and experiences correspondingly low displacements. The reliability of these measurements can be judged by numerical manipulation of the data to give estimates of the X and Z–direction components of TMJ velocity. Comparison of the integrated acceleration measurements with differentiated displacement cal-

93

(a) X   (b) Z
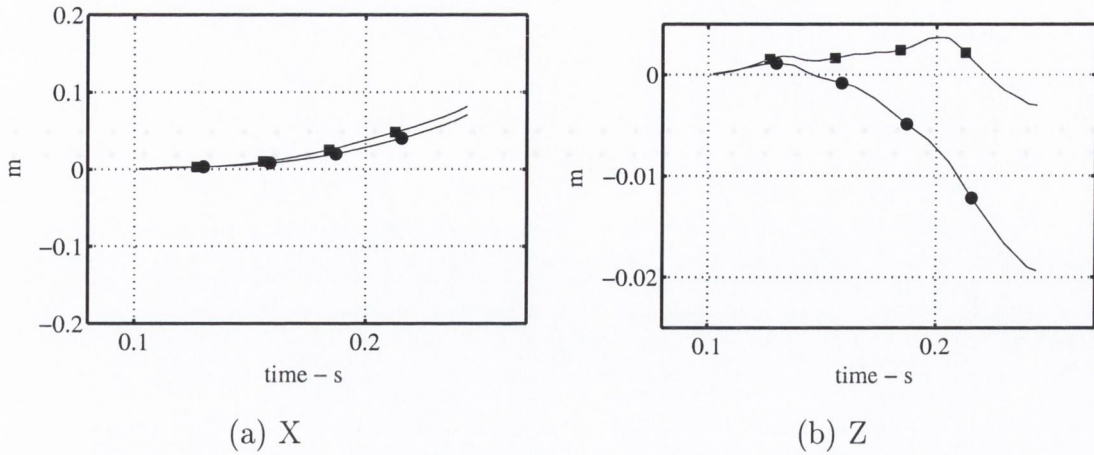
Figure 5.5: TMJ_X and TMJ_Z displacements (■) compared to COG_{head_X} and COG_{head_Z} displacements (•).

culations provides a good basis for validating these measurements, see figure 5.6. The high–frequency noise and low–frequency drift that characterise numerical differentiation and integration respectively are present in these computed velocity traces, but it can be seen that there is close agreement between both sets of data. It is concluded that there is good accuracy in these experimental measurements.

(a)   (b)
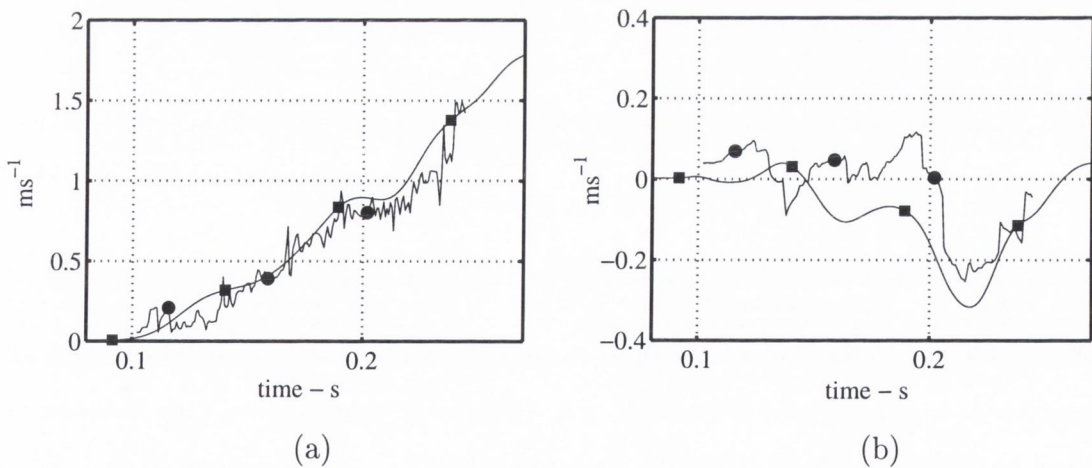
Figure 5.6: $\dot{P}_{TMJ_X}$ and $\dot{P}_{TMJ_Z}$: integrated acceleration data (■) and differentiated displacement data (•).

94

5.3 ICR Calculations

Typical X and Z time–histories of the computed locus of ICR_{head} are shown in figure 5.7. During retroflexion, the locus migrates from a superior and posterior location to close to the TMJ and then to a superior and anterior location, see figure 5.8. A clearer indication of ICR behaviour is given in figure 5.9. It can be seen
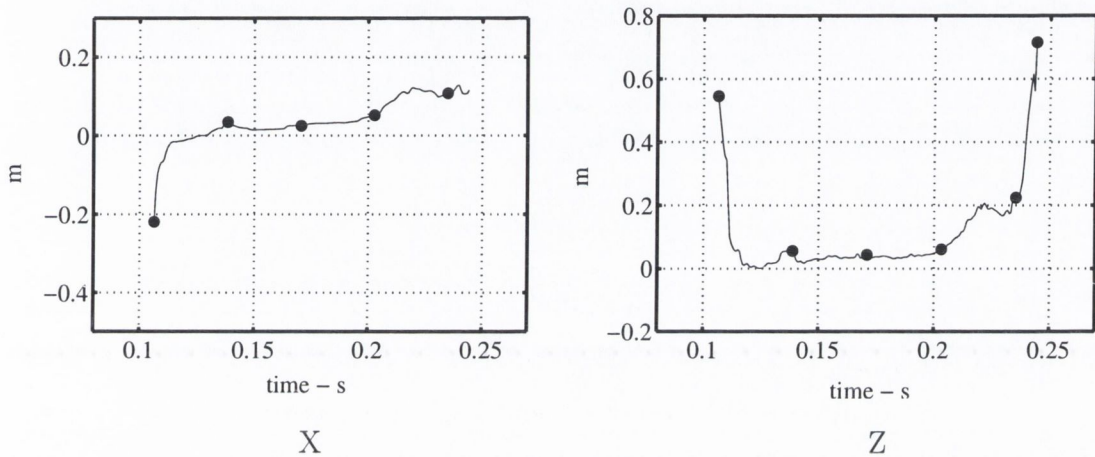
Figure 5.7: X and Z displacement components of ICR_{head} during retroflexion.

that during the early and late stages of retroflexion (from t = 0.102s to t = 0.130s and from t = 0.223s to t = 0.243s) the locus of ICR_{head} lies far from the TMJ. However, during the majority of the retroflexion period (from t = 0.130s to t = 0.223s), the ICR_{head} lies close to the TMJ. When $\dot{\theta}_{head}$ is not significant, the ICR lies far from the TMJ. As $\dot{\theta}_{head}$ increases, the ICR is rapidly pulled in closer to the TMJ. As $\dot{\theta}_{head}$ decreases again to zero at maximum retroflexion ($t = 0.180s$), the locus of the ICR once again migrates away from the TMJ. There are considerable difficulties associated with ICR measurements, and the resulting locus is highly sensitive to instrumentation error. The greatest ambiguity occurs during the initial and final stages of retroflexion, when $\dot{\theta}_{head}$ is small. The ICR does not necessarily lie within the body and by definition ICR_{head} must lie at infinity when $\dot{\theta}_{head} = 0$. The resolution of the instrumentation used to calculate P_{sled_X} and $P_{head/sled_X}$ was limited by the crenellated strip over which the slotted opto–switch passed. The tooth and gap widths were each 0.001m and the resulting resolution was ±0.001m.
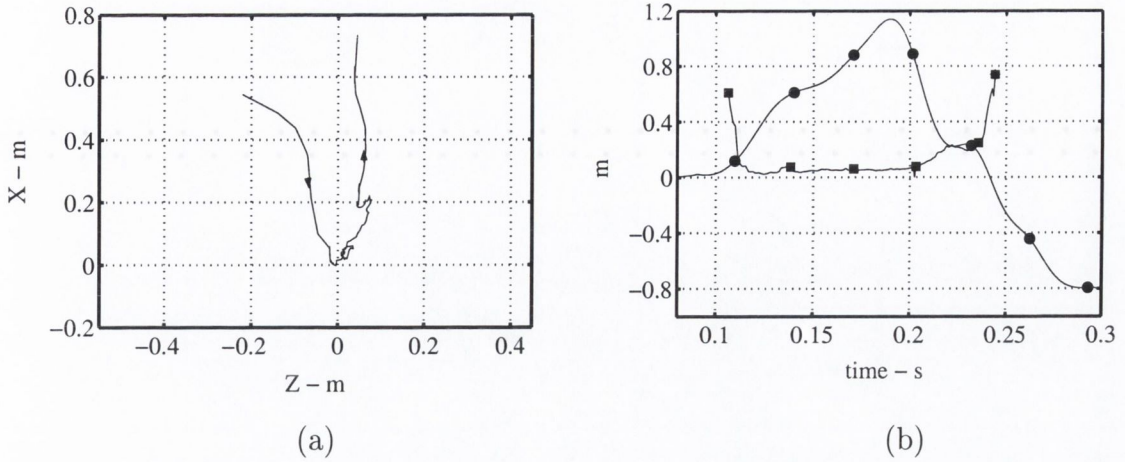
Figure 5.8: (a) Locus of ICR_{head}; (b) distance from TMJ to ICR (■) and $\dot{\theta}_{head}$ (•) – not to scale – during retroflexion.

This is sufficient to cause considerable error in the locus of ICR_{head} during the initial stages of retroflexion. However, the magnitude of error is dramatically reduced as $\dot{\theta}_{head}$ increases.

There is some conflict between the accelerometer data and the computed locus of ICR_{head} during the initial stages of retroflexion. According to figure 5.3, loading is compressive throughout retroflexion. In contrast, the ICR_{head} measurements indicate an initial tensile load as the ICR lies to the left of the TMJ and direction of head rotation is anti–clockwise, see figure 5.9a. The most likely explanation for this inconsistency is that the actual loading is minor, as the measured displacements indicate. The measured TMJ accelerations at the onset of retroflexion are small and fluctuating while the ICR measurements are unreliable because $\dot{\theta}_{head}$ is small. The result is that the two measurements err each side of zero.

96
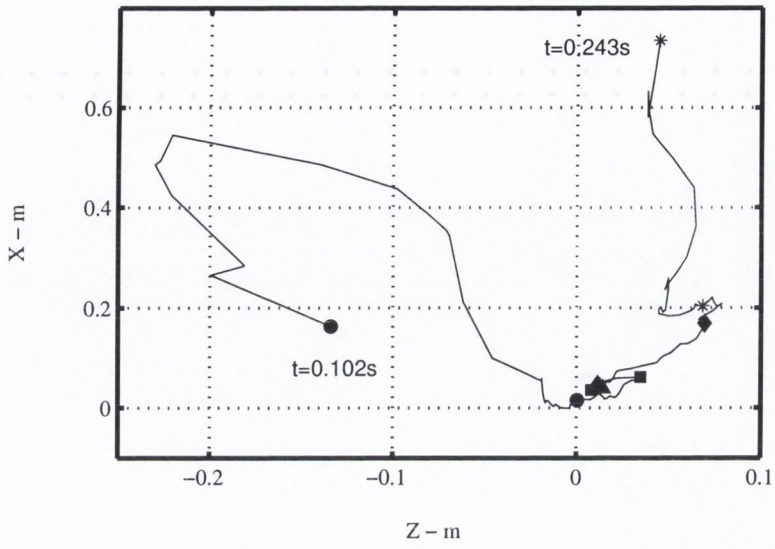
(a)
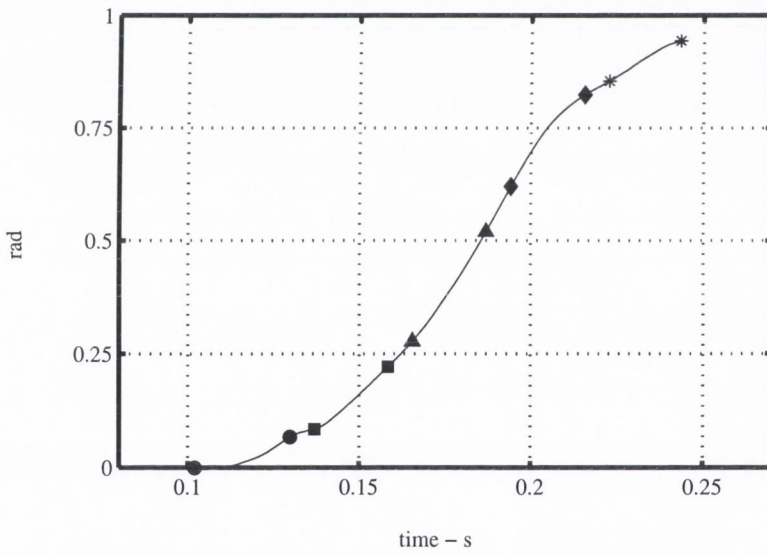
(b)

Figure 5.9: (a) Locus of ICR$_{head}$; (b) θ_{head}: t = 0.102s–0.130s ($\bullet$), t = 0.137s–0.159s ($\blacksquare$), t = 0.166s–0.187s ($\blacktriangle$), t = 0.194s–0.216s ($\blacklozenge$), t = 0.223s–0.243s ($\star$).

Chapter 6

Cadaveric Specimen Testing

It has been proposed that rapid excessive mouth–opening occurs because the mandible does not keep up with head motion during the retroflexion sequence of whiplash [51, 31, 52, 23]. During physiological mouth–opening, rotation is accompanied by anterior translation of the condyles towards the crest of the articular eminence. Supporters of the proposed Inertial Injury Theory (IIT) have claimed that when this occurs rapidly, stretching or tearing of the soft–tissue components in the joint occurs due to hypertranslation of the condyles, see appendix B. Function and dysfunction of the TMJ is strongly dependent on its structural and material properties as these determine response characteristics to external loading. This can be used to assess the likelihood of internal joint derangement during the whiplash sequence.

Detailed qualitative descriptions of TMJ morphology [89, 53, 100, 101] have not been followed by quantitative analyses and there is little published information regarding either structural or material properties of the joint. Variable collagen content, fibre orientation and geometry of the TMJ preclude the adaptation of existing data from tests on other ligamentous materials. The task of acquiring this information is complicated by the unavailability of *in vivo* human TMJ's for dissection and the uncertainty of tissue alterations occurring in *in vitro* specimens. Further, due to geometric complexity, knowledge of individual material properties does not easily equate to overall structural understanding. Similarly, measuring

macroscopic joint behaviour masks the contributions of individual structures in the joint. Finally, it is not sufficient to determine quasi–static joint properties: the short time–frame of the whiplash incident dictates that tissue properties under dynamic conditions may also be important (quasi–static refers to purely elastic properties, and excludes all visco–elastic effects). All of this information is crucial to this thesis and an attempt has been made to address some of these omissions.

6.1   Specimen Storage

In vivo human specimens are clearly not available for mechanical testing and an alternative must be found. Human cadaveric specimens are the only feasible choice while remaining within an engineering environment, although some very useful information could certainly be achieved through testing with *in vivo* primates. A mixed–gender sample of five cadaveric TMJ specimens was used in this investigation. The exact histories of these specimens were not available, but all were preserved in a 10% formalin solution. The impact of this mode of storage on the tissue properties needs to be addressed as there are postmortal morphological, chemical and mechanical changes and these may interact with each other.

Several researchers have investigated the effects of preservation on the mechanical properties of soft–tissue specimens. Hirsch & Galante [102] tested annulus fibrosis specimens from human intervertebral discs and found that immersion in aqueous solution caused tissue swelling that significantly affected the mechanical properties of the tissue. Elongation was found to have increased by nearly 65% while residual deformation had doubled and energy dissipation had increased by a factor of three during tensile testing. These are serious changes and direct immersion of the specimen in aqueous solution is clearly not a successful means of preservation for mechanical testing. Hirsch & Galante [102] also found that exposure to air resulted in progressive weight loss in all samples due to evaporation and this also compromised tensile properties. The most successful procedure was freezing of the samples under a CO_2 snow and thawing at a relative humidity of 100% before testing.

However, the latter method was not available for this study and an alternative was required. The TMJ's used in this investigation were not dissected prior to testing. A protective layer of skin and other fatty tissue surrounding the joint absorbed liquid and provided a physical block between the joint and the aqueous solution. This prevented swelling of the joint tissues. Increased elasticity of the surrounding layers of skin due to swelling is not important since human fascia lata already has highly elastic properties [103] and does not significantly influence joint stiffness. Viidik et al. [104] found that although other researchers claimed that ligaments lose their mechanical properties within two hours after death, most of these had stored their samples in air. In contrast, Viidik et al. [104] stored their ligaments within intact and closed knee joints in formaldehyde until testing was due to commence. They found no changes after four days storage at room temperature, and that collagenous tissue was resistant to autolysis. This indicates that cadaveric tissue stored in formaldehyde is resistant to mechanical changes if the sample is surrounded by a sacrificial layer of fatty tissue.

6.2   Experimental Objectives

The geometry of the TMJ is complex but the locations of the principal structures within the joint are well established. This geometric information, combined with data regarding the material properties of the principal structures, could be used to construct a model of dynamic behaviour of the TMJ. However, material properties of individual joint structures can only be measured accurately using specimens of uniform length and cross–sectional area (CSA) and by applying load along the long–axis of each structure. This was not feasible because none of these structures had uniform length or CSA and attempts at measuring these parameters are subject to error. In addition, stretching along the long–axis involves clamping both ends of each tissue and this causes problems with slippage at the clamp/tissue interface. Such an approach would require a considerably larger sample size than was available.

Testing Mode

The difficulty in obtaining cadaveric samples dictated a degree of compromise: not all parameters of interest could be measured and a specific focus needed to be established. The Inertial Injury Theory states that damage occurs due to anterior hypertranslation of the condyles. The direction of this motion is shown in figure 6.1. Uni–axial stretching of the TMJ along this axis yields the stiffness of the joint in that direction.

(a)   (b)
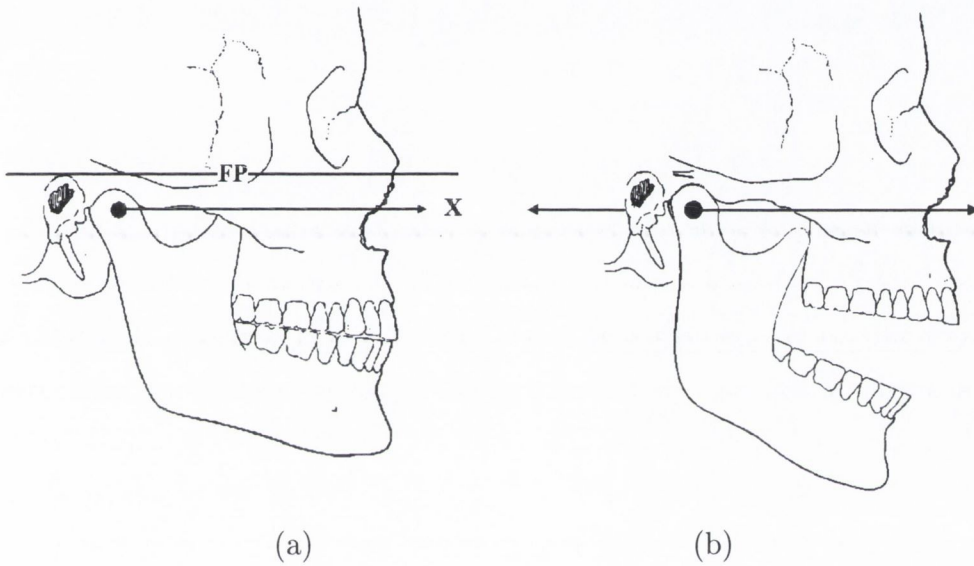
Figure 6.1: (a) Orientation of stretch–axis (X) and the Frankfort plane (FP). (b) Stretch direction with mouth open.

This method characterises structural rather than material properties of the joint. It is then no longer necessary to remove each tissue from its in situ location, measurements of lengths and CSA become unnecessary, and the overall structural stiffness in the direction of stretch is directly measured. Structural stiffness is defined here in terms of Hooke's Law: i.e. the ratio of uni–axial force to displacement in a given direction. Displacement within the joint caused by a given external load can then be calculated. This process is less complete than measuring material properties of the individual structures, but it provides sufficient information to determine

whether overall joint displacement for a given load remains within physiological limits. The Frankfort plane is the horizontal plane of the skull normal to the sagittal plane and the orientation of uni–axial stretch was chosen to be parallel to this, along the axis of proposed anterior condylar motion, see figure 6.1a.

Mouth–opening

Sled–tests with the dummy showed that mouth–opening and closing occurred during retroflexion. The effect of this on the force–extension characteristics of the TMJ required investigation, but reproducing this motion during a tensile test was not realistic. Instead, tests were performed with a number of fixed levels of mouth–opening, see figure 6.1b. The maximum level of mouth–opening measured on the dummy was $19°$, see section 4.1. The fixed angles of mouth-opening chosen for the cadaveric tests were $0°$, $5°$, $10°$ and $15°$.

Tissue Dissection

Stability in the TMJ is provided by several reinforcing structures, see appendix B. The relative importance of these was investigated by progressive dissection of the samples at the end of each testing process. The structures were dissected incrementally and force–extension tests were carried out at each stage. Individual strength contributions could then be estimated from resulting changes in the force–extension curve. Distal tissue was necessarily excised first, and the order of dissection is given in table 6.1. This permitted an assessment of the relative contributions of the respective joint structures to overall stiffness.

1	lateral ligament
2	lateral capsule
3	2/5 of the posterior attachment
4	medial capsule, but synovial membrane still complete
5	all tissue except the remaining posterior attachment removed

Table 6.1: Order of tissue dissection.

6.3   Experimental Setup

The Instron

Uni-axial force–extension tests were performed using an Instron 1011 tensile loading machine fitted with a 50N load transducer. This provides position control and a load read–out. The maximum extension speed was limited to 500mm/min: thus only quasi–static tests could be carried out on this machine. The extension–rate for all tests was 10mm/min.

Acrylic Mounting

Each specimen was mounted in cold cure dental acrylic blocks which provided a flat surface for connection to the Instron grips. Figures 6.2 and 6.3 show a schematic and a photograph of a mounted specimen respectively. Each specimen consisted of a section of temporal bone (A), the external auditory meatus (F) and a portion of the mandible (B). The articular eminence (C), condyle (D) and coronoid process (E) are obscured by soft–tissue, but the posterior border of the mandible is clearly discernible. The acrylic mounting blocks (G and H) were attached to the upper and lower Instron grips respectively. All muscle tissue entering the capsule was dissected.

Details of the Experimental Rig

The lower Instron grip is fixed, while the upper grip moves vertically (in the X–direction) during testing. The acrylic mounting blocks (G and H) were rigidly connected to the Instron grips and this ensured that the applied axial load passed through the TMJ with zero bending moment, see figure 6.3.

It was necessary to facilitate the curved motion of the condyle as it moved on the articular eminence: axial load from the Instron was applied in the X–direction but forward translation of the condyle is accompanied by Z–direction motion of the condyle due to the slope of the articular eminence (see figure 6.2). This movement was facilitated by a sliding mechanism (K) located between the mandible and

103
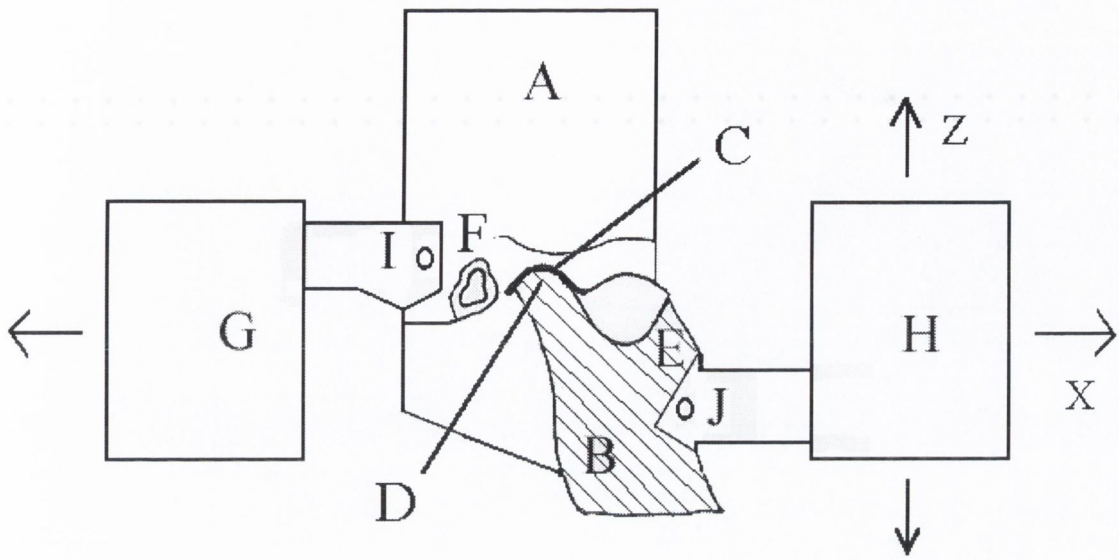
Figure 6.2: Schematic of sagittal section of mounted specimen showing bony components mounted between acrylic blocks.

the lower Instron grip, see figure 6.3. Precision guide rods and linear bearings housed in an aluminium block permitted friction–free sliding of the mandible in the Z–direction.

A hinge–block located between the upper Instron grip and block G was used to vary the relative angle between the skull and mandible for the mouth–opening tests, see figure 6.3. Set–screws were used to lock the mandible at any desired angle up to a maximum of 15°. Mouth–opening altered the position of block H relative to the lower Instron grip and this was accommodated via the sliding mechanism previously described.

Mounting Procedure

The Frankfort plane was identified and the correct occlusal relationship between the mandible and skull was marked. Holes were drilled in the temporal bone and mandible at I and J respectively (see figure 6.2), and 4mm steel pins were inserted as anchor points. The specimen was then clamped with the Frankfort plane oriented vertically. Temporary shuttering was constructed around the steel
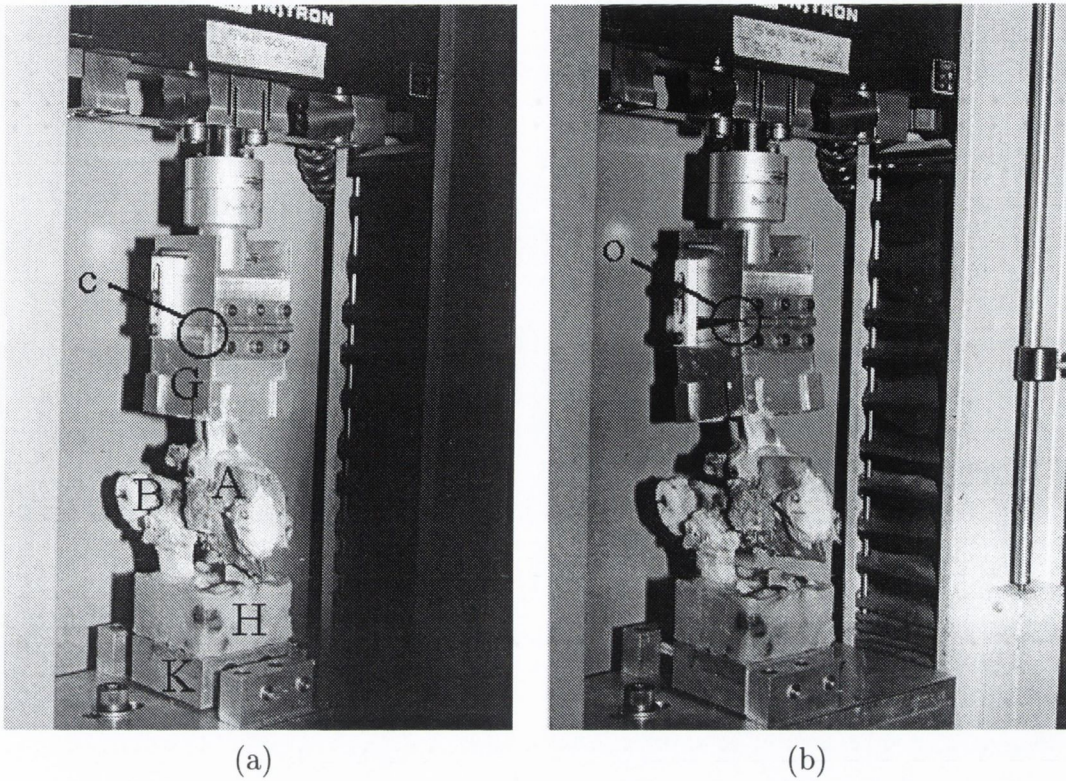
Figure 6.3: Specimen mounted in tensile loading machine: (a) mouth closed (c);
(b) mouth opened 15° (o).

pin at I and filled with acrylic mix. When set, the specimen was rotated through
180° and the procedure was repeated at J. This provided two strong acrylic rods
protruding from the skull and mandible. These were then set into blocks G and H
using a similar method, see figure 6.3. The samples were mounted in the Instron so
that the load read–out was zero prior to each test. Each specimen was a different
size and the rest–position of the upper Instron grip varied accordingly.

6.4 Results

6.4.1 Standard Force–elongation Tests

Force–extension curves under quasi–static conditions are presented first. Three specimens were tested in the mouth–closed configuration. The first (sp1) was damaged during preliminary testing. Typical results for the second (sp2) are shown in figure 6.4. Each of the six curves nominally represents the same test: after each force–extension cycle the upper Instron grip was lowered to the original rest position and the test was repeated. It can be seen that there is some variation between equal tests on the same specimen, and this proved characteristic of all soft-tissue testing.
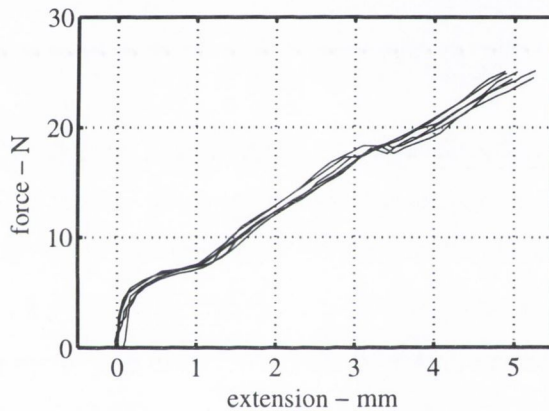
Figure 6.4: Force–extension, mouth closed, unedited: sp2.

A number of characteristics can be identified. The beginning of the curve has a high slope, but this is an artefact of the experimental procedure and can be explained. The geometry of each specimen varied so the zero–stretch distance between the Instron grips was found empirically for each specimen after it had been mounted in the Instron. However, because the sample was mounted vertically, when the upper grip moves during testing, the load measured by the Instron includes the mass of the upper half of the specimen and its attachments. The method of adjusting the upper Instron grip in the rest position until the load read–out is zero causes the mass of the skull section to be initially supported by

the lower portion (the mandible). As the skull section is lifted during testing, its mass is then carried by the upper Instron grip, causing the rise in load evident at the onset of testing. This is clearly not part of the structural stiffness of the TMJ and must be factored out. The exact mass of the skull section is difficult to measure as much of the tissue originates in the skull and inserts into the mandible, making it difficult to judge where the mass is held. However, as all specimens were subsequently stretched to failure, the final mass of both sections could be measured. This provides a good estimate of the original mass, even though soft tissue around the joint has been dissected, see table 6.2. The large variation in mass between specimens is due to differences in the amount of surrounding bone included and is not a reflection of anatomical differences between samples.
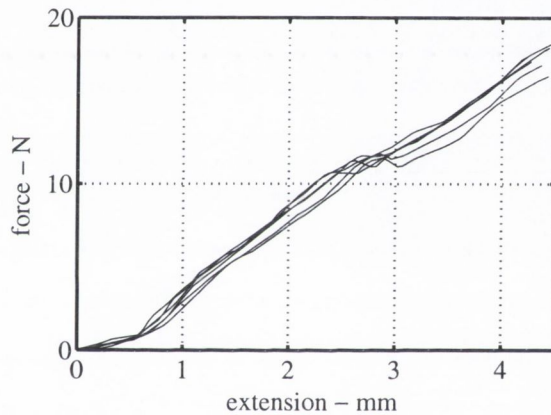

Figure 6.5: Force–extension, mouth closed: sp2.

	Acrylic block and aluminium hinge assembly (kg)	upper joint portion (kg)	total mass (kg)	Offset weight (N)
sp2	0.4876	0.193	0.6806	6.68
sp3	0.4876	0.260	0.7476	7.33
sp4	0.4876	0.05	0.5376	5.27

Table 6.2: Masses of the rig components.

It can be seen from figure 6.4 that some of the curves do not begin at the origin: there is some extension (always less than 1mm) without a resisting load. This is due to slack within the TMJ and has also been factored out to allow better comparison between tests. The data in all subsequent graphs is presented with both load and extension offsets factored out: figure 6.5 presents these alterations applied to the data from figure 6.4.

The resulting curve shows three linear regions. The first section of the curve (up to 0.6 mm stretch) shows a gentle slope (1.38N/mm), followed by 2mm of linear load increase at a higher rate (5.17N/mm). At 3.3 mm stretch, tissue slippage occurs and this results in a discontinuity in the curve. Each specimen was rigidly mounted in acrylic, so slip occurred within the TMJ rather than at the specimen/acrylic interface. The cause of this was difficult to ascertain, as access to the TMJ was obscured by the capsule. It may be the equivalent of *in vivo* clicking, where during mouth–opening the disc is first anteriorly displaced from its normal position over the condyle and then jumps back to its original position with an audible click, see appendix B. It may also result from contact between the lateral ligament and the lateral pole of the condyle: as the condyle moves anteriorly during stretching, the ligament may be pulled forward by the lateral pole until it develops sufficient resistance and returns to its normal position.

However, the effect of this discontinuity on the overall force–extension curve is not significant and there is a broadly linear increase in load as the condyle approaches the crest of the articular eminence. The slope of the curve before and after the discontinuity is the same, suggesting that after some internal rearrangement the same stretch–pattern continues. There is no evidence of an increase in the slope of the curve as extension reaches 5mm. An increase in slope would suggest the approach of the elastic limit and its clear absence confirms that 5mm extension lies within physiological limits. This is an expression of the fact that during normal mouth–opening the condyles travel anteriorly to the crest of the articular eminence.

The same tests were carried out on specimen 3 (sp3) and specimen 4 (sp4), see figure 6.6a&b. Considerable variation between the three samples is evident.
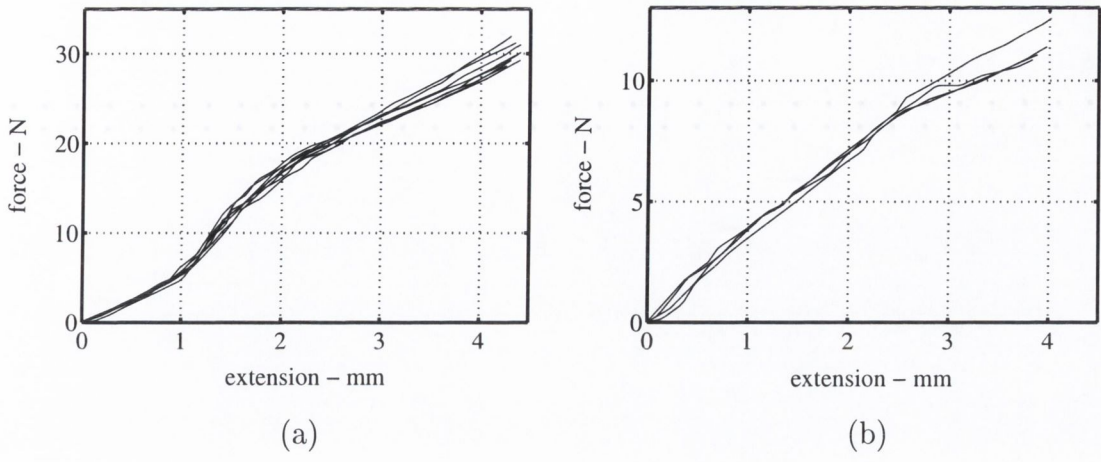
Figure 6.6: Force–extension, mouth closed: (a) sp3; (b) sp4.

Figure 6.7 shows averages for each of the three specimens. Sp3 is clearly far stiffer than the two others: more than twice the load is required to cause 5mm anterior displacement of the condyle for sp3 compared with sp4. This is most likely due to the considerable variation in geometry between different TMJ's, even between the two halves of the same joint [89]. Subsequent inspection of the articular surfaces revealed that the slope of the articular eminence varied between samples and this affected the load required to cause anterior displacement of the condyle. A steeper sloping eminence is more resistant to anterior motion of the condyle.

Figure 6.7: Force–extension, mouth closed: sp2 (■), sp3 (▲) and sp4 (●).

6.4.2 Mouth–opening Tests

The effect of mouth–opening on the foregoing force–extension tests was investigated using the experimental setup described in section 6.3. The relative angle between the mandible and skull was set to 0°, 5°, 10° and 15°. Figures 6.8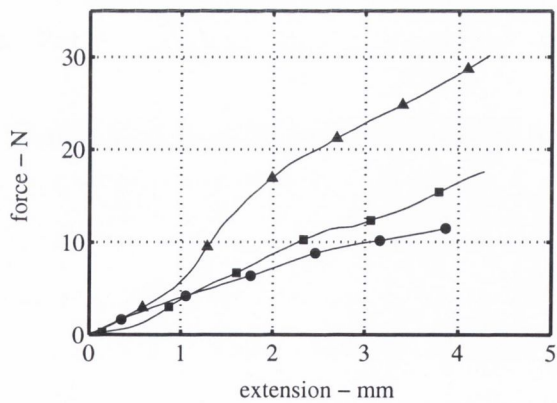 and figure G.1 in appendix G show the results of these tests for sp3 and sp4 (sp2 was not tested in this manner): (a)–(e) show repeated tests at fixed angles of 0°, 5°, 10° and 15° respectively, while (e) shows the averages of these. Mouth–opening causes no major changes in the force–extension characteristics of the specimens tested, but a number of features can be identified. The characteristics for sp3 and sp4 are broadly similar.

Specimen 3

There was good repeatability between similar tests for this specimen. Increasing mouth–opening increases the stiffness during the first 1.5 millimetres of stretch, but substantially decreases the joint stiffness as the extent of stretching is increased to 5mm. The overall effect of mouth–opening is a reduction in resistance to protrusion of the condyles, see figure 6.8e.

Specimen 4

Increasing the angle of mouth–opening produced no increase in stiffness during the first millimetre of stretch for sp4. There is more scatter in all data from these tests. However, the predominant trend of overall decrease in stiffness as the angle of mouth–opening is increased is clearly illustrated in figures G.1 and G.2 in appendix G.

Comment

The results show that mouth–opening facilitates protrusion of the condyles. The reason is that during physiological mouth–opening the condyles rotate and translate to reduce loading within the TMJ. Similarly, these tests on cadaveric specimens show that rotation of the condyles reduces the resistance to the translation

110
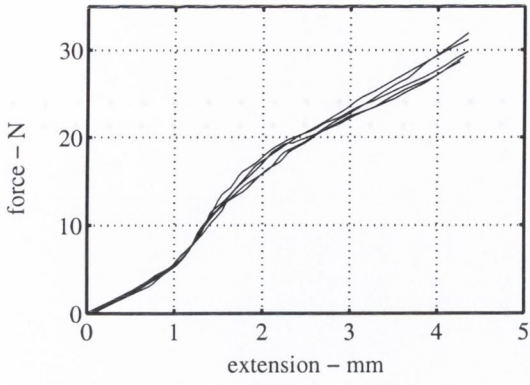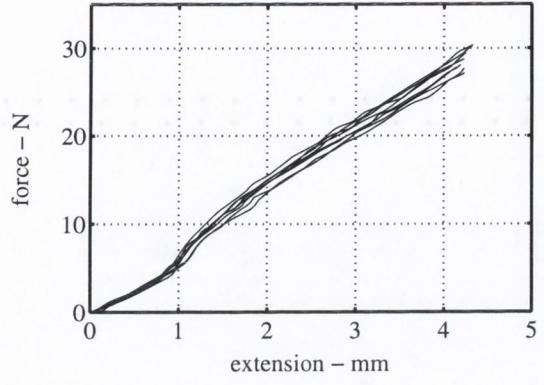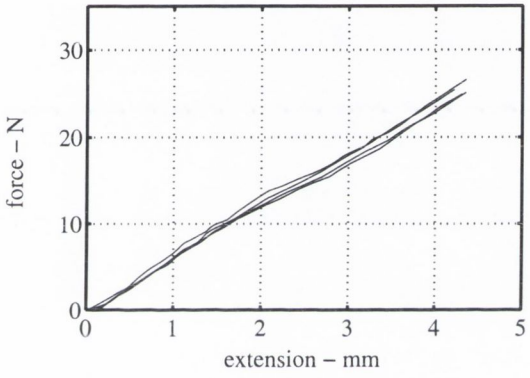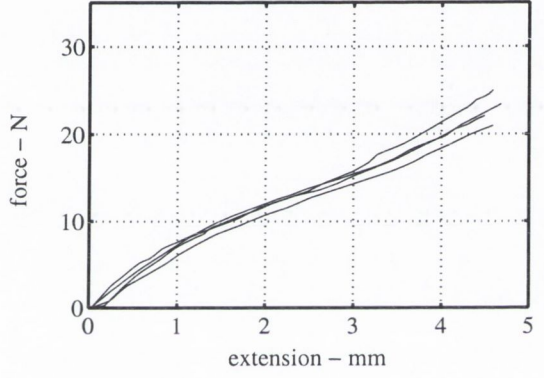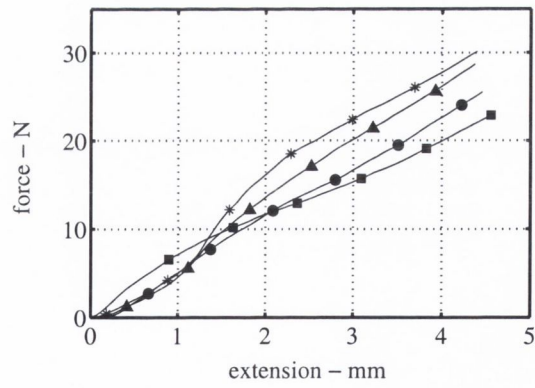
Figure 6.8: (a) – (d): Force–extension, sp3 at fixed mouth-opening angles; (e) averages: $* = 0°$, ▲$= 5°$, ●$= 10°$, ■$= 15°$.

necessary for mouth–opening. It should be noted that rotating the mandible in mouth–opening automatically causes some protrusion of the condyles and this is in addition to the 5mm protrusion occurring during the stretch test.

6.4.3   Tissue Dissection

The relative importance of individual joint structures was assessed by successive dissection of the joint tissues. The order of dissection is given in table 6.1: the lateral ligament was dissected first in all samples. Figure 6.9a–d shows the force–extension curves for sp3 from repeated protrusion tests with the lateral ligament dissected. Mouth–opening angles were set to $0°$, $5°$, $10°$ and $15°$ respectively. Figure 6.9e shows the average of each of these. Figure G.5 in appendix G shows the same results for sp4. The lateral ligament is composed of stiff collagenous fibres and is the primary ligamentous reinforcement of the TMJ. It is taut in almost all joint configurations, including the close–packed position [53]. Dissection of this ligament considerably reduces the stability of the TMJ, but its orientation is such that it provides least resistance to anterior motion: the latter places the ligament under compressive loading and collagenous materials have low compressive strength. However, there is sufficient CSA in the ligament to provide some resistance to condylar protrusion and it can be seen that the resisting force measured was reduced by ca. 20% after dissection of the ligament, see figure 6.10. The lateral ligament is connected close to the condylar neck. This is near the centre of rotation of the mandible for the first 10–15° (pure rotation stage). Thus mouth–opening would not be expected to affect the tension within the ligament and figure 6.10 shows that mouth–opening does not significantly alter the influence of the lateral ligament.

6.4.4   Final Dissection of each TMJ

The primary structures of the TMJ remaining after dissection of the lateral ligament are the posterior attachments, medial and lateral collateral ligaments and the capsular ligament. The results of sequential dissection of these from sp3 are

112
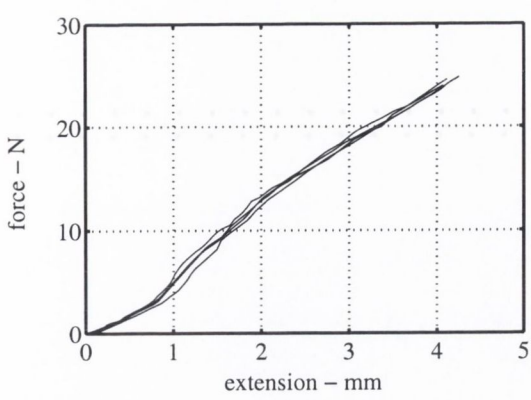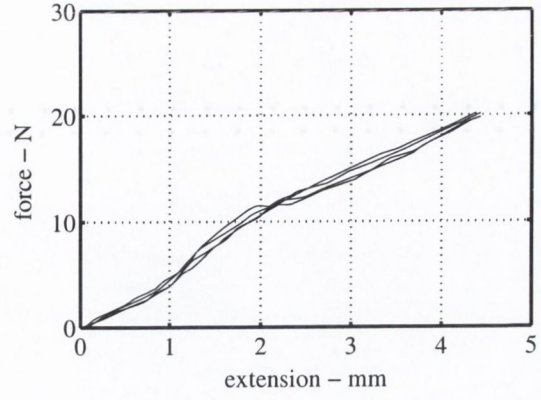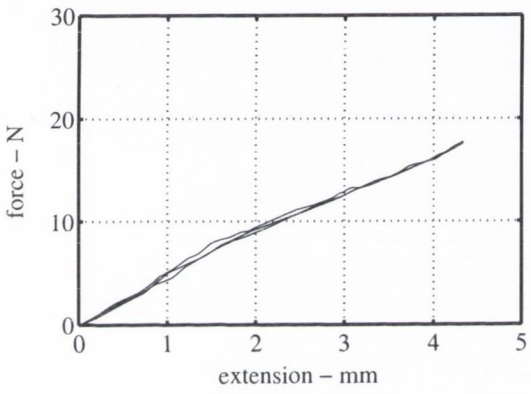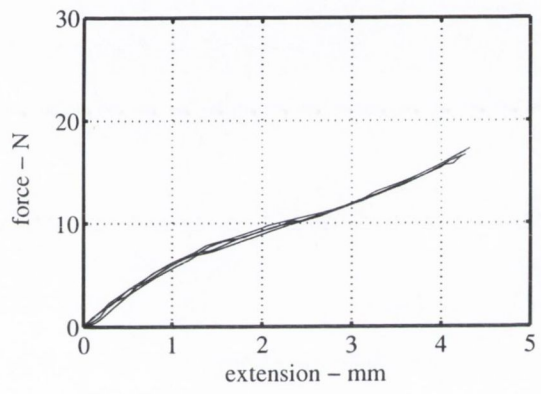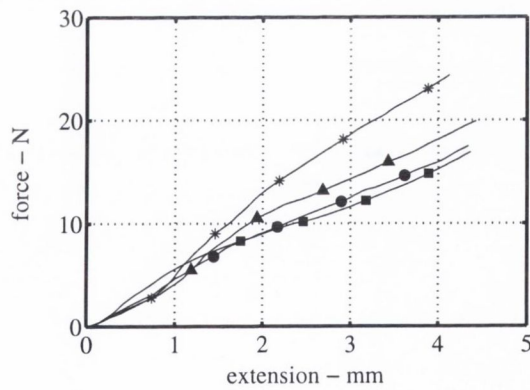
Figure 6.9: Force–extension, sp3, lateral ligament dissected: (a)–(d) mouth open; (e) averages: $* = 0°$, $\blacktriangle = 5°$, $\bullet = 10°$, $\blacksquare = 15°$.
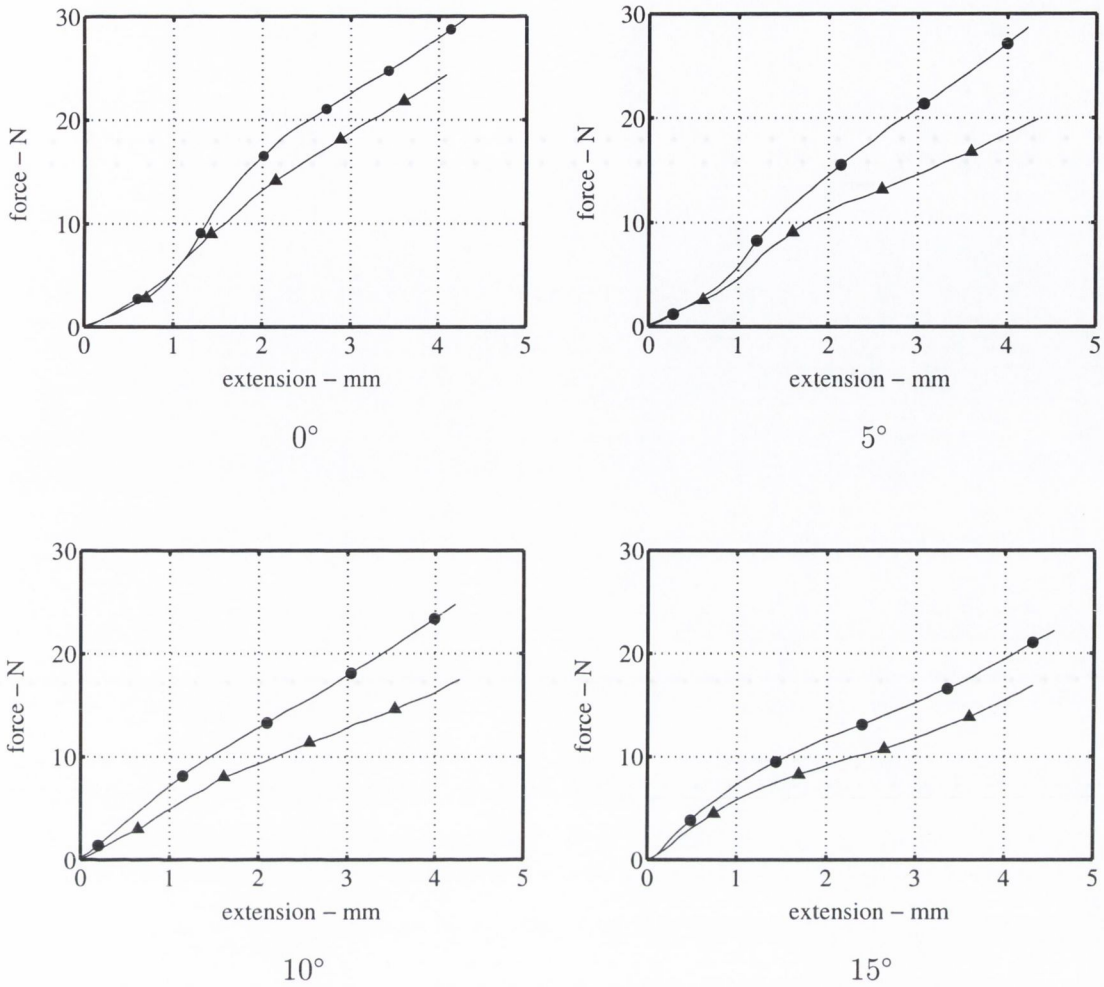
Figure 6.10: Force–extension, sp3: before (•) and after (▲) dissection of the lateral ligament.

shown in figure 6.11. The same tests were also performed on sp2 and sp4 and results from these are shown in appendix G, see figures G.6 and G.7.

The posterior attachments provide strong resistance to anterior motion of the condyle. When the only remaining tissues are 3/5 of the posterior attachments, considerable joint stiffness is still present (17N at 4mm stretch). The overall effect of tissue dissection is a steady decrease in the force required to cause protrusion of the condyle: there is no single structure responsible for resisting anterior hypertranslation. Instead, stability in the joint is derived from a combination of stretching of the posterior attachments and compression of the lateral ligament

114
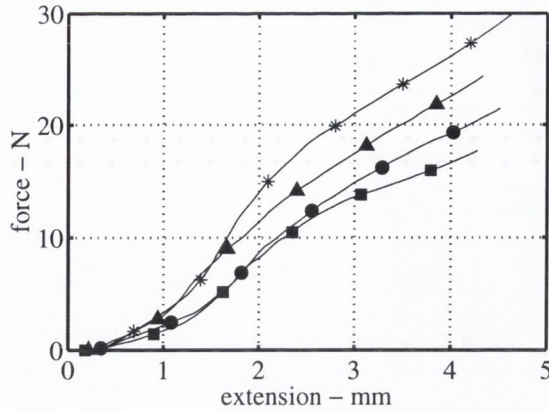
Figure 6.11: Dissection of sp3: * = complete joint. ▲ = lateral ligament removed, • = lateral ligament and lateral capsule, (including lateral collateral ligament) removed, ■ = lateral ligament, lateral capsule and 2/5 posterior attachments removed.

and the lateral and medial collateral ligaments. Figure 6.11 indicates that no single structure bears all of the load and so it is unlikely that damage will be incurred through excessive stretching or compression as a result of these relatively low forces.

6.4.5 Visco–elastic Tissue Properties

The quasi–static force–extension tests indicated that TMJ injury during whiplash is unlikely to result from excessive joint motion. However, non–rigid structures exhibit visco–elastic properties in which the response to loading is strain–rate dependent. The time-frame of a whiplash event is short and so it was necessary to determine whether visco–elastic tissue properties significantly influenced the loading pattern at the TMJ. Theoretical models describing features of elasticity in fluids began with the Maxwell model (mid–nineteenth century) and this was followed by the Kelvin and Voigt models. The basic building blocks of these are combinations of springs and dashpots arranged in series and/or parallel. These models are conceptual analogues of a wide variety of physical systems, and have considerably furthered understanding of biological tissue behaviour. Their suc-

115

cessful application involves some measurement of loss modulus (damping) in the tissue being measured.

Since then, a number of empirical laws predicting injury probability for a given strain–rate have been developed. These began crudely with the Acceleration and Force Criteria. Newton's Second Law forms the basis of the former, which resulted from Colonel Stapp's early experiments: Stapp measured human tolerance to high–g sled accelerations [105]. The Acceleration Criterion predicts severe chest injury if acceleration pulses of 3ms duration (or longer) exceed 60g. However, these tolerance estimations were based on sled accelerations rather than occupant kinematics. Eiband [106] used Stapp's data to demonstrate that tolerance could be inversely correlated to exposure duration.

The Force Criterion was developed after collaboration between General Motors and Wayne State University. Experimental crash–tests with cadavers were used to predict chest tolerance to distributed loads. However, it became clear that soft–tissue injury to vital organs was more critical for occupant survival than bone damage and that existing empirical laws regarding tolerance to force and acceleration were inadequate. Neathery et al. [107] developed the Compression Criterion which predicted critical chest compression as 40%. Above this value, multiple rib fractures are likely, thus exposing the lung and heart to serious injury.

Soft–tissue injuries can occur due to excessive deformation that is rate sensitive [108]. The Compression Criterion fails to account for this rate sensitivity and in response to this Lau & Viano developed the Viscous Criterion (VC) [108]. This predicts that the critical velocity for strain–rate type injuries is 3m/s. Below this level, actual compression is considered more critical than strain–rate when assessing the likelihood of serious soft–tissue injuries.

Visco–elastic Considerations for the TMJ in Whiplash

The foregoing injury criteria were developed to predict life–threatening trauma thresholds, and their applicability to TMJ injuries during whiplash has not been established. The retroflexion phase of head motion occurs over ca. 130ms: 5mm stretch in 130ms is a stretch velocity of only 0.38ms^{-1}. This is far below the

116

threshold level of 3m/s for the VC. However, the TMJ is not a vital organ and is exposed to the possibility of inertial damage from which the heart and lungs are adequately protected. It is therefore likely that the VC is not a suitable predictor for soft tissue trauma to the TMJ and independent tests were required to determine the significance of visco–elastic tissue properties.

The tensile testing machine used to perform the quasi–static force/extension tests described previously was not capable of applying the desired extension rates, and an alternative apparatus was required. A dynamic materials testing analyser (DMTA) was used to measure damping in the TMJ. This precision device is used in the polymer industry to provide dynamic stiffness and damping measurements over a range of frequencies. The testing temperature was set to 37°C (although the storage temperature prior to testing had been room temperature). Retroflexion of the head occurs over a period of 130ms. This is a close approximation to a 1/4 sine wave motion, and corresponds to a frequency of ca. 2Hz. The frequency range for the DMTA was thus chosen as 0–30Hz. The DMTA requires tissue samples whose approximate dimensions were 1 x 4 x 20mm. A single human cadaveric TMJ was used: the entire capsule and lateral ligament were excised and stored in a 10% formaldehyde solution. This tissue sample was cut into two strips for separate testing. The orientation of the fibres was not noted, but the properties of the sample were thought to be quite anisotropic. The strips were carefully clamped at either end and an actuator was then used to apply a predefined strain. The resulting load was measured and the accompanying software provided graphical information about tensile $\tan \delta$ and tensile $\log E'$ over the frequency range measured. The loss and storage moduli of the sample can then be readily calculated from the following definitions.

Elastic modulus:

$$E' = (\sigma/\varepsilon) \cos \delta$$

Storage modulus:

$$E'' = (\sigma/\varepsilon) \sin \delta$$

117

Complex Modulus:

$$E* = \sqrt{(E')^2 + (E'')^2}$$

Phase Angle:

$$\tan \delta = \frac{E''}{E'}$$

Tensile $\log E'$ and $\tan \delta$ for the two samples are given, see figure 6.12a&c and figure 6.12b&d respectively. Large experimental scatter is evident. The increase in elastic modulus over the 10min testing period is a result of moisture loss in the sample. Tan δ can be seen to decrease correspondingly, 6.12b&d. There is an increase in the elastic modulus of sample I as the excitation frequency is increased, see figure 6.12a, but this trend was not borne out in sample II, see figure 6.12c. The elastic modulus calculated with this mode of testing varied between 2MPa and 6MPa and showed no definite trend over the frequency range measured.

A comparison can be made between these values and the elastic modulus from the quasi–static force–extension tests. The CSA of the TMJ is difficult to measure but can be estimated at 15mm^2. The force at 5mm stretch varied between 13N and 35N (extrapolating from figure 6.6a). These correspond to stresses of 0.86 – 2.3MPa. Strain in the tissue fibres is also difficult to measure, but an extension of 5mm represents ca. 30% strain. The resulting elastic modulus is 2.8–7MPa. Thus there is good agreement between the two modes of testing.

Figure 6.12b&d shows that $\tan \delta$ varies between 0.11 and 0.21. From this, the maximum viscous contribution to the overall modulus was ca. 20%. The implication is that although there was evidence of strain dependent resistance to loading over the frequency range measured, the extent of this was not critical.
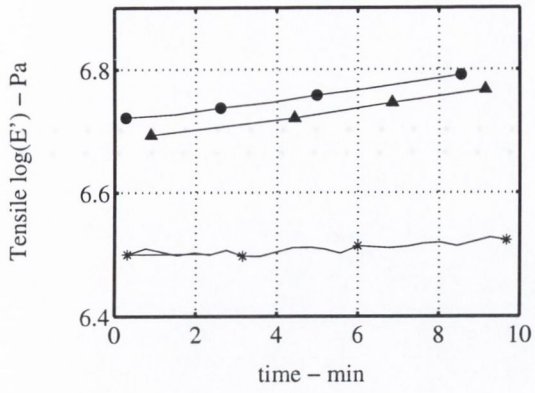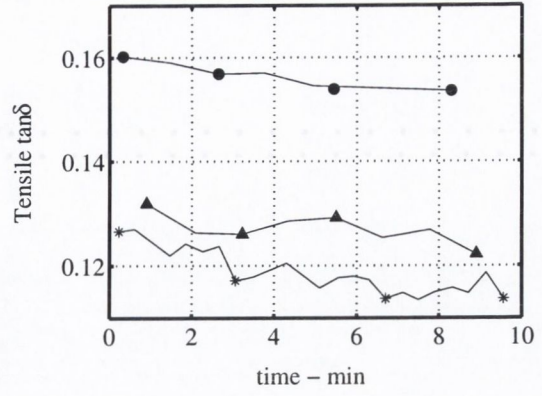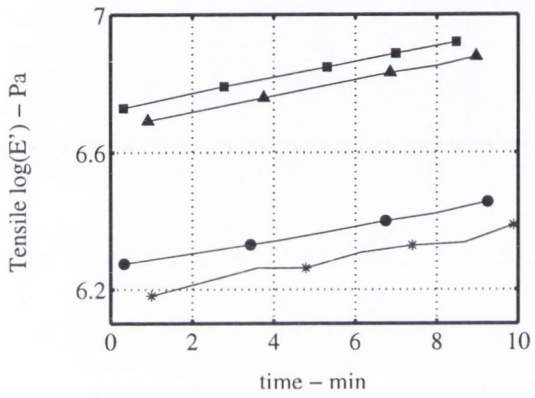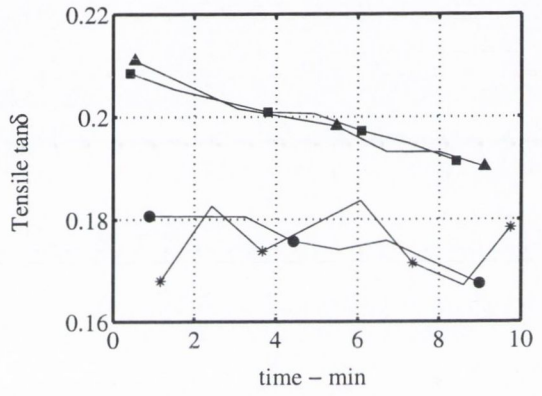
Figure 6.12: DMTA data: (a)&(b): sample I; (c)&(d): sample II; $*$ = 1Hz, $\blacktriangle$= 5Hz, $\bullet$= 10Hz, $\blacksquare$= 30Hz.

Chapter 7

Mathematical Models

The magnitude and direction of loading at the TMJ during the whiplash sequence need to be quantified. It has been acknowledged that experimental difficulties prevented measurement of relative acceleration between the head and jaw. The simple application of Newton's Second Law to find reaction forces at the TMJ was therefore not possible, and an alternative means was required. This chapter addresses the issue of TMJ reaction forces during functional biting using a free body diagram (FBD). A further mathematical model of the head and jaw is formulated using Lagrange's method for deriving the equations of motion of a system. The results of simulations using this model are compared to the experimental data. A parametric analysis was then performed to illustrate the stability of the model over a considerable range over parameter values. This model is then used to estimate TMJ loading during the retroflexion phase of whiplash.

7.1   Free body diagram

Early researchers were convinced that the mammalian TMJ is non load bearing [109, 110, 111, 112, 113, 114]. However, it has since been generally accepted that the TMJ *is* load bearing during functional movements [115, 116, 117, 118, 119, 120, 121, 122]. The design of the temporomandibular disc is ideal for load distribution across the articular surfaces [123], providing strong evidence favouring the theory

that the disc is load bearing, see appendix B. Experimental verification of this has proved difficult to obtain: Brehnan et al [118] used pressure sensitive foil inserted between the articular surfaces of the TMJ in macaques and found low-level loading (ca 13N) during molar chewing. However, the uncertainty in this measurement was stressed. Hylander [117] measured bone strain in the condylar neck and found qualitatively that the TMJ is loaded by a compressive reaction force during the power stroke of mastication, but failed to quantify the load.

A simplified model of the mandible during biting can be used to show that there is considerable loading across the articular surfaces in functional biting. Figure 7.1 shows a sagittal plane FBD of the mandible. The principal force generators during biting (masseter, medial pterygoid and temporalis muscles) and the corresponding reaction forces have been approximated as point loads. These are: occlusal or bite force (F_b) acting at an angle ϕ to the vertical, muscle force (F_m) acting at an angle θ to the vertical and the orthogonal components of TMJ reaction force (F_{j_x}, F_{j_z}). The line of action of tensile load in the temporomandibular ligament (F_l) is also shown. There is no load on this ligament during bilateral biting, see appendix B. For equilibrium, the sum of the forces in the X and Z directions and their moments about any fixed point are zero. Taking moments about the TMJ gives:

$$F_b r_b - F_m r_m = 0, \qquad (7.1)$$

where clockwise moments are positive, r_b and r_m are the respective moment arms of F_b and F_m about the TMJ, and the joint reaction forces (F_{j_x}, F_{j_z}) have no moment about the TMJ. Equation 7.1 and figure 7.1 show that the magnitude of the bite force F_b is less than the applied muscle force F_m by a factor of $\frac{r_b}{r_m} \cos(\theta - \phi)$. (This is a common physiological condition: skeletal muscle tends to act at a mechanical disadvantage.) A vertical force balance gives:

$$F_m \cos\theta - F_b \cos\phi - F_{j_z} = 0, \qquad (7.2)$$

and since equation 7.1 dictates that $F_m \cos\theta > F_b \cos\phi$, this implies that there must be a vertical compressive reaction force in the TMJ. Van Eijden et al [124] investigated muscle activation for various pre-defined bite-forces measured at the
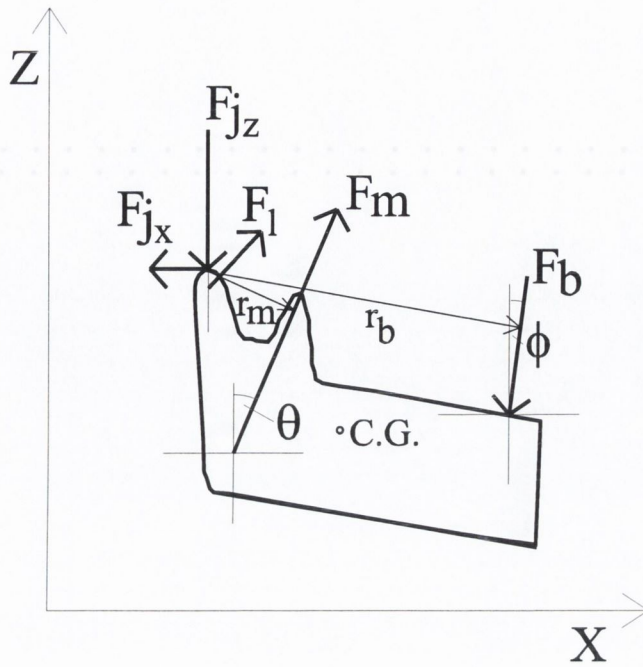
Figure 7.1: Free body diagram of the mandible during functional chewing.

second pre-molars and registered a maximum bite force of ca 606N $\pm$ 84N. If a bite force of 600N is applied and the angles $\theta, \phi \simeq 0$ and $r_b \simeq 1.5 r_m$, then by equations 7.1 and 7.2 the vertical reaction force at the TMJ will be ca 300N. The horizontal reaction force (F_{j_x}) is smaller:

$$F_m \sin \theta - F_b \sin \phi - F_{j_x} = 0. \tag{7.3}$$

The angles θ and ϕ will be small in most functional positions. The mechanical disadvantage of the muscle force dictates (as before) that $F_m \sin \theta > F_b \sin \phi$ and the horizontal joint reaction force required for balance is therefore compressive.

This FBD model is a major simplification : the actions of the digastric muscle and the lateral pterygoid should also be accounted for, see appendix B. Further, the force vector generated by the temporalis depends on the recruitment levels of its anterior and posterior fibres. However, this analysis does show that considerable vertical loading at the TMJ occurs during functional biting, and gives an indication of the resilience of the TMJ to external loading.

7.2 Kinematic Model

The experimental work presented can be used to construct a mathematical model of jaw behaviour during retroflexion of the head. Jaw kinematics are determined by its inertial characteristics, head motion and the biomechanical constraints linking the mandible to the skull. This is a classical dynamics problem and a mathematical model is a good auxiliary method of investigation. There are certain advantages of such a model over its physical counterpart, the principal one being that it allows a parametric analysis beyond that which can be achieved in a physical model. This provides a means to measure how small variations in structural, inertial or geometric properties are likely to influence the dynamic behaviour of the TMJ. In this manner, a mathematical model can be used to eliminate additional experimental work. The experimental evidence is used to calculate values for the model parameters: if the simulations show good correlation between the model and the dummy, then a parametric analysis using the model can be used to investigate the stability of the dummy. However, strict simplifications are necessary to allow the governing differential equations of the system to be derived. A number of techniques are available, and the Lagrangian approach has been applied in this analysis.

7.2.1 Model Setup

Lagrange's Method

Lagrange's method provides a systematic plan for writing down the equations of motion for any dynamical system. This involves finding expressions for the kinetic and potential energies of a system. Standard differentiation routines are then used to derive the equations of motion. In doing so, this method removes the need to recognise peculiarities within a given system: a rigid set of rules is simply applied. The rules for deriving the equations of motion from the energy functions are presented here, for a rigorous derivation see Synge & Griffith [99].

Let T and V be the kinetic and potential energies of a system respectively.

Then if q_i are the generalised coordinates,

$$\frac{d}{dt}\frac{\partial T}{\partial \dot{q}_i} - \frac{\partial T}{\partial q_i} + \frac{\partial V}{\partial q_i} = 0 \qquad (7.4)$$

There is one equation for each degree of freedom (DOF) of the system (one gener-alised coordinate is required for each DOF). When suitable boundary conditions are applied, these equations can be solved by numerical integration. In this inves-tigation a low order Runge–Kutta integration scheme was implemented using the ODE23.m routine in Matlab.

7.2.2 History

The literature contains one previous attempt at modelling the dynamics of the head, neck and mandible. Schneider, Zernicke & Clark [70] expanded an existing head–neck model developed by Tien & Huston [125]. Results of crash simulations using their jaw/head/neck model led them to predict very large angles of mouth–opening for simulated impact speeds of 6.71ms^{-1} and 13.41ms^{-1}: 1.17rad and 1.11rad respectively. Translation of the mandible was also reported. However, the biomechanical constraints produced by the muscles and ligaments were not included in this model as these parameters were unknown. Thus jaw motion in this model was governed by its inertial characteristics. The low inertia of the jaw coupled with the high strength of the elevator muscles strongly compromises the validity of these simplifications. In addition, there is no comment on their finding that a higher impact velocity produced a smaller peak jaw–opening angle. This result is certainly counter–intuitive, yet it is not addressed in their discussion.

7.2.3 Possible model types

The advantage of constructing a mathematical model on the basis of the forego-ing experimental work is that head kinematics (θ_{head} and its derivatives) during retroflexion have all been measured and can be used as input to the model. This has the dual benefit of reducing the complexity of the solution by one DOF as well

as eliminating complicated initial conditions. The values of θ_{head}, $\dot{\theta}_{head}$ and $\ddot{\theta}_{head}$ are read by the Matlab solver at each integration time–step.

It is desirable to begin mathematical modelling with a simple concept. Initial models considered are shown in figure 7.2. A number of assumptions were
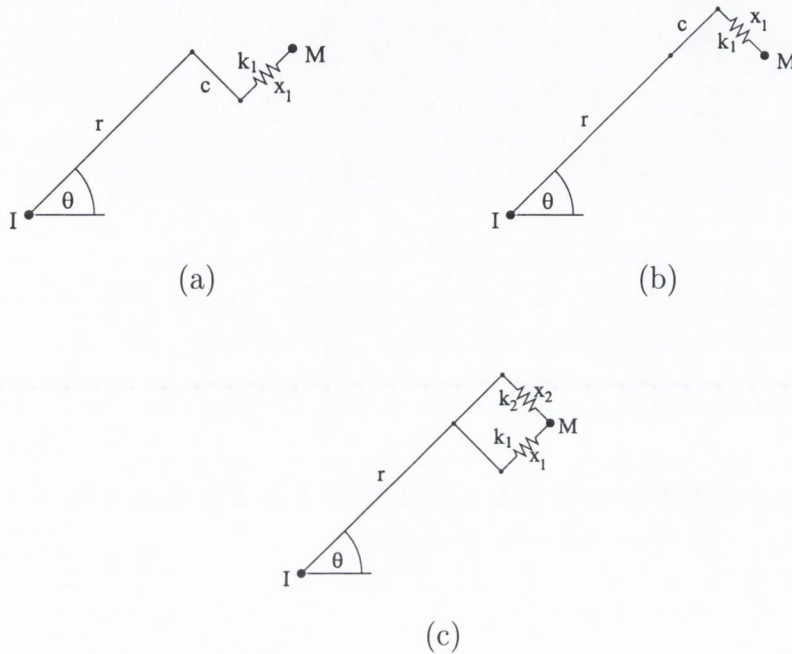
Figure 7.2: Basic spring models.

necessary to allow a simplified modelling process:

- The skull and mandible were treated as rigid bodies.

- The head has a fixed centre of rotation.

- Stiffness of the jaw elevator muscles was linearised.

- Biomechanical constraints were purely elastic, and did not include visco–elastic (damping) components.

- The mass ratio between the head and jaw is such that jaw kinematics do not significantly affect head behaviour.
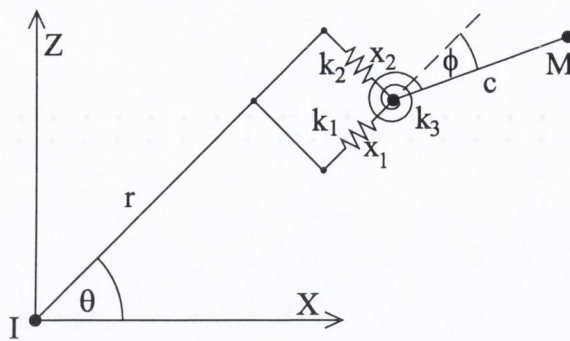
Figure 7.3: Final kinematic model.

The spring models of figures 7.2a&b are basic. In these two DOF systems, the head rotates through an angle θ about a fixed point at I. The mandible is a point mass M with one DOF: motion is limited to each of the x_1 directions shown. A linear spring of stiffness k_1 resists motion along the x_1 direction. This is a poor representation of reality: the mandible is capable of orthogonal displacements in the sagittal plane and figure 7.3 shows an improved model where motion in the x_1 and x_2 directions is permitted and there are corresponding restraining spring forces $(k_1x_1$ & $k_2x_2)$. However, the mandible is not a point mass: it is a rigid body with inertial characteristics that include a rotational inertia which is ignored by a point mass approximation of the mandible. Accurate modelling of kinematic behaviour of the mandible must include a jaw which is a rigid body with a distributed mass.

Figure 7.3 shows the final model. The head is a rigid body rotating through an angle θ about a fixed point I. The TMJ lies at a radius r from I. The mandible is also a rigid body with a centre of mass at M located a fixed distance c from the TMJ. The mandible has three DOF, all in the sagittal plane. These are sufficient to define planar motion of a rigid body. Two orthogonal displacements $(x_1$ & $x_2)$ are resisted by linear springs, k_1 and k_2 respectively. The mandible rotates through an angle ϕ, resisted by a rotational stiffness k_3.

Damping has not been included in this model, as maximum displacements were desired. The effect of including damping components would be to reduce the displacements of the three generalised coordinates.

7.2.4 Derivation of energy functions

The total kinetic energy function is the sum of the linear and rotational components of energy of M, the centre of mass of the mandible. The linear kinetic energy of M is obtained from the derivative of its position. Let the origin of the system lie at I and P_M be the position of the centre of mass of the mandible. Then

$$P_M = (r + x_1)e^{j\theta} - x_2 j e^{j\theta} + ce^{j(\theta-\phi)}. \tag{7.5}$$

The derivative of equation 7.5 gives the linear velocity of M:

$$\dot{P}_M = j\dot{\theta}(r + x_1)e^{j\theta} + \dot{x}_1 e^{j\theta} + x_2\dot{\theta}e^{j\theta} - j\dot{x}_2 e^{j\theta} + jc(\dot{\theta} - \dot{\phi})e^{j(\theta-\phi)}. \tag{7.6}$$

Let T_L be the linear kinetic energy of M. By definition,

$$T_L = \frac{1}{2}M \left| \dot{P}_M \right|^2, \tag{7.7}$$

where $\left| \dot{P}_M \right|^2$ is the product of $\dot{P}_M$ and its complex conjugate. After some simplification, it can be seen that

$$
\begin{aligned}
\left| \dot{P}_M \right|^2 = \quad & (r + x_1)^2\dot{\theta}^2 + \dot{x}_2^2 - 2(r + x_1)\dot{\theta}\dot{x}_2 + 2c\dot{\theta}(r + x_1)(\dot{\theta} - \dot{\phi})\cos\phi \\
& -2c\dot{x}_2(\dot{\theta} - \dot{\phi})\cos\phi + c^2(\dot{\theta} - \dot{\phi})^2 + \dot{x}_1^2 + x_2{}^2\dot{\theta}^2 \\
& +2\dot{x}_1 x_2\dot{\theta} + 2c\dot{x}_1(\dot{\theta} - \dot{\phi})\sin\phi + 2cx_2\dot{\theta}(\dot{\theta} - \dot{\phi})\sin\phi.
\end{aligned} \tag{7.8}
$$

from which we have

$$
\begin{aligned}
T_L = \frac{1}{2}M \Big[& (r + x_1)^2\dot{\theta}^2 + \dot{x}_2^2 - 2(r + x_1)\dot{\theta}\dot{x}_2 + 2c\dot{\theta}(r + x_1)(\dot{\theta} - \dot{\phi})\cos\phi \\
& - 2c\dot{x}_2(\dot{\theta} - \dot{\phi})\cos\phi + c^2(\dot{\theta} - \dot{\phi})^2 + \dot{x}_1^2 + x_2{}^2\dot{\theta}^2 \\
& +2\dot{x}_1 x_2\dot{\theta} + 2c\dot{x}_1(\dot{\theta} - \dot{\phi})\sin\phi + 2cx_2\dot{\theta}(\dot{\theta} - \dot{\phi})\sin\phi \Big]
\end{aligned} \tag{7.9}
$$

The moment of inertia (I) of a rod of mass M, length $2l$ about its centre is $I = \frac{1}{3}Ml^2$. The rotational kinetic energy (T_R) of a body with a moment of inertia I rotating through an angle θ is given by

$$T_R = \frac{1}{2}I\dot{\theta}^2. \tag{7.10}$$

Thus the rotational kinetic energy of the mandible is

$$T_R = \frac{1}{6} M c^2 \dot{\phi}^2. \tag{7.11}$$

The total kinetic energy function (T) for the spring model in figure 7.3 is the sum of equations 7.9 and 7.11.

$$
\begin{aligned}
T = \frac{1}{2} M \Big[&(r + x_1)^2 \dot{\theta}^2 + \dot{x}_2^2 - 2(r + x_1) \dot{\theta} \dot{x}_2 + 2c\dot{\theta}(r + x_1)(\dot{\theta} - \dot{\phi}) \cos \phi \\
&- 2c\dot{x}_2 (\dot{\theta} - \dot{\phi}) \cos \phi + c^2 (\dot{\theta} - \dot{\phi})^2 + \dot{x}_1^2 + x_2{}^2 \dot{\theta}^2 + 2\dot{x}_1 x_2 \dot{\theta} \\
&+ 2c\dot{x}_1 (\dot{\theta} - \dot{\phi}) \sin \phi + 2cx_2 \dot{\theta} (\dot{\theta} - \dot{\phi}) \sin \phi \Big] + \frac{1}{6} M c^2 \dot{\phi}^2 \quad (7.12)
\end{aligned}
$$

The potential energy of the system is the sum of the gravitational and elastic energies. However, an order of magnitude analysis showed that the former is insignificant and can be excluded. The elastic energy in the system is the sum of the spring energies. The potential energy in a linear spring of stiffness k with extension x is

$$V_S = \frac{1}{2} k x^2.$$

The total potential energy function is thus given by

$$V = \frac{1}{2} k_1 x_1^2 + \frac{1}{2} k_2 x_2^2 + \frac{1}{2} k_3 \phi^2. \tag{7.13}$$

The three equations of motion can then be obtained by applying equation 7.4 to each of the three generalised coordinates (x_1, x_2 and ϕ) respectively.

$$
\begin{aligned}
Lx_1 = \ & M\ddot{x}_1 + Mx_2 \ddot{\theta} + 2M\dot{x}_2 \dot{\theta} + Mc(\ddot{\theta} - \ddot{\phi}) \sin \phi + 2Mc\dot{\theta}\dot{\phi} \cos \phi \\
& - Mc(\dot{\theta}^2 + \dot{\phi}^2) \cos \phi - M(r + x_1)\dot{\theta}^2 + k_1 x_1 = 0
\end{aligned} \tag{7.14}
$$

$$
\begin{aligned}
Lx_2 = \ & M\ddot{x}_2 - M(r + x_1)\ddot{\theta} - 2M\dot{x}_1 \dot{\theta} + 2Mc\dot{\theta}\dot{\phi} \sin \phi + Mc(\ddot{\theta} - \ddot{\phi}) \cos \phi \\
& - Mc(\dot{\theta}^2 + \dot{\phi}^2) \sin \phi - Mx_2 \dot{\theta}^2 + k_2 x_2 = 0
\end{aligned} \tag{7.15}
$$

$$
\begin{aligned}
L\phi = \ & \frac{4}{3} Mc^2 \ddot{\phi} - Mc\ddot{\theta} - 2Mc\dot{x}_1 \dot{\theta} \cos \phi - Mc(r + x_1)\ddot{\theta} \cos \phi + Mc\ddot{x}_2 \cos \phi \\
& + Mc(r + x_1)\dot{\theta}^2 \sin \phi - Mc(\ddot{x}_1 + x_2\ddot{\theta} + 2\dot{x}_2\dot{\theta}) \sin \phi \\
& - Mcx_2 \dot{\theta}^2 \cos \phi + k_3 \phi = 0
\end{aligned} \tag{7.16}
$$

These equations were derived and then verified using the symbolic toolbox on Matlab. The Runge Kutta scheme requires a system of equations of the form

$$[A]\{\ddot{q}_i\} = [B] \tag{7.17}$$

where A is the coefficient matrix of the second order derivatives of the generalised coordinates q_i, and B contains all other terms (functions of q_i, first order derivatives and constants). Initial conditions for position and first derivative of each generalised coordinate are required. These were all set to zero. The matrix A is given by

$$A = \begin{bmatrix} M & 0 & -Mc\sin\phi \\ 0 & M & Mc\cos\phi \\ -Mc\sin\phi & Mc\cos\phi & \frac{4}{3}Mc^2 \end{bmatrix}. \tag{7.18}$$

The Runge Kutta scheme then solves for $\ddot{q}_i = [A]^{-1}[B]$ and it is critical that the determinant $[A]^{-1}$ is non–zero. Since

$$det[A] = \frac{1}{3}M^3c^2 \tag{7.19}$$

the special cases when M or c are zero are trivial, and so a solution will always be possible for this model. Matlab scripts were used to integrate this system of equations.

7.2.5 Parameter Values

The choice of values for spring coefficients, distances and head kinematics critically influences the value of numerical modelling. The approach adopted was to calculate values for each parameter based on the fore–going experimental work and then measure the effect of varying each of these individually.

Spring stiffnesses k_1 and k_2 represent internal stiffness within the TMJ while k_3 is the rotational stiffness representing the passive muscle forces of the jaw elevators. Values for k_1 and k_2 have been approximated from the cadaveric tissue tests reported in chapter 6. From figure 6.7 it can be seen that the force required to cause 5mm protrusion varies between 15 and 35N. The simple average of 25N was

used. If a linear stiffness is assumed, this gives an internal stiffness coefficient for the TMJ of 5000N/m. Preliminary tensile tests where the TMJ was stretched in the superior/inferior direction rather than the anterior/posterior direction showed that stiffness within the TMJ was reasonably isotropic. Therefore initial values of 5000N/m were chosen for both k_1 and k_2.

The rotational stiffness k_3 was chosen by simplifying the stress/stretch—ratio data of Hawkins and Bey [75], see figure 3.7. Sled testing of the physical model showed a maximum mouth–opening of ca. 20°. The three main jaw elevator muscles are the masseter, temporalis and the medial pterygoid. If the normal distance of each to the TMJ is ca. 30mm, then 20° of mouth–opening will induce 10.9mm stretch in each muscle. This results in stretch ratios varying from 1.18 – 1.27, depending on the resting length of each muscle. Noting (as before) that the passive muscle response is linear in this stretch–ratio range, the torque components from each muscle based on the stress and stretch–ratio data described in chapter 3 have been summed in table 7.1. Thus mouth–opening of 20° produces a torque of 0.272Nm and this was used to calculate $k_3 = 0.78$Nm/rad from $T = k_3\phi$.

The mass of the jaw was approximated at M = 0.2kg, the distance from the mass centre of the jaw (M) to the TMJ was measured as 0.05m, and the distance from the TMJ to the centre of rotation of the head was taken as r = 0.04m. This latter value is taken as the approximate case where ICR_{head} remains close to the c_o axis, the base of the skull on the neck. This was used in favour of the measured locus of ICR_{head}, because a stable and simplified model was desired, and the measured locus of ICR_{head} is highly sensitive to error, see chapter 5. The values for head kinematics were interpolated at each integration time–step from the experimental measurements of a 9.2 km/h $\triangle v$ impact.

7.2.6 Results

The results of the simulation with the parameter values listed in table 7.2 are given in figures 7.5 and 7.6. Velocities, displacements and the prescribed head kinematics (θ_{head} and $\dot{\theta}_{head}$, respectively) are shown. The strongly oscillating curves reflect

Muscle	Masseter	Medial Pterygoid	Temporalis
cross-sectional area per pair (cm²)	6.8	3.8	8.4
resting length (mm)	60	55	40
stretched length (mm)	70.9	65.9	50.9
stretch ratio	1.180	1.198	1.272
stress (N/cm²)	0.384	0.403	0.503
force (N)	2.61	1.53	4.226
radius (mm)	30	30	35
torque (Nm)	0.078	0.046	.147
Total torque (Nm)	0.271		

Table 7.1: Torque calculations from passive elevator muscles.

the absence of damping in the system. It can be seen that x_1 and x_2 displacements are small, but that ϕ rises steadily to a maximum of 0.43rad between $t = 0.1$s and $t = 0.173$s. These results indicate that considerable mouth-opening occurs but that displacements within the TMJ are small.

parameter	M	r	c	k_1	k_2	k_3
value	0.2kg	0.04m	0.05m	5000N/m	5000N/m	0.78Nm/rad

Table 7.2: Model parameters.

The angle ϕ represents mouth-opening and there is quite a good correlation between mouth-opening measured on the dummy and ϕ predicted by this model, see figure 7.4. The somewhat larger degree of mouth-opening predicted by the Lagrangian model is due to the fact that no damping has been included. After

the mouth has closed, the comparison between the two curves loses validity: the mouth–opening curve for the experimental data is the integrated difference be-
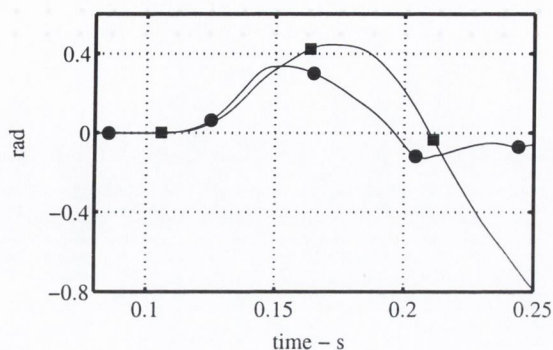

Figure 7.4: Mouth–opening: experimental (•) and predicted (■).

tween $\dot{\theta}_{head}$ and $\dot{\theta}_{jaw}$. When the mouth closes, there is high–frequency noise due to 'occlusal contact' between the model head and jaw, see section 4.1. In the simulation, there is no occlusal contact to prevent negative mouth–opening, and so realistic comparison can only be made while ϕ is still positive.

7.2.7 Parametric Analysis

The following simulation results demonstrate the stability of the model over a considerable range of parameter values. For each simulation, one parameter was varied, while those not under investigation were maintained as in table 7.2. The computed value of each parameter under investigation was both doubled and halved and the results are given.

Mass Dependency

One uncertainties in the physical model was the influence of the inertia of the tongue. The effect on mouth–opening of varying the mass of the mandible was investigated. Figure 7.7a shows the effect of varying jaw mass, with all other model parameters the same as in table 7.2. The predicted mouth–opening curve is stable over a large range of mass variations. The effect of varying M from 0.1kg to 0.3kg
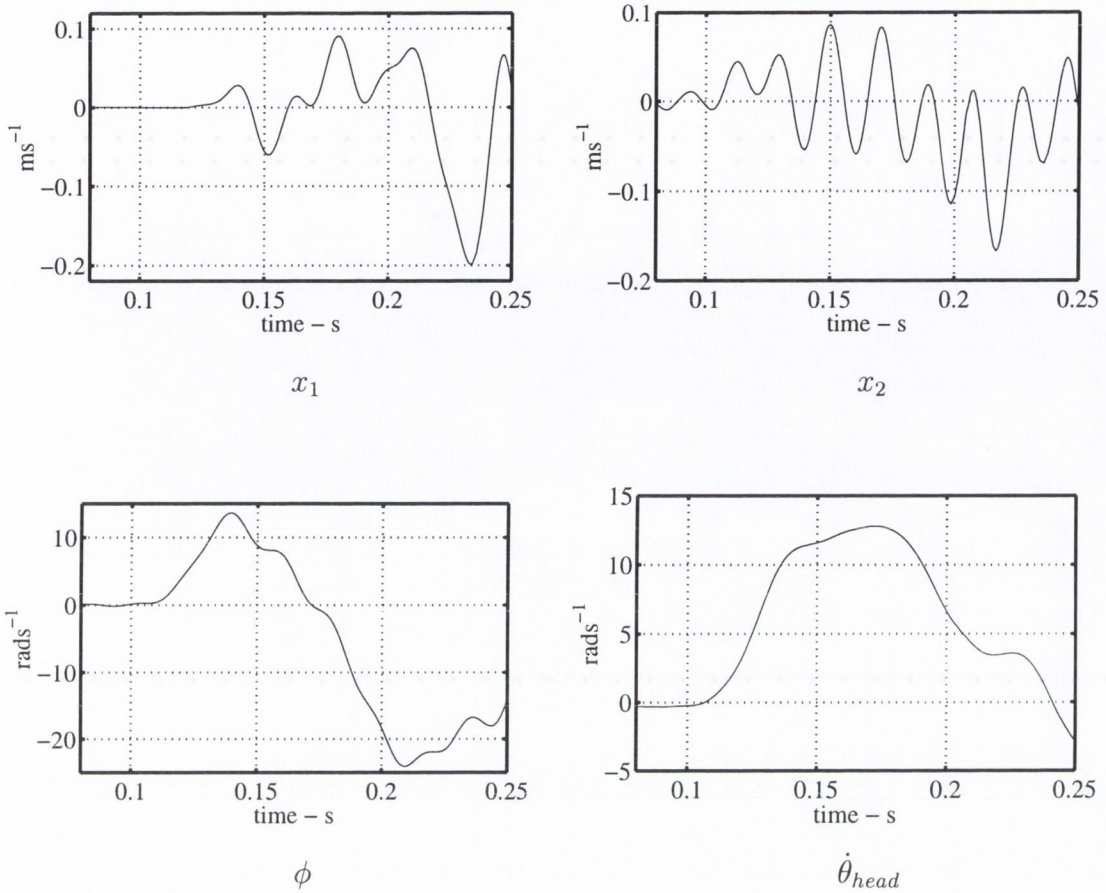
Figure 7.5: Simulation results: velocities. The model input $\dot{\theta}_{head}$ is also shown.

is as expected: increased mass increases the maximum value of mouth–opening, and also increases the period of mouth–opening. The former is due to increased inertial resistance to head retroflexion, while the latter is because natural frequency is inversely proportional to the square–root of mass. The effect of mass variation on internal joint displacements (x_1 and x_2) is seen in figure 7.7b&c: increased inertia causes larger displacements, as expected. As with mouth–opening, there is no evidence of dramatic changes over the mass range presented.
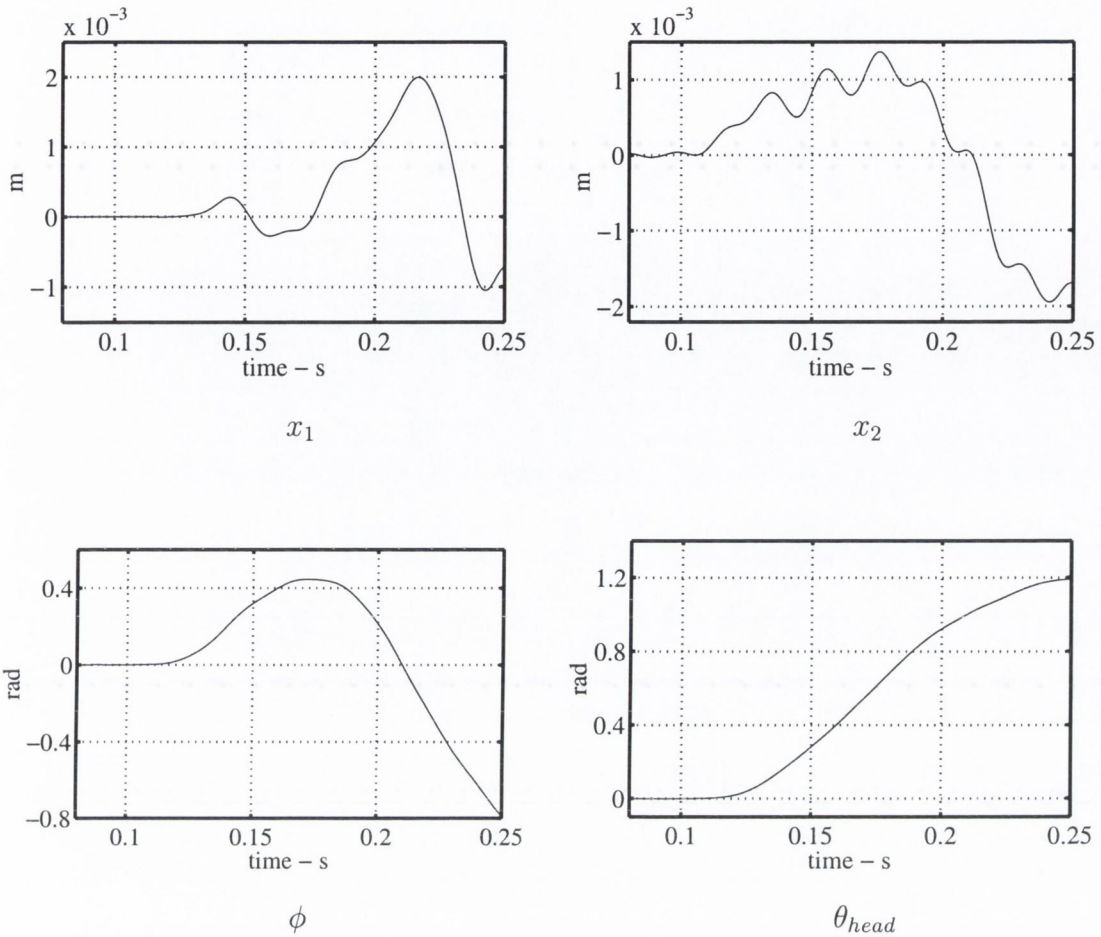
Figure 7.6: Simulation results: displacements. The model input θ_{head} is also shown.

Spring Stiffness

The influence of varying k_1 and k_2 is shown in figure 7.8. It is clear that mouth–opening remains largely unaffected by the internal linear stiffnesses within the joint. This is because the spring forces governed by k_1 and k_2 pass through the centre of rotation of ϕ, and therefore do not resist ϕ. The displacements x_1 and x_2 are reduced (as expected) by increases in linear spring stiffness. In fact, from comparison of figures 7.7b&c and figures 7.8b&c, it can be seen that increasing k_1 and k_2 has a broadly reciprocal effect to increasing M. In contrast, the angle of mouth–opening is strongly influenced by variations in the rotational stiffness k_3, see figure 7.9.
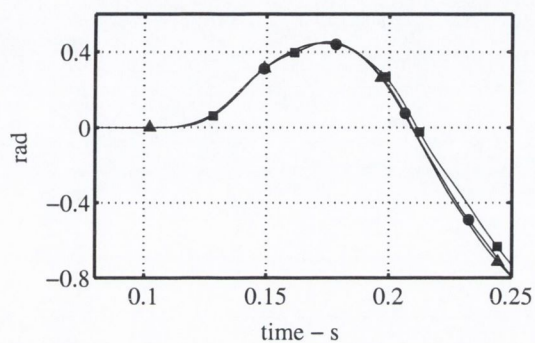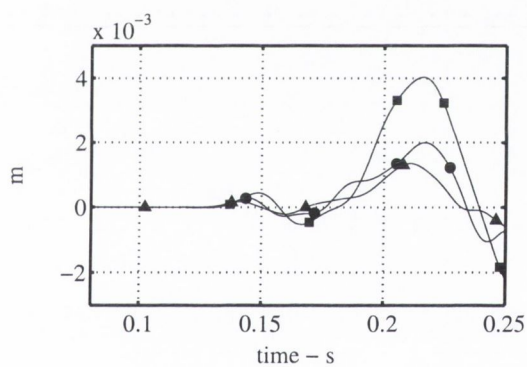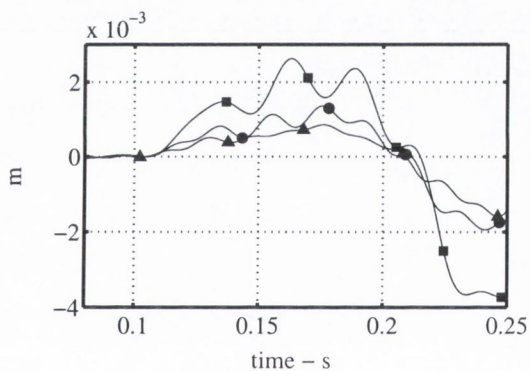
134

ϕ
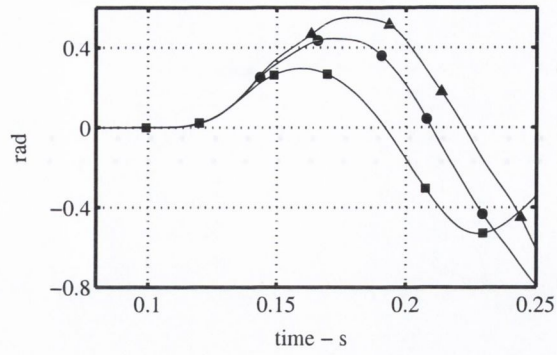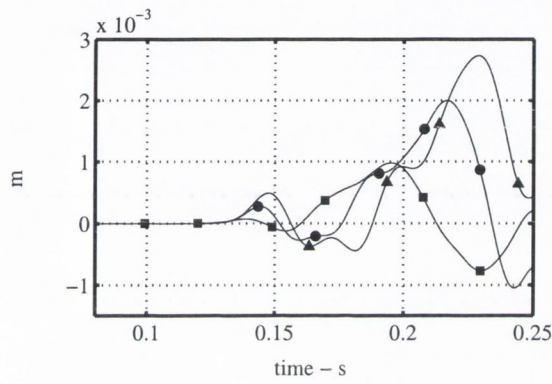
x_1
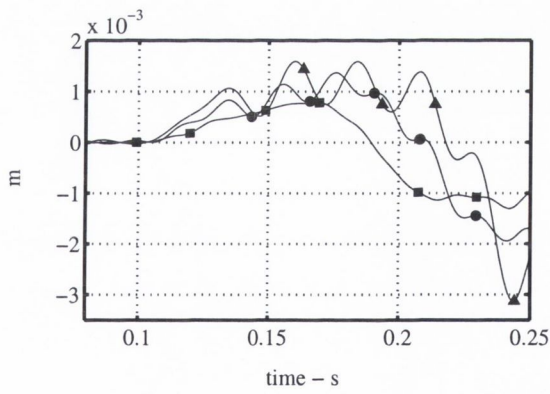
x_2

Figure 7.7: Influence of varying M on ϕ, x_1 and x_2: $M = 0.1$kg ($\blacksquare$), $M = 0.2$kg ($\bullet$), $M = 0.3$kg ($\blacktriangle$).
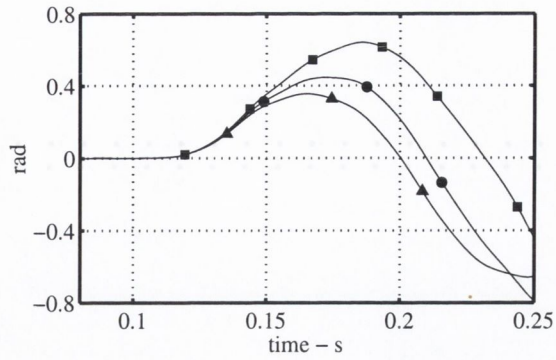
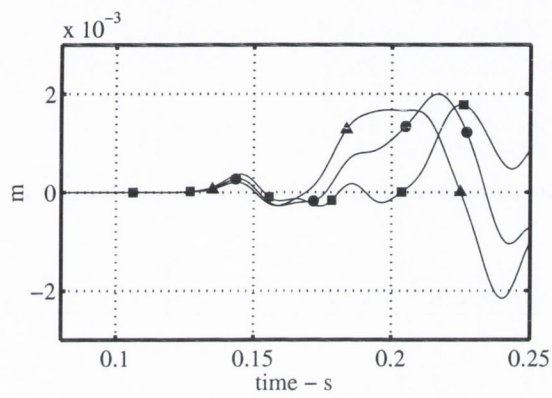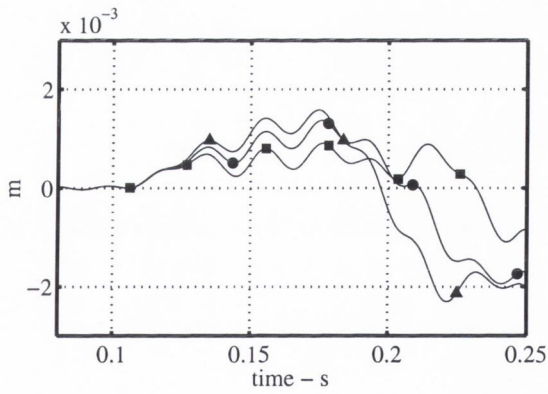Figure 7.8: Influence of varying k_1 and k_2 on ϕ, x_1 and x_2: k_1 and $k_2 = 2500\text{N/m}$ (■), k_1 and $k_2 = 5000\text{N/m}$ (●), k_1 and $k_2 = 7500\text{N/m}$ (▲).

ϕ

x_1

x_2

Figure 7.9: Influence of varying k_3 on ϕ, x_1 and x_2: $k_3 = 0.39$Nm/rad ($\blacksquare$), $k_3 = 0.78$Nm/rad ($\bullet$), $k_3 = 1.19$Nm/rad ($\blacktriangle$).

137

Influence of Link Lengths c and r

The influence of the lengths of links c and r was investigated, see figures 7.10 and 7.11. Changes in c represent different sizes of mandible: a larger mandible is subject to larger torques, and hence higher levels of mouth–opening. The internal joint displacements (x_1 and x_2) are not significantly affected by this. It should be noted that in the *in vivo* case a larger jaw would probably be accompanied by larger restraining muscle forces, and this would counterbalance the increased level of mouth–opening shown here. The effect of misjudgement in the location of ICR_{head} can be seen from variations in the length of link r. This affects each
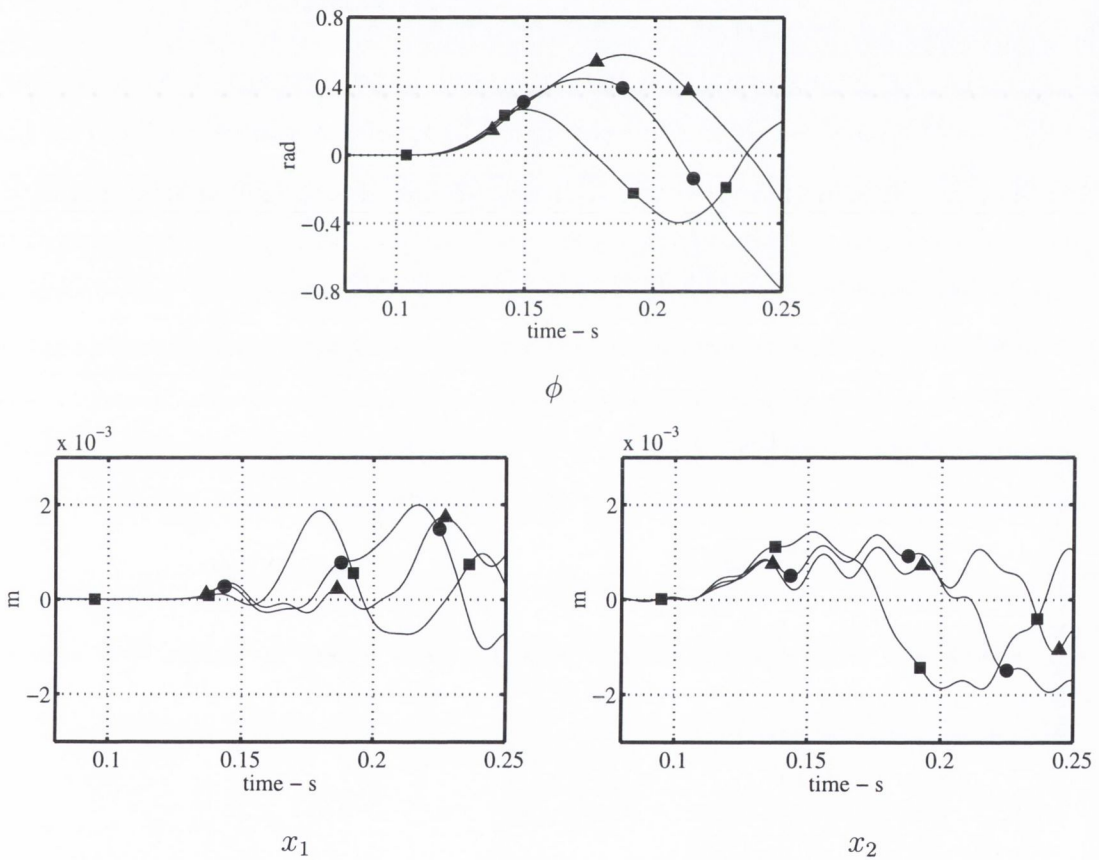

Figure 7.10: Influence of varying c on ϕ, x_1 and x_2: $c = 0.0025$m ($\blacksquare$), $c = 0.005$m ($\bullet$), $c = 0.0075$m ($\blacktriangle$).

of the generalised coordinates (x_1, x_2 and ϕ) in a broadly linear manner. This is because forces on a rotating body with a fixed centre are proportional to the radius of rotation.
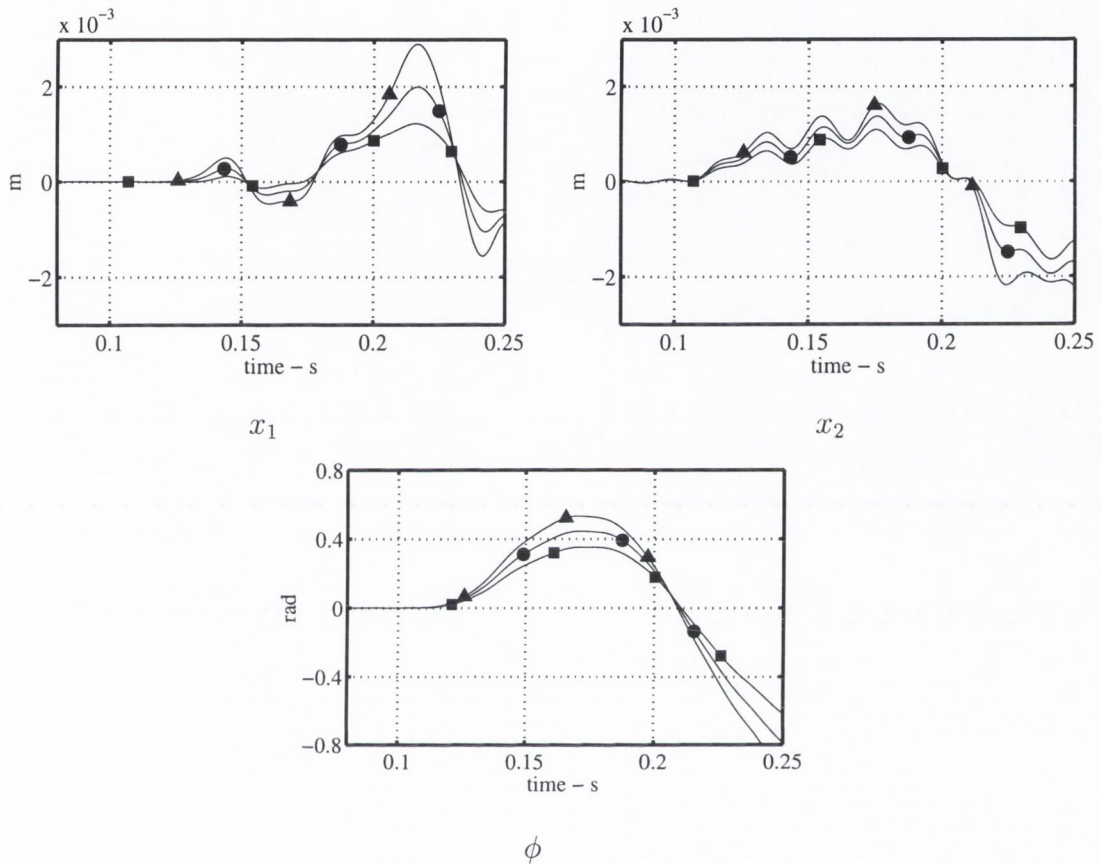
Figure 7.11: Influence of varying r on ϕ, x_1 and x_2: $r = 0.2$m (■), $r = 0.4$m (•), $r = 0.6$m (▲).

Influence of Angular Kinematics of the Head

Variations in the rotational behaviour of the head occur with changes in impact severity. In general, larger angles of retroflexion can be expected with higher impact severity, though resistance to head rotation increases non-linearly with head rotation angle [64]. These variations in head kinematics influence the response of the mandible. Mertz and Patrick [64] carried out rear-end collision tests using

cadavers and have published time histories of head retroflexion angle (θ_{head}) for impact velocties of 16km/h and 36.8 km/h. These correspond to $\triangle v$'s of 14.5 and 23.7 km/h respectively and therefore provide a good basis for testing the response of the model to higher $\triangle v$ equivalent collisions. The angular velocity and acceleration of the head were estimated by fitting polynomials to the angular displacement data and then differentiating the latter.
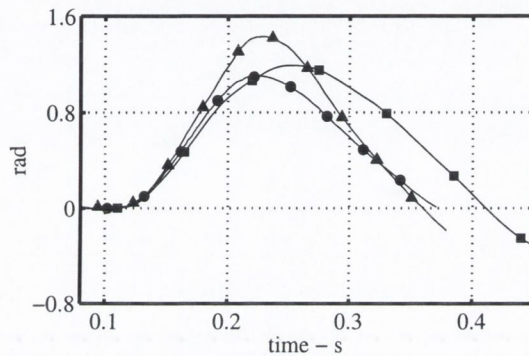

Figure 7.12: Head rotation angle for various impact severities: $\triangle v = 9.2$ km/h ($\bullet$), 14.5 km/h ($\blacksquare$) and 23.7 km/h ($\blacktriangle$).

Figure 7.12 shows the variation of head rotation angle with increasing impact severity. Figure 7.13 shows the effect on x_1, x_2 and ϕ of applying this varied head motion as input to the kinematic model. It can be seen that all three primary model parameters vary in a broadly linear manner with increased impact severity. Further, doubling the equivalent $\triangle v$ does not substantially alter the maximum angle of mouth-opening (ϕ), nor are the joint displacements (x_1, x_2) substantially increased. This may in part be due to differences between the test set-up devised by McConnell et al. [20] compared with the test set-up used by Mertz & Patrick [64]. Nonetheless, the model is remarkably insensitive to increases in impact severity.
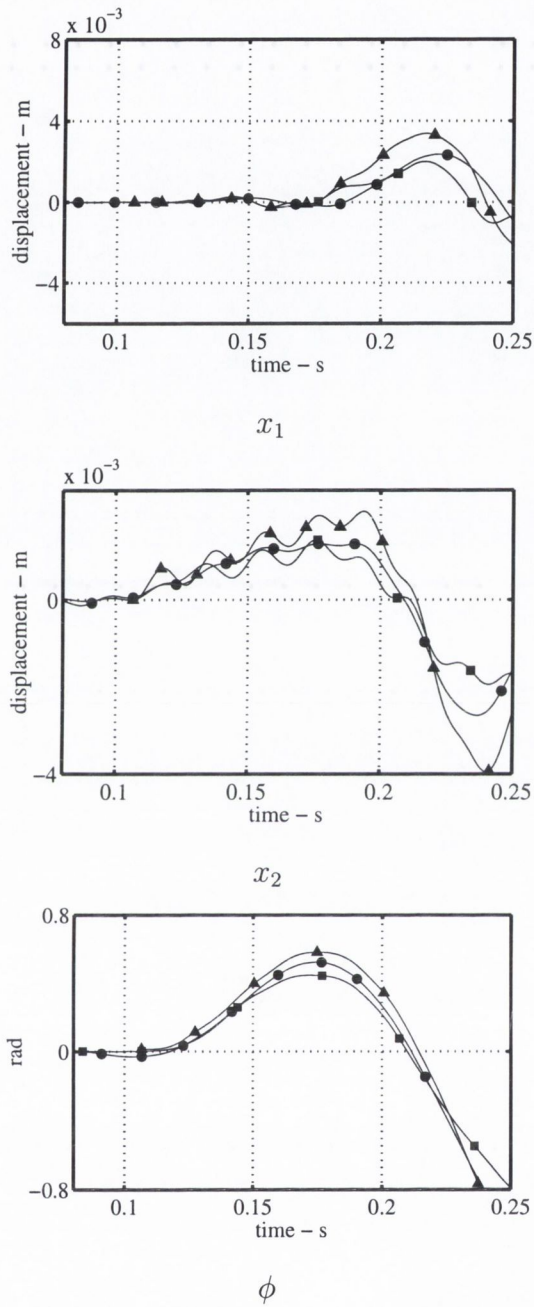
140

x_1

x_2

ϕ

Figure 7.13: Influence of varying impact severity on x_1, x_2 and ϕ: $\triangle v = 9.2$ km/h ($\blacksquare$), $\triangle v = 14.5$km/h ($\bullet$), $\triangle v = 23.7$km/h ($\blacktriangle$).

141

7.3 Estimation of TMJ Reaction forces

The kinematic model described in figure 7.3 has orthogonal springs of stiffness k_1 and k_2 connecting rigid links c and r. These linear springs model the resistance to stretch of the soft tissue within the TMJ. It follows that an estimate of the orthogonal forces developed in the TMJ during the simulation can be found from the respective products of k_1x_1 and k_2x_2. Table 7.1 shows the parameter values chosen for the basic simulation, which models the 9.2km/h $\triangle v$ impact described by McConnell et al [20]. The linear stiffnesses k_1 and k_2 are both 5000N/m. Figure 7.6 shows the variation of x_1 and x_2 during retroflexion. The corresponding forces developed by the spring displacements are given in figure 7.14. The maximum

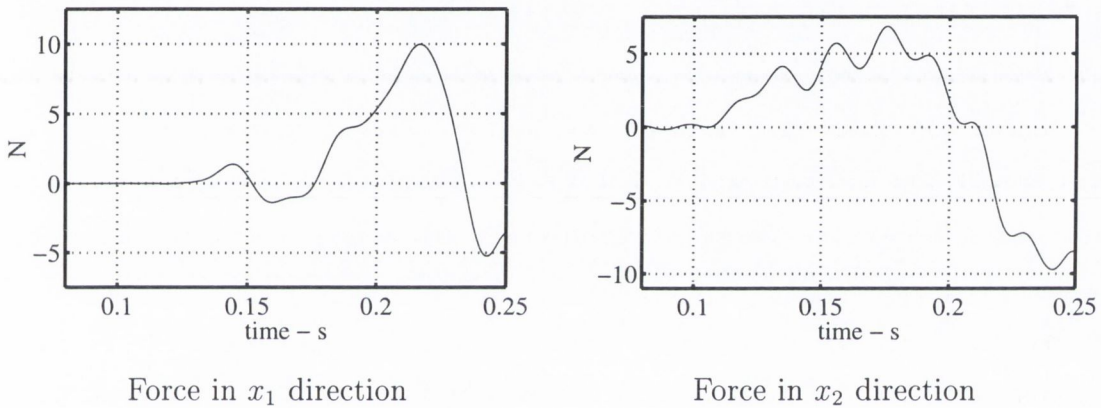Force in x_1 direction   Force in x_2 direction

Figure 7.14: Inertial forces at the TMJ calculated from simulation.

forces generated are 10N and 6.6N in the x_1 and x_2 directions respectively. The orientations of x_1 and x_2 are fixed in the model head and therefore change during retroflexion, but relative to the TMJ they remain fixed. Positive forces are tensile.

7.3.1 Effect of Parametric Variations on Force Calculations

It is necessary to check whether the parametric analysis presented in section 7.2.7 produces significant variation in inertial load generated at the TMJ. The same method is applied as before: for each simulation, one parameter was varied while those not under investigation were maintained as in table 7.2. The computed

value of each parameter under investigation was both doubled and halved and the resulting forces at the TMJ are given. The force-time curves in each case directly mirror the displacement-time curves for the parametric analysis in section 7.2.7. The obvious exceptions to this are the simulations in which the linear spring stiffnesses k_1 and k_2 are varied.

Mass Variation

Force in x_1 direction   Force in x_2 direction
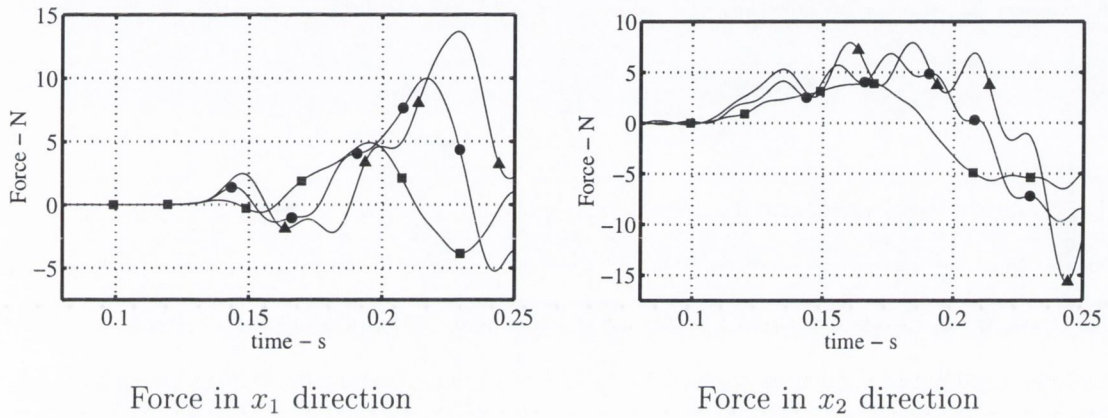
Figure 7.15: Influence of varying M on internal joint loading: $M = 0.1$kg ($\blacksquare$), $M = 0.2$kg ($\bullet$), $M = 0.3$kg ($\blacktriangle$).

Linear Spring Stiffness Variation

Force in x_1 direction   Force in x_2 direction

Figure 7.16: Influence of varying k_1 and k_2 on internal joint loading: k_1 and $k_2 = 2500$N/m ($\blacksquare$), k_1 and $k_2 = 5000$N/m ($\bullet$), k_1 and $k_2 = 7500$N/m ($\blacktriangle$).

143

Rotational Spring Stiffness Variation
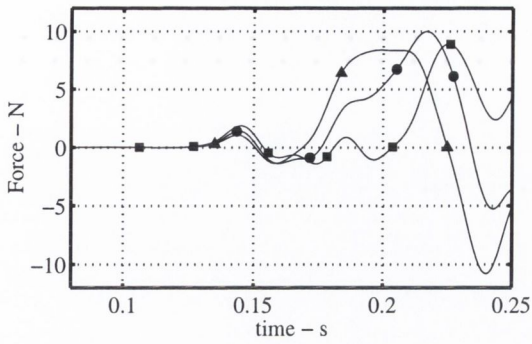
Force in x_1 direction
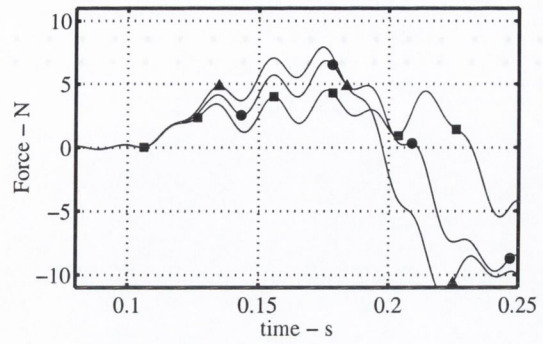
Force in x_2 direction

Figure 7.17: Influence of varying k_3 on internal joint loading: $k_3 = 0.39$Nm/rad (■), $k_3 = 0.78$Nm/rad (•), $k_3 = 1.19$Nm/rad (▲).

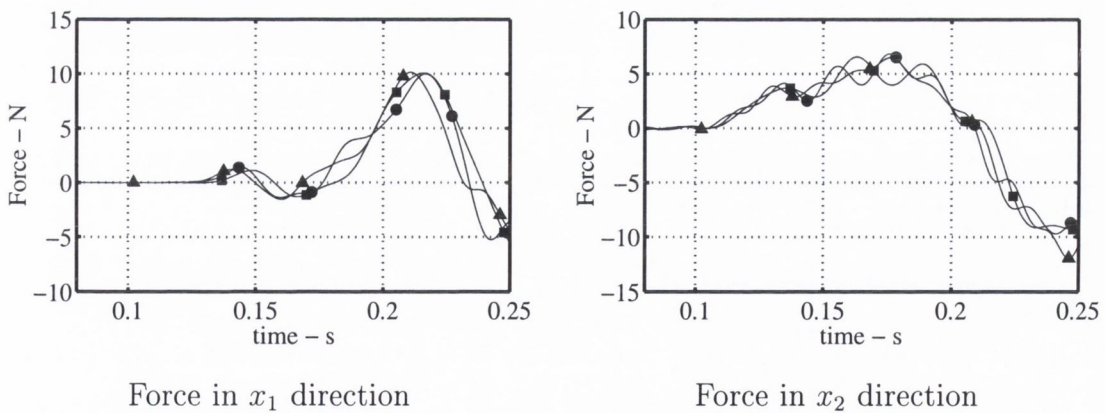## Influence of Link Lengths c and r

Force in x_1 direction

Force in x_2 direction

Figure 7.18: Influence of varying c on internal joint loading: $c = 0.0025$m (■), $c = 0.005$m (•), $c = 0.0075$m (▲).
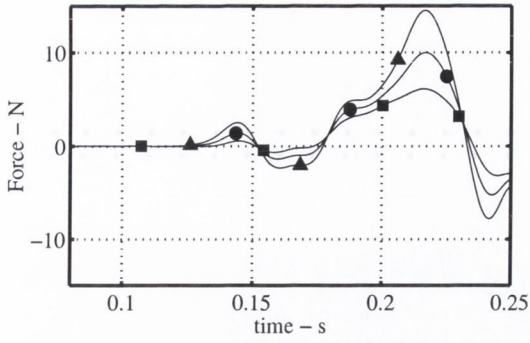
Force in x_1 direction
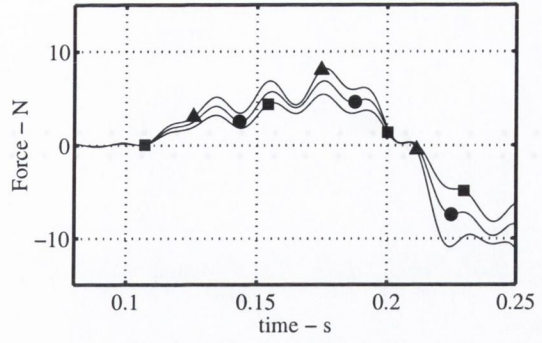
Force in x_2 direction

Figure 7.19: Influence of varying r on internal joint loading: $r = 0.2$m ($\blacksquare$), $r = 0.4$m ($\bullet$), $r = 0.6$m ($\blacktriangle$).

Impact Severity Variations
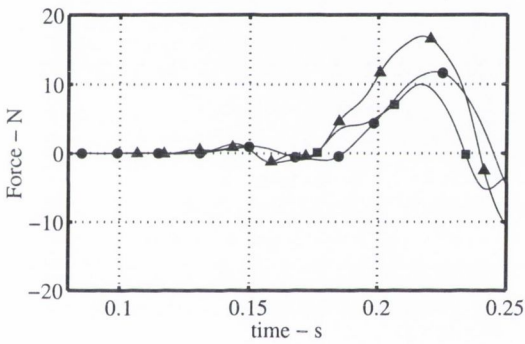
Force in x_1 direction
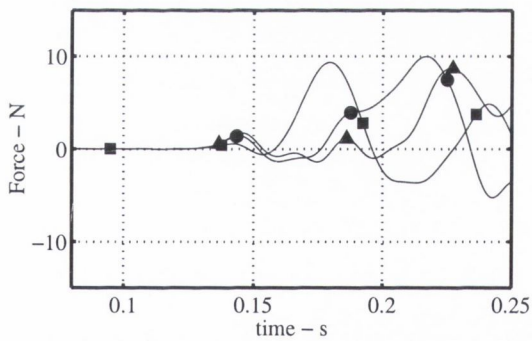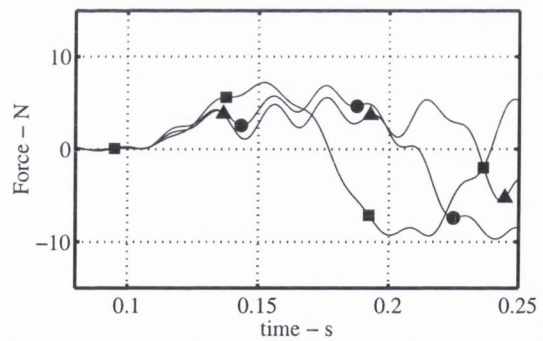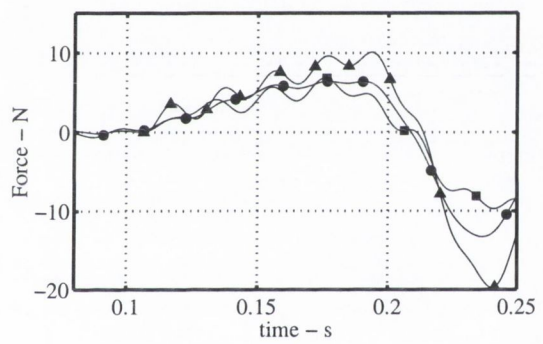

Force in x_2 direction

Figure 7.20: Influence of varying impact severity on internal joint loading: $\triangle v = 9.2$ km/h ($\blacksquare$), $\triangle v = 14.5$km/h ($\bullet$), $\triangle v = 23.7$km/h ($\blacktriangle$).

Comment

None of the forces generated in these simulations exceed the reaction forces generated during functional biting. The vertical reaction force at the TMJ during maximum bite force is ca 300N, see section 7.1, while the maximum inertial load calculated is 16.5N for a $\triangle v$ of 23.7km/h, see figure 7.20. These results suggest

145

that the inertial load developed at the TMJ during retroflexion are of a lower magnitude than the reaction forces in the TMJ during functional movements.

However, it should be emphasised that strict simplifications were necessary when formulating the kinematic model of the head and jaw used in these simulations. The importance of this is addressed in chapter 8.

Chapter 8

Discussion

The clinical evidence of TMJ injuries during whiplash indicates that a significant number of patients who have suffered whiplash also exhibit TMJ symptoms: mainly clicking, myofascial pain and limited jaw motion. The major limitation of these reports has been discussed: it is often not clear whether symptoms were pre–existing or have been caused by the accident. The issue of litigation coupled with the subjective nature of self–evaluated reporting considerably compromises the external validity of such reports. Further, few distinguish between direct and indirect impact of the mandible. The latter does not constitute a genuine whiplash injury and yet this category has not been factored out. The similarity between the symptoms of TMJ injuries and the symptoms of a number of other unrelated illnesses is striking. Finally, it is possible that post–accident neurological changes affect the normal function of the mandible, leading to the development of classic MPD symptoms. The result of these uncertainties is that in some cases the same evidence has been used to argue both for and against the likelihood of a causal link between whiplash and TMJ dysfunction.

The clinical evidence can be criticised but is not meaningfully categorised as true or false. In contrast, the two main injury theories arising from this evidence can be readily judged on a true or false basis. These are the Inertial Injury Theory (IIT) and the Late TMJ Injury Theory (LTIT). The results of the experimental investigations described in this thesis lead to a number of conclusions.

8.1 Discussion of Results

The Degree of Mouth–opening

Considerable angular velocity differentials were measured during sled–tests with model jaw muscles corresponding to the passive state. The equivalent $\triangle v$ was 9.2km/h. A low velocity rear–end impact is therefore likely to cause mouth–opening if the jaw musculature is relaxed. It is noteworthy that mouth–opening occurs early during the retroflexion phase, see figure 4.7. The IIT implies that mouth–opening continues until maximum retroflexion has been reached, following which mouth–closing occurs during the flexion stage of head motion. However, the current model indicates that both opening and closing have been completed well before maximum retroflexion has been reached. The natural frequency of jaw motion is higher than that of the head because of the high mass–ratio between the head and jaw, and a head–rest designed to prevent mouth–opening would therefore need to be placed very close to the head. However, the maximum level of mouth–opening measured did not exceed 20°, which lies well within the physiological envelope and will not cause injury. This contradicts the claims of the IIT that rapid excessive mouth-opening occurs during retroflexion: the IIT does not account for the fact that stretching of the bulky, powerful jaw elevator muscles quickly prevents excessive mouth–opening.

Sled–testing using the 25% active model jaw muscles indicated a dramatically reduced level of relative motion between the head and jaw. The increased muscle stiffness further increases the natural frequency of jaw motion and figure 4.10 shows that mouth–opening and closing are completed in the first 50ms after retroflexion begins. The magnitude of opening has now been reduced to ca. 1–2°. With the 50% active model jaw muscles, the relative angular velocity between the head and jaw was negligible (see figure 4.12) and mouth–opening was completely prevented, see figure 4.13. Thus, if there is any significant muscle activity, then the strength of the jaw elevator muscles precludes mouth–opening.

148

Kinematic Behaviour of the TMJ

Orthogonal accelerometers placed at the TMJ showed that the resultant sagittal plane X and Z accelerations of the TMJ do not exceed 30ms^{-2} during the retroflexion phase. Howard et al. [126] have published similar results from volunteer testing, and it now seems conclusive that the IIT is wrong in predicting tensile loading at the TMJ during retroflexion.

The reason for these surprisingly low accelerations can be found from measurements of head, sled and TMJ displacements during retroflexion. The rearward motion of COG_{head} relative to the sled is cancelled by forward motion of the sled relative to ground. The resulting absolute displacement of the head relative to ground is small and positive throughout the retroflexion sequence. These displacement calculations allow the locus of ICR_{head} to be plotted, and this serves as a useful visual aid. In the initial 10–20ms post impact, when $\dot{\theta}_{head}$ is not significant, ICR_{head} lies far from the TMJ. As $\dot{\theta}_{head}$ increases, ICR_{head} is rapidly pulled in closer to COG_{head}. ICR_{head} is the locus of points that are instantaneously at rest, and since the TMJ lies close to COG_{head}, the inertia of the head acts to protect the TMJ from high accelerations. The effect of the high inertia of the head is that the collision impact is converted to a ramp response at the TMJ. McConnell et al. [20] have reported that during the first 60ms of head motion almost pure rotation occurs and this is in agreement with the ICR measurements made in this investigation: figure 1.10 shows that the ICR is almost stationary during much of the retroflexion sequence.

Dynamics of the TMJ during Whiplash

A simple FBD of the mandible demonstrates that there is considerable compressive loading at the TMJ during functional biting. A bite force of 600N will generate a vertical reaction in the TMJ of ca 300N. In contrast, calculation of joint forces using the kinematic displacements of the linear springs in the kinematic model in chapter 7 shows that the inertial forces generated in the TMJ do not exceed 20N in any of the simulations. This suggests that the inertial forces developed during

149

the whiplash maneouvre are smaller than the load developed during physiological biting. This result should be treated with caution as major simplifications were necessary in formulating the kinematic model. However, the difference between loading of ca 300N in functional chewing compared to inertial loading of only 20N is striking. This neatly illustrates the low mass yet high muscle strength regime under which the mandible operates.

Force–extension tests on cadaveric specimens

Function and dysfunction of the TMJ depends on the strength of its constituent tissues. During physiological mouth–opening, rotation is accompanied by anterior translation of the condyles towards the crest of the articular eminence. The IIT claims that during the retroflexion phase of whiplash, rearward motion of the head and excessive mouth–opening combine to cause hypertranslation of the condyles, leading to stretching or tearing of the soft tissues of the TMJ. It has been seen that the anterior capsule is the weakest portion of the TMJ and tests were therefore performed to investigate internal joint resistance to excessive translation of the condyles.

Tensile tests using embalmed cadaveric specimens have indicated that significan loads are required to cause anterior dislocation of the condyles. Considerable variation between specimens was found, and the force required to extend the condyle anteriorly by 5mm varied between 15–35N. This motion lies within physiological limits. The effect of mouth–opening on the force/extension characteristics was investigated: with the mandible fixed at 15° opening, the force required for 5mm anterior displacement was reduced by nearly 50%. The influence of visco–elasticity was investigated and found to be at most 20% of the static stiffness of the joint. It is possible that a combination of strong anterior loads acting on the condyle together with visco–elastic loading and mouth–opening would cause soft–tissue damage through hypertranslation. However, it has already been seen that such forces do not act on the TMJ, and injuries of this form do therefore not occur.

Tensile tests on these cadaveric specimens following successive dissection of the joint tissues have shown that the stiffness of the TMJ derives from the strength

of several individual structures. This indicates that there is no single soft-tissue component responsible for structural stiffness.

Lagrangian model

A simplified Lagrangian model of the jaw and head was developed: head motion was purely rotational and muscle forces were linearised. Input to the model was provided by the experimentally measured rotational kinematics of the head, and simulations on Matlab show a good correlation with the experimental sled data, particularly with regard to mouth–opening. This has been used as a basis to vary each model parameter and investigate its overall influence on jaw kinematics. A strongly linear relationship between parameter value and jaw response was found in every case. The model is therefore stable over the range of values measured, and variations in these parameters are unlikely to affect the behaviour of the experimental model. This conveniently obviates the need to carry out a parametric analysis with the physical model. The significance of the simulation results are that the considerable geometric variations present due to age and sex differences are unlikely to be sufficient to cause injury in one category where another remains unharmed: increasing the mass of the mandible by 50% only increases maximum mouth–opening by 25%. Increasing the distance from the mass centre of the mandible to the TMJ by 50% increases maximum mouth–opening by 35%. A 50% increase in distance from the TMJ to c_o increases mouth–opening by 20%. Increasing the impact Δv from 9.2 km/h to 23.7 km/h increases maximum mouth–opening by 30%. Thus it is clear that while all of these parameters influence the jaw, there is no evidence that variation in a single parameter will significantly alter the kinematic behaviour of the jaw.

8.1.1 Limitations in the Experimental Work

Several simplifications were necessary to facilitate construction of the sled–test dummy, see chapter 3, and the effect of these on the experimental results should be assessed.

The Digastric Muscle

The simplification offered by the omission of the hyoid bone and digastric muscle is considerable. Supporters of the IIT have claimed that during retroflexion, the suprahyoid and infrahyoid muscles have insufficient time to stretch, thereby anchoring the mandible and increasing the possibility of hypertranslation and excessive mouth–opening [31]. However, the proposed inability of the depressor muscles to lengthen quickly is cancelled by the same inability in the elevator muscles – and the strength of the depressors is far less than that of the elevators [127], as the former do not perform power functions. Active contraction of the jaw depressor muscles can be disregarded as involuntary clenching will tend to close the mouth rather than open it. The digastric muscles are stretched by head retroflexion, but it is critical at what stage during head motion and by how much. Static range of motion tests suggest that the digastrics are only significantly stretched after ca. 0.8rad of retroflexion of the head. From figure 4.7 it is clear that if this is the case, the effect of passive stretching of the digastrics during the later part of retroflexion is to increase mouth–opening only after the mouth has almost fully closed. Angular velocity measurements of the head and jaw on the current model have shown that mouth–opening and closing occur in the early stages of retroflexion. Thus stretching of the digastrics might prolong mouth–opening, but it will not act to increase its magnitude.

Further, if the digastrics are only stretched during the latter stages of retroflexion, then the presence of (even poorly placed) headrests will curtail retroflexion and significant stretching of the digastrics will not occur.

Non–Zero Incident Angle Impacts

The RID III neck is designed for testing in the sagittal plane only, and non–zero incident angle impact tests were therefore not possible. However, the mandible is not as vulnerable to oblique impacts as the neck. The range of sagittal plane motion of the neck is severely limited by prior rotation of the head in the horizontal plane and a seated occupant looking sideways is more likely to suffer neck injuries

than an occupant facing forward. However, this argument does not hold for the jaw. The range of motion of the mandible is not significantly altered by coronal plane rotations of the head and the soft tissues of the jaw are therefore not pre–stressed by horizontal head rotations.

Translations within the neck

The *in vivo* neck has some facility for linear displacement at the facet joints. This is not modelled in the RID III neck, where only rotational translations are permitted about each of the nine pin–joints. The effect of this on head acceleration should be assessed. The base of the neck is accelerated forward after impact, while the head remains initially stationary. The response of the head is to minimise its kinetic energy: it does this by limiting the linear and rotational velocities of its mass center. In the case of the RID III neck, there is no facility for pure translations and the linear accelerations of the mass centre of the head are thus increased. In the *in vivo* case, some of the forward acceleration of the base of the neck is absorbed by (rearward) linear translations within the neck and is therefore not transferred to COG_{head}. Thus the linear accelerations of COG_{head} are harsher in the RID III environment than in the *in vivo* case. The measured accelerations at the TMJ using the RID III neck were found to lie below physiological limits and it can therefore be concluded that accelerations in the *in vivo* case will likewise lie below the physiological limit.

Increased Impact Severity

The aim of this thesis was to investigate the dynamic response of the jaw to low velocity rear–end impacts. The impact levels tested in this investigations are at the threshold of injury for human volunteer tests. The pneumatic impact cylinder used was not capable of accelerating the sled beyond the $\triangle v$ equivalent of 9.2km/h. However, the Lagrangian model shows that mouth-opening and loading at the TMJ lies within physiological limits for higher impact severities up to $\triangle v$'s of 23.7km/h.

8.1.2   Limitations in the Kinematic Model

The formulation of the kinematic model based on Lagrange's equations involved approximating head motion as purely rotational. This is not strictly accurate: the experimental work has shown that the dominant movement of the head is rotational throughout retroflexion, but some linear acceleration of the COG_{head} does occur. The effect of this on inertial loading of the TMJ in the numerical simulations has not been accounted for. The finding in chapter 7 that maximum inertial loading at the TMJ does not exceed 20N is based on this assumption.

Chapter 9

Conclusions

The results indicate that the mandible and TMJ are not harmed during a low-velocity rear–end collision. Excessive levels of mouth–opening do not occur during whiplash resulting from $\triangle v$'s up to 9.2km/h. Muscle bracing has a pronounced effect on mouth–opening: if there is any significant jaw muscle bracing, mouth–opening is prevented altogether. Acceleration at the skull portion of the TMJ measured during sled–testing are low. This is because the proximity of the TMJ to COG_{head} protects the former from high acceleration levels. An order of magnitude comparison between TMJ reaction forces during functional biting and inertial loading during retroflexion shows that the former produces much larger forces.

Soft–tissue tests of *in vitro* specimens have been used to quantify some of the structural properties of the TMJ. The effects of mouth–opening and visco-elasticity are significant but insufficient to cause injury during whiplash. The Lagrangian model indicates that even significant parametric variations are unlikely to affect loading at the TMJ during whiplash.

The Late TMJ Injury theory proposes that post–accident neurological changes cause radiated pain to the TMJ. It has been noted that this theory cannot be experimentally validated. However, none of the findings of this investigation conflict with this theory. A review of the literature has shown that there is some connection between TMJ injuries and whiplash. It is unlikely that TMJ injuries occur during the whiplash event: it is therefore be concluded that TMJ injuries

arising from a whiplash accident develop in the post–accident period. This adequately explains the frequent delay in the onset of symptoms. This theory also acknowledges that the neck is far more vulnerable to direct whiplash injuries than the jaw. The Late TMJ Injury Theory is therefore the most plausible explanation of TMJ injuries during whiplash.

The implication is that an investigation of crash kinematics is not a suitable means of assessing the likelihood of TMJ disorders following whiplash. Instead, an assessment of the extent of neuromuscular changes emanating from the neck region is probably a better indicator of TMJ disorders following whiplash.

9.1 Future Work

A major clinical study eliminating the ambiguity present in existing reports would be a very useful contribution to this area of research. The expansion of the present two–dimensional Lagrangian model of the jaw to a three-dimension model would give insight into the effects of non–direct impacts. Full integration of such a three-dimensional model of the human jaw into a crash investigation package such as Madymo could considerably improve future vehicle safety design.

Bibliography

[1] M. R. Trimble. *Post-traumatic Neurosis.* John Wiley and Sons, 1981.

[2] R. T. McIntyre. Opening remarks of the symposium on whiplash injuries. *International Record of Medicine*, 169:2, 1956.

[3] J. R. Gay and K. H. Abbott. Common whiplash injuries of the neck. *J Am Med Assoc*, 152:1698, 1953.

[4] D. M. Severy, J. H. Mathewson and C. O. Bechtol. Controlled automobile rear end collisions, an investigation. *Canadian Services Medical Journal*, 11:727–759, 1955.

[5] M. M. Braaf and S. Brosner. Whiplash injury of the neck – fact or fancy? *Int Surg*, 46:176–182, 1966.

[6] S. A. Hirsch, P. J. Hirsch and H. Hiramoto. Whiplash syndrome – fact or fiction? *Orthop Clin North Am*, 19:791–795, 1988.

[7] C. Maimaris, M. R. Barnes and M. J. Allen. Whiplash injuries of the neck: a retrospective study. *Injury*, 19(5):393–396, 1988.

[8] A. Watkinson, M. G. Gargan and G. C. Bannister. Prognostic factors in soft tissue injuries of the cervical spine. *Injury*, 22(4):307–309, 1991.

[9] C. H. Schutt and F. C. Dohan. Neck injury to women in automobile accidents. *JAMA*, 206(12):2689–2692, 1968.

[10] M. Hohl. Soft tissue injuries of the neck in automobile accidents: factors influencing prognosis. *J Bone Jt Surg*, 56A(8):1675–1682, 1974.

[11] I. Macnab. Acceleration injuries of the cervical spine. *J Bone Jt Surg*, 46A:1797–1999, 1964.

[12] C. L. Ewing, D. J. Thomas, G. W. Beeler, L. M. Patrick and D. B. Gillis. Dynamic response of the head and neck of the living human to -G_x impact. In *12th Stapp Car Crash Conference*, 424–439, 1968.

[13] C. L. Ewing, D. J. Thomas, L. M. Patrick, G. W. Beeler and M. J. Small. Living human dynamic response to -G_x impact acceleration. In *12th Stapp Car Crash Conference*, 400–415, 1968.

[14] C. L. Ewing and D. J. Thomas. Torque versus angular displacement response of the human head to -G_x impact acceleration. In *17th Stapp Car Crash Conference*, New York, 309–342, 1973.

[15] D. T. Watts, E. S. Mendelson, H. N. Hunter, A. T. Kornfield and J. R. Poppen. Tolerance to vertical acceleration required for seat ejection. *J Aviation Med*, 18:554, 1947.

[16] L. W. Schneider, D. R. Foust, B. M. Bowman, R. G. Snyder, D. B. Chafin, T. A. Abdelnour and J. K. Baum. Biomechanical properties of the human neck in lateral flexion. In *19th Stapp Car Crash Conference*, Warrendale, PA, 455–485, 1975.

[17] K. Langwiede. Passenger injuries in collisions and their relations to the general speed scale. In *17th Stapp Car Crash Conference*, New York, 1–34, 1973.

[18] C. W. Gadd, C. C. Culver and A. M. Nahum. Study of responses and tolerances of the neck. In *15th Stapp Car Crash Conference*, New York, 256–268, 1971.

[19] W. E. McConnell, R. P. Howard, H. M. Guzman, J. B. Bomar, J. H. Raddin, J. V. Benedict, H. L. Smith and C. P. Hatsell. Analysis of human test subject kinematic responses to low velocity rear end impacts. SAE No. 930889, Biodynamic Research Corporation, San Antonio, Texas, 1993.

[20] W. E. McConnell, R. P. Howard, J. VanPoppel, R. Krause, H. M. Guzman, J. B. Bomar, J. H. Raddin, J. V. Benedict and C. P. Hatsell. Human head and neck kinematics after low velocity rear–end impacts: understanding whiplash. SAE No. 952724, Biodynamic Research Corporation, San Antonio, Texas, 1995.

[21] J. H. Pringle. Displacement of the mandibular meniscus and its treatment. *Br J Surg*, 6:385–389, 1918–1919.

[22] C. Wakeley. The mandibular joint. *Ann R Coll Surg (Eng)*, 2:111–120, 1948.

[23] R. H. Roydhouse. Whiplash and temporomandibular dysfunction. *The Lancet*, 1341–1342, 1973.

[24] V. H. Frankel. Temporomandibular pain syndrome following deceleration injury to the cervical spine. *Bulletin, Hospital for Joint Disease*, 26(1), 1965.

[25] V. H. Frankel. Whiplash injuries to the neck. In C. Hirsch and Y. Zottermann, editors, *Cervical Pain*. Pergamon Press, 1972.

[26] D. C. McKay and L. V. Christensen. Whiplash injuries of the temporomandibular joint in motor vehicle accidents: speculations and facts. *J Oral Rehab*, 25:731–746, 1998.

[27] R. I. Brooke, P. G. Stenn and K. J. Mothersill. The diagnosis and conservative treatment of myofascial pain dysfunction syndrome. *J Oral Medicine*, 844-852, 1977.

[28] R. I. Brooke and P. G. Stenn. Postinjury myofascial pain dysfunction syndrome: its etiology and prognosis. *J Oral surg*, 846–850, 1978.

[29] S. J. Harkins and J. L. Marteney. Extrinsic trauma: a significant precipitating factor in temporomandibular dysfunction. *J Prosthetic Dentistry*, 271–272, 1985.

[30] E. Truelove, J. Burgess, S. Dworkin, L. Lawton, E. Somers and M. Schubert. Incidence of trauma associated with temporomandibular disorders. *J Dent Res*, 64(1):339, 1985.

[31] S. Weinberg and H. L. Lapointe. Cervical extension–flexion injury (whiplash) and internal derangement of the temporomandibular joint. *J Oral Maxillofac Surg*, (45):653–656, 1987.

[32] A. G. Pullinger and A. A. Monteiro. History factors associated with symptoms of temporomandibular disorders. *J Oral Rehab*, 15:117–124, 1988.

[33] S. Kopp. Pain and functional disturbances of the masticatory system – a review of etiology and principles of treatment. *Swed Dent J*, 6:49, 1982.

[34] R. A. Meyer. Clicking sounds owing to temporomandibular injury. *J Am Dent Assoc*, 248:38, 1982.

[35] A. Hohmann, K. Wilson and R. C. Nelms. Surgical treatment in temporomandibular joint trauma. *Otolarynologic Clinics of North America*, (16):549, 1983.

[36] A. P. Heise, D. M. Laskin and A. S. Gervin. Temporomandibular joint pain secondary to cervical musculoskeletal injury. *J Oral Maxillofac Surg*, 1990.

[37] A. P. Heise, D. M. Laskin and A. S. Gervin. Incidence of temporomandibular joint symptoms following whiplash injury. *J Oral Maxillofac Surg*, 1992.

[38] J. Burgess. Symptom characteristics in patients reporting blunt trauma and/or whiplash injury. *J Craniomandib Disord Facial Oral Pain*, 5:251–257, 1991.

[39] B. D. Pressman, F. G. Shellock, J. Schames and M. Schames. Magnetic resonance imaging of temporomandibular joint abnormalities associated with cervical hyperextension/hyperflexion (whiplash) injuries. *JMRI*, 2:569–574, 1992.

[40] C. Brady, D. Taylor and M. O'Brien. Whiplash and temporomandibular joint dysfunction. *J Irish Dent Assoc*, 39(3):69–72, 1993.

[41] T. Magnusson. Extra-cervical symptoms after whiplash trauma. *Cephalalgia*, 14(3):223–227, 1994.

[42] T. C. S. Probert, D. Wiesenfeld and P. C. Reade. Temporomandibular pain dysfunction disorder resulting from road traffic acidents – an Australian study. *Int J Oral Maxillofac Surg*, 23:338–341, 1994.

[43] R. Garcia Jr. and J. A. Arrington. The relationship between cervical whiplash and temporomandibular joint injuries. *J Craniomandib Pract*, 14(3):233–238, 1996.

[44] J. Stenger. Whiplash. *Basal Facts*, 2:128–134, 1977.

[45] C. Molin. Studies in mandibular pain dysfunction syndrome. *Swed Dent J*, 66:1(suppl no. 4), 1973.

[46] R. M. Ricketts. Understanding your TMJ. *American Institute for Bioprogressive Education*, 1985.

[47] R. I. Brooke and H. J. Lapointe. Temporomandibular joint disorders following whiplash. *Spine*, 7(3):443–454, 1993.

[48] J. P. Wiens. Acquired maxillofacial defects from motor vehicle accidents: statistics and prosthodontic considerations. *J Prosth Dent*, 63:172–181, 1990.

[49] J. L. Balla. The late whiplash syndrome: a study of an illness in Australia and Singapore. *Cult Med Psych*, 6:191–210, 1982.

[50] J. L. Balla. The late whiplash syndrome. *Aust New Zeal J Surg*, 50:610–614, 1980.

[51] J. Mannheimer, R. Attanasio, W. Cinotti and R. Pertes. Cervical strain and mandibular whiplash: Effects upon the craniomandibular apparatus. *Clincial Preventive Dentistry*, 11(1):29–32, 1989.

[52] A. G. Pullinger and D. A. Seligman. Trauma history in diagnostic groups of temporomandibular disorders. *J Oral Surg*, 71:521–534, 1991.

[53] P. E. Mahan. *The temporomandibular joint in function and pathofunction*, chapter 2. Quintessence Publishing, 1980.

[54] E. Lader. Cervical trauma as a factor in the development of TMJ dysfunction and facial pain. *J Craniomandib Pract*, 1(2):87–90, 1983.

[55] G. B. Whatmore and D. R. Kohli. *The physiopathology and treatment of functional disorders*. Grune and Stratton, 1974.

[56] N. A. Shore. *Temporomandibular joint dysfunction and occlusal equilibriation*. J. P. Lippincott & Co., 1976.

[57] H. Myrhaugh. The incidence of ear symptoms in cases of malocclusion and temporomandibular joint dysfunction. *Br J Oral Surg*, 2:28–32, 1964.

[58] D. W. Darling and S. L. Kraus. Relationship of head posture and rest position of the mandible. *J Prosth Dent*, 52(1):111–115, 1984.

[59] D. F. Goldstein and S. L. Kraus. Influence of cervical posture on mandibular movement. *J Prosthet Dent*, 52(3):421–426, 1984.

[60] C. H. Boyd. The effect of head position on EMG evaluation of representative mandibular positioning muscle groups. *J Craniomandib Pract*, 5(1):50–54, 1987.

[61] D. M. Severy and J. H. Mathewson. Automobile barrier impacts. *Highway Research Board Bulletin*, 91:39, 1954.

[62] D. M. Severy. Automobile crash effects. *Engineering Section, California Traffic Safety Conference, Sacramento, California*, 1954.

[63] H. Mertz and L. M. Patrick. Investigation of the kinetics and kinematics of whiplash. *SAE*, 670919, 1967.

[64] H. Mertz and L. M. Patrick. Strength and response of the human neck. In S. H. Backaitis and H. J. Mertz, editors, *Hybrid III – The first human–like crash test dummy*. SAE, 121–146, 1994.

[65] D. F. Huelke and G. S. Nusholtz. Cervical spine biomechanics: a review of the literature. *J Orth Res*, 4:232–245, 1986.

[66] T. J. Szabo and J. B. Welcher. Human subject kinematics and electromyographic activity during low speed rear impacts. *SAE*, 962432, 1996.

[67] T. Matsushita, T. B. Sato, K. Hirabayashi, S. Fujimura, T. Asazuma, and T. Takatori. X–ray study of the human neck motion due to head inertia loading. In *38th Stapp Car Crash Conference*, New York, 55–64, 1994.

[68] K. Ono and M. Kanno. Influences of the physical parameters on the risk to neck injuries in low impact speed rear–end collisions. In *International IRCOBI Conference on the Biomechanics of Impacts*, 201–212, 1993.

[69] D. H. West, J. P. Gough and G. T. K. Harper. Low speed rear–end collision testing using human subjects. *J Acc Recon*, 1:22–26, 1993.

[70] K. Schneider, R. F. Zernicke and G. Clark. Modelling of jaw–head–neck dynamics during whiplash. *J Dent Res*, 68(9):1360–1365, 1989.

[71] R. P. Howard, J. V. Benedict, J. H. Raddin and H. L. Smyth. Assessing neck extension–flexion as a basis for temporomandibular joint dysfunction. *J Oral Maxillofac Surg*, 49:1210–1213, 1991.

[72] J. H. Koolstra, T. M. G. J. Van Eijden, W. A. Weijs and M. Naeije. A three dimensional mathematical model of the human masticatory system predicting maximum possible bite–forces. *J Biomechanics*, 21:563, 1988.

[73] A. V. Hill. The heat of shortening and the dynamic constants of muscle. *Proc R Soc (B)*, 126:136–195, 1938.

[74] A. F. Huxley. Muscle structure and theories of contraction. In J. A. V. Butler and B. Katz, editors, *Progress in Biophysics and Biophysical Chemistry*. The MacMillan Company, New York, 6–318, 1957.

[75] D. Hawkins and M. Bey. A comprehensive approach for studying muscle-tendon mechanics. *J Biomechanics*, 116:51–55, 1994.

[76] H. Yamada. Strength of biological materials. Baltimore, 1970.

[77] A. M. Gordon, A. F. Huxley and F. J. Julian. Contraction of muscle cells. *J Physiol*, 184–170, 1966.

[78] A. Manns and M. Spreng. EMG amplitude and frequency at different muscular elongations under constant masticatory force or EMG. *Acta Physiol Lat Ann*, 27:259, 1977.

[79] B. R. Jewell and D. R. Wilkie. An analysis of the mechanical components of frog striated muscle. *J Physiolog*, 143:515–540, 1958.

[80] G. I. Zahalak. A distribution moment approximation for the kinetic theory of muscular contraction. *Math Biosci*, 55:89–114, 1981.

[81] G. I. Zahalak. A comparison of the mechanical behaviour of the cat soleus muscle with a distribution moment model. *J Biomech Eng*, 108:131–140, 1986.

[82] S. H. Backaitis and Mertz. *HYBRID III, The first human like crash test dummy*, chapter 1. SAE Intl., 1994.

[83] H. J. Clemens and K. Burow. Experimental investigation on injury mechanisms of cervical spine at frontal and rear–front vehicle impacts. In *16th Stapp Car Crash Conference*, New York, 76–104, 1972.

[84] C. L. Ewing and D. J. Thomas. Human head and neck responses to impact acceleration. Joint Army Navy Monograph, No. 21, 1972.

[85] F. A. Baragar and J. W. Osborn. A model relating patterns of human jaw movement to biomechanical constraints. *J Biomechanics*, 17(10):757–767, 1984.

[86] M. R. Seemann, W. H. Muzzy and L. S. Lustick. Comparison of human and Hybrid III head and neck response. In *30th Stapp Car Crash Conference*, 291-313, 1986.

[87] J. Y. Foret-Bruno, F. Dauvilliers and C. Tarriere. Influence of the seat and headrest stiffness on the risk of cervical injuries in rear impact. In *Proc. 13th ESV Conference*, number 91-S8-W-19, Paris, France, 1991.

[88] M. Y. Svensson and P. Lovsund. A dummy for rear-end collisions – development and validation of a new dummy neck. In *Neck Injuries in Rear–End Collisions*. Department of Injury Prevention Goteborg, 1993.

[89] W. E. McDevitt. *Functional Anatomy of the Masticatory System*. Wright, 1989.

[90] J. W. Osborn and F. A. Baragar. Predicted pattern of human muscle activity during clenching derived from a computer assisted model: symmetric vertical bite forces. *J Biomechanics*, 18(8):599–612, 1985.

[91] R. Craik and C. Oatis. *Gait analysis: Theory and Application*. Mosby, 1995.

[92] P. J. Davis and P Rabinowitz. *Methods of numerical integration*. Academic Press, 1984.

[93] J. R. W. Morris. Accelerometry – a technique for the measurement of human body movements. *J. Biomechanics*, 6:729–736, 1973.

[94] M. Whittle. *Gait analysis: an introduction*. Butterworth Heinemann, 1996.

[95] B. R. Durward, G. D. Baer, and P. J. Rowe. *Functional human movement: measurement and analyis*. Butterworth Heinemann, 1999.

[96] A. T. M. Willemson, C. Frigo, and H. B. K. Boom. Lower extremity angle measurement with acceleromters - error and sensitivity. *IEEE Transactions of Biomedical Engineering*, 38(12), 1991.

[97] E.Y.S. Chao. Justification of tri-axial goniometer for the measurement of joint rotation. *J. Biomechanics*, 13:989–1006, 1990.

[98] H. S. Gill, J. Morris, E. Biden, and J. J. O'Connor. Optometric methods in gait analysis. In J. F. Orr and J. C. Shelton, editors, *Optical measurement methods in biomechanics*. Chapman and Hall, 1997.

[99] J. L. Synge and B. A. Griffith. *Principles of Mechanics*, chapter 4. McGraw–Hill, Tokyo, 3 edition, 114–116, 1959.

[100] W. F. Bell. *Clinical management of temporomandibular disorders*. Year Book Publishers Inc, New York, 1982.

[101] H. Sicher. Functional anatomy of the temporomandibular joint. In B. C. Sarnat, editor, *The Temporomandibular Joint*. C. C. Thomas and Co., Springfield, Illinois, 1951.

[102] C. Hirsch and J. Galante. Laboratory conditions for tensile tests in annulus fibrosis from human intervertebral discs. *Acta Orthop Scand*, (38):148–162, 1967.

[103] C. M. Gratz. Tensile strength and elasticity tests on human fascia lata. *J Bone Jt Surg*, 13:334, 1931.

[104] A. Viidik, L. Sandquist and M. Magi. Influence of postmortal storage on tensile strength characteristics and histology of rabbit ligaments. *Acta Orthop Scand*, 7–38, 1965.

[105] J. P. Stapp. Voluntary human tolerance levels. In *Impact Injury and Crash Protection*. C. C. Thomas and Co., Illinois, Springfield, 308–349, 1970.

[106] A. M. Eiband. Human tolerance to rapidly applied acceleration: A survey of the literature. In *National Aeronautics and Space Administration*, number NASA memo no. 5–19–59E. NASA, 1959.

[107] R. F. Neathery. An analysis of chest response data and scaled performance recommendations. In *18th Stapp Car Crash Conference*, volume 74188, Warrendale, PA, 459–493, 1974.

[108] Lau V. and Viano D. The viscous criterion – bases and applications of an injury severity index for soft tissues. In *30th Stapp Car Crash Conference*, 1986.

[109] D. Roberts and I. Tattersall. Skull form and the mechanics of mandibular elevation in mammals. *Amer Mus Novitates*, (2536):1–9, 1974.

[110] I. Tattersall. Cranial anatomy of archeolemurinae (lkemuroidea primates). *Anthropol Pap Am Mus Natl Hist*, 52:1–110, 1973.

[111] G. Steinhardt. Anatomy and function of the temporomandibular joint. *Inter Dent J*, 8:155–156, 1958.

[112] J. H. Scott. A contribution to the study of mandibular joint function. *Brit Dent J*, 94:345–349, 1955.

[113] M. Robinson. The temporomandibular joint: thoery of reflex controlled non-lever action of the mandible. *J Am Dent Assoc*, 33:1260–1271, 1946.

[114] G. H. Wilson. The anatomy and physics of the temporomandibular joint. *J Natl Dental Assoc*, 8:236–241, 1920.

[115] J. C. Barbenel. The biomechanics of the temporomandibular joint. *J Biomechanics*, 5:251–256, 1972.

[116] P. Gingerich. The human mandible: lever, link, or both? *Am J Phys Anthropol*, 1979.

[117] W. Hylander. An experimental analysis of temporomandibular reaction force in macaques. *Am J Phys Anthropol*, 51:433, 1979.

[118] K. Brehnan, R. L. Boyd, J. Laskin, C. H. Gibbs and P. Mahan. Direct measurement of loads in the temporomandibular joint in macaca arctoides. *J Dent Res*, 60(10):1820–1824, 1981.

[119] H. Sicher. *Oral Anatomy*. C.V. Mosby and Co., St Louis, 1951.

[120] J. M. Smith and R. J. G. Savage. The mechanics of mammalian jaws. *School Science Review*, (40):289–301, 1959.

[121] A. W. Crompton and K. M. Hiiemae. How mammalian molar teeth work. *Discover*, 5:23–34, 1969. Yale Peabody Museum.

[122]

[123] J. W. Osborn. The disc and the human temporomandibular joint. *J Oral Rehab*, 12:279–293, 1985.

[124] T. M. G. J. van Eijden, P. Brugman, W.A. Weijs, and J. Oosting. Coactivation of jawmuscles: recruitment order and and level as a function of bite force direction and magnitude. *J Biomechanics*, 5:475–485, 1990.

[125] C. S. Tien and R. L. Huston. Biodynamic modelling of the head–neck system: Field accidents, data collections, analysis, methodologies and crash injury reconstructions. *SAE No. P159*, 359–364, 1985.

[126] R. P. Howard, C. P. Hatsell and H. M. Guzman. Temporomandibular joint injury potential imposed by the low velocity extension flexion maneuver. *J Oral Maxillofac Surg*, 53:256–262, 1995.

[127] G. J. Pruim, H. J. de Jongh and J. J den Dosch. Forces acting on the mandible during bilateral static bite at different bite force levels. *J Biomech*, 13:755–763, 1980.

[128] L. A. Rees. The structure and function of the temporomandibular joint. *British Dental Journal*, 96(125), 1954.

[129] K. Nakazawa and K. Kawimura. *Anatomical Atlas of the Temporomandibular Joint*. Quintessence Publishing, 1991.

[130] L. Bannister, M. Berry, P. Collins, M. Dyson, J. Dussek and M. Ferguson, editors. *Gray's Anatomy*, chapter 6. Churchill Livingstone, 38 edition, 516-521, 1995.

[131] H. Meyer. Das Kiefergelenk. *Archiv fuer Anatomie und Physik*, 1865.

[132] W. Wallish. Das Kiefergelenk. *Zeitschrift fuer Anatomie und Entwicklungsgeschichte*, 64(533), 1922.

[133] Y. Wang. The function of temporal, masseter, digastric and external pterygoid muscles in different positions of the mandible and occlusion during mandibular movement. In *Theses of stomatologic medicine*. Beijing Medical College, 1984.

[134] B. S. Kraus, R.E. Jordan and L. Abrams. *Dental anatomy and occlusion*. Williams and Wilkey, Baltimore and London, 1969.

[135] R. P. Juniper. The superior pterygoid muscle. *British J Oral Surg*, 19(21), 1981.

[136] P. G. Grant. Biomechanical significance of the instantaneous centre of rotation: The human temporomandibular joint. *J Biomechanics*, 6:109–113, 1973.

[137] W. Jinbao, X. Xiaoming and S. Jingen. Analysis of the open–closing movement of the human temporomandibular joint. *Acta Anat*, 1:213–216, 1988.

[138] J. Chen and K. Buckwalter. Displacement analysis of the temporomandibular condyle from magnetic resonance images. *J Biomechanics*, 26(12):1455–1462, 1993.

[139] Y. C. Fung. *Biomechanics: Mechanical properties of living tissue.* Springer Verlag, 1993.

Appendix A

Glossary of Medical Terms

Acoustic neuroma   Neoplasm derived from cells of the nervous system

Aetiology   The science of the cause of a disease

Anterior   Relating to the front portion of the body or limbs

Arthrography   X–ray technique for examining joints

Auriculo–temporal   Relating to the auricle of the ear and the temporal region

Autolysis   Postmortal breakdown of tissue under the actions of its own enzymes

Avascular necrosis   Lack of blood to organs resulting in death

Bruxism   Habit of grinding the teeth, leading to excessive wear

Collagen	A protein that is the principal constituent of white fibrous connective tissue. It is relatively inelastic and has a high tensile strength.
Contralateral	Referring to the opposite side
Crepitation	Crackling or grating feeling produced by bone rubbing on bone or roughened cartilage
Deviation	A departure from normal mouth–opening, usually involving lateral motion of the mandible during opening
Effusion	Escape of fluid from blood vessels or lymphatics into a tissue or cavity
Epidemiology	The study of epidemic disease, with a view to finding means of future control and prevention
fascia	A sheet of fibrous tissue that envelops the body beneath the skin
Fasciculi	Small bundles
Frankfort plane	A horizontal plane of the skull
Frontal plane	The plane that extends down the long axis of the body, dividing it into front and rear halves

Histology	The study of the structure of tissue
Hyaline cartilage	The most common type of cartilage: elastic material with a matrix of chondroitin sulphate in which fine collagen fibrils are embedded.
Ipsilateral	Referring to the same side
Labyrinthitis	Inflammation of the middle ear labyrinth
Lateral	Relating to the side portion of the body or limbs
Magnetic resonance imaging	Diagnostic technique based on the analysis of the absorption and transmission of high–frequency radio waves by the water molecules in tissue placed in a strong magnetic field. T1 and T2 are two characteristic relaxation times after the magnetic resonance pulse has been applied. These are used for tissue identification
Medial	Relating to the central portion of the body or limbs.
Myofascial	Of or relating to the fascia surrounding muscle tissue
Myospasm	Muscular contraction
Neuralgia	Nerve pain
Occlusal	Pertaining to occlusion or closure

Oedema	Accumulation of liquid causing abnormal swelling of the tissues
Osteoarthritis	Degenerative or hypertrophic arthritis
Osteoarthrosis	Osteoarthritis
Posterior	Relating to the back portion of the body or limbs
Process	A thin prominence or protruberance
Proprioception	The response to motion, mechanical stress and position due to contraction of muscles, movements of joints and changes in position of the body
Reduction	Anterior displacement of the disc, preventing forward translation of the condyle, thereby limiting mouth–opening. The extent of reduction is affected by the slope of the articular eminence
Referred pain	Pain occurring at a location distant from the source
Retro–orbital	Referring to the rear of the eye sockets
Rhinorrhea	Discharge from the nasal mucus membrane
Sagittal plane	The plane that extends down the long axis of the body, dividing it into right and left halves

Septum	Wall dividing two cavities
Temporo–parietal	Relating to the temporal and parietal regions
Tinnitus	Unexplained noises in the ear
Vocal dystonia	Abnormal tonicity in vocal tissues

Appendix B

Anatomy

Detailed descriptions of the functional anatomy of the head and neck are available in a plethora of textbooks. This appendix is based on the work of McDevitt [89], Rees [128] and Nakazawa and Kamimura [129] and provides an outline of the anatomy of the neck and a more detailed description of the structure and function of the mandible and TMJ. A brief description of muscle physiology is also given.
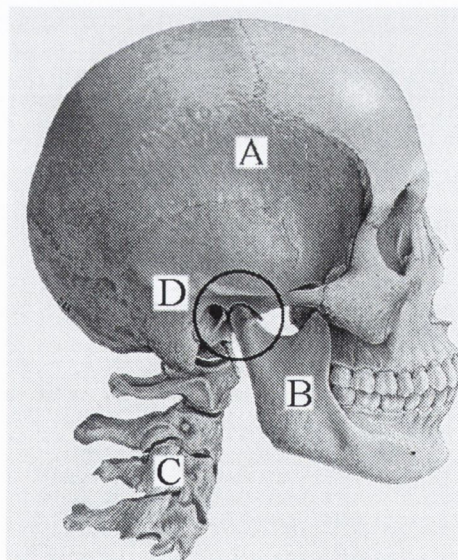
Figure B.1: Bony structures of the head and neck: the skull (A), mandible (B), vertebrae of the neck (C) and TMJ (D).

The Neck

The human neck is an almost cylindrical structure linking the head to the trunk. It is connected superiorly to the seat of the skull via the atlas and inferiorly to the thoracic vertebrae. The neck houses several vital components (including the jugular vein) but these are not significant in low velocity impacts. Rather the functional anatomy is determined by the cervical vertebrae and their controlling muscles and ligaments.

The Cervical Vertebrae

Seven cervical vertebrae form the skeleton of the neck, see figure B.2. These are a continuation of the lumbar and thoracic vertebrae, collectively forming the spinal column. The cervical vertebrae are oblong and broad. Articulation between the cranium and the vertebral column provides a wider range of motion than in the rest of the spine. The first vertebra (c_o) is called the atlas and is quite different from the others, see figure B.2. It supports the skull by articulation with the condyles of the occipital bone which is seated in the base of the skull, see figure B.4. The atlas has no body and no spinous process. It is a bony ring divided by a lateral mass on either side into an anterior and posterior arch. This lateral mass is a thick, load bearing section of bone and it makes the atlas the widest of the cervical vertebrae. The transverse processes are wide and act as strong levers for muscle actions. The axis (the second cervical vertebra) is an axle for rotation of the atlas and head around the odontoid process, see figure B.2.

There are three atlanto-axial joints: one pair between the lateral masses and a median pair between the dens of the axis and the anterior arch and transverse ligament of the atlas. Movement at the atlanto-axial joint occurs simultaneously at all three of these and results almost exclusively in pure rotation. The shape of the articular surfaces is such that rotation causes the axis to ascend into the atlantal ring and this limits stretch on the lateral joint capsules. The normal range of motion has been measured as 41.5°, but there are large variations between individuals (range 29–54°) [130].
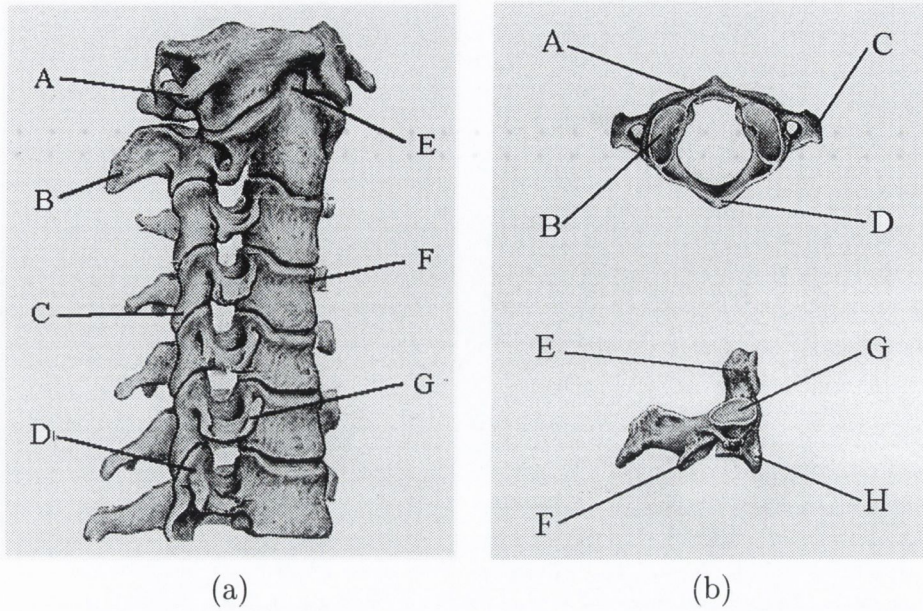
Figure B.2: Bony structures of the neck: (a) cervical vertebrae: transverse process (A), spinous process (B), inferior articular process (C), lateral process (D), odontoid process (E), superior articular process (F), anterior tubercle (G); (b) atlas A – D, axis E – H: anterior arch (A), superior articular surface (B), transverse process (C), posterior tubercle (D), odontoid process (E), inferior articular surface (F), superior articular surface (G) and body of axis (H).

Muscles and Ligaments of the Neck

The vertebral column is protected and reinforced by a very large number of muscles and ligaments. Figures B.3 and B.4 show some (but not all) of the major neck muscles and ligaments. It is clear that these combine to produce a highly complex layered sheath surrounding the vertebral column. They have the collective property of making the neck a structure which can bend but also allows for some translation in the horizontal plane. The mobility of the neck is remarkable: a 50th percentile male skull has a mass of ca. 4.5kg and yet the neck muscles are sufficiently powerful to facilitate rapid yet precise head movements in all directions. Modelling the response of the neck to rear impact is discussed in chapter 3.
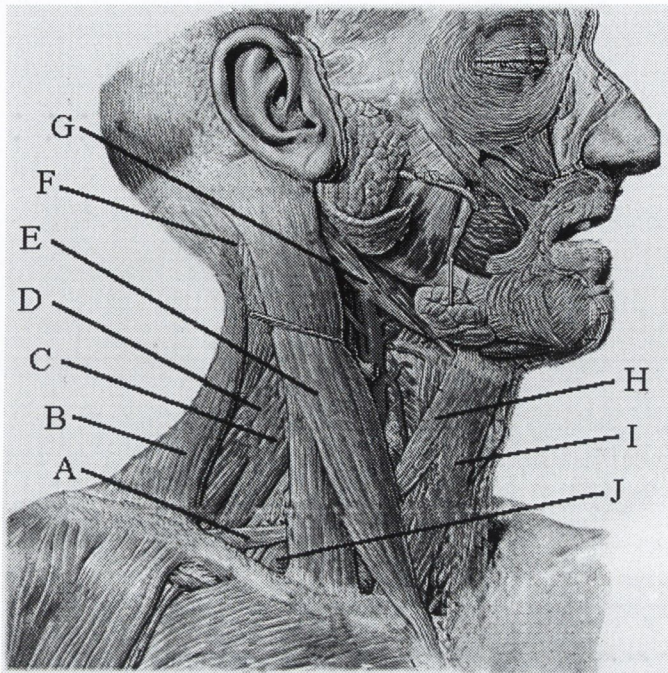
Figure B.3: Muscles of the neck: omohyoid – inferior belly (A), trapezius (B), scalenus medius (C), levator scapulae (D), sternocleidomastoid (E), splenius capitis (F), digastric muscle – inferior belly (G), omohyoid – superior belly (H), sternohyoid (I) and scalenus anterior (J).

The Mandible and Temporomandibular Joint

The Mandible

The TMJ has traditionally received less attention from anatomists than the larger synovial joints of the human body. Leonardo da Vinci and Vesalius described the elevator muscles of the mandible in the fifteenth and sixteenth centuries respectively. In the eighteenth century, Ferrein gave a description of jaw movements. By the mid nineteenth century, the study of anatomy had become more formalised – the first edition of Gray's Anatomy appeared in 1858 – and the TMJ was analysed successively by two German anatomists, Meyer in 1865 [131] and Wallish in 1922 [132]. However, the most important work on the anatomy of the TMJ was carried out at The Queens University of Belfast by Leonard Rees and pub-
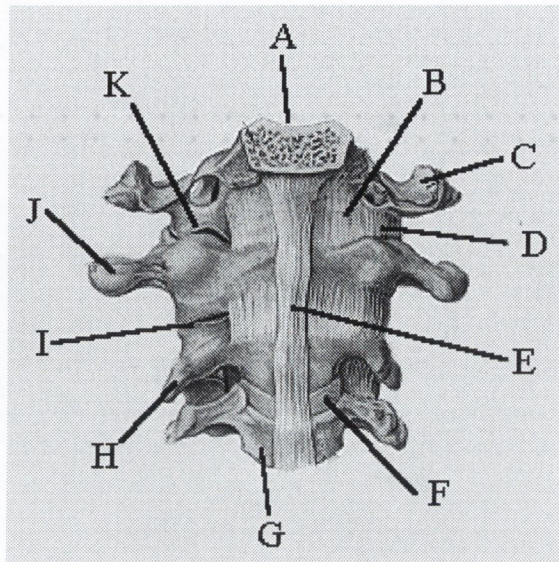
Figure B.4: Anterior view of ligaments and articulations of first three cervical vertebrae: occipital bone (A), atlanto-occipital membrane (B), skull (C), articular capsule (D), anterior longitudinal ligament (E), intervertebral disc (F), third cervical vertebra (G), axis (H), atlanto–axial joint (I), atlas (J) and atlanto–occipital joint (K).

lished posthumously in 1954 (as Rees was killed in an aircraft accident). Although the basic anatomy was well established by that stage, there was considerable debate regarding histology and function. Rees's fundamental work investigated the structure, composition and function of the disc of the TMJ.

The mandible is the mobile part of the human masticatory system. It must be capable of fine tuned movements for speech while at the same time produce considerable crushing forces for the ingestion of food. It is a U-shaped bone built around a central neurovascular supply, see figure B.5. There are several bony processes which enable the mandible to carry out its primary functions:

1. The alveolar process, which supports the teeth in a horizontal arch.

2. The muscular processes, surrounding the coronoid process.
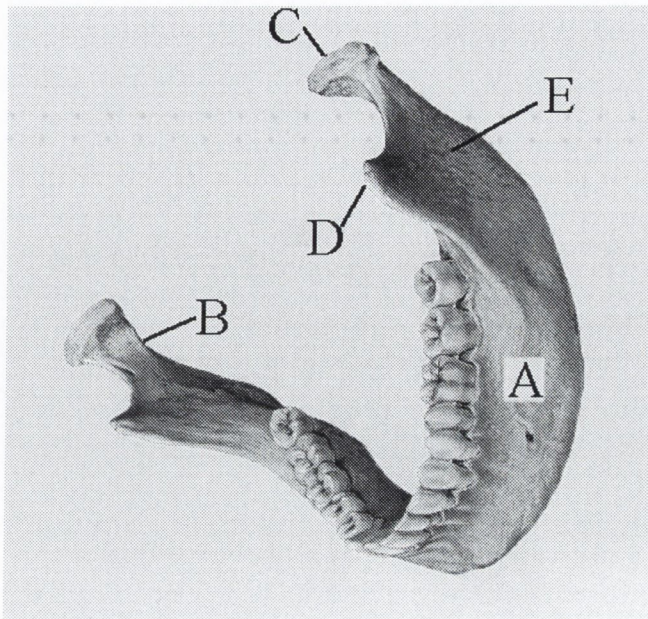
Figure B.5: Bony structures of the mandible: body of the mandible (A), neck of the mandible/condylar process (B), condyle (C), coronoid process (D) and ramus (E).

3. Articular processes, which stabilise the moving bone and provide hinging and pivoting surfaces and fulcra for the application of force. The articular surfaces of the teeth provide a limit to vertical motion of the mandible while the right and left condylar processes dictate the pivoting movements.

The Temporomandibular Joint

The TMJ is composed of the condylar process of the mandible and the glenoid structures in the base of the skull. The TMJ closely demonstrates the correlation between structure and function – a freely movable hinge–joint whose articular surfaces are comprised mainly of collagen (rather than hyaline cartilage seen in most other joints of the body. [53]). The condylar process is made up of a slim neck and a semi–cylindroid condyle. The condyle is about twenty millimetres from pole to pole and ten millimetres thick, see figure B.6. There is great variability in the form of the condyle, even between the two sides of the same subject [89]. The
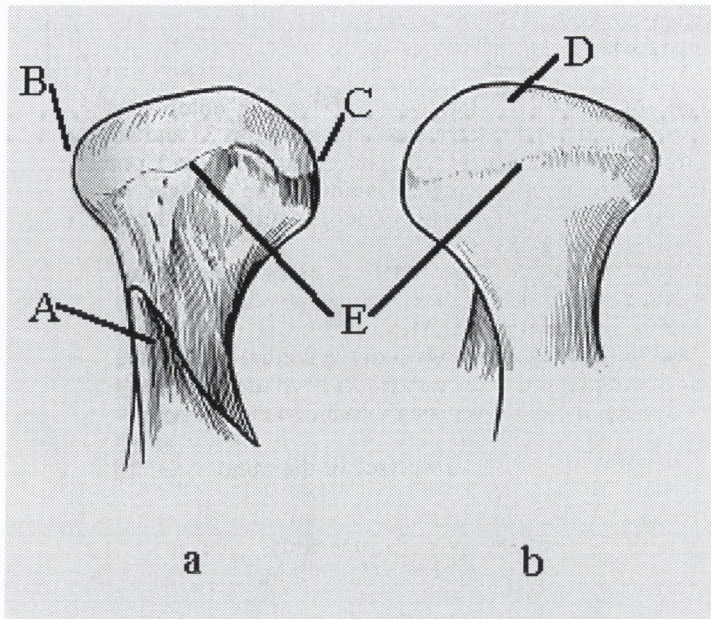
Figure B.6: (a) Anterior and (b) posterior views of the condyle: condylar neck (A), lateral pole (B), medial pole (C), articular surface (D) and the border of the articular surface (E).

antero–superior surface is the articulating surface. The articular surface stretches the whole width of the condyle and all surrounding surfaces curve away from the articulating face.

The Glenoid Structures

The TMJ is housed in the squamous portion of the temporal bone. The skull portion of the joint consists of a vault-like hollow posteriorly, called the glenoid fossa, and a slope rising out of the fossa anteriorly, known as the articular eminence, see figure B.7. The glenoid structures form the fixed articulating part of the TMJ, and the shape of the fossa corresponds roughly to that of the mandibular condyle. The articular eminence, rising anteriorly out of the fossa, provides a downward guide for the anteriorly moving condyle. The bony surfaces of the joint (condyle and fossa) constitute only a loose fit and soft–tissue fills the remaining space.
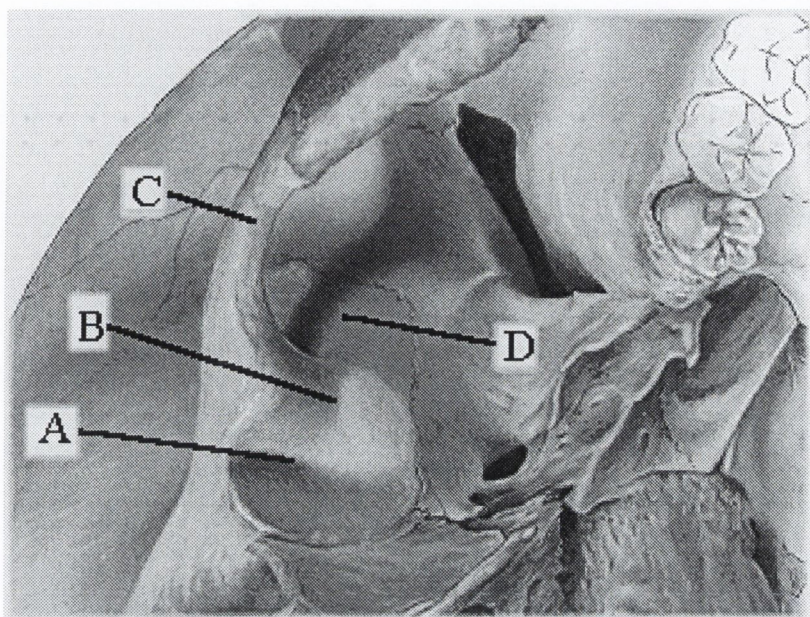
Figure B.7: The glenoid structures: glenoid fossa (A), articular eminence (B), zygomatic arch (C) and pre–glenoid plane (D).

Soft–tissue components of the TMJ.

The primary soft–tissue components of the TMJ are the articular disc, articular capsule, ligaments and muscles. Those surfaces directly subjected to load–bearing pressure are provided with a smooth layer of fibrous tissue that is highly resistant to rubbing and shear stress and is tightly bound to the joint surface. This specialised surface is thickest where the stress is greatest and most often applied [100] [101]. Consequently, it is not present in the side-walls of the glenoid fossa. The synovia are specialised secretory membranes which provide a nutrient, lubricating and cleansing service for the load–bearing surfaces.

The Articular Disc

The space between the articular surfaces of the TMJ is occupied by the articular disc, see figure B.8. This continuous structure fits snugly over the condyle and is closely adapted to the surfaces of the glenoid fossa. The disc is attached to
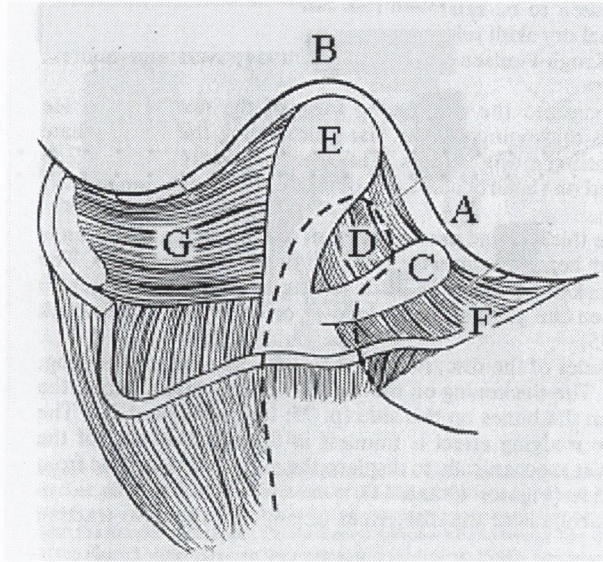
Figure B.8: The articular disc: glenoid fossa (A), articular eminence (B), anterior band of disc (C), intermediate zone of disc (D), posterior band of disc (E), anterior extension of disc (F) and bilaminar zone of disc (G).

the condyle (B), pre–glenoid plane (C), capsule of the TMJ (D), posterior wall of the glenoid fossa (E), muscle tissue (F) and to the middle ear (G), see figure B.9. The superior part of the lateral pterygoid gains insertion into the disc and adjacent parts of the masseter and temporal muscles are also connected to the disc. However, there is considerable variation between individuals and in some cases masseter and temporalis may have no insertion at all [128]. The disc is essentially a collagenous structure but its composition is complex. Rees's findings supported the popular (but not consensus) opinion on the type and degree of movement in the two cavities of the joint. At that time there was some disagreement on whether the disc travelled anteriorly with the condyle during mouth–opening, as it was contended that the posterior attachments of the disc to the temporal bone would prevent anterior disc motion. Rees found several factors indicating that the condyle and disc assembly do both travel anteriorly in mouth–opening, but at differing rates. He found that the lateral pterygoid gains true tendinous insertion into the anterior portion of the disc and that the posterior attachment of the disc to the temporal bone consists of loose, fibro-elastic tissue stretchable by ca. 7–10mm

in a dissected specimen [53]. Further, the disc is tightly bound down onto the condyle at both poles, and since the anterior pull exerted by the lateral pterygoid during mouth–opening [133] is near the axis of the condyle, this allows the latter to rotate (i.e. mouth–opening) as the disc is pulled forwards. The result is that the disc translates more slowly than the condyle and the condylar ridge contacts differing portions of the disc at various stages of translation. There is an approximate 2:1 ratio of condyle to disc displacement in mouth–opening. These motions were observed in specimens dissected in the sagittal plane. Rees also identified four distinct transverse portions of the disc with varying thickness, see figure B.8.

- an anterior band, which is moderately thick but relatively narrow.

- an intermediate zone. This is much thinner and narrower.

- a posterior band. This is the thickest and the widest portion.

- the posterior attachment, a thick and spongy bilaminar region that delaminates posteriorly into a stretchable temporal attachment and a stiff mandibular attachment. Loose, areolar connective tissue fills the space between these two attachments [53].

Rees postulated that the purpose of these bands with thicker and thinner zones was to make the disc more flexible and allow it to change its shape as it slides forward. This would permit a more stable locus of translation for the condyles, as they would then not be constrained to follow the often rough contours of the temporal surface.

The capsule of the TMJ

The capsule of the TMJ is a loose, tapering, thin-walled cuff of white collagenous tissue enclosing the bony parts and the disc of the joint, see figure B.10. The capsule surrounds the joint cavities. The upper joint cavity (or compartment) is between the glenoid fossa and the superior surface of the disc, while the lower joint cavity is between the articular surface of the condyle and the inferior surface
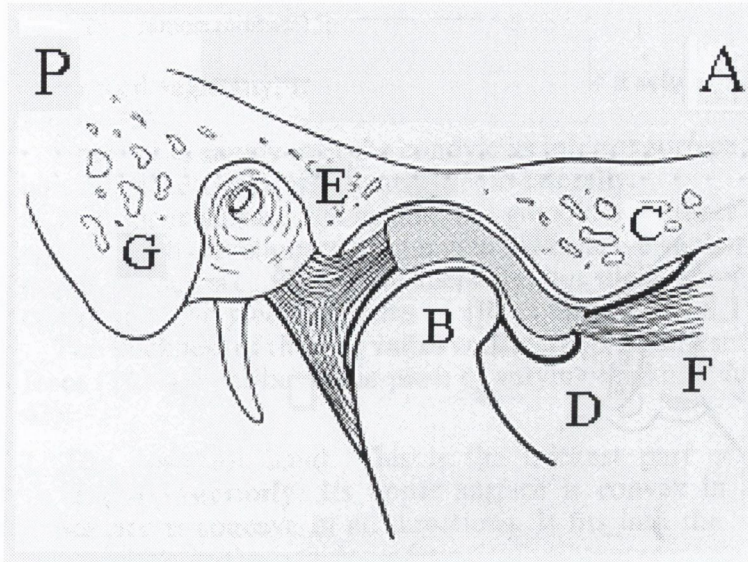
Figure B.9: Sagittal section of attachments to the disc: condyle (B), pre–glenoid plane (C), capsule (D), posterior wall of fossa (E), lateral pterygoid (F) and middle ear (G).

of the disc. These compartments play a vital role in articulation of the joint in mouth–opening, see section B. The capsule performs several functions:

- enclose and delineate the two joint cavities.

- confine the synovial fluid. This is the fluid that cleans and feeds the joint.

- provide continuity of attachment from muscle to disc: there are muscle attachments into the disc, and these must pass through the capsule.

- provide a weak restraining action. Anteriorly, the capsule is very weak and often entirely absent.

Ligaments of the TMJ

As the capsule is thin, it is inadequate to support and limit joint movement. The temporomandibular ligament, the collateral ligaments and other accessory ligaments act as supporting structures for this purpose. The temporomandibular
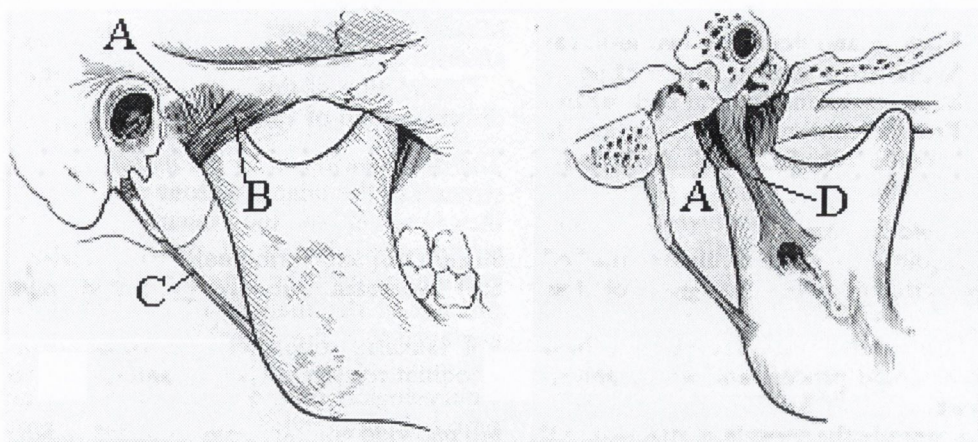
Figure B.10: Sagittal section of the capsule and ligaments of the TMJ: capsule (A), temporomandibular ligament (B), stylomandibular ligament (C) and spheno-mandibular ligament (D).

ligament is the primary ligamentous reinforcement of the joint, see figure B.10. It is a fan–shaped structure and its location prevents posterior motion of the condyle as well as providing lateral stability. The accessory ligaments (sphenomandibular and stylomandibular) provide little overall stability to the joint [89].

Muscles

The muscles involved in mastication are divided into mouth–closing groups for biting and mouth–opening groups for separating the jaws. The mouth–closing group consists of the masseter, medial and lateral pterygoids and the temporalis. However, the function of the lateral pterygoid is not straightforward. The mouth–opening group is divided into the suprahyoid and infrahyoid muscles. These groups are presented separately.

Masseter

The masseter is a bulky, rectangular mass on the side of the face. It is attached between the lateral surface of the ramus of the mandible and the zygomatic arch and lies just beneath the skin. For functional purposes, the masseter can be divided

into a superficial and deep part, see figure B.11. The internal structures of the masseter and medial pterygoid muscles are dominated by the presence of large tendinous septa, which enlarge the areas available for attachment of the muscle fasciculi. This allows the masseter to have a multi–pennate structure and greatly increases both power and the options for directional pull. As a result the major bulk of tissue is in the middle of the masseter [89]. The masseter is designed for crushing and grinding of food. In addition to elevating the mandible, the masseters can exert anterior vectors by the spread of contraction from the most anterior to the most posterior fasciculi [134].
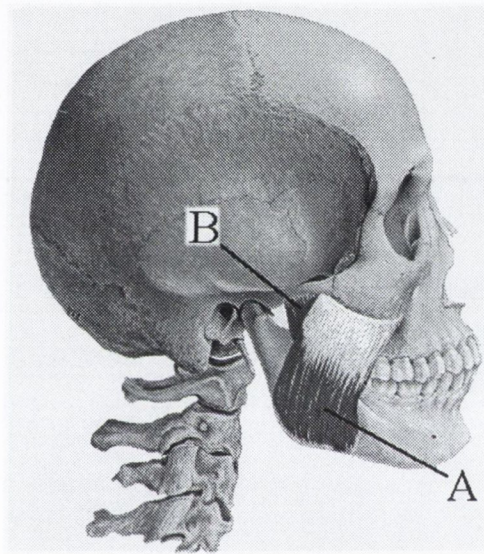
Figure B.11: The masseter muscle: superficial (A) and deep portions (B).

Medial Pterygoid

The medial pterygoid is a thick, rectangular, powerful mass of muscle tissue arising from the area around the pterygoid fossa and inserting into the medial surface of the ramus of the mandible, see figure B.12. It is not as thick or as wide as the masseter. In cooperation with the masseter it forms a sling that elevates the mandible for occlusion with bilateral contraction and produces lateral movement of the mandible with unilateral contraction.
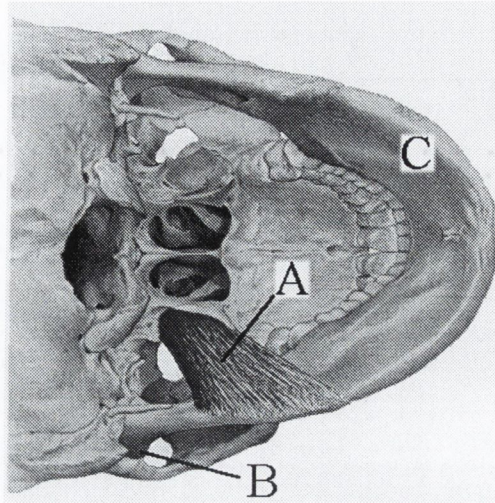
Figure B.12: The medial pterygoid muscle (A), condyle (B) and body of the mandible (C).

Lateral Pterygoid

The lateral pterygoid muscle consists of a superior and an inferior head, see figure B.13. The superior head originates from the infratemporal surface of the great wing of the sphenoid bone and inserts into the capsule and disc of the TMJ. Laterally, the origin blends with the temporalis muscle. Since the disc is firmly attached to the condyle at the lateral and medial poles, and posteriorly to the neck of the condyle between the poles, the superior head may be considered to have a stirrup–like ligamentous attachment to the condylar process of the mandible [135]. This means that traction applied to the disc is also indirectly applied to the neck of the mandible. The superior head of the lateral pterygoid is active during posterior movement of the ipsilateral condyle. The inferior head originates from the lateral surface of the lateral pterygoid plate and inserts into the anterior portion of the neck of the condyle. The function of the inferior head is to protrude the ipsilateral condyle/disc assembly to manoeuvre the hingeing axis of the mandible into functional positions. It is also active in rotating the mandible in simple depression and helps prevent superior and distal displacement of the condyle. It is not an elevator muscle.
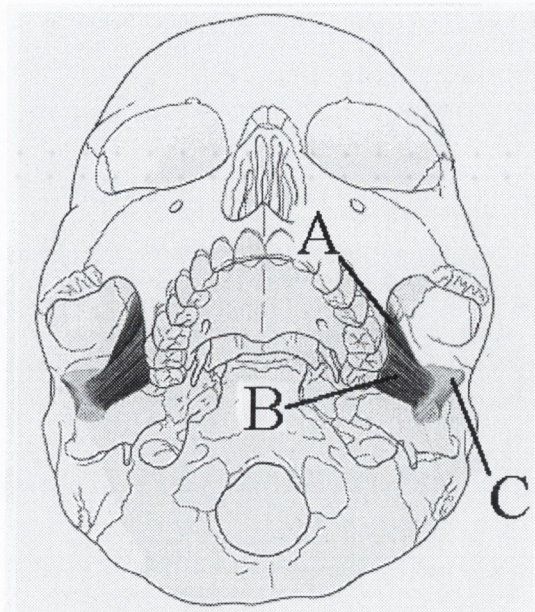
Figure B.13: The lateral pterygoid muscle: superior head (A), inferior head (B) and condyle (C).

Temporalis

This is a bipennate muscle with a fan–shaped origin and very large, tough tendons of insertion into the coronoid process, deep temporal crest and anterior border of the ramus of the mandible, see figure B.14. This muscle has been divided into anterior, middle and posterior sections on the basis of area of origin and direction of the fibres. The anterior fibres arise from the anterior portion of the temporal fossa and run almost straight downwards. The middle fibres arise from the wide area in the middle of the temporal fossa and run downward with a slight anterior inclination. The posterior fibres run from the posterior part of the temporal fossa and run anteriorly. All three insert into the area around the coronoid process of the mandible, giving the muscle its fan shape. This muscle is designed for producing a strong bite force.
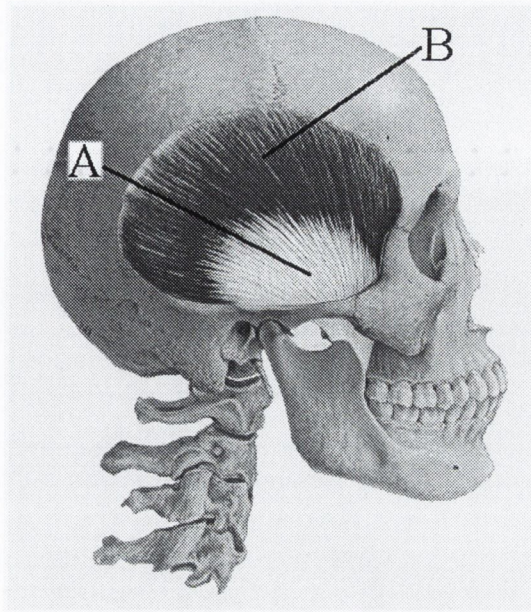
Figure B.14: The temporalis tendon (A) and muscle (B).

Hyoid muscles

The suprahyoid muscles are located in the floor of the mouth and act to pull the mouth downward for opening and raise the floor of the mouth for swallowing. These are the digastric, stylohyoid, mylohyoid and the geniohyoid, see figure B.15.

Digastric

The digastric has two bellies located antero–posteriorly that are united by a long intermediate tendon. Both bellies insert into the tendon, which is not fixed directly to the hyoid bone, but is connected by a loop of fibrous connective tissue. The intermediate tendon passes through the stylohyoid muscle at its insertion onto the hyoid bone. The anterior belly arises from the digastric fossa on the posterior wall of the anterior portion of the mandible, see figure B.15. The digastric muscle is the primary mouth–opening muscle. It achieves this when the hyoid bone is stabilised by the infrahyoid muscle group.
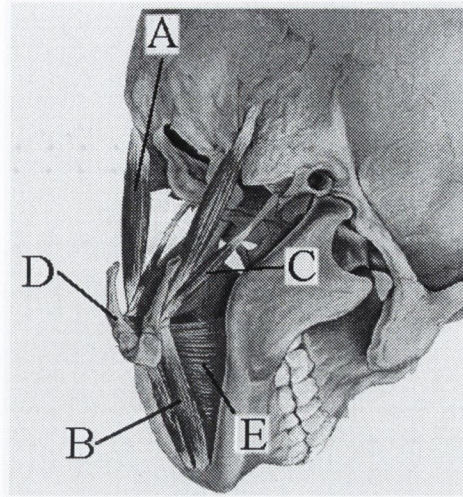
Figure B.15: The suprahyoid muscles: digastric, posterior (A) and anterior (B) bellies, stylohyoid (C), hyoid bone (D) and omohyoid (E), geniohyoid not shown.

Stylohyoid

This arises from the styloid process of the temporal bone and inserts into the body of the hyoid bone. The stylohyoid raises the floor of the mandible during swallowing.

Mylohyoid

This forms the floor of the mouth.

Geniohyoid

The geniohyoid consists of a pair of narrow muscles located superior to the mylohyoid. This muscle aids in opening the mouth when the hyoid bone is stabilised.

Functional considerations

Contraction of the digastric muscle applies traction to the body of the mandible near the midline, in an inferior and posterior direction. If the anterior and posterior bellies are considered to act as one, then the mechanical advantage of the digastric muscle is the greatest of all for achievement of depression of the mandible [89].

The remaining suprahyoids may contribute to depression of the mandible but are probably not very significant in this respect. These muscles are movers of the hyoid bone and elevate the floor of the mouth when the mandible is stabilised. The infrahyoid group of muscles aids stabilisation and movement of the hyoid bone, and has only a peripheral function in the masticatory system. Thus the supra and infra–hyoid group of muscles do not significantly affect the mandible during the retroflexion manoeuvre of the head.

Mechanics of Mouth–opening

The importance of Rees's work lies in the fact that he attempted to correlate structure with function in the TMJ, rather than merely mapping the topography of his dissections. He identified distinct phases of mouth–opening and closing and barely altered versions of his diagrams and descriptions can be found in many standard textbooks. Mouth–closing is essentially the reverse of mouth–opening, so only the opening phases are described here.
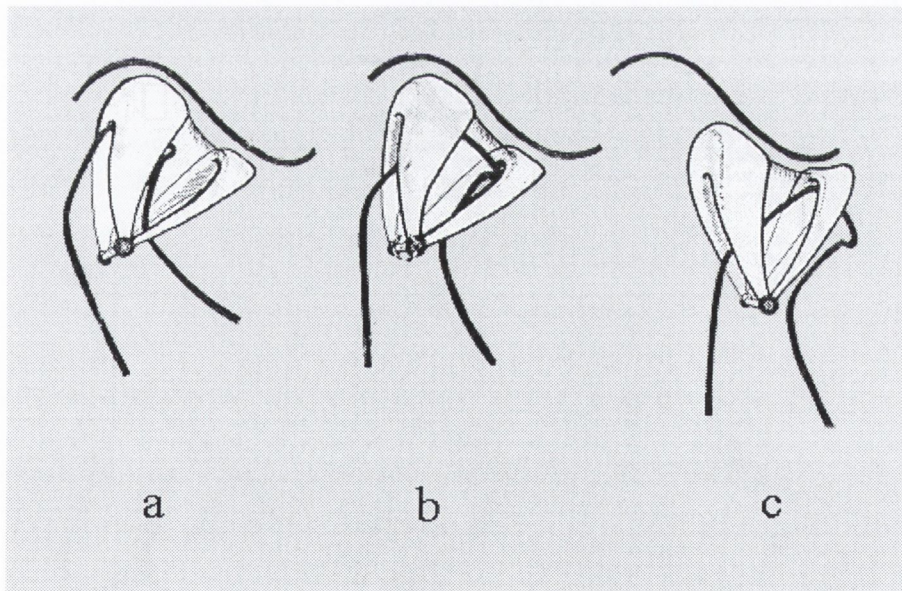
Figure B.16: Relationship between disc, condyle and fossa: (a) mouth closed; (b) opening; (c) fully open.

- **Occlusal Phase** This is when the mouth is closed with upper and lower teeth interlocking, see figure B.16a. The posterior band of the disc fills the deepest part of the fossa. The bilaminar region is relaxed but the attachments of the disc to both condylar poles are taut. This means that further rearward motion of the condyle will draw the disc with it, and such motion will be limited by the temporomandibular ligament (TML) and by tension of the meniscus from its anterior attachments.

- **Retruded Opening Phase** The condyles rotate about the intercondylar axis, which remains approximately stationary. The condylar ridge slides forward by 5–6 mm to the intermediate zone of the meniscus, see figure B.16b. The upper surface of the meniscus is simultaneously beginning to slide forwards on the temporal bone.

- **Protrusive Opening Phase** The intercondylar axis moves forward and downward on the slope of the articular eminence as the condyles continue to rotate *about this axis* (subsequent research has shown this latter statement to be incorrect: the true axis of rotation of the mandible is not the intercondylar axis. When a rigid body rotates about an axis which is itself translating, the locus of the overall axis of rotation will not be the original point [136, 137]. The biomechanical significance of the instantaneous centre of rotation of the mandible is reflected in the difference between using the intercondylar axis instead of the true centre of rotation of the mandible for static joint loading calculations [136]. The condylar ridge moves further forward on the lower surface of the intermediate zone, which is interposed between the anterior slope of the condylar articular surface and the articular eminence during this movement. The bilaminar region and its temporal attachment are stretched about 6–9mm by this motion.

- **Extreme Protrusive Opening Phase** The posterior portion of the disc has now been stretched to near its limit. The condyles are still moving forward and down as well as rotating and when close to maximum opening the condylar ridge slips over the anterior band of the disc, see figure B.16c.

194

This may produce an audible click in some people. This occurs when the disc is prevented from travelling further forward by its fully stretched temporal attachment. The limit of forward motion of the condyle is through the discal attachments at the condylar poles and by the temporomandibular ligament. Soft tissue is sucked in to fill the gap left posteriorly by the forward travelling condyle.

Recent publications have confirmed most of Rees's findings. Displacement analysis of the *in vivo* condyle using Magnetic Resonance Imaging (MRI) has given conclusive evidence that Rees's description of condylar motion during mouth–opening is correct [138]. However, there have been advances in understanding the function of the disc, notably from Osborn & Baragar at the University of Alberta in Edmonton. Osborn [123] concluded that the function of the disc is to destabilise the joint, thereby facilitating increased mobility. In addition, the presence of the disc acts to protect the fibrous tissue covering the osseous structures of the TMJ, whose purpose is to allow low–friction slide, spin and roll of the articular surfaces over each other. The rough contours of the osseous structures might otherwise puncture this fibrous layer. The disc is stabilised on the condyle by biomechanical rather than neuromuscular means, though proprioception in the ligaments will cause the muscles to fire also. The temporomandibular ligament must always be almost taut [85] and the volume of free movement of the mandible decreases to a minimum at full mouth–opening. Osborn & Baragar have since focussed on the prediction of bite forces but include Cartesian coordinates of origin and insertion points as well as cross-sectional areas for the elevator muscles of the mandible. These aided scaling and locating the model muscles in the dummy used in this thesis.

Early researchers considered that the mammalian TMJ was non load bearing [109, 110, 111, 112, 113, 114]. However, it is now generally accepted that the TMJ *is* load bearing during functional movements [115, 116, 117, 118, 119, 120, 121, 122]. Using pressure sensitive foil inserted into the TMJ's of macaques, it has been shown that the maximum loading in the joint during molar chewing is ca. 13N [118]. However, this was a difficult experimental process, and was not readily repeatable.

Muscle Structure and Function

Structure of skeletal muscle

The following text and diagrams are based on Fung's *Biomechanics – Mechanical Properties of Living Tissue* [139]. The units of skeletal muscle are the muscle
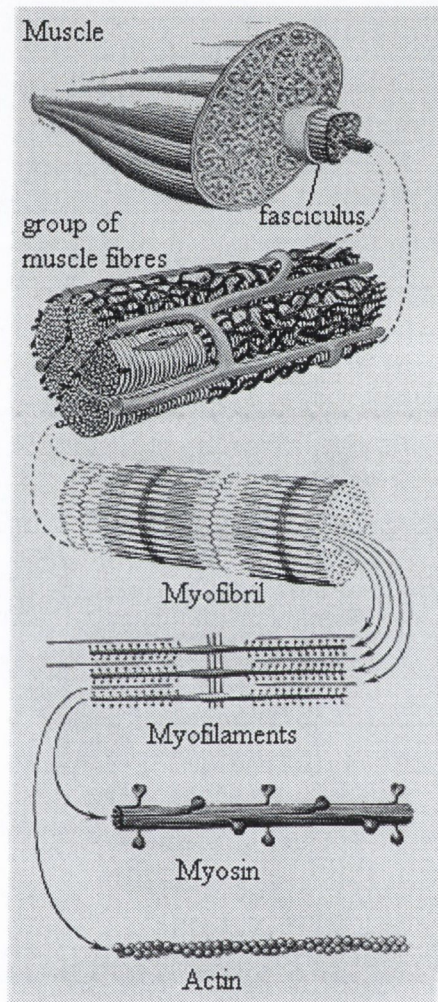
Figure B.17: Organisational hierarchy of skeletal muscle.

fibres, each of which is a single cell provided with many nuclei, see figure B.17. These fibers are arranged in bundles or fasciculi of various sizes within the muscle. Connective tissue fills the spaces between the muscle fibres within a bundle. Each bundle is surrounded by a stronger connective sheath, and the whole muscle is again surrounded by an even stronger sheath. Skeletal muscle fibres are

elongated (diameter 10–60μm) and vary in length from several millimetres to several centimetres. The fibres may run the whole length of the muscle, but often extend only part of the length, ending in tendinous or other connective tissue intersections. The flattened nuclei of muscle fibres lie immediately beneath the cell membrane. The cytoplasm is divided into longitudinal threads or myofibrils, each 1μm in diameter. The myofibrils are divided into isotropic (I) and anisotropic (A) bands, see figure B.18. These I and A bands are bisected transversely by the Z and H bands respectively. If the muscle contracts greatly, the I and H bands may narrow to extinction, but the A bands remain unaltered. Each of the myofibrils is composed of arrays of myofilaments. These are divided transversely by the Z bands into serially repeating regions called sarcomeres, see figure B.18. Two types of myofilament are distinguishable in each sarcomere. The fine ones are
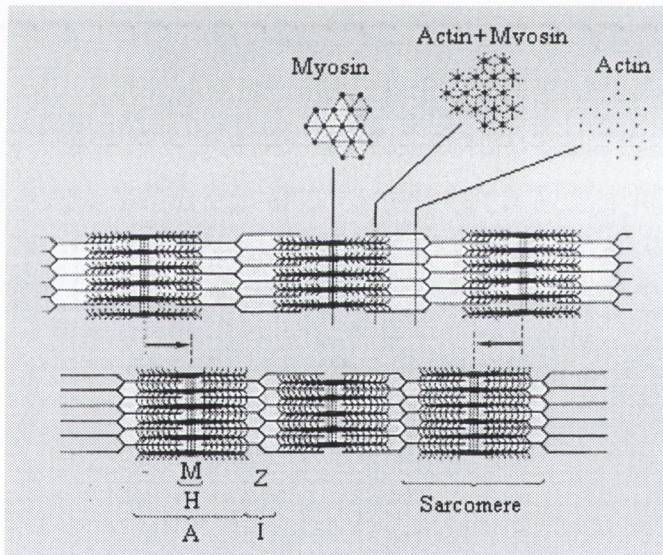
Figure B.18: Structure of a myofilament, showing the spatial arrangement of actin and myosin molecules.

actin molecules, while the thick ones are myosin molecules. The actin filaments are each attached at one end to a Z band and are free at the other to interdigitate with the myosin filaments. The spatial arrangements of these fibres are shown figure B.17. The A bands are the myosin filaments, while the I band is the part of the actin filaments not overlapping with the myosin. The H bands are the middle

region of the A bands into which the actin filaments have not penetrated. The M band lies transversely across the middle of the H bands, and this consists of fine strands of interconnecting adjacent myosin filaments. The hexagonal pattern of arrangement is shown in figure B.18. The structures of the actin and myosin filaments are shown in the last two sketches of figure B.18. Since the 1950's theories and experiments on muscle contraction have concentrated on the cross bridges. The interaction between the actin and myosin filaments is responsible for muscle contraction. The mechanics of this was first identified by Huxley [74] and is now known as the Sliding Element Theory of Muscle Action.

Single Twitch and Wave Summation

Skeletal muscle responds to stimulation by nervous, chemical or electrical impulses. Each adequate stimulation produces a single twitch lasting a fraction of a second. Successive twitches add up to produce a stronger phenomenon, see figure B.19. A single isometric twitch is shown in the lower left corner, and this is followed by successive twitches at varying frequencies. If the frequency exceeds 10Hz, overlap occurs between the twitches. A critical frequency is reached at which successive contractions can no longer be distinguished and this is known as a fused tetanus.
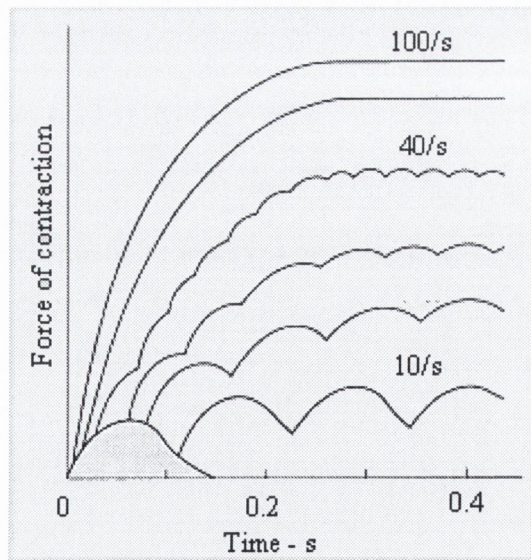
Figure B.19: Wave summation and tetanisation.

Appendix C

MHD's – Frequency Response Characteristics

This appendix shows the Frequency Response Characteristics for the MHD's.
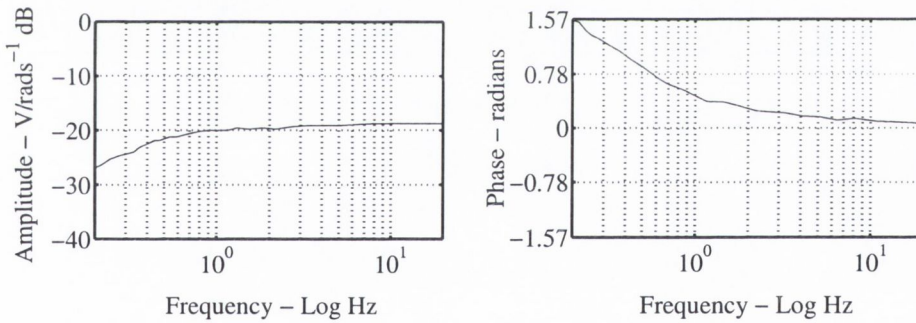
Figure C.1: Magnitude and phase characteristics of M458.
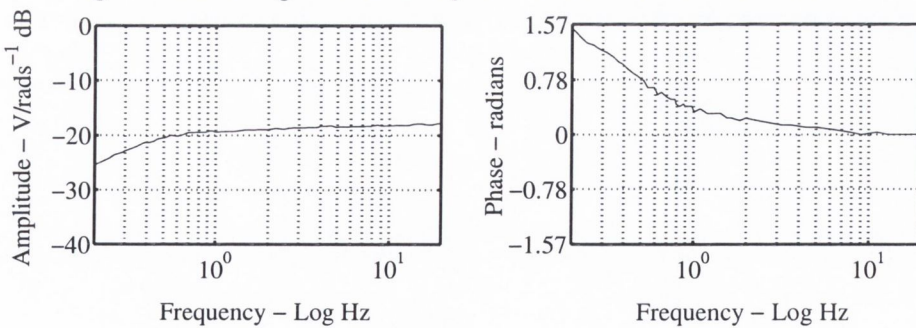
Figure C.2: Magnitude and phase characteristics of M479.

Appendix D

Jaw Template
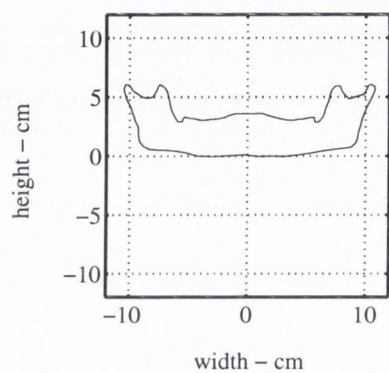
(A)
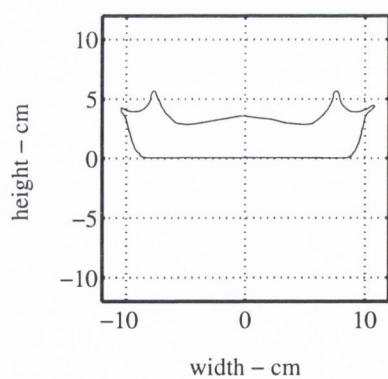
(B)

Figure D.1: Development of 50% male mandible (A) and template for model jaw (B).

Appendix E

Model Muscles

This appendix shows the scaled force/stretch–ratio relationships for the model muscle bundles. The target curve is a scaled multiple of the Yamada curve from figure 2.5, accounting for resting length and cross–sectional area of each muscle. Percentage muscle activity is linearly scaled from the data in figure 3.7.

masseter   medial pterygoid

temporalis
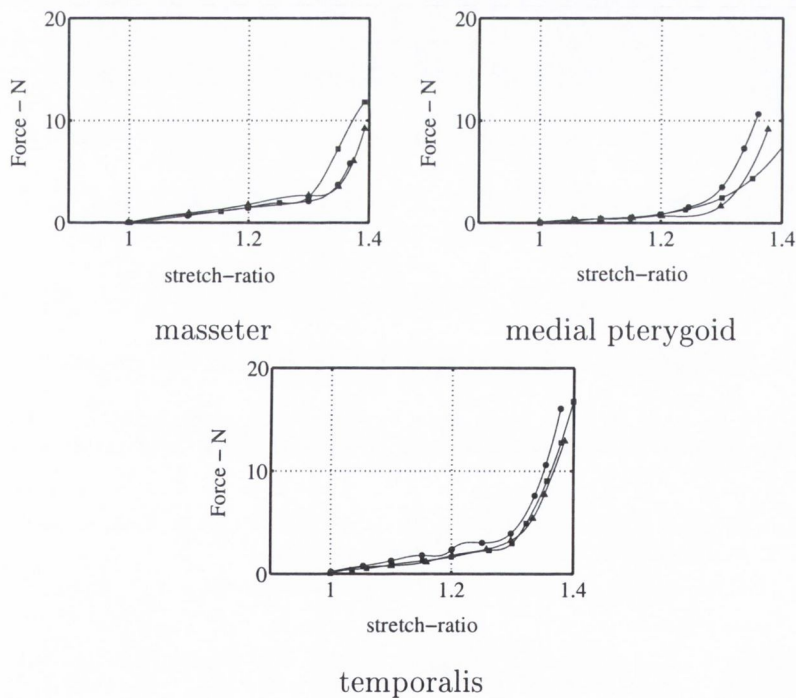
Figure E.1: force/stretch–ratio, 0% active: Yamada (■), model1 (•) and model2 (▲).

masseter

medial pterygoid

temporalis
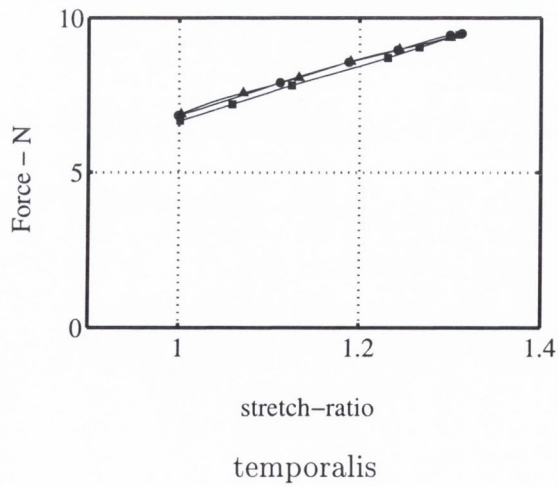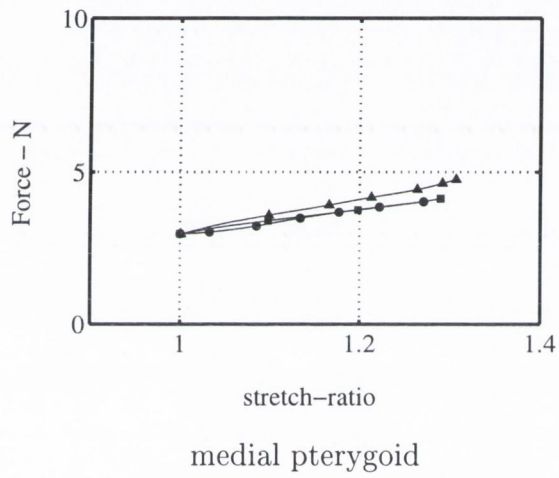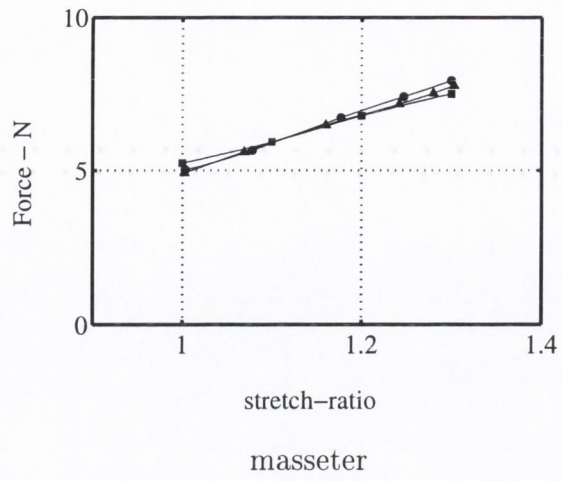
Figure E.2: Force/stretch–ratio, 25% active: Yamada (■), model1 (•) and model2 (▲).

masseter

medial pterygoid

temporalis
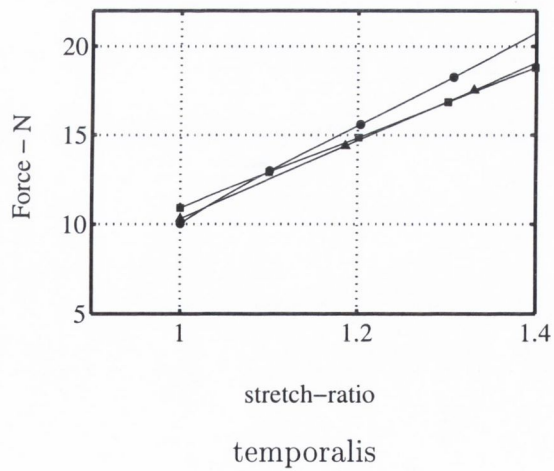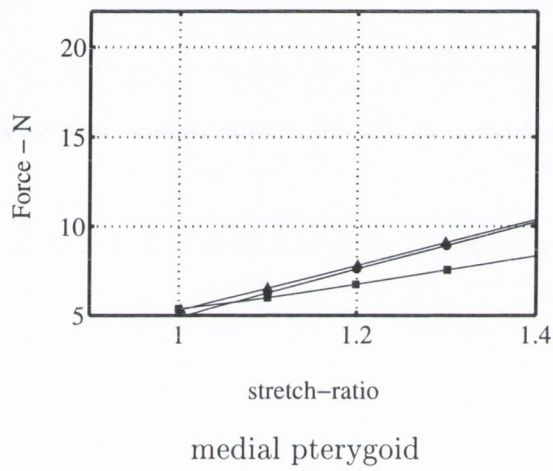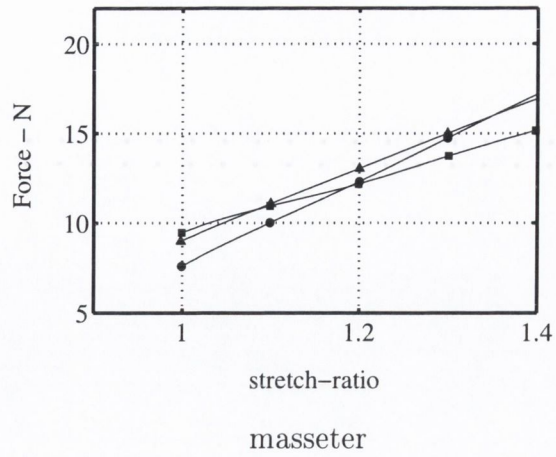
Figure E.3: Force/stretch-ratio, 50% active: Yamada (■), model1 (•) and model2 (▲).

Appendix F

Additional Sled Tests

This appendix includes additional sled–tests as described in chapter 4.
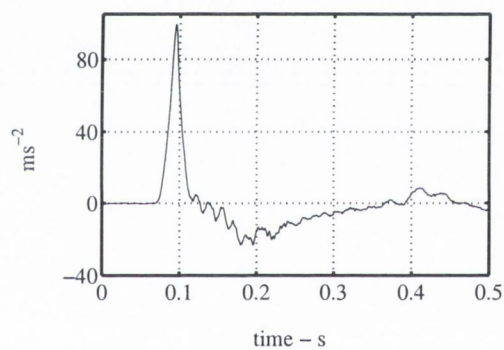
(a) Sled acceleration.
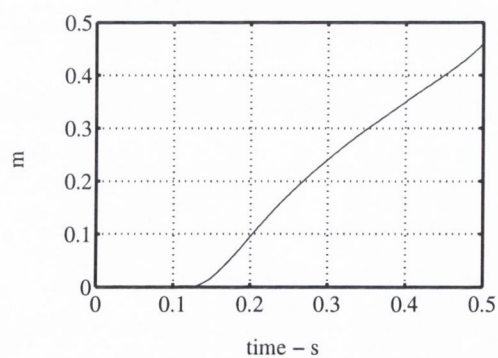
(b) Sled displacement.

Figure F.1: Passive jaw muscle sled–test data – II.
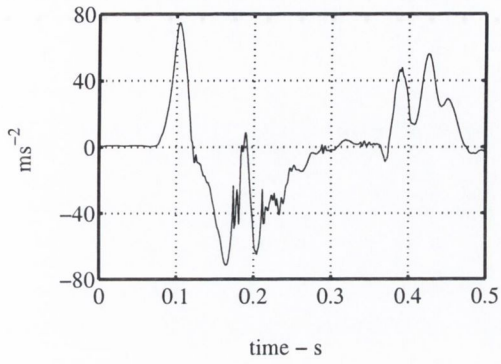
(e) Head linear acceleration.
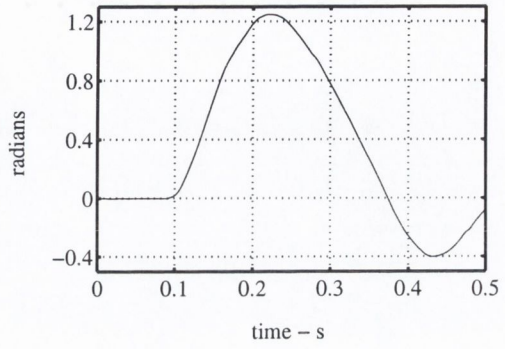
(f) Head angular displacement.
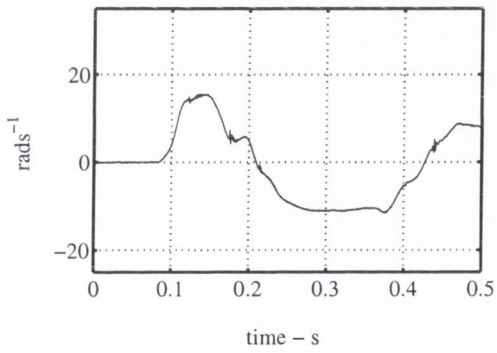
(c) Head angular velocity.
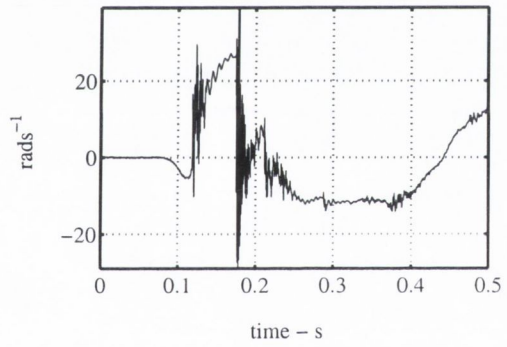
(d) Jaw angular velocity.

Figure F.2: Passive jaw muscle sled–test – II, additional data.
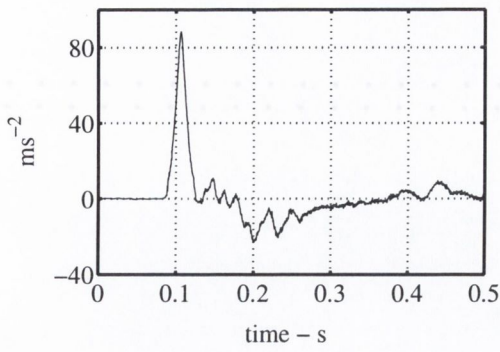
(a) Sled acceleration.
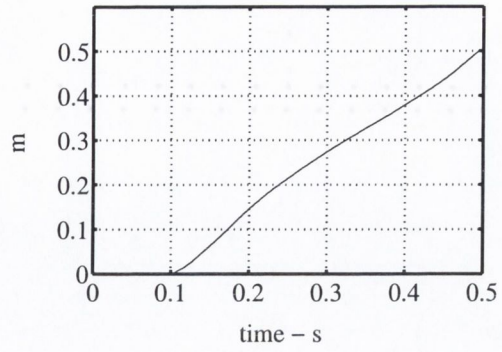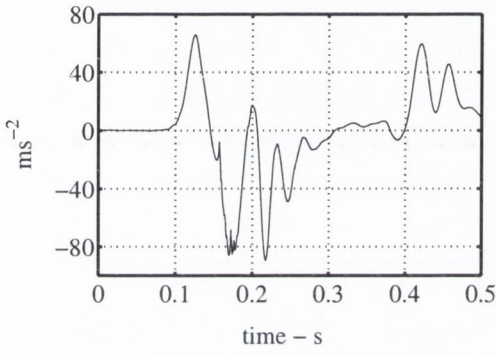
(b) Sled displacement.

(e) Head linear acceleration.
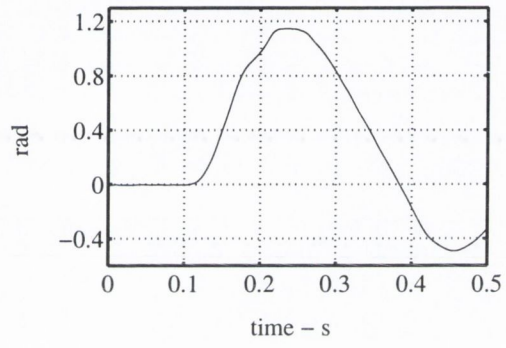
(f) Head angular displacement.
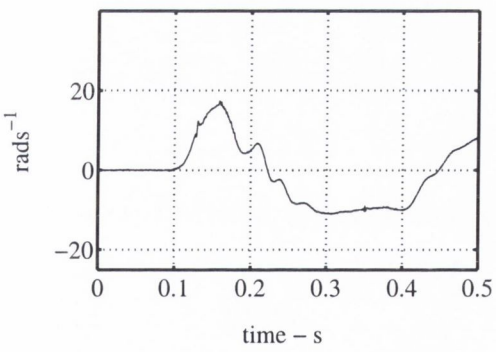
(c) Head angular velocity.
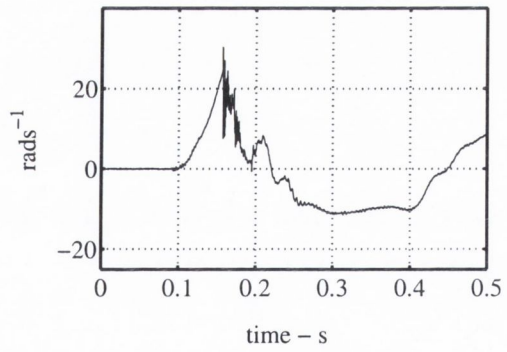
(d) Jaw angular velocity.

Figure F.3: 25% active jaw muscle sled–test data – II.

Appendix G

Cadaveric Tissue Tests
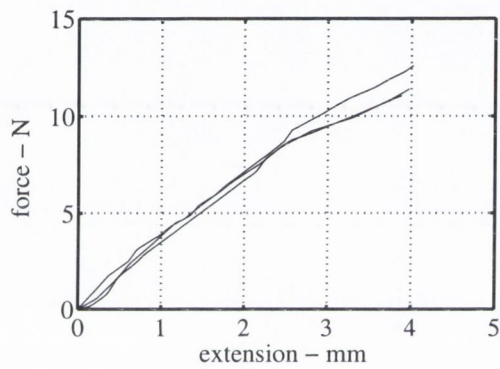
(a) 0°
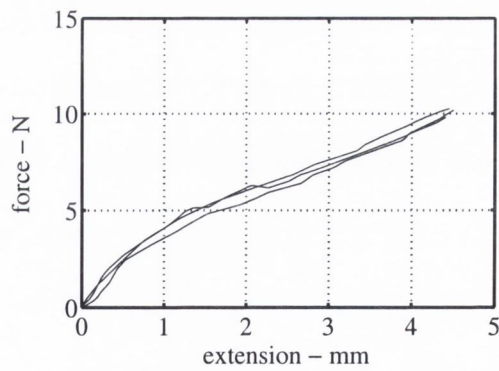
(b) 5°

Figure G.1: Force–extension tests, sp4 at fixed mouth-opening angles.
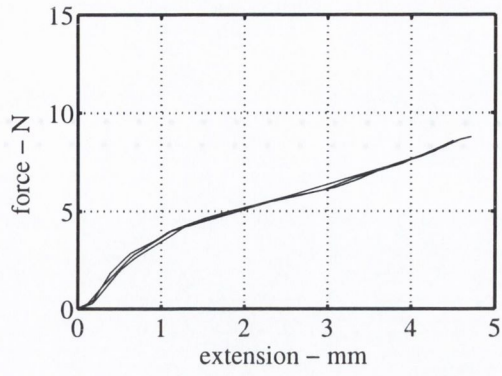
(a) 10°
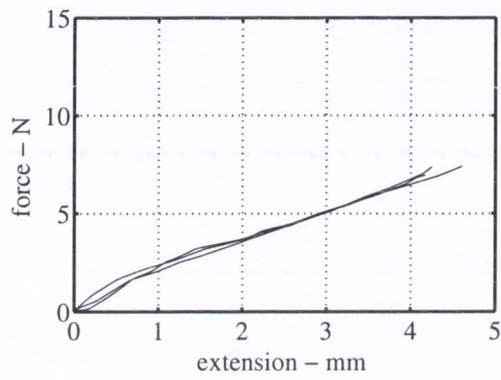
(b)15°
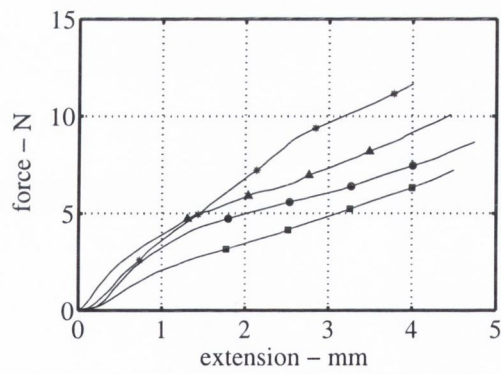
(c)

Figure G.2: a&b: Force–extension tests, sp4 at fixed mouth-opening angles: (c) averages: * = 0°, ▲ = 5°, • = 10°, ■ = 15°.

208
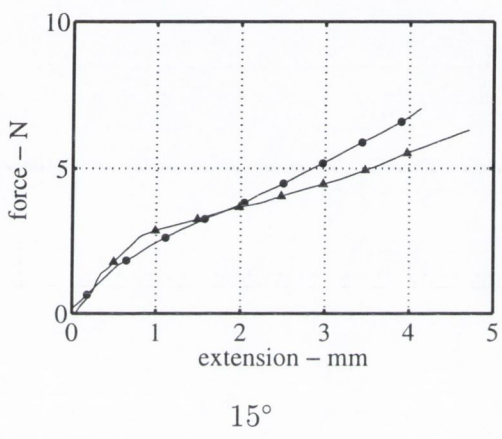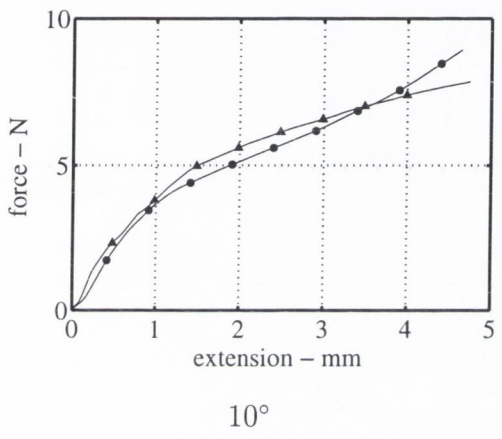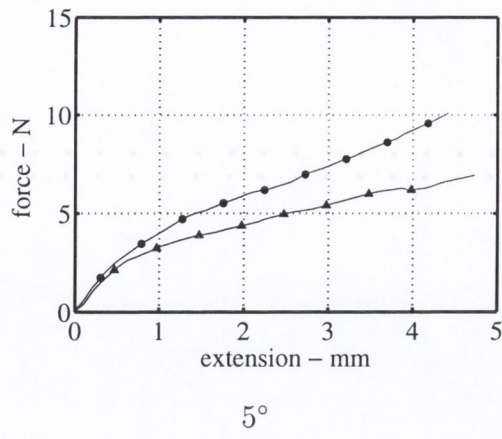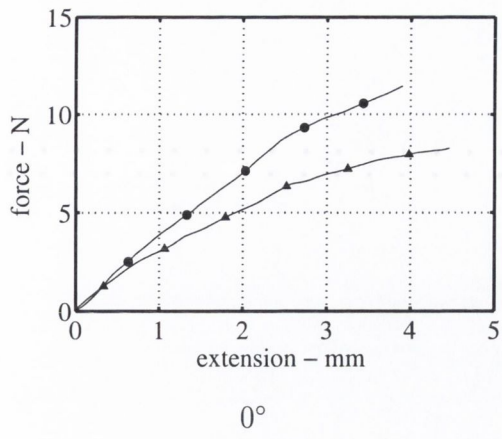
Figure G.3: Force–extension, sp4: before (•) and after (▲) dissection of the lateral ligament.
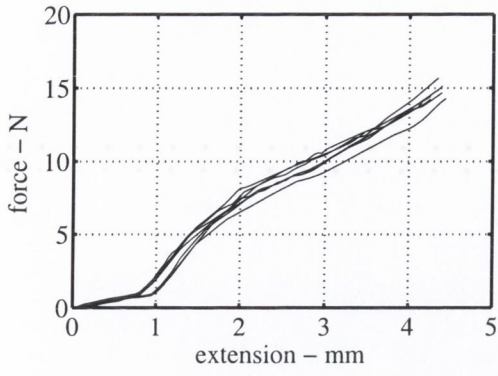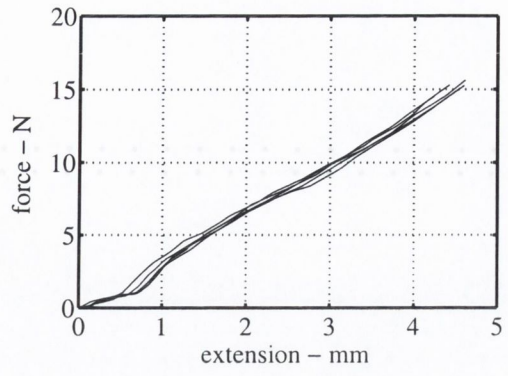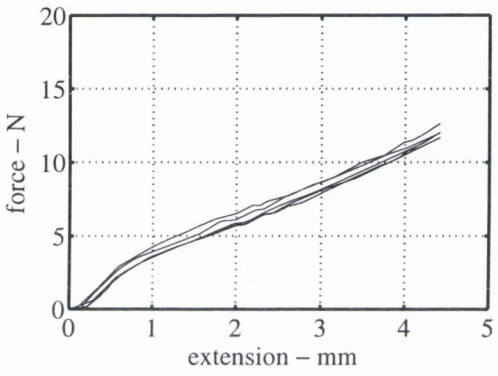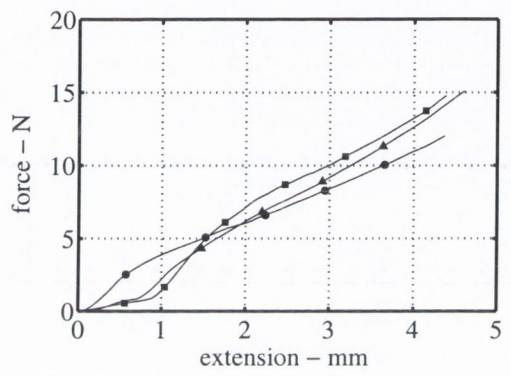
Figure G.4: Force–extension, lateral ligament dissected, sp2: (a) – (c) mouth open, (d) averages: ■ = 0°, ▲ = 5°, • = 10°.
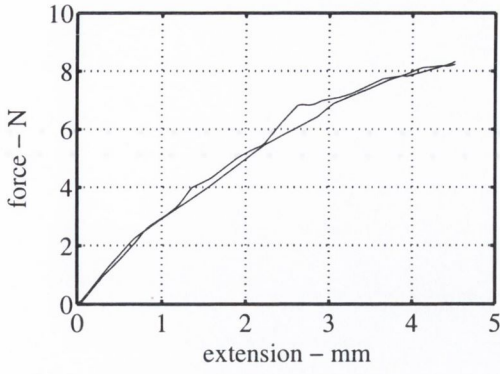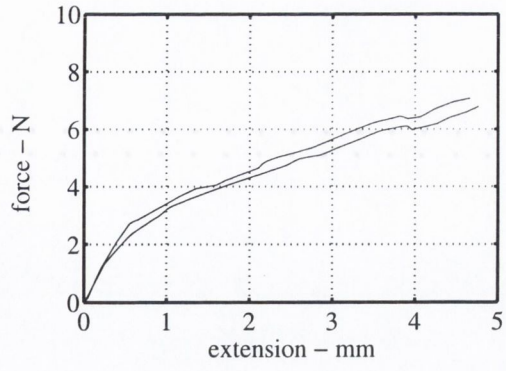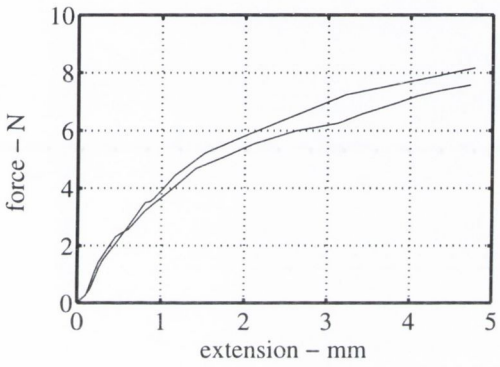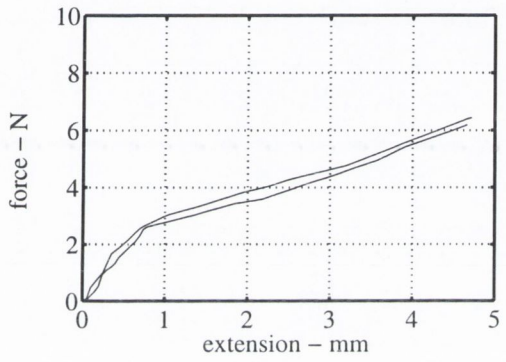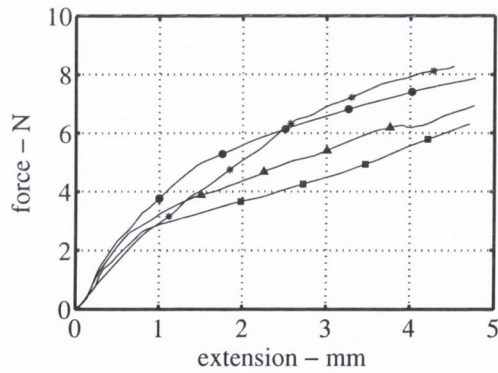
Figure G.5: Force–extension, lateral ligament dissected, sp4: (a)–(d) mouth open, (e) averages: $*$ = 0°, ▲ = 5°, • = 10°, ■ = 15°.
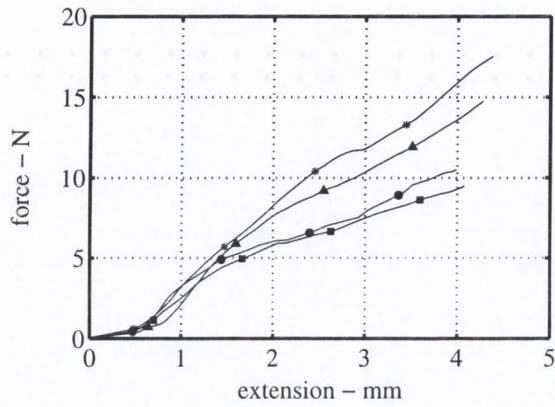
Figure G.6: Dissection of sp2: * = complete joint, ▲ = lateral ligament removed, • = lateral ligament and lateral capsule (including lateral collateral ligament) removed, ■ = lateral ligament, lateral capsule and 2/5 posterior attachments removed.
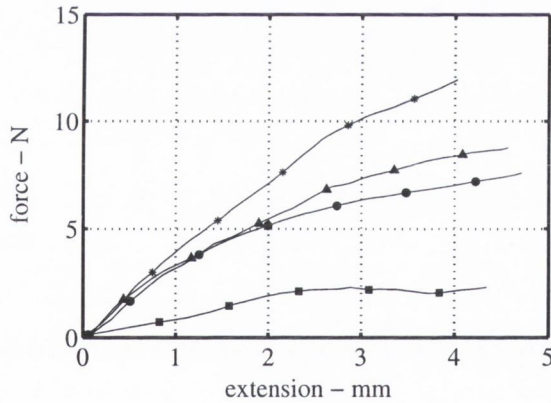

Figure G.7: Dissection of sp4: * = complete joint, ▲ = lateral ligament removed, • = lateral ligament and lateral capsule (including lateral collateral ligament) removed, ■ = lateral ligament, lateral capsule and 2/5 posterior attachments removed.